Predicting Orthostatic Vasovagal Syncope With Signal Processing and Physiological Modelling

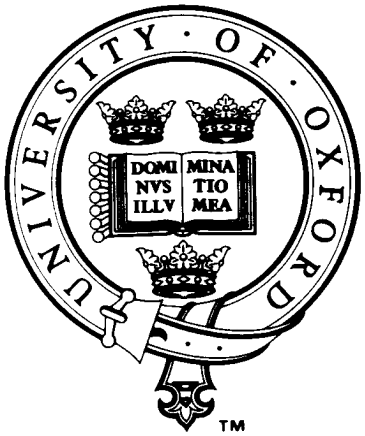

Mark Ebden
Wolfson College

Supervised by
Professor Lionel Tarassenko
Submitted: Michaelmas Term, 2006

This Thesis is submitted to the Department of Engineering Science, University of Oxford, in fulfilment of the requirements for the degree of Doctor of Philosophy. This thesis is entirely my own work, and except where otherwise stated, describes my own research.

Predicting Orthostatic Vasovagal Syncope With Signal Processing and Physiological Modelling

Mark Ebden
Wolfson College

Doctor of Philosophy
Michaelmas term 2006

Orthostatic vasovagal syncope is the sudden loss of consciousness resulting from a temporary impairment of cerebral blood flow, within approximately an hour of standing. Patients who suffer from this problem have "vasovagal syndrome". The purpose of this thesis was to devise a method to detect the syndrome following the assumption of upright position.

Data from 106 syncopal patients undergoing head-up tilt table testing (HUT) were acquired, including electrical activity of the heart (electrocardiogram), blood pressure, oxygen saturation, and cerebral perfusion parameters from near-infrared spectroscopy (NIRS). The data set was examined with the aim of generating automatic diagnoses. Comparison of the rate-pressure product (blood pressure multiplied by heart rate) during the time of syncope with a recommended threshold, in addition to comparison with monitoring the fall of systolic blood pressure during prolonged tilt, yielded an 84% accuracy rate for vasovagal syndrome.

The thesis reviewed the techniques used on the aforementioned time series by previous researchers, emphasising the concepts underlying "time-frequency analysis", a method for analysing nonstationary signals. Since even healthy patients experience time-varying frequency information in their haemodynamics, a transform known as the Smoothed Pseudo-Wigner Ville Distribution (SPWVD) is well suited to their analysis. This distribution was applied to RR tachograms, plots of heart period against time. After the smoothing parameters of the SPWVD were chosen based on artificial data, the optimised transform was then applied to a second artificial tachogram to calculate the LF/HF (low- to high-frequency) ratio, an indicator of heart rate variability. The computed LF/HF ratio tracked the expected value within an error margin of 3.6%. Finally, by applying the same transform to clinical data, it was proved to offer better resolution than an alternative known as the Lomb periodogram.

Classical techniques from the literature predicting vasovagal syncope were found to fail on the current data set: out of 29 tests, only two yielded statistically significant differences between the two patient groups. These were compared with the author's time-frequency analysis of RR tachograms, linear regression of heart rate, and examination of NIRS oscillations and changes on tilt. Of these, the ICFV during time period P3 was found to perform best (negative predictive value: 0.86). A linear classifier was used to combine the best four predictors; it achieved an overall accuracy of 0.88.

Following the data-driven approach, an analytical modelling approach was undertaken. In order to define an appropriate model that traded off simplicity with comprehensiveness, the mechanisms of vasovagal syncope were reviewed. A model of orthostasis was developed, validated, and used toward parameter estimation from patient data. Three parameters (baroreceptor operating point, cardiac effectiveness, and baroreflex gain) were gleaned from the supine baseline recording to "normalise" the model for a given patient, before four new parameters (sympathetic and parasympathetic gains at the sino-atrial node, peripheral vasoconstriction gain, and total blood volume) were estimated from the data collected in the upright position. The expectation was that this approach would improve feature extraction (and hence prediction accuracy) as well as the clinical interpretation of the results. However, the modelling approach was found to offer no significant improvement upon the data-driven signal processing results: a linear classifier on the four post-tilt parameters yielded a negative predictive value of just 0.69. This result may have been due to inaccuracies in the time series data owing to instrumentation error. It is also possible that the modelling approach was not able to provide the quality of feature extraction necessary for predicting vasovagal syncope in the elderly.

Finally, methods to predict syncope during mid- to late HUT were examined. Using information derived from heart rate and baroreflex sensitivity, a technique was developed to ease patient comfort by terminating the test approximately 2 minutes before syncope was expected to occur.

Acknowledgments

Funding for this thesis was generously provided by Oxford BioSignals Ltd and NSERC, the Natural Sciences and Engineering Research Council of Canada. Essential advice and guidance were administered by Prof. Lionel Tarassenko as well as Drs. Adam Darowski and James Price.

I am grateful for the collaboration and other assistance of researchers at the following institutions. Aston University: Profs. David Lowe and Ian Nabney. King's College London: Profs. Jane and Jeremy Ward. Manchester University: Prof. Paul Beatty, Mr. Patrick Cherry, and Prof. Alan Jackson. Massachusetts Institute of Technology: Dr. Thomas Heldt and Profs. Roger Mark and George Moody. Politecnico di Milano: Prof. Sergio Cerutti. Università di Bari: Prof. Mariavittoria Pitzalis. Università di Bologna: Dr. Elisa Magosso and Prof. Mauro Ursino. University of British Columbia: Mr. Parry Fung. University of California at San Diego: Distinguished Prof. John B. West. University College London: Dr. Murad Banaji, Prof. David Delpy, and Dr. Ilias Tachtsidis. University of McGill: Prof. Leon Glass.

Members of the Signal Processing and Neural Networks Group and its associated researchers formed a good working environment in all respects: Drs. Vernon Bailey and Peter Bannister; Mr. Thomas Brennan; Drs. Shelley Cazares, Michael Chappell, and Gari Clifford; Messrs. William Cobern, Richard Germuska, Oliver Gibson, and Alistair Hann; Drs. Nick Hughes and Dileepan Joseph; Mr. Mark Larsen; Miss Lisa Lazareck; Drs. Laura Mason, Patrick McSharry, and Stephen Payne; Miss Tingying Peng; Mr. Alex Rowley; and Drs. Sunay Shah, Neil Townsend, and Simukai Utete. I also thank the employees of Oxford BioSignals, in particular Dr. Emma Braithwaite, Messrs. David Clifton and Stuart Cove, and Dr. Charles Potter.

For technical consultation and assistance I am indebted to Messrs. Roger Belcher, John Hastings, and Christopher Rabson. For translations, I thank Messrs. Matteo Aquilina and Simone Ghislandi, and Misses Tania Tam and Anna Vassileva. For Matlab and numerical computing issues I thank Prof. Nick Trefethen. For statistical consultation, I thank Prof. Emeritus F.H.C. Marriott. For data acquisition assistance and patient information I thank Mmes. Janet Burton and Sheena Davie. For administrative support I thank Miss Jan Minchington, Ms. Val Mitchell, and the staff at Wolfson College. I owe thanks to the examiners of the PRS report, Prof. David Edwards and Dr. Janet Efstathiou, and the examiners of this thesis, Drs. Clare Elwell and Stephen Payne.

Finally, it may be a truism to say that doctorates are challenging, but they can still surprise in the nature of that challenge. It is for this reason that most of my thanks is reserved for family and friends, for their love.

Contents

List of Figures

List of Tables

Chapter 1

Introduction

1.1 The Need for Syncope Prediction

Syncope is the sudden loss of consciousness resulting from a temporary impairment of cerebral blood flow. Although recovery is always rapid, syncopal attacks (faints) are accompanied by the loss of upright posture, and hence present a real danger: syncope accounts for up to 3% of emergency room visits and 6% of hospital admissions [124]. Patients with recurrent syncope (frequent episodes) endure a quality of life comparable to sufferers of rheumatoid arthritis or chronic lower back pain [109].

There are many reasons why a patient might suffer from recurrent syncope. Since standing up is often sufficient to cause a faint, these patients are sometimes referred for a clinical test known as head-upright tilt-table testing (HUT). This test involves tilting a patient from the supine position to a nearly vertical position, with the support of an angled hospital bed (see Figure 1.1). In this way, the challenge of upright posture — referred to medically as "orthostasis" — is mimicked in a controlled environment, allowing the doctor to observe symptoms and cardiovascular reactions prior to collapse. Although HUT functions as a rich source of information in the forming of a diagnosis, it can take up to an hour for the patient to faint in this manner, known as orthostatic vasovagal syncope.

This occupation of valuable physician time is the primary disadvantage of HUT, leading to many attempts to shorten the test. The experiments usually involve examination of the cardiovascular data in the minutes that follow the tilt, in an effort to diagnose patients by predicting their tendency to faint during prolonged HUT, but a reliable predictor has not yet been developed.

Previous work in the area of syncope prediction has focused on the analysis of one or at most two channels of data, such as the electrocardiogram (defined in Section 1.4.2). In contrast, the current work is distinguished not only by the novelty of some of the analyses of these individual data streams, but

moreover by the methods to combine multiple data streams in forming a prediction. The use of multiple inputs was deemed necessary given the heterogeneity of the syncopal population, the topic of the next chapter.

The remainder of this chapter serves to introduce the relevant medical terminology and context, to define the type of patient data under review in the present analyses, to summarise the method in which the data was collected, and to outline the scope of the thesis.

1.2 Historical Background

Syncope has a rich history: having fascinated people for centuries, it has elicited many speculations on its causes, and today remains improperly understood. The following timeline introduces some of the medical terminology applied in later chapters.

First Phase

The first historical phase focused on causes, the pathophysiology (i.e. the associated functional changes) of vasovagal syncope, and the natural history of various entities.

1628: W. Harvey observed the unusual languor of blood from patients fainting during a blood removal procedure [223], thereby unknowingly describing the "vasodilatory" effect of vasovagal syncope. Vasodilation refers to the expansion of blood vessels.

1773: J. Hunter observed the scarlet colour and languor of blood from a bleeding fainter, providing further unwitting proof of the vasodilation which is characteristic to vasovagal syncope.

1888: M. Foster deduced that inadequate cerebral blood flow is an essential component of syncope.

1895: L. Hill first asserted that vasodilation plays an important role.

1907: W. Gowers recognised the concurrence of vasodilatory and "bradycardic" components during fainting. A bradycardia is an abnormally slow heart rate, below 60 beats per minute; it results from high activity in the vagus nerve. Gowers coined the term "vasovagal" to refer first to the vasodilatory and second to the vagally-mediated bradycardic component characteristic of the syncope.

1932: Sir Thomas Lewis extended Gowers' findings while coining the term "vasovagal syncope" [108].

1940s: Tilt table testing began to be used to explore the response of the body to changes in position.

1956: E. Sharpey-Schafer hypothesised that vasovagal syncope is caused by increased left ventricular contraction triggering a "Bezold-Jarisch reflex" [184]. (This is explained more fully in the next chapter.) His theory grew in popularity until the 1990s, when it began to be assessed more critically.

Second Phase

In the early 1980s, several studies concluded that the cause of syncope is not clear for many patients [91].

Researchers turned to more pragmatic approaches.

Early 1980s: Subgroups with high mortalities were identified to tackle this new perspective practically.

Mid 1980s: Much electrophysiological testing led to an understanding of the roles — and limitations — of syncope tests; studies also showed that syncope in the elderly is often a complicated product of medications, comorbid diseases, and physiological changes. (A comorbid disease is one which occurs simultaneously with another.)

Mid 1980s to early 1990s: HUT was proven to be an excellent diagnostic tool for syncope patients.

1990s: Various international symposia were held on the topic of syncope or its subtopics. Panels were convened to strive for a consensus on controversial aspects.

1992: The Vasovagal International Study (VASIS) proposed a three-pronged classification scheme for vasovagal syncope [200]. This proved popular, and helpful minor modifications were later suggested [31, 92].

2001: An international "Task Force on Syncope" was created by the European Society of Cardiology, which then published "Guidelines on management (diagnosis and treatment) of syncope" [3].

1.3 Classification and Pathology

Syncope is a symptom rather than a discrete pathological entity; its causes are many, and in fact over 100 can be identified in the literature. A useful approach is to divide these causes into three broad classes [63], for prognostic reasons — in keeping with the philosophy of the "second phase" identified in the previous section. These three classes are the following:

1. Cardiovascular causes (25–30% of patients; usually the most dangerous)
2. Non-cardiovascular causes (20–40%)
3. Unknown causes (30–50%; often more benign)

In many studies, the percentages vary considerably beyond the ranges given above, owing to the diverse selection criteria applied to recruit patients. However, it is becoming possible to reduce the percentage of "unknown" causes as diagnostic methods improve. In particular, HUT and a technique known as "carotid sinus massage" have proved to be two important techniques in increasing the percentage of successful diagnoses. Chapter 2 provides an overview of the causes of the most common types of syncope, according to a more comprehensive classification system with five types.

There exists a consensus that regardless of the cause of syncope, the final pathway is always a transient cerebral hypoperfusion, i.e. poor blood flow to the brain. It has been shown that a 6- to 8-second total cessation of cerebral blood flow [173], or a systolic blood pressure below 60 mmHg [185], is associated with syncope. However, there is still uncertainty regarding the mechanisms causing this cerebral hypoperfusion in patients.

Figure 1.1: An illustration of head-upright tilt table testing, at the Radcliffe Infirmary Falls Clinic.

1.4 Available Data

1.4.1 Patients

The Falls Clinic at the Radcliffe Infirmary, Oxford, receives a steady stream of patients suffering from unexplained falls. The typical subject is an elderly person referred by his or her primary care physician since the patient history alone is not sufficient to form a diagnosis.

Since a large number of these patients suffer from syncope, the Falls Clinic provides an ideal data source for investigation. The data under investigation in this thesis were acquired from January 2002 to November 2004 at the Falls Clinic during the execution of HUT: ordinarily lasting less than two hours, each test was performed under the supervision of a qualified physician. The protocol will be detailed in Chapter 4.

1.4.2 Measurements

Physiological signals were recorded noninvasively before, during, and after orthostasis. Most of this recording relied on the Software Monitor, a patient-monitoring system developed during the late 1990s in the University of Oxford Signal Processing and Neural Networks Group [210]. The other instrument used was the NIRO-300, from Hamamatsu. The signals recorded were as follows:

Electrical activity of the heart: Electrocardiograms, also known simply as cardiograms or ECGs, record cardiac electrical activity in millivolts (mV); a typical example is depicted in Figure 1.2.

Blood pressure: The force per unit area that circulating blood exerts on arterial walls is defined as blood pressure (BP). This measurement is divided into systolic and diastolic readings, registering the pressure during cardiac contraction and relaxation respectively. The usual unit of measurement is millimetres of mercury (mmHg). If a physician reports a BP of 120/80, this means that the BP is oscillating once per heartbeat between a maximum (systolic) BP of 120 and a minimum (diastolic) BP of 80 mmHg.

Pulse Oximetry: The quantity of oxygen present in blood vessels can drift slowly up or down, as a person's blood supply and demands vary. Oxygen is transported using haemoglobin, a blood protein. Depending on whether oxygen molecules are bound to haemoglobin at a given time, the protein is also referred to as oxyhaemoglobin or deoxyhaemoglobin. Oxygen saturation is expressed as a percentage, by dividing the actual amount of haemoglobin-carried oxygen by the (theoretical) maximum oxygen capacity and multiplying by 100.

Cerebral perfusion changes: In many patients, cerebral blood perfusion (the extent to which blood reaches its target tissues and organs) was recorded. The details will be described in Chapter 3.

Additional processing of the above data was also performed, either offline or in real time within the recording equipment itself. The most important parameter derived from the ECG was heart rate (HR), measured in beats per minute. For convenience, the R peak — identified in Figure 1.2 — was extracted as a reference point to identify the timing of each heart beat. (See Appendix A.) Counting R peaks over a given period of time represents a standard way to calculate HR; for the current work, instantaneous HR was approximated by first finding the "RR interval", the time which elapses between two consecutive R peaks. A beat-to-beat estimate of HR (in beats per minute) was then obtained from this interval.

1.5 Data-Driven versus Physiological Modelling Approaches

The analysis carried out in this thesis is concerned primarily with the goal of predicting the result of HUT, based on the data recorded during a period of supine rest and during tilt, with the secondary aim of automating the *diagnosis* of syncope. As mentioned earlier, one of the novel aspects of this thesis is

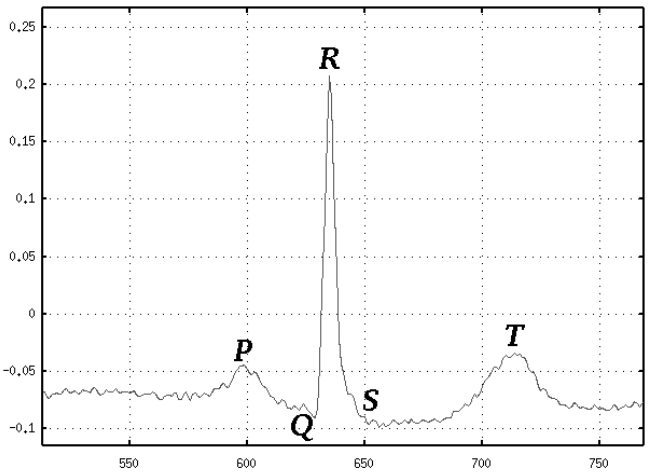

Figure 1.2: A segment of a typical electrocardiogram (ECG), here representing one heart beat. The vertical and horizontal axes measure electrical potential and time, respectively, in arbitrary units. The letters P through T represent points of interest; most importantly, "R" corresponds to the moment at which the ventricles (the largest chambers in the heart) contract, pulsing blood through the circulatory system. [39]

the use of multiple data streams as part of this analysis. Single-parameter analysis is of limited use in the analysis of a multi-factorial problem such as syncope. Therefore, the analysis of multiple parameters was thought likely to yield greater understanding.

There are two main ways that multiple data streams can be analysed: data-driven approaches and analytical modelling. The former involves computing n parameters from m available data streams by running n independent algorithms, such as cross-spectral analysis. In contrast, the latter involves constructing a software model of how the m measurable quantities can be expected to interact, and using a given patient's data to estimate n selected parameters within that model. In either case, the n parameters can then be integrated using a linear combination or neural network and the result can be compared to some threshold in order to determine whether a patient should be diagnosed as abnormal. Alternatively, the n parameters can be subjected to cluster analysis or dimensionality reduction to observe patterns in their distribution.

The choice between data-driven approaches and physically-based models often arises in biomedical engineering. Data-driven approaches can be computationally simpler than modelling, since the latter requires multiple runs of the model for the purpose of parameter fitting. In addition, data-driven approaches do not require as thorough a knowledge of the underlying system; indeed, it is theoretically possible to classify data reliably using a parameter of completely unknown origin.

However, data classification in biomedical engineering is often, as in the present case, a *diagnosis* which must be justified to a physician. This is where one of the advantages of physically-based models becomes evident: the results are often easier to explain to the medical community. This is because a physician can appreciate a diagnosis more readily when it is based on the calculated abnormality of a particular physiological quantity. A second important advantage of modelling is that in some cases it provides superior feature extraction: this occurs when models are able to make abstractions of a kind not possible with the data-driven approach. More precisely, raw clinical data can be extended when they are used to fit the parameters of a given model; for example, a control model of how blood pressure provides negative feedback on heart rate can be used with clinical data to estimate the gain of such a system in a given patient. A third advantage of analytical modelling is that it can provide physiological insight if a new or extended model is able to reproduce clinical data faithfully. For instance, deBoer *et al.* [42] used a beat-to-beat model of blood pressure and heart rate to refine the understanding of the causal pathways relating the two.

The two approaches, data-driven and analytical model-based, need not be pursued in isolation. Hybrids are possible, for example when a knowledge-based model contains as a unit a data-driven representation. As a second example, the signal processing normally associated with a data-driven approach can influence the development of a physiological model in at least two ways:

- Specifying causal links between parameters, by determining their transfer function, or analysing their phase lag
- Identifying new parameters of interest to add to the model

The thesis approaches the problem of syncope prediction using first the data-driven approach (Chapters 4 through 6), followed by the analytical model-based approach (Chapters 7 and 8). This plan is described in more detail below.

1.6 Overview of the Thesis

The next chapter defines key physiological concepts and then delineates the different ways in which syncope can occur, before describing the current diagnostic protocols for syncope. Chapter 3 focuses on how these concepts have been investigated to develop our understanding of syncope, with a view to being

able to predict it. This chapter also reviews most of the signal processing literature of relevance to the dianosis and prediction of syncope.

Chapter 4 introduces the data acquisition from the Falls Clinic patients and evaluates the use of straightforward syncope diagnosis techniques to analyse these patients. The following chapter describes the time-frequency analysis of beat-by-beat heart rate, using a distribution named the Smoothed Pseudo Wigner-Ville Distribution (SPWVD). The aim is to devise a new method of interpreting ECGs, suited to the task of predicting syncope in the elderly population. This method is then applied in Chapter 6, using the first few minutes of ECG data collected after tilt during HUT. In addition to this analysis, the performance of other syncope predictors is reported.

The signal processing approach to the problem of syncope prediction is followed by a physiological modelling approach described in Chapters 7 and 8. The construction of an accurate model requires a level of physiological detail beyond that described in Chapter 2; the aim of Chapter 7 is therefore to summarise the essential physiological mechanisms for each of three hypothetical causes of vasovagal syncope. This understanding informs the development of the "Orthostasis Model", a lumped-parameter model described in Chapter 8. After the model is validated, it is used to estimate parameters for the Falls Clinic patients. These parameters are in turn used in an attempt to predict syncope, as was previously done in Chapter 6. A comparison of the results of Chapters 6 and 8 concludes the chapter.

Chapter 9 examines syncope prediction in the later stages of HUT. The aim becomes no longer to try to save the clinician time, but rather to increase patient comfort by avoiding syncope if it is certain. Finally, Chapter 10 summarises the findings of the thesis and reviews the relevance of the results of physiological modelling with respect to those of signal processing. It finishes by making suggestions for future work.

Chapter 2

The Diagnosis and Treatment of Recurrent Syncope

2.1 Introduction

This chapter reviews how syncope is diagnosed and treated by the medical community. Although various subclassification schemes exist, the categories used in the remainder of the thesis are defined as follows [3]:

1. Orthostatic hypotension
2. Cardiac arrhythmias as primary cause
3. Structural cardiac or cardiopulmonary disease
4. Cerebrovascular syndromes
5. Neurally mediated reflex syndromes

(See Figure 2.1.) After these five types of syncope are described, this chapter will discuss how syncope is diagnosed and treated. However, two physiological concepts not particular to syncope require explanation first: the baroreflex and cerebrovascular autoregulation.

Figure 2.1 (Next page): A quantitative interpretation of the various types of syncope, based primarily on information from [3]. Values of parameters are not sufficient for a diagnosis, and must be interpreted alongside qualitative factors, including patient history. The ideal starting point for the diagnosis includes a careful history and physical examination, followed by supine and upright BP measurements and a standard 12-lead ECG. Abbreviations: HR = Heart Rate; BP = Blood Pressure; CSM = Carotid Sinus Massage; CBF = Cerebral Blood Flow; ECG = electrocardiogram.

Figure 2.1:

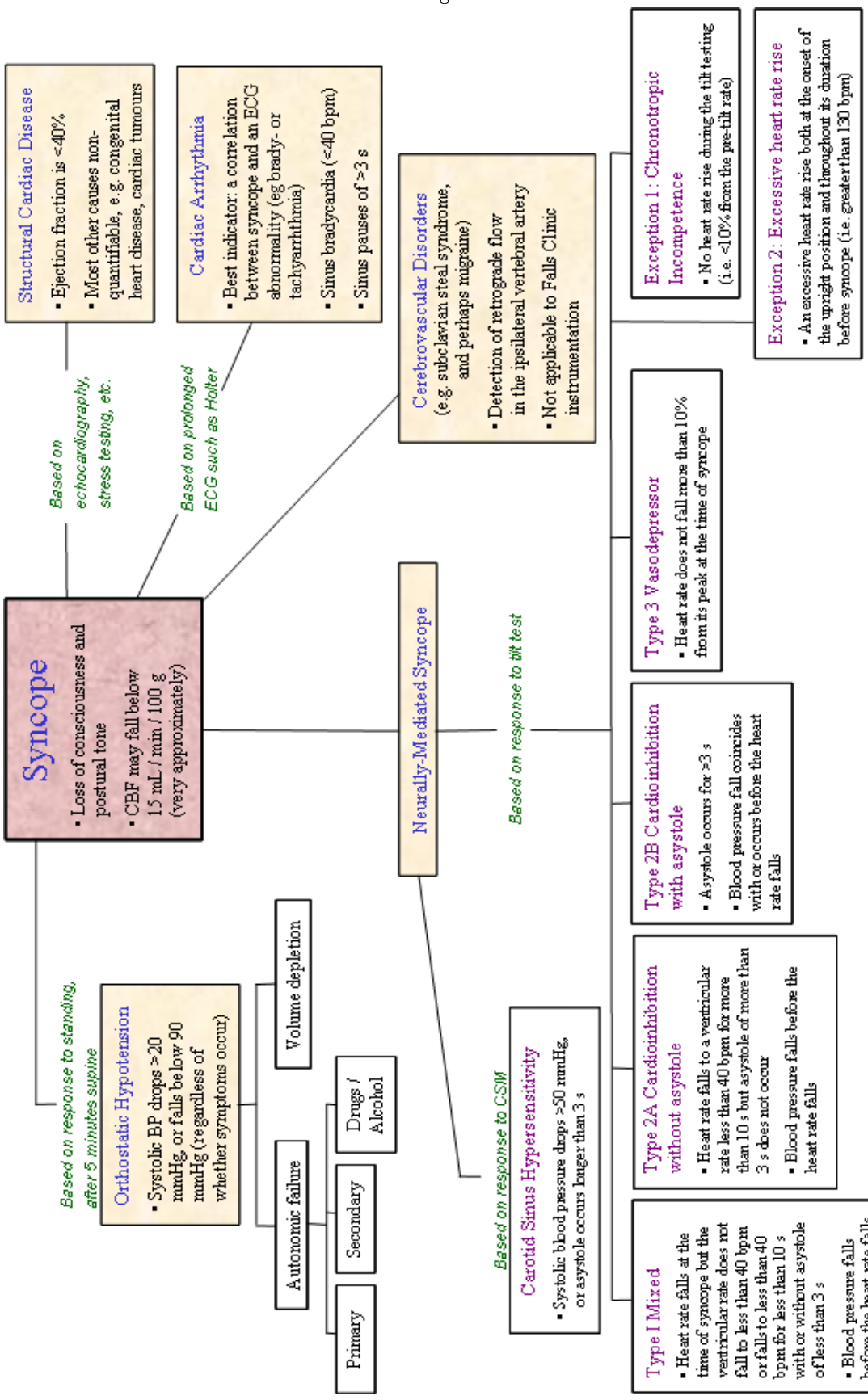
Syncope
▪ Loss of consciousness and postural tone
▪ CBF may fall below 15 mL / min / 100 g (very approximately)
Based on response to standing, after 5 minutes supine
Orthostatic Hypotension
▪ Systolic BP drops ≥20 mmHg or falls below 90 mmHg (regardless of whether symptoms occur)
Primary
Secondary
Autonomic failure
Drugs / Alcohol
Volume depletion
Based on response to CSM
Carotid Sinus Hypersensitivity
▪ Systolic blood pressure drops >50 mmHg, or asystole occurs longer than 3 s
Based on response to tilt test
Neurally-Mediated Syncope
Type I Mixed
▪ Heart rate falls at the time of syncope but the ventricular rate does not fall to less than 40 bpm or falls to less than 40 bpm for less than 10 s with or without asystole of less than 3 s
▪ Blood pressure falls before the heart rate falls
Type 2A Cardioinhibition without asystole
▪ Heart rate falls to a ventricular rate less than 40 bpm for more than 10 s but asystole of more than 3 s does not occur
▪ Blood pressure falls before the heart rate falls
Type 2B Cardioinhibition with asystole
▪ Asystole occurs for >3 s
▪ Blood pressure fall coincides with or occurs before the heart rate falls
Type 3 Vasodepressor
▪ Heart rate does not fall more than 10% from its peak at the time of syncope
Exception 1: Chronotropic Incompetence
▪ No heart rate rise during the tilt testing (i.e. <10% from the pre-tilt rate)
Exception 2: Excessive heart rate rise
▪ An excessive heart rate rise both at the onset of the upright position and throughout its duration before syncope (i.e. greaterthan 130 bpm)
Based on prolonged ECG such as Holter
Cardiac Arrhythmia
▪ Best indicator: a correlation between syncope and an ECG abnormality (eg brady- or tachyarrhythmia)
▪ Sinus bradycardia (<40 bpm)
▪ Sinus pauses of >3 s
Based on echocardiography, stress testing, etc.
Structural Cardiac Disease
▪ Ejection fraction is <40%
▪ Most other causes non-quantifiable, e.g. congenital heart disease, cardiac tumours
Cerebrovascular Disorders
(e.g. subclavian steal syndrome, and perhaps migraine)
▪ Detection of retrograde flow in the ipsilateral vertebral artery
▪ Not applicable to Falls Clinic instrumentation

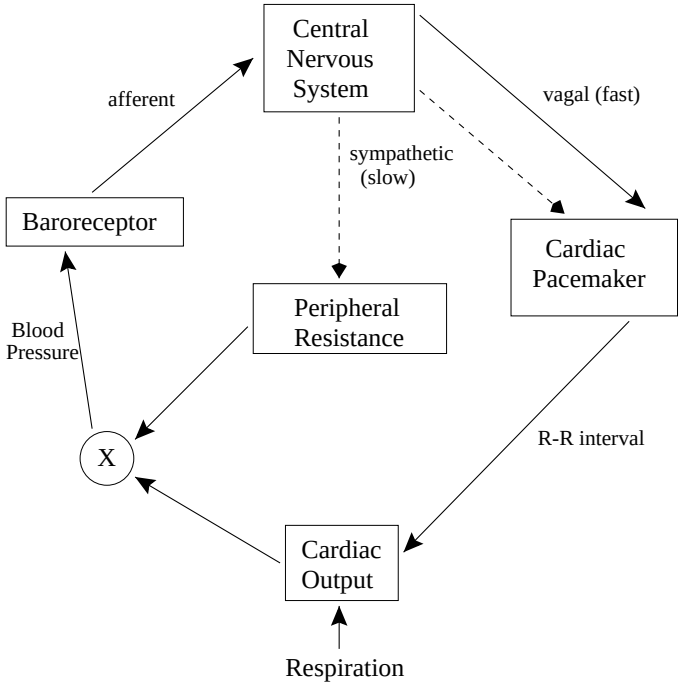

Figure 2.2: Schematic diagram of the baroreflex (From Clifford [39], adapted from deBoer *et al.* [42]).

2.2 Physiological Background

2.2.1 The Baroreflex

The "baroreflex" is a negative feedback system which smooths transient BP (blood pressure) changes, as illustrated in Figure 2.2. A decrease in BP reduces the stretch in blood vessel walls, and this relaxation is detected by pseudo-strain gauges known as "baroreceptors". These pressure receptors help govern the activity of the sympathetic nervous system: a decrease in BP is countered by an increase in sympathetic nervous outflow, and vice versa. When BP falls, the baroreceptors therefore cause a compensatory rise in cardiac output as well as an increase in peripheral resistance (the total resistance to flow of blood in the systemic circuit) via vasoconstriction. These two responses act to raise BP back towards its initial value.

2.2.2 Cerebrovascular Autoregulation

The brain must maintain a steady flow of nutrients to its cells, countering challenges from the rest of the body such as low BP or high levels of oxygenation. This process is known as cerebral autoregulation. It is believed that the brain's primary mechanism for accomplishing this task involves the control of cerebral blood flow (CBF) with a negative feedback loop [219]. The feedback involves vasoconstriction

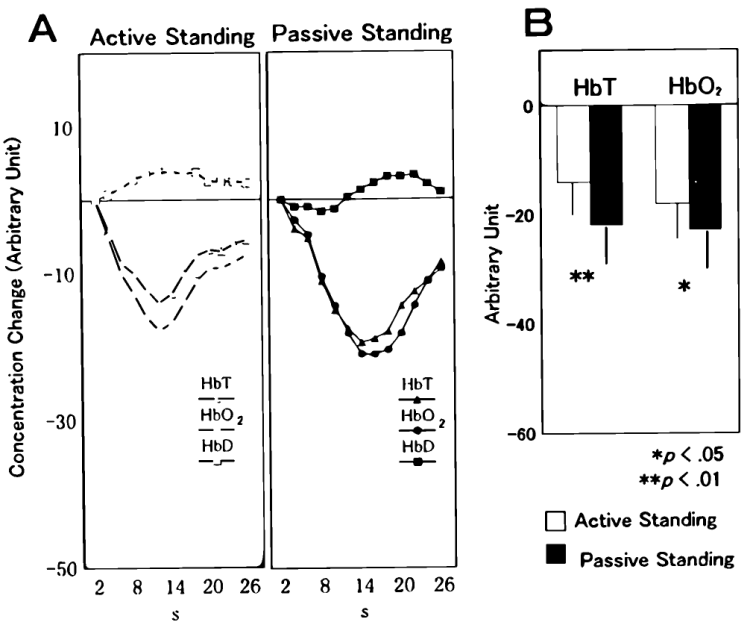

Figure 2.3: **A.** Changes in HbT (total haemoglobin), HbO_2 (oxyhaemoglobin), and HbD (deoxyhaemoglobin) concentrations in young subjects upon standing. **B.** Comparison of the maximum variation in HbT and HbO_2 in young subjects during active and passive standing. [207]

and vasodilation of elements in the arterial vasculature. It should be noted that although CBF and cerebral oxygenation are kept fairly constant for a large range of blood pressures, at very high or very low BP cerebral autoregulation fails and hence blood flow and oxygenation can decrease or rise severely.

Cerebral perfusion changes have been analysed in patients undergoing orthostatic stress. Figure 2.3A shows that haemoglobin deoxygenates steadily for approximately ten seconds after standing, and then begins to recover at a slightly slower rate. The degree of deoxygenation varies with the manner in which the patient assumes the upright position, as can be shown in Figure 2.3B. (Note that "passive standing" involves being carefully pulled upright by a nurse, minimising patient effort.)

Cerebral autoregulation is known to become impaired owing to the ageing process [207], and hence some of the elderly Falls Clinic patients (see Section 4.2) will be affected by poor CBF control. However, syncope can result from several causes and the role of cerebral autoregulation in syncope is still a matter of debate. Thus far it is known that CBF is similar in healthy and syncopal patients immediately upon standing [34,65,180], and when differences do appear later during prolonged orthostasis, they are followed by syncope only after a significant time lag [102]. Hence, it is not at all certain that impaired control of CBF is a common cause of syncope. Second, some groups have argued that cerebral vasoconstriction can precede vasovagal syncope [65, 68, 102, 191] but it is perhaps more likely that vasodilation occurs

instead [34, 103, 179].

Owing to these uncertainties, cerebral autoregulation is not included in the classification scheme defined in Figure 2.1. However, the topic will be considered again in the next chapter.

2.3 Syncope Classification

Orthostatic Hypotension

Orthostatic hypotension is characterised by a large decrease in BP upon standing or at the start of HUT. The problem can be caused by the failure of the body to react to the proper extent during the orthostatic stimulus: for example, HR does not increase sufficiently, or more commonly, the blood vessels do not vasoconstrict sufficiently. The decrease in BP can take place within a few minutes (frank orthostatic hypotension) or over a significant fraction of an hour ("dysautonomic response" to standing).

Many of the elderly take medications with side effects which exacerbate orthostatic hypotension. (For instance, anti-hypertension drugs can directly oppose the vasoconstriction which accompanies healthy orthostasis.) However, another important reason why the elderly are susceptible to orthostatic hypotension is the attenuation of the autonomic nervous system with ageing. Specifically, the subsystems that commonly degrade are blood volume regulation and baroreflex sensitivity. In the case of a healthy baroreflex, the initial decrease in BP on standing is at least partially mitigated. However, in elderly patients with less sensitive baroreceptors, changes in BP (whether positive or negative) cannot be detected as effectively, and hence BP can decrease relatively unchecked upon standing.

Besides autonomic failure (primary, secondary, and drugs- or alcohol-related), another cause of orthostatic hypotension is volume depletion, resulting for example from haemorrhage, diarrhoea, or Addison's disease. Patients with any form of hypovolaemia (low blood volume) are prone to lower cerebral perfusion for obvious reasons.

Cardiac Arrhythmia / Structural Heart Disease

The causes of cardiac-related syncope are often multifactorial, although in general, impaired cardiac output prevents the heart from matching the brain's vascular demands under certain circumstances. The individual factors resulting from the cardiac difficulties may include arrhythmia (irregular heart beat), compromised haemodynamics, and neurally mediated problems. For example, the arrhythmia rate, the status of left ventricular function, and the adequacy of vascular compensation — including the potential

impact of neural reflex effects — are all important. The most common cardiac causes of syncope [63] will not be described in further detail here.

Cerebrovascular (Steal Syndromes)

In steal syndromes, blood is diverted from its expected path to the brain. The most common type is "subclavian steal syndrome", caused when the arterial circulation to the arm is occluded in a key vessel called the subclavian artery. Blood is shunted from one path to another, and this can result in retrograde flow during arm exercise, when the demands of the arm muscles increase. The retrograde flow sucks blood away from the brain, and syncope can result.

Neurally Mediated Syncope

Proposed aetiologies for the various types of neurally mediated syncope are illustrated in Figure 2.4. The first box identifies vasovagal syncope, the most common form of neurally mediated syncope. Although "head-up tilt" syncope appears in the second box, it is generally classified as a subtype of vasovagal syncope as well. Since this subtype forms the main subject of the thesis, henceforth it will be referred to by its formal name, *orthostatic vasovagal syncope.*

As can be seen from the figure, all forms of neurally mediated syncope are reflex reactions, mediated by neurons. The trigger pathway of vasovagal syncope is still a matter of considerable debate, and forms the subject of Chapter 7. For present purposes, it will be assumed that orthostatic vasovagal syncope is evoked as follows:

1. Subject stands or is tilted upright passively.
2. Roughly a quarter of the subject's blood is redistributed in response to this orthostatic stress. Venous pooling occurs in the legs.
3. Decreased venous return is an obvious result.
4. Tachycardia, vasoconstriction, and increased inotropy (more forceful cardiac contractions) attempt to compensate — as they should. *Everything up to this point represents a more or less normal compensatory reaction to orthostatic stress.*
5. However, in vasovagal syncope patients, the forceful ventricular contractions may activate hypersensitive cardiac receptors. This triggers an afferent pathway[1] consisting of left ventricular vagal C

[1] An afferent pathway conveys neural impulses *to* a nerve centre, whereas an efferent pathway conveys them *away.*

fibres[2].

6. This phenomenon, known as the Bezold-Jarisch reflex, ultimately reduces sympathetic tone and increases parasympathetic tone. (See Appendix B for an overview of these two systems.)

7. These changes in tone result in vasodilation and bradycardia, to induce hypotension (low BP).

8. When cerebral perfusion falls sufficiently, syncope results.

Despite the popularity of this 30-year-old hypothesis, a growing number of studies have challenged it [71,73] and have offered more plausible alternatives: errors in central nervous system processing, involving chemicals such as serotonin and delta opioids; or hormonal problems, such as the effect of vasopressin on baroreceptor sensitivity. These theories are explored more fully in Chapter 7.

Vasovagal syncope is commonly subdivided into three types — cardioinhibitory, vasodepressor, and mixed — and two "exceptions", using a scheme known as the "VASIS" classification [200]. These five cases are described at the bottom of Figure 2.1.

2.4 Differential Diagnosis

The procedure to diagnose a patient with recurrent syncope results in what is known as a differential diagnosis. It is known as such since one diagnosis is selected out of several different possibilities; these were summarised in Figure 2.1. Procedures vary from physician to physician, depending on his/her opinions on what constitutes the best approach, as well as the healthcare system of the host country. Numerous flowcharts have been proposed to diagnose the various types of syncope in preparation for treatment [25, 26, 79, 196]. A recent flowchart was compiled by the Task Force on Syncope [3] and is reproduced in Figure 2.5. Some key points to accompany the flowchart are outlined in Table 2.1. The following is a discussion of the primary diagnostic methods for syncope, structured approximately on the green-shaded steps in this figure.

2.4.1 Initial Evaluation

It is widely accepted that a thorough patient history is the most important component of syncope diagnosis, identifying a potential cause of syncope in nearly half of patients. Basic laboratory tests comprise

[2]C fibres are examples of nerves which affect the autonomic nervous system (ANS), the part of the nervous system that handles our "unconscious" functions such as digestion or heart beat regulation. The ANS is divided into sympathetic and parasympathetic branches, which have a push-pull effect, e.g., the former increases our heart and respiration rates, while the latter reduces them.

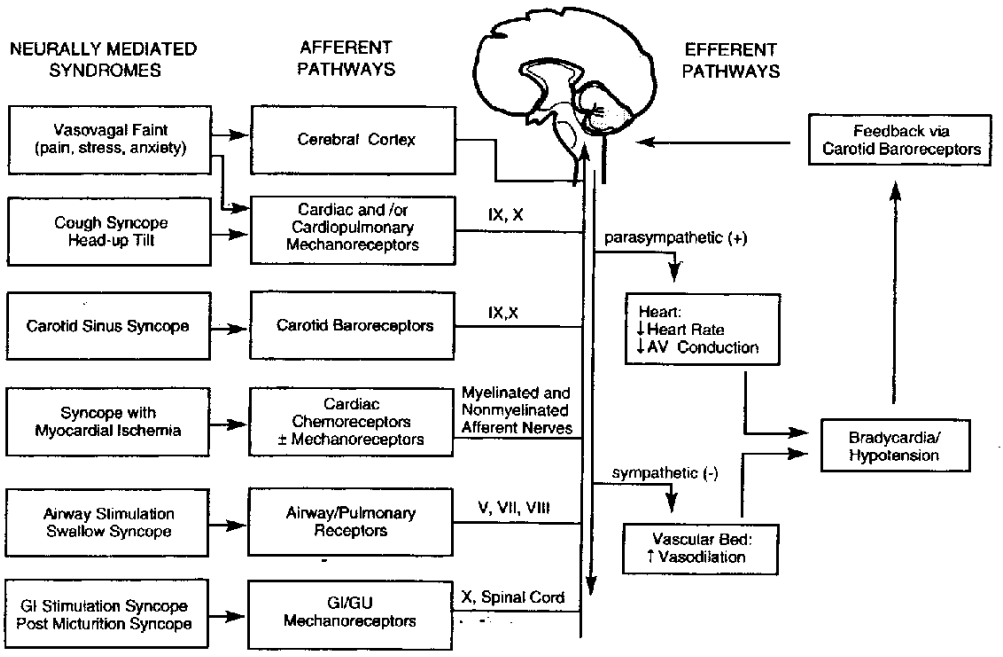

Figure 2.4: Proposed pathways of neurocardiogenic syncope, including vasovagal syncope. The specific pathways are disputed, being poorly understood: head-up tilt may use an afferent pathway not shown, and all humoral mechanisms have been overlooked in this diagram. However, the list of syndromes and explanation of efferent pathways are less controversial. In the upper central portion of the diagram, afferent nerve traffic is believed to reach the NTS (nucleus tractus solitarius) within the medulla (see Appendix B). Roman numerals refer to standard designations for the cranial nerves. A (+) sign means the effect is increased, whereas a (-) sign signifies diminished effect. GI = gastrointestinal; GU = genitourinary. [13]

If the patient has ...	**The first diagnostic step is ...**
Suspected heart disease	Echocardiography and prolonged electrocardiographic monitoring (if non-diagnostic, electrophysiological studies should follow)
Chest pain suggestive of ischaemia	Stress testing, echocardiography, and electrocardiographic monitoring
A young age, without suspicion of heart or neurological disease	Head-upright tilt table testing
Syncope during neck turning	Carotid sinus massage
Syncope during effort	Echocardiography and stress testing

Table 2.1: Conditions overriding Figure 2.5. Explanations of terms in the right-hand column can be found in Section 2.4.2. Ischaemia is low oxygen concentration in tissues, usually due to obstruction of the arterial blood supply or simply inadequate blood flow.

part of the initial evalution if syncope may be due to loss of circulating volume, or if a syncope-like disorder with a metabolic cause is suspected.

The results of the initial evaluation are diagnostic in certain situations. Orthostatic hypotension is diagnosed when BP decreases significantly upon standing or at the start of HUT after lying supine

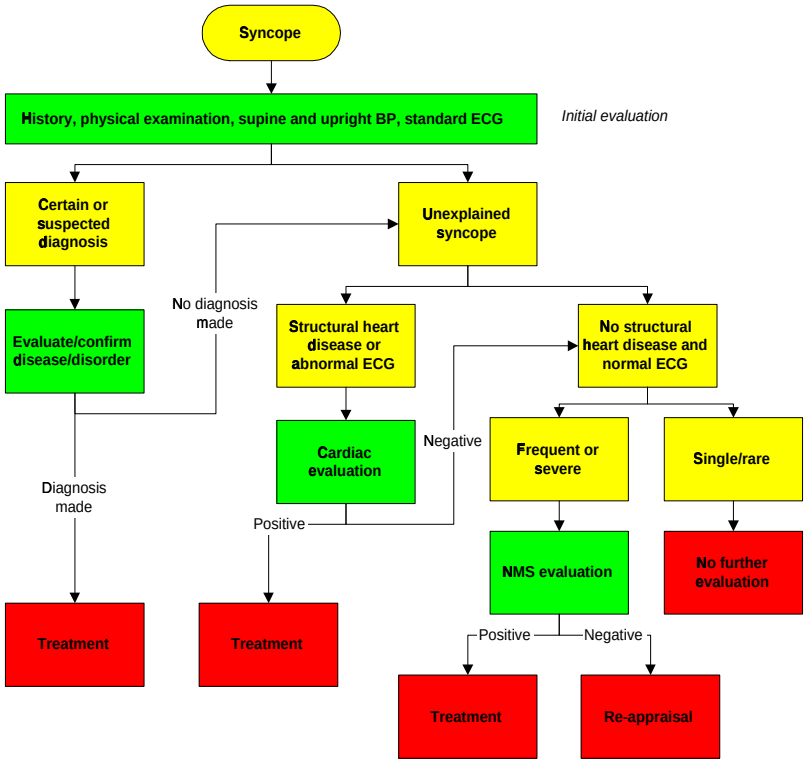

Figure 2.5: The flow diagram proposed by the Task Force on Syncope of an approach to the evaluation of syncope. BP = blood pressure; ECG = electrocardiogram; NMS = neurally mediated syncope. [3]

for five minutes. Hence it can be diagnosed either during the initial evaluation or later during HUT (see Section 2.4.3). There is disagreement on the extent and type of the decrease required to secure a diagnosis. Popular criteria include systolic BP falling more than 20 mmHg, diastolic BP falling more than 10 mmHg, and (less commonly) systolic BP falling below 80 or 90 mmHg. This will be discussed further in Chapter 4.

Vasovagal syncope is diagnosed if precipitating events such as fear, severe pain, emotional distress, connection to instrumentation, or prolonged standing are associated with typical prodromal[3] symptoms. HUT can further help to classify the type of syncope as Type I, IIA, IIB, or III [200], but in the elderly, "there is no evidence to support the use of head-up tilt studies as part of the initial[4] evaluation" [3].

Situational syncope is easily diagnosed if syncope occurs during or immediately after urination, defaecation, coughing or swallowing. Cardiac ischaemia-related syncope is diagnosed when symptoms are present with ECG evidence of acute ischaemia with or without heart attack, i.e., irreversible heart muscle injury. Arrhythmia-related syncope is diagnosed by ECG if there exists any of a number of specific

[3]Medically, a prodrome is an early symptom indicating the onset of an attack.
[4]The word *initial* is important here, for there is of course ample evidence of the usefulness of HUT.

problems, which will not be detailed here in the interests of brevity.

2.4.2 Cardiac Evaluation

The cardiac evaluation may involve "echocardiography", i.e. ultrasonic analysis of the heart. This can ascertain patient risk by determining the type and severity of heart disease; however, this test allows a final diagnosis in only a few cases — e.g. severe aortic stenosis (narrowing of the aorta, a major artery) and atrial myxoma (a tumour in the atrium).

A more common test is electrocardiographic monitoring, of one of the following two general types:

Non-invasive: Holter monitoring, external ECG event monitoring. When there is a high pre-test probability of identifying an arrhythmia, syncope patients with structural heart disease should undergo Holter monitoring (a 24-hour ECG). However, external ECG event monitoring should be used when the mechanism of syncope remains unclear after full evaluation. This monitor records (to a small memory) only cardiac events of potential interest, instead of the entire ECG.

Invasive: ECG event monitoring via an Implantable Loop Recorder. This alternative is growing rapidly in popularity. It has further been suggested that there may be value in combining the ILR with measurement of electrical activity in the brain (electroencephalography), CBF, hormonal and blood sugar changes, and, above all, the haemodynamic response [143].

When a correlation between syncope and an electrocardiographic abnormality (brady- or tachyarrhythmia) is detected, ECG monitoring can be considered diagnostic. Second, when syncope occurs during sinus rhythm (a normal heart beat), arrhythmic causes are excluded. In the absence of such correlations, additional testing is usually warranted.

A third test sometimes used during the cardiac evaluation is electrophysiological testing, which, like ECG monitoring, can be divided into two types [79]:

Non-invasive: Transoesophageal electrophysiological study. This test begins with the insertion of a thin, flexible tube into the nostril. The tube is then advanced to the back of the throat, where it can influence the electrical activity of the heart and record the resulting behaviour.

Invasive: Intracardiac electrophysiological study. This test begins by inserting a thin, flexible catheter into a vein in the leg. The catheter is pushed up to the heart, guided by x-ray fluoroscopy. Once there, its functionality is similar to that of non-invasive electrophysiological testing.

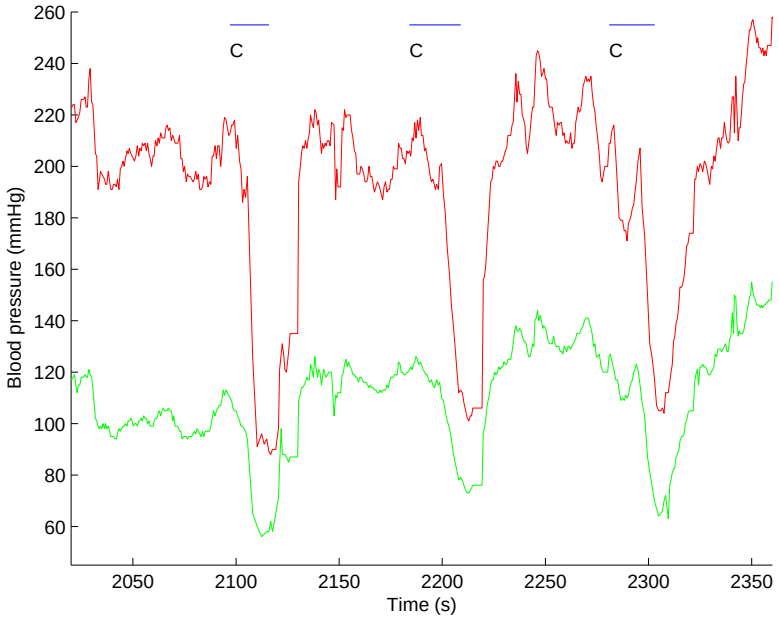

Figure 2.6: A plot of systolic (red) and diastolic (green) BP during three periods of carotid sinus massage (CSM, denoted by blue horizontal lines). Since CSM elicited immediate marked decreases in BP, this patient was diagnosed with vasodepressor carotid sinus hypersensitivity (CSH).

These electrical stimulate-and-record methods can determine the cause of a tachycardia. They are good diagnostic tests in patients with coronary artery disease, markedly depressed cardiac function, or simply unexplained syncope. Patients with bifascicular block (a particular conduction problem in the heart) often benefit from types of electrophysiological study as well.

2.4.3 NMS Evaluation

Carotid Sinus Massage

Cartotid sinus massage (CSM) is a technique to uncover problems in the baroreceptors (see Section 2.3) of a person's neck area. Before performing CSM, baseline measurements of HR and BP are first noted. Then a physician firmly massages the right carotid artery for 5–10 s where the pulse is strongest. If the BP decreases by more than 50 mmHg, the patient is likely to have vasodepressor carotid sinus hypersensitivity (CSH). If the heart stops beating for more than three seconds, the diagnosis is cardioinhibitory CSH. If both these phenomena occur, the patient has "mixed" CSH. The symptoms of vasodepressive CSH are demonstrated clearly by the BP traces shown in Figure 2.6: note the large decreases immediately following CSM.

CSM is usually comprised of either five seconds of massage in the supine position, or ten seconds of

massage supine followed by massage while upright if not successful. Predictably, the former approach yields lower positive rates: just ignoring the upright position misses the diagnosis in about a third of cases [32,150]. The Task Force on Syncope [3] favours the second method, and the protocol at the Falls Clinic (described in Chapter 4) is similar to this.

Head-Upright Tilt Table Testing

Head-upright tilt table testing (HUT) has reasonable specificity and sensitivity[5] when performed correctly. A general outline of the test is:

1. A passive, supine phase of 20–45 minutes

2. A tilt to 60–80° from horizontal, for about 45 minutes

3. The test ends earlier if syncope occurs; patient should then be immediately returned to the supine position for recovery

Two well-known protocols are the Westminster protocol [51] and, more recently, the Newcastle protocol [93]. In general, the latter appears to be in remarkable agreement with the other tilt procedures in the literature, but areas of contention do exist, including:

Fasting: It has been suggested [199] that "patients should fast for at least 3 hours before testing, or overnight in preparation for early morning studies". However, the Newcastle protocol disagrees: "Patients, in particular those over 60 years old, should be fasted for no more than two hours before the procedure in order to avoid the confounding effects of relative dehydration and hypotension." This is backed by a reference to Benditt and Grubb [15]. As [199] and [93] both come from highly respected contributors to the field (Sutton and Bloomfield on one side, *versus.* Kenny *et al.* who then reference Benditt and Grubb), the jury remains out on this point. However, interestingly, Benditt and Kenny later sat on the international Task Force on Syncope [3] which concluded that "patients should fast for at least 2 hours before the test". Since the ingestion of just 16 ounces of water five minutes before HUT has been shown to impact HUT results [112], it is likely that the choice whether to fast or not in the preceding hours also has a bearing on the test outcome.

[5] Specificity and sensitivity are true negative and true positive rates, respectively. Specificity is the probability that a screening test is negative given that the person does not have the disease, and sensitivity is the probability that a test is positive given that the person has the disease.

Drugs: Very often, experimenters administer drugs such as isoproterenol or nitroglycerin during HUT to increase the rate of positive response. Since this is not the practice at the Falls Clinic in Oxford, owing to concerns about decreasing the test's specificity and patient well-being, such drugs will not be discussed in detail here.

An alternative to HUT is the application of lower-body negative pressure (LBNP), whereby the patient's legs are surrounded by a hermetic tube which is then partially evacuated. The effect of LBNP is to draw blood into the legs from the upper body, to simulate orthostasis. This was not employed in the Falls Clinic since the use of the tilt table is the preferred test.

2.4.4 Other Diagnostic Tests

The above explanation of the differential diagnosis represents only a summary of the most common recommendations and practices. Other tests which have not been described in full include exercise testing, for exertion syncope; cardiac catheterisation and angiography, for suspected myocardial ischaemia; neurological and psychiatric evaluation, when no particular physiological cause of syncope is suspected; and the ATP (adenosine triphosphate) test, whose diagnostic value remains to be validated.

2.5 Treatment

When deciding on treatment, two important factors to consider are the frequency of syncope occurrence, and the public health risk. In other words, patients who do not suffer from frequent syncope can enjoy minimal treatment, but airline pilots and truck drivers should be carefully attended regardless.

Orthostatic Hypotension

As this is most often caused by drug-induced autonomic failure, an obvious treatment is to stop, reduce the dose of, or replace the drugs in question. Of course, for some drugs, especially vasodilators and diuretics, this is difficult. However, educating the patient regarding the various circumstances that influence systolic BP (e.g. standing, heat, exertion, large meals), and developing strategies to combat an individual's problems (e.g. encouraging small but frequent meals, discussing leg crossing and squatting) is an easy treatment. Higher salt intake, fluid intake, and the volume-expander "fludrocortisone" are often advised, while support stockings and abdominal binders can reduce vascular pooling. The newer drug "midodrine" increases peripheral resistance and reduces gravitational downward displacement of central volume.

Cardiac Arrhythmias as Primary Cause

The severity, nature, and setting of the arrhythmia must be considered. Treatment can include installing a pacemaker or implantable cardioverter-defibrillator (ICD), administering drugs such as beta blockers, or surgically excising cardiac tissue.

Structural Cardiac or Cardiopulmonary Disease

Treatment is not always possible, especially for patients suffering from primary pulmonary hypertension or restrictive cardiomyopathy (heart problems of an undiagnosed cause). However, when the problem is myocardial ischaemia, pharmacological therapy and revascularisation (returning blood flow to the area) are usually appropriate. For other problems, in general treatment should be aimed directly at improving the specific structural lesion or its consequences.

Vascular Steal Syndromes

Angioplasty or other forms of corrective surgery are ordinarily effective for subclavian steal syndrome. Angioplasty is the surgical repair of a blood vessel, either by inserting a balloon-tipped catheter to unblock it, or by reconstructing or replacing part of the vessel.

Neurally Mediated Reflex Syncopal Syndromes

An obvious treatment involves the physician explaining the risk of the syndrome, and reassurance about the prognosis. Equally obvious is avoidance of trigger events as much as possible, e.g. a causal situation such as an emotional upset in situational syncope. Stopping or reducing the dose of a hypotensive drug treatment for a concomitant condition can help. Cardiac pacing can help patients with cardioinhibitory or mixed carotid sinus syndrome, as well as those with frequent cardioinhibitory vasovagal syncope, those with severe physical injury, and the elderly. Volume expansion by salt supplements, an exercise programme or head-up tilt sleeping (sleeping at an angle in excess of 10°) can assist posture-related syncope. Finally, "tilt training" (tilting the patient daily to increase tolerance) in patients with vasovagal syncope may be useful.

2.6 Conclusion

Classification of the various types of syncope is possibly reaching maturity. This represents a significant improvement over the situation two decades ago, when classification schemes were still inchoate. The

diagnosis and treatment of recurrent syncope remains a controversial endeavour, although recent attempts to form a consensus have helped streamline such procedures to a certain extent.

Research using signal processing has the potential to uncover new causal pathways or, alternatively, to pioneer a novel treatment strategy. As explained in Section 1.4.2, patients in the Falls Clinic who underwent HUT between January 2002 and November 2004 had the following vital signs monitored: ECG, BP (using an inflatable cuff on the arm), beat-by-beat BP, oxygen saturation, and cerebral perfusion. Syncope diagnostic protocols often involve the first two or three of these (ECG and BP). Hence, out of the five types of syncope listed at the start of this chapter, the data recorded during these studies should help with the diagnosis of the first and last. (Although some cardiac arrhythmias also have the potential to be detected from the data included within the data set, this field of investigation was not pursued during the thesis, for the following reasons: first, some arrhythmias would be missed owing to the lack of some of the tests described in Section 2.4.2; second that the development of algorithms to detect the various types of arrhythmias is a non-trivial exercise.)

As stated in Chapter 1, the primary purpose of this thesis is the prediction, rather than diagnosis, of syncope. Whereas a diagnosis is achieved using as much information as possible (for example, all data recorded during prolonged HUT), predictions need to be made as early as possible during a test — for example, by analysing only the supine data and the data recorded immediately after tilt.

Orthostatic hypotension requires only five minutes to diagnose; hence, little value exists in devising a predictor to substitute for the traditional test described in Section 2.4.1. However, as explained in Section 2.4.3, the accurate diagnosis of vasovagal syndrome requires a much longer test; it is here that investigations into syncope *prediction* will be most useful. Such investigations are the subject of Chapters 5 and 6, using the Oxford Falls Clinic patient database (see Section 1.4). Since a good *prediction* is one that matches the *diagnosis*, techniques for automated diagnosis are described first. Results from these can set the benchmark for prediction algorithms, and so Chapter 4 concentrates on syncope diagnosis using the same Falls Clinic HUT database. As an introduction to these chapters, Chapter 3 examines the signal processing relevant to both syncope diagnosis and syncope prediction.

Chapter 3

Instrumentation and Signal Processing for the Investigation of Syncope

3.1 Introduction

The previous chapter described the physiological background and tests for syncope; the present chapter focuses on the instrumentation and signal processing which have been used for the diagnosis and prediction of syncope. To begin, the next section reviews previous work in chronological order. This is followed by a technical description of the instrumentation selected for data acquisition in the Oxford Falls Clinic. Finally, the largest section is reserved for a literature review of the research undertaken with these measurements, with a focus on signal processing.

3.2 Historical Background of Signal Acquisition and Processing

The following timeline outlines the history of the technological contributions which appear in this chapter.

1816: René Théophile Hyacinthe Laënnec invented the stethoscope.

1881: Samuel Siegfried von Basch invented the sphygmomanometer, allowing the first non-invasive measurement of BP. (Earlier devices were somewhat bloody.)

1896: Scipione Riva-Rocci invented a simpler, more accurate sphygmomanometer.

1901: Willem Einthoven invented the string galvanometer to create accurate electrocardiograms.

1905: Nikolai Korotkoff fully described auscultatory[1] sounds, using the stethoscope and Riva-Rocci

[1] Auscultation is the act of listening for sounds within the body.

sphygmomanometer. These sounds are still used today by virtually every physician making a blood pressure measurement.

1936: Karl Matthes invented a basic oxygen saturation meter for the ear using two wavelengths of light.

Early 1940s: Glen Millikan developed a lighter version of Matthes' device for use in aviation.

1965: Interest in heart rate variability (HRV) was stirred when E.H. Hon and S.T. Lee discovered that foetal distress and its resultant HR change are preceded by alterations in interbeat heart intervals.

1965: James Cooley and John Tukey invented the modern version of the Fast Fourier Transform (FFT). (Earlier attempts to speed up Fourier transforms in fact date as far back as Gauss.)

1972: Takuo Aoyagi invented the modern version of the pulse oximeter.

1977: Jobsis van der Vliet outlined the use of near-infrared spectroscopy (NIRS) as a tool to monitor oxygenation. Working systems were later developed in the 1980s and used to monitor cerebral blood flow.

Late 1980s: The possible role of HRV in risk stratification took a step forward: HRV was thought to be a predictor of mortality after an acute myocardial infarction. (Later this was shown to be activity-dependent.)

1992: HR and BP were chosen as the two key parameters in a classification scheme aimed at subdividing vasovagal syncope [200].

1996: A Task Force of the European Society of Cardiology standardised the common HRV techniques [115].

3.3 Instrumentation

For each data stream introduced in Section 1.4.2, the technical details of acquisition will now be described.

3.3.1 Electrocardiography

An electrocardiogram (ECG) records the changes in cardiac electrical voltage throughout each heart beat. The surface ECG is constructed by measuring the electrical potential between various points of the body; in the present work the electrodes were placed near the right shoulder, on the left side of the chest, and

near the left hip. The signals from the three leads were digitised with 12-bit accuracy at a sampling rate of 256 Hz.

3.3.2 Beat-by-beat Blood Pressure

Beat-by-beat blood pressure was measured using a Finapres device, a noninvasive continuous finger BP monitor. The word Finapres stands for FINger Arterial PRESsure, and this quantity is measured continuously using a volume-clamp method. The finger arteries are clamped at a fixed diameter — although intra-arterial pressure changes continuously — by applying an external pulsating pressure via an inflatable bladder mounted in a finger cuff and a fast-acting servo system. Finapres uses the Physiocal criteria of Wesseling [224] for the setpoint criteria determination; the diameter at which the finger arteries are clamped is determined from an infrared plethysmograph mounted in the finger cuff such that transmural pressure is zero and intra-arterial and cuff pressure are equal both in shape and in level at all times [85]. Systolic, diastolic, and mean BP are output once per heartbeat.

Arthritic fingers in the elderly can hinder the digital pressure readings of the Finapres. One study experienced difficulties in 45% of patients because of this problem [6], and at the Falls Clinic (see Section 4.2) this may have influenced the recordings of some patients.

3.3.3 Intermittent Brachial Blood Pressure

Brachial blood pressure was measured intermittently using a self-inflating oscillometric BP measurement module, connected via flexible tubing to an inflatable cuff, placed around the upper arm. The term "oscillometric" indicates measurement of the oscillations caused by the arterial pressure pulse within the arm, transmitted via cuff and tube to the central pressure sensor. The point of maximal oscillation corresponds to mean arterial BP, while diastolic and systolic BP are derived from pressure measurement at heuristically-determined amplitudes of the oscillating signal. [44].

3.3.4 Pulse Oximetry

Arterial oxygen saturation was measured using pulse oximeters on the shoulder, elbow, wrist, and finger. The reflectance (or, in the case of the finger probe, transmittance) of a dual wavelength LED signal allows variations in infrared attenuation (caused by blood pulsing in the artery) to be recorded. This attenuation waveform is digitised with 16 bits and sampled at 81.3 Hz, and the SMP also outputs one SpO_2 figure at the end of each heart beat.

Figure 3.1: Photograph of the NIRO-300. The display unit (large monitor) plots real-time traces of the parameters listed on page 28, while the measuring unit (small box at right) interfaces with the probe (shown at the other end of the cable, at lower left) on the patient's forehead.

3.3.5 Cerebral Perfusion Changes

Most syncope diagnostic procedures focus on the ECG and BP, and do not assess local cerebrovascular and metabolic autoregulation capacities. However, by definition syncope is intimately related to cerebral hypoperfusion. To maintain consciousness, the brain requires roughly 11–19 ml/min/100 g of blood flow [189]. Average flow is approximately 55 ml/min/100 g, with much of that servicing gray matter [106]. Limited information about the blood flowing to the brain can be acquired in several ways:

- Transcranial dopplerimetry
- Xenon-133 uptake
- Single-photon computed tomography (SPECT)
- Carotid angiography
- Near-infrared spectroscopy (NIRS)

The last method, noninvasive NIRS monitoring as used in the Oxford Falls Clinic, is most relevant here. The NIRO (Near-InfraRed Oxygenation) device is a non-invasive instrument for measuring changes in cerebral haemodynamics, including the concentration changes of oxy- and deoxyhaemoglobin and a metabolic indicator (explained below), by placing a sensor unit on the forehead [46]. (See Figure 3.1 for a photograph of the NIRO.) The data can be digitised at one of several sampling rates; the highest rate, 6 Hz, was usually chosen for the current research. Two independent methods are employed simultaneously:

(a) Light Attenuation in the Near-Infrared

The Beer-Lambert Law reflects the linear relationship between concentration and absorption in a clear solution:

$$A = \log_{10}\left(\frac{I_0}{I}\right) = \alpha(\lambda)\, c\, d \tag{3.1}$$

where A is the attenuation of a beam of light travelling through the solution, I_0 is the incident light intensity (immediately before the light enters the solution), I is the transmitted light intensity (immediately after the light exits the solution), $\alpha(\lambda)$ is a wavelength-dependent "extinction coefficient" of the absorbing solution (in micromolar^{-1} cm^{-1}), d is the distance the light travels through the solution (the "pathlength", in cm), and c is the concentration of the absorbing compound (analyte), in micromolar.

However, the human head is a scattering medium, not a clear solution. Hence, the Modified Beer-Lambert Law is used:

$$A = \log_{10}\left(\frac{I_0}{I}\right) = \alpha(\lambda)\, c\, d\, B + G \tag{3.2}$$

where G is an additive term to account for scattering loss, and B is a multiplier to account for the increased optical pathlength due to scattering — a photon must travel further to reach a given point when scattering occurs.

For the NIRO, a laser diode provides the incident radiation. An emitter and a detector are placed on the forehead, 5 cm apart. Using the Modified Beer-Lambert Law, the density changes of various chromophores (i.e. compounds which absorb light in the spectral region of interest) can be measured:

- O_2Hb: Oxyhaemoglobin[2]
- HHb: Deoxyhaemoglobin
- cHb: Total haemoglobin
- CtOx: Oxydised cytochrome (an indicator of metabolic activity)

Because the additive term G is unknown, only the variations in these densities, and not the absolute values, can be determined. In normal patients undergoing HUT, O_2Hb often decreases slightly before settling to

[2]See note on page 5.

a new equilibrium [122, 205]. The difference between the two time series O_2Hb and HHb, referred to as Hb_{diff}, may on tilt decrease to a smaller extent in normal controls than in patients with severe degeneration of the autonomic nervous system [205]. Furthermore, it has been shown that O_2Hb undergoes rhythmic oscillations with a frequency of about 0.1 Hz, thought to reflect the periodic contraction and relaxation of cerebral arteries known as vasomotion [47, 123]. The amplitude of these oscillations is posture-dependent [204, 206], and has been hypothesised to reflect the degree of cerebral sympathetic stimulation on tilt. Finally, this amplitude declines with age [182] and hence in the elderly Falls Clinic patients the oscillations should be detectable but small.

(b) Spatially-Resolved Spectroscopy (SRS)

If the spacing between the emitter and detector d is widened slightly, the attenuation A will increase accordingly. At $d \approx 5$ cm, most of this small increase will be due to added absorption, as opposed to extra scattering. Using photon diffusion theory [202], the rate at which absorption changes as distance increases $\left(\frac{\partial A}{\partial d}\right)$ can be used to calculate the following measures:

- $THI = k\,(O_2Hb + HHb)$: Total Haemoglobin Index
- $TOI = \frac{O_2Hb}{O_2Hb+HHb}$: Tissue Oxygenation Index

where k is a constant that arises from the photon diffusion calculations. While THI provides a measure of the quantity of blood in the area of measurement, TOI describes how oxygenated the blood is. One would expect a syncopal patient to experience a decrease in both of these parameters immediately before fainting, as the brain becomes deprived of blood (lower THI) and hence exhausts the remaining oxygen in the blood (lower TOI).

3.4 Parameters for Signal Processing

The key paper on classification of vasovagal syncope [200] made use of just two signals: systemic BP, and heart rate. Indeed these are the two most common parameters involved in syncope diagnosis, although minimal signal processing is required. Beat-to-beat assessment of these parameters is useful to keep track of transients around the time of syncope; hence the importance of devices such as the Finapres.

This section will outline relevant signal processing parameters, including BP, HR, HRV, cerebral perfusion changes, and PTT. Studies which yielded negative results or which used instrumentation not

available in the current research are not included in this review (e.g. [5,12,28,61,62,136,181,188,190]).

3.4.1 Heart Rate

A graph which quantifies the fluctuations in heart rate (HR) over short time periods is called a tachogram (from the Greek word *tachos* for speed). The rate of contraction of the heart is sampled once per beat (and hence unevenly in time), being taken as the inverse of the interval which occurs between consecutive QRS complexes (known as an "RR interval", as explained in Section 1.4.2). The tachogram is the resulting plot of RR interval versus time. Since the Fourier transform algorithm requires even sampling, the tachogram is often resampled using interpolation.

3.4.2 Heart Rate Analysis for Syncope Prediction

Heart rate (HR) during supine rest probably offers no predictive insight with respect to HUT-induced syncope; when a significant difference in baseline HR is observed between fainters and controls [8, 50, 140, 142, 155, 165], it is probably due to chance or poor patient selection. The kurtosis and variance of resting HR have been used in combination with other parameters to predict syncope, with only moderate success [137].

Upon tilt, an increase in HR in normal and syncopal subject groups is a universal finding in the literature [9, 36, 53, 88, 101, 114, 136, 168, 207, 208, 229], as it represents an important part of the normal autonomic response to assuming the upright position; however, several studies have demonstrated that the degree of HR increase is greater in tilt-positive patients. Sumiyoshi *et al.* [198] reached this conclusion examining the absolute beats-per-minute increase, during the first five minutes after tilt. Mallat *et al.* [116] observed that the mean HR in vasovagal syncope patients in the first six minutes of tilt reflected a higher than normal percentage increase over baseline. Marangoni *et al.* [119] found that the increase in HR from baseline during all stages of the test after 3 minutes of tilt was higher in tilt-positive than in tilt-negative patients.

The same research group found that the HR itself (as opposed to the change) was higher from the start to the end of the upright portion of HUT. Similar results have been found by other groups, who often examined just the early response to tilt. For example, Furlan *et al.* [56] reported that vasovagal syncope patients experience higher heart rates during the second minute of tilt compared to healthy controls. Marangoni *et al.* [119] observed a similar HR difference but during all stages of the tilted

portion of the test. In contrast to these examples, Kochiadakis *et al.* [99] found that patients previously diagnosed with vasovagal syncope experience lower HR during the 4 minutes after tilt than controls; however, the predictive analysis was confounded by the fact that 40% of these patients were tilt-negative for their test. As a second counter-example, Novak *et al.* [140] showed that during the same period, HR is lower among tilt-positive vasodepressive syncope patients than either controls or tilt-negative syncopal patients; however, this finding was probably influenced by the fact that the HUT-positive patients under study happened to have significantly lower supine HR than the controls.

Attempts to examine the HR response within subsets of the syncopal population have led to interesting results. The vasodepressive syncope patients under study by Novak *et al.* [140] were subdivided into two groups: those who fainted during the first 25 minutes, and those who fainted after an isoproterenol infusion after 25 minutes. The study found that early fainters have lower heart rates during the first four minutes after tilt, as well as during the supine baseline recording, as compared to the late fainters or to controls. Sumiyoshi *et al.* [198] divided their vasovagal syncope patients similarly, using 15 minutes as the cutoff rather than 25. They then calculated the HR increase upon tilt by subtracting baseline HR from the highest HR observed in the first 5 minutes after tilt. In this manner, early fainters (< 15 minutes) were found to have higher HR increases than patients who maintained consciousness throughout the test. These findings do not reinforce one another but they do support the hypothesis that the fainting population is heterogeneous.

Finally, the variance and kurtosis of HR have been considered for their predictive value [137]. Kurtosis, which reflects the convexity of a histogram, is calculated as

$$b_1 = \frac{\sum_{i=1}^{n} (X_i - \overline{X})^4}{n\sigma^4}, \tag{3.3}$$

where n represents the number of HR data points X_i, with standard deviation σ.

The several relevant HR analyses found in the literature are summarised in Table 3.1.

3.4.3 Heart Rate Variability

Heart rate variability (HRV) is a measure of the beat-to-beat fluctuations in HR. A normal resting heart undergoes periodic variations in its RR interval, and the frequency spectrum of a tachogram often reveals

Test	Parameter of Interest	Periods Measured	Positive Test Criterion	Patient Group	First Author
T1	HR	Second minute after tilt	Mean value is higher than some threshold	22 H+ (16±1) 22 H– (20±1)	Furlan [56]
T2–T6	HR	Last 30 s of baseline; five 30-s periods starting 3 min after tilt & ending 20 min later	Change from baseline in bpm is greater than some threshold (approximately +13 bpm, depending on which of the five periods is analysed: 3, 5, 10, 15, 20)	42 S+ (51 ±20) 95 S– (52±19)	Marangoni [119]
T7	HR	Last 10 min of baseline; first 6 min of tilt	The highest rate sustained for > 30 s is more than 18 bpm above the baseline mean	Study 1: 70 S+, 28 S– (50±17) Study 2: 28 S+, 71 S– (49±19)	Mallat [116]
T8	HR	Last 8 min of baseline	Mean value is below some threshold	23 S+ (17–62) 10 H– (18–40)	Novak [140]
T9	HR	First 4 min of tilt	Mean value is below some threshold	23 S+ (17–62) 10 H– (18–40)	Novak [140]
T10	HR kurtosis	10 min baseline	Value is above some threshold	21 S+ (29±18), 20 H– (29±8)	Naschitz [137]
T11	HR variance	10 min baseline	Value is above some threshold	21 S+ (29±18), 20 H– (29±8)	Naschitz [137]

Table 3.1: Syncope prediction tests, based on heart rate analysis in the literature. Predictive algorithms introduced in this chapter are identified as T1, T2, and so on, for later reference. min = minute, bpm = Beats Per Minute, HR = Heart Rate, S = Patients with recurrent syncope, H = otherwise healthy patients, + = HUT-positive, - = HUT-negative.

two or three peaks, at known frequencies[3]:

0.15–0.4 Hz (HF): This variation in RR interval occurs in phase with respiration, and is known as respiratory sinus arrhythmia (RSA). RSA reflects a cardio-deceleration during expiration (due to vagal efferent traffic to the sinus node), and a cardio-acceleration during inspiration (due to the sudden absence or attenuation of such parasympathetic activity).

0.04–0.15 Hz (LF): Although a peak in this range is very common, the cause of these "Mayer waves" (also known as the "ten-second rhythm") is less clear. They are thought to be due to a delay in baroreflex feedback mechanisms [42] (see Section 2.3), but other possibilities exist, most notably an oscillator in the brainstem mandated to modulate peripheral resistance. Within the LF range, a peak near 0.1 Hz is common.

[3]HF, LF, and VLF are abbreviations for high-, low-, and very low frequency, respectively.

Less than 0.04 Hz (VLF): Besides the two common peaks, there often exists a strong spectral component below 0.04 Hz as well. The physiological origin is uncertain; for example, one possible contributor is the influence of circadian (roughly 24-hour) rhythms. Understandably, some HRV measurement techniques ignore this spectral contribution altogether.

In addition, spectral density at different frequencies may be regulated not only by central and peripheral neural input, but also by complicating factors such as the ratio of beta-adrenergic to muscarinic receptor densities in the heart [23, 35, 118].

There are various quantifications of HRV, using the time domain, frequency domain, or both [39]. In 1996 the Task Force of the European Society of Cardiology aimed to standardise HRV measurement [115], and its compilation of existing techniques is often referenced in studies. Popular examples include:

- SDANN, the standard deviation of the averages of NN intervals (i.e. "normal-to-normal" intervals, which are the RR intervals resulting from sinus node depolarisation[4] in all 5-minute segments of a recording)
- pNN50, the number of pairs of adjacent NN intervals differing by more than 50 ms in the recording, divided by the total number of NN intervals
- RMSSD, the square root of the mean of the squares of differences between adjacent NN intervals
- LF/HF ratio, the power in the low frequency range (0.04–0.15 Hz) divided by that in the high frequency range (0.15–0.4 Hz); typically within a five-minute segment

Heart Rate Variability and Head-Upright Tilt Table Testing

Many research groups have examined HRV behaviour during head-upright tilt table testing (HUT). It has been shown that under these circumstances, an autoregressive method for estimating the spectral content of the HR time series can be as effective as an FFT method [7]. Some problems may exist with the reproducibility of time-domain HRV metrics in syncopal patients [97], but the HRV Task Force recommended that both time- and frequency-domain methods be used regardless of the problem being studied [115].

Numerous studies have investigated the putative link between HRV and the sympathovagal balance. Parasympathetic blockade (for example with drugs) abolishes the HF component and diminishes the LF component. Subsequent beta-sympathetic blockade removes the residual LF component, leading

[4]This depolarisation is exhibited in Figure 1.2. Beats that do not originate from the sinus node are known as "ectopics".

to an extremely steady heartbeat [4]. Therefore, fluctuations above 0.15 Hz are mediated purely by the parasympathetic system, whereas lower frequency oscillations are jointly governed sympathetically and parasympathetically. Such findings are consistent with the delays associated with the autonomic nervous system: parasympathetic responses occur usually within a single heartbeat, whereas sympathetic responses require up to 20 seconds; hence the sympathetic system acts as a low-pass filter. Such filtering occurs at the sino-atrial node [19]. It should be pointed out that the clinical interpretation of the LF and HF components is still highly controversial [45].

For this reason, HRV is probably a less straightforward measure of autonomic system activity than plasma catecholamine concentration or sympathetic activity as measured by microneurography[5]. However, there exists a consensus that, in healthy individuals, HRV increases upon orthostatic stress (e.g. HUT), whereas autonomic neuropathy (e.g., problems resulting from ageing or diabetes) curbs this HRV increase and in fact can lead to a decrease in HRV during HUT [36, 101, 207]. This is an important finding since autonomic neuropathy can contribute to orthostatic hypotension and vasovagal syncope. (For example, in Figure 2.1, manifesting as "Autonomic failure" or "Type 3: Vasodepressor" syncope.)

Spectral Heart Rate Variability in Syncope Research

Autonomic neuropathy is merely one of the many possible causes of syncope [3], and this multifactorial nature may be responsible for some of the apparent contradictions [190] amongst HRV analysis findings. Upon tilting syncopal patients, HRV tends to rise in the young but to decrease in the elderly[6] [111,132,144, 164]; hence HRV changes cannot be correlated easily with syncope test positivity, despite studies which argue the opposite [101]. However, consideration of the age of the patient may assist prognosis: Lipsitz *et al.* [111] found that amongst young people, HUT-positive patients (fainters) experience a greater increase in HRV than HUT-negative patients; further, Ruiz *et al.* [175] found that age is the major determinant of autonomic behaviour during HUT. In summary there is a need for interpreting HRV data in the context of the patient's age and medical history, which together will narrow down the suspected causes of syncope.

[5] Microneurography involves inserting a microelectrode to study conduction in individual nerve fibres or bundles of fibres.
[6] The definitions of young and elderly vary from paper to paper, but generally the minimum age to qualify as elderly ranges from about 60 [175] to 70 [111].

3.4.4 Heart Rate Variability for Syncope Prediction

Results in the literature for HRV techniques have been conflicting, and so far no indicator has been widely accepted for predicting syncope. Two examples of the past use of HRV in syncope prediction are as follows:

LF: The LF spectral band was defined as 0.04–0.15 Hz; the last five minutes of baseline recording were compared with the first five minutes after tilt. A change below a certain signed percentage was deemed predictive of syncope [101].

LF/HF: The ranges of 0.06–0.15 Hz and 0.15–0.40 Hz were defined as LF and HF ranges respectively (see Section 3.4.3); the first four minutes after tilt were observed. An LF/HF ratio below a certain threshold was deemed predictive of syncope [98].

Numerous other tests of equal interest are described in Tables 3.2 and 3.3; using the aforementioned two tests as examples (T14 and T20), the others are similarly listed. Some tests were excluded owing to their similarity to others [59, 163].

A possible shortcoming of many tests listed in this table, and the tables which follow in this chapter, is that the heterogeneity of vasovagal syncope is not always recognised: syncopal patients are usually represented as a single cohort, to be compared with normals. Guzmán *et al.* [71] examined vasovagal syncope patients and found that those with cardioinhibitory and "mixed"[7] syncope experience a rise in HRV during prolonged HUT, whereas vasodepressive patients experience a decrease. Gielerak *et al.* [59] found similar results, but only for the late stages of HUT; in fact, immediately after tilt vasodepressive patients had experienced a large rise in LF/HF. These papers may be used to support the hypothesis that cardioinhibitory syncope is due to the Bezold-Jarisch reflex (involving hypersensitive cardiac mechanoreceptors; see Section 2.3) whereas a peripheral component could be suspected in vasodepressive syncope.

Elderly Patients

Unfortunately, analysis of elderly patients is often less fruitful than that of young patients [175], due in part to comorbidity (simultaneity of diseases) and in part to autonomic degeneration. The elderly suffer from comorbidity more than any other age group, so a given syncope patient is likely to have

[7] Recall that "cardioinhibitory" and "mixed" are terms used in the classification scheme [200] depicted in Figure 2.1.

been diagnosed previously with other disorders which might affect his or her cardiovascular system. Few elderly patients suffer from vasovagal syncope and no other disorder; one third of people over the age of 65 take three or more prescribed medications [3]. As to the issue of autonomic degeneration, it is known that ageing decreases autonomic activity [3]. Hence, traditional autonomic indicators such as the LF/HF ratio are less effective in predicting syncope results in the elderly. Ruiz *et al.* described how detrimental the effects of ageing can be on traditional HRV analysis [175], since ageing lowers the spectral energies under study.

3.4.5 Blood Pressure and Related Parameters

With few exceptions [101], most studies find that upon tilt (see Section 1.4), systolic and diastolic BP decrease slightly in healthy subjects, yet recover within one or two minutes, heading for equilibria not far from their supine values [9, 40, 53, 78, 87, 106, 119, 126, 127, 207, 229].

Some authors have looked at the product of SBP (systolic blood pressure) and HR, known as the "rate-pressure product" (RPP). This measure of myocardial work has been found to be lower at the end of positive tilt tests than at the end of negative tests — an RPP below 7000 mmHg/min is a reasonable sign that the subject has fainted [185, 186].

A second parameter of interest is baroreflex sensitivity. Introduced in Section 2.3, the baroreflex has been implicated in vasovagal syncope and orthostatic hypotension [11, 87, 131, 134, 156, 212]. The primary methods to calculate baroreflex sensitivity (BRS) are as follows [148]:

Sequence technique: Measuring the regression slope for sequences of beats where spontaneous SBP changes are coupled with similar RR-interval changes [8]

Cross-correlation: Between the RR interval and SBP time series

Modulus: Of the RR-SBP transfer function, centred at 0.1 Hz

Autoregressive moving average (ARMA) model: Of the closed-loop RR-SBP transfer function

Statistical dependence: Of the RR interval on SBP fluctuations

Spectral technique (a.k.a. "α coefficient"): If P_{RR} and P_{SBP} are the spectral powers of RR intervals and SBP, respectively, for a given frequency range (for example, the LF or the HF range) and

[8] This technique also permits the calculation of the Baroreflex Effectiveness Index (BEI), defined as the number of baroreflex sequences divided by the total number of beat series in which SBP progressively increased or decreased irrespective of RR-SBP coupling.

a given signal duration (usually 128 to 1024 beats), then:

$$BRS = \alpha = \sqrt{\frac{P_{RR}}{P_{SBP}}}. \tag{3.4}$$

Blood Pressure Variability

Just as HR varies periodically with time, particular peaks can be found in the spectrograms of BP as well. However, the physiology responsible for these oscillations is only partly related to HRV. For example, the HF component of systolic BP variability (BPV) is not likely to be autonomically related as it rises (rather than falls) with orthostatic stress [53]; it is more probably related simply to respiratory mechanical effects on haemodynamics [192]. Indeed, spectral analysis of systolic BP waves using an autoregressive algorithm [155], the discrete Fourier Transform [94, 140], or a more advanced, multiresolution wavelet analysis [120,121], appears unable to dissimilate tilt-positive vasovagal syncope patients from tilt-negative patients or controls, during supine rest or the early stages of tilt. Hence BPV seems to be less useful than HRV for syncope prediction research.

3.4.6 Blood Pressure for Syncope Prediction

As with HR, occasional findings of differences in averaged supine BP between syncopal patients and controls [94,140,142,163,187] are not relevant to the present work.

Very few authors note significant differences in BP between positive- and negative-testing patients during the first few minutes after tilt. At least three exceptions exist. Marangoni *et al.* [119] found that tilt-positive patients had lower mean BP (MBP) values immediately after tilt and throughout the remainder of the test than tilt-negative patients. Second, averaging the first four minutes after tilt, Kochiadakis *et al.* [99] observed lower systolic BP values in tilt-positive vasovagal syncope compared to controls. Third, some groups [50] have found that the maximum MBP attained during the course of tilt is higher in tilt-negative patients.

In a prospective BP study following encouraging retrospective analysis, Pitzalis *et al.* [165] demonstrated that if more than 14 "blood pressure reductions" occurred in the first 15 minutes of tilt, the patient was likely to faint (80% sensitivity, 85% specificity). (A "blood pressure reduction" was considered to occur when any heart beat's corresponding systolic BP fell below that of the lowest reading obtained during a supine baseline recording.) This result indicates that the change in BP from supine to

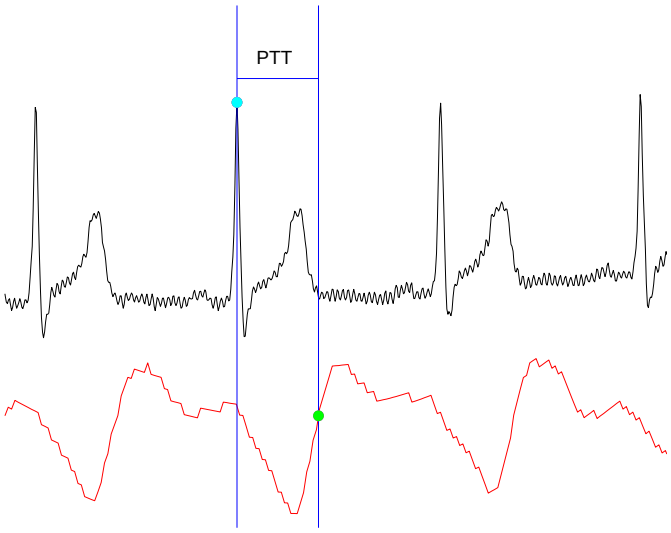

Figure 3.2: A typical PTT measurement involves the ECG (upper, black trace) and PPG (photoplethsymogram, the lower, red trace). In this thesis it is defined as the interval between the QRS complex (cyan dot) and the subsequent point of maximum slope in the PPG (green dot). Alternatively, two PPG traces taken from different sites on the body can be compared. An explanation of how these traces are measured is provided in Section 3.3.4.

upright may be as important as the actual post-tilt BP itself.

Finally, many authors have found that syncopal patients often have lower than normal baroreflex sensitivities [11, 87, 131, 134, 212]. A low BRS is thought to interfere with a subject's ability to withstand gravitational stress. (Two recent studies claim the opposite to be true [155, 156], but the significance of their results is mitigated by partial correlations among tilt test positivity, age, and resting HR.)

Following this review of BP and BRS with regards to syncope prediction, three promising noninvasive tests are summarised in Table 3.4.

3.4.7 Pulse Transit Time

Pulse transit time (PTT) is the time taken for the pulse waveform to traverse a given path in the arterial system. It reflects solely the speed of pulse conduction, known as pulse waveform velocity (PWV). As an example, one of the many possible definitions of PTT is the time elapsing between the ECG QRS complex (the onset of ventricular contraction) and the point of maximum slope in a photoplethysmogram (PPG, from a pulse oximeter) at the finger-tip. This concept is demonstrated in Figure 3.2.

As the PWV is dependent on blood pressure, there exists a link between PTT and BP. This relationship

is often masked by other effects, but if those could be corrected for, PTT could be used as a potentially more reliable alternative to continuous blood pressure readings. For nearly a century, many investigations have attempted to quantify the BP-PTT relationship, although without unqualified success [55, 58, 214]. Notwithstanding this, PTT could be an interesting parameter in the study of syncope, but it has only been explored to a very limited extent [137].

Syncope Prediction

In the one study on the topic of PTT and syncope prediction, it was found that a high PTT standard deviation, before or immediately after tilt, might be associated with vasovagal syncope [137]. The same group found that the ratio of post- to pre-tilt PTT was higher among the syncopal subjects. These tests are summarised in Table 3.5. Given the difficulties in interpreting the significance of PTT, the metric has not yet played an important role in syncope prediction research.

3.4.8 Cerebral Perfusion Changes

NIRS has the potential to offer insight into the role of cerebral autoregulation in syncope, identified in Section 2.2.2. One group found that after healthy elderly patients stand up, cortical oxyhaemoglobin decreases while deoxyhaemoglobin increases [126, 127]. Since this did not occur in young controls, it may demonstrate that the regulation of cerebral oxygenation changes with age. Another study found that middle-aged or elderly patients with sympathetic failure experience a very large (11.6 μmol L^{-1}) decrease in O_2Hb upon standing [78]. However, the observed O_2Hb fall may have been due to an inordinate decrease in BP, as opposed to an abnormality of cerebral autoregulation: BP fell on average by 72 mmHg during the same interval. O_2Hb undergoes its clearest changes in the final minutes prior to syncope; for example, Szufladowicz *et al.*reported a consistent decrease on average 3.3 minutes prior to syncope (standard deviation: 2.8 minutes) [203].

Syncope Prediction

In hypovolaemic young or middle-aged normal subjects, a steady decrease in O_2Hb in the upright position might indicate a propensity to faint [40]. However, the cost of the instrumentation means that NIRO parameters have not yet been studied thoroughly by many other researchers interested in syncope prediction.

3.5 Conclusion

A thorough literature search reveals that parameters which yield useful discriminatory information in the study of syncope are HR, HRV, BP, BRS, PTT, and O_2Hb. Most techniques are currently restricted to academic interest; besides the simple methods described in Figure 2.1, no technique has risen to a level of universal acceptance by physicians. The next chapter will describe the use of these parameters in automating the diagnosis of syncope in the Oxford Falls Clinic patients.

Test	Parameter of Interest	Period(s) Measured	Positive Test Criterion	Patient Group	First Author
T12	VLF (0.01–0.05 Hz)	Last 8 min of baseline	Value is above some threshold	23 S+ (17–62) 10 H– (18–40)	Novak [140]
T13	VLF (0.01–0.05 Hz)	First 4 min of tilt	Value is above some threshold	23 S+ (17–62) 10 H– (18–40)	Novak [140]
T14	LF (0.04–0.15 Hz)	Last 5 min of baseline, first 5 min after tilt	Percent change is smaller than some threshold	42 S+, 27 S– (16–75, 42±18)	Kouakam [101]
T15	LF (0.06–0.15 Hz)	First 4 min after tilt	Value is below some threshold	44 S+ (52±14) 20 H– (48±12)	Kochiadakis [98]
T16	LFnu, i.e. LF/(LF+HF)	Second 5 min after tilt	Value is higher than some threshold	40 S+, 62 S– (15–85, 44±21)	Ruiz [175]
T17	LF/HF ratio, where LF = 0.06–0.15 Hz and HF = 0.15–0.40	Last 4 min of baseline, first 4 min after tilt	Change is negative, not positive	44 S+ (52±14) 20 H– (48±12)	Kochiadakis [98]
T18	LF/HF ratio, where LF = 0.04–0.15 Hz and HF = 0.15–0.4 Hz	Second 5 min after tilt	Value is above some threshold	40 S+, 62 S- (15-85, 44±21)	Ruiz [175]
T19	LF/HF ratio, where LF = 0.04-0.15 Hz and HF = 0.15-0.5 Hz	First 5 min after tilt	Value is below some threshold	15 S+ (32±14) 15 S– (33±13) 14 H-, 1 H+ (34±12)	Morillo [132]
T20	LF/HF ratio, where LF = 0.06-0.15 Hz and HF = 0.15-0.40	First 4 min after tilt	Value is below some threshold	44 S+ (52±14) 20 H– (48±12)	Kochiadakis [98]
T21	LF/HF ratio, where LF = 0.04-0.15 Hz and HF = 0.15-0.4 Hz	Last 5 min of baseline, first 5 min of tilt	Change is downwards, not upwards	42 S+, 27 S– (16-75, 42±18)	Mangin [117], Kouakam [101] (similar test)

Table 3.2: Syncope prediction tests, from frequency-domain heart rate variability analysis in the literature. LF = Low Frequency, LFnu = Low Frequency in Normalised Units, VLF = Very Low Frequency, HF = High Frequency. See Table 3.1 for a guide to the other abbreviations.

Test	Parameter of Interest	Periods Measured	Positive Test Criterion	Patient Group	First Author
T22	PNN50	First 5 min after tilt	Value is above some threshold	15 S+ (32±14) 15 S– (33±13) 14 H-, 1 H+ (34±12)	Morillo [132]
T23	RMSSD	Final 5 min of baseline, first 5 min after tilt	Change is positive	17 S+, 11 S– (52±20)	Lippmann [110]

Table 3.3: Syncope prediction tests, from time-domain heart rate variability analysis in the literature. RMSSD = Root Mean Square of Successive Differences, PNN50 = Percentage of adjacent differences in Normal-to-Normals that are greater than 50 ms. See Table 3.1 for a guide to the other abbreviations.

Test	Parameter of Interest	Periods Measured	Positive Test Criterion	Patient Group	First Author
T24	SBP	Ten minutes of baseline, first 15 minutes after tilt	More than 14 post-tilt readings are lower than the mean baseline value	165 S–, 73 S+ (34±15)	Pitzalis [165]
T25	BRS	Last 300 beats of baseline	Mean value is lower than some threshold	9S+, 1S–, 8H– (20-42, 30±6)	Béchir [11]
T26	BRS	First 300 beats after tilt	Mean value is lower than some threshold	9S+, 1S–, 8H– (20-42, 30±6)	Béchir [11]

Table 3.4: Syncope prediction tests, based on the analysis of systolic blood pressure (SBP) and spontaneous spectral baroreflex sensitivity (BRS) via the spectral technique. See Table 3.1 for a guide to the other abbreviations.

Test	Parameter of Interest	Periods Measured	Positive Test Criterion	Patient Group	First Author
T27	PTT	10 min baseline, first 600 beats after tilt	Percent change is above some threshold	21 S+ (29±18), 20 H– (29±8)	Naschitz [137]
T28	σ_{PTT}	10 min baseline	Value is above some threshold	21 S+ (29±18), 20 H– (29±8)	Naschitz [137]
T29	σ_{PTT}	First 600 beats after tilt	Value is above some threshold	21 S+ (29±18), 20 H– (29±8)	Naschitz [137]

Table 3.5: Syncope prediction tests, based on the analysis of pulse transit time in the literature. PTT = pulse transit time, σ = standard deviation. See Table 3.1 for a guide to the other abbreviations

Chapter 4

Signal Analysis for the Diagnosis of Syncope

4.1 Introduction

Head-upright tilt table testing (HUT) of patients at the Radcliffe Infirmary Falls Clinic was introduced in Section 1.4. The objective of this chapter is to summarise how the data were collected, introduce the impact that tilting had on each of the data streams, describe how patients were selected or excluded for analysis, and most importantly, present the results of the signal analysis for the diagnosis of two types of syncope described in Figure 2.1: neurally-mediated syncope (including the sub-types of orthostatic vasovagal syncope and carotid sinus hypersensitivity), and orthostatic hypotension.

4.2 Patient Protocol at the Falls Clinic

The Falls Clinic HUT protocol will first be described in full and then compared to the established protocols described in Chapter 2. The procedure ran as follows:

1. The patient was asked to lie down whilst a physician applied the recording probes listed in Section 1.4.2.
2. Once the setup was complete, at least ten minutes of quiet baseline data were recorded.
3. The patient was tilted gently to simulate standing. The mean angle of tilt was 70°, and the standard deviation 5°. (The angle varied because frail patients preferred lower inclinations.)

4. The upright patient's data were observed over the next few minutes for signs of orthostatic hypotension (recall that this is a rapid decrease in systolic BP).

5. After this initial period, monitoring continued for signs of vasovagal syndrome (e.g. sweating or tachycardia, after many minutes). Occasionally the physician spoke to the patient.

6. If the patient announced a need to be returned to the supine position, the test was concluded. However, if no symptoms developed after 30–45 minutes, carotid sinus massage (CSM) was performed to test for carotid sinus hypersensitivity (CSH).

7. CSM could elicit large transient decreases in BP or HR, sometimes leading to syncope. Regardless, following CSM, the patient was returned to the supine position.

8. For most patients, a second tilt was then executed. This tilt lasted no more than a few minutes, and a standard mercury sphygmomanometer was used in place of the oscillometric cuff. The purpose was to compare BP in the lying and standing positions as accurately as possible.

Owing to the variation in the angle of tilt from patient to patient, it was necessary to confirm, via a statistical test, that the angle did not demonstrably affect the likelihood of fainting. (In at least one other data set, the angle did have some effect [186].) Confirmation for the current database was achieved with a Mann Whitney U value of 216 out of 384, lower than the critical value of 267. Angle was therefore considered not to influence tilt test positivity.

The Falls Clinic protocol may be contrasted with the recently published Newcastle protocol for CSM [93] in three different respects:

Angle of tilt: The Newcastle protocol recommends that "the patient should lie supine for a minimum of 5 minutes" and remain supine during CSM, whereas at the Falls Clinic, CSM was initiated while upright (70°), after being upright for at least 30 minutes. The protocol recommends performing CSM at a tilted position only after CSM in the supine position fails, but recognises that 30% of subjects will experience a positive response in the latter and not the former.

Length of time: The Newcastle protocol recommends 5 seconds of massage, acknowledging that "some authors recommend continuing CSM for 10 seconds if there is no asystole after 5 seconds, but this is not our practice". At the Falls Clinic, each CSM lasted an average of 12 seconds (standard deviation: 4 s).

Post-procedure rest period: The Newcastle protocol recommends 10 minutes of supine rest following the procedure, which in their experience "reduced neurological complication rates". At the Falls Clinic, a rest was granted following CSM, but it usually lasted much less than 10 minutes.

Importantly, none of these differences affected the results reported in the thesis.

4.3 The Database

The data were collected over a period of 33 months with the intention of testing approximately 100 patients. The importance of statistical power calculations for determining data set size becomes more relevant in the design of prospective trials as follow-up work (see Section 6.6).

The epidemiology of the Falls Clinic patients is described in Figure 4.1 and Table 4.1. "Syncope" was said to occur when the doctor felt that the patient had lost consciousness, or would have lost consciousness within seconds of continuing the test, if the latter had not been terminated. "Presyncope" was said to occur when a patient felt symptoms of nausea, lightheadedness, cold sweating, and/or pallor, making continuation of the test difficult.

"Orthostatic hypotension" was diagnosed if systolic BP fell by more than 20 mmHg within approximately three minutes after head-up tilt. This was measured using a mercury sphygmomanometer, usually as a part of Step 8 in Section 4.2. As discussed in Section 2.4.1, the diagnosis of orthostatic hypotension is a non-trivial task. The determination of whether or not systolic BP fell by more than 20 mmHg was necessary to ensure consistency.

"Carotid sinus hypersensitivity" was diagnosed when systolic BP fell by more than 50 mmHg within approximately 30 seconds of CSM, concurrently with a feeling of lightheadedness. It was also diagnosed if an asystole lasting 3 seconds or more occurred immediately following CSM. These two types of CSH are known as vasodepressive (VCSH) and cardioinhibitory (CCSH), respectively.

Finally, "vasovagal syndrome" was diagnosed when the patient's BP fell during prolonged HUT to such an extent that syncope occurred or was thought to be imminent. It was also diagnosed in cases where BP fell steadily and the patient requested that the test be terminated. The decrease in systolic BP was between 60 and 120 mmHg, and the decrease in diastolic BP was between 30 and 100 mmHg.

A label of "Perhaps" was selected rather than "Yes" or "No" when any of the three following sources of information conflicted: the annotated log of events compiled during HUT, the HR and BP data acquired

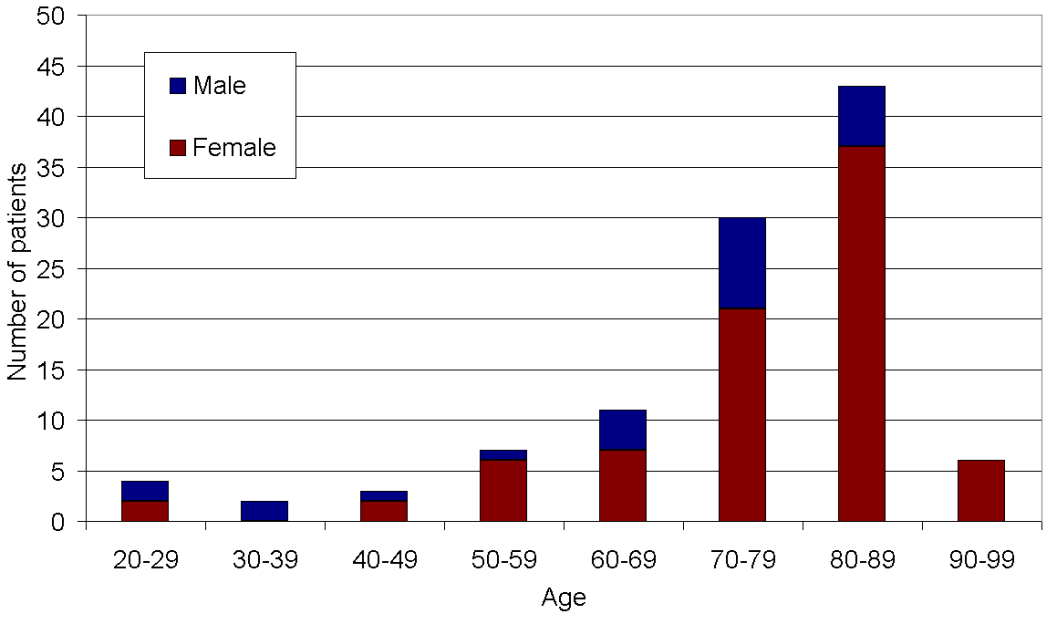

Figure 4.1: Age distribution for Falls Clinic patients. Seventy-five per cent of the patients were 70 or older, and 76% were female.

	Syncope	**Presyncope**	**Orthostatic Hypotension**	**Carotid Sinus Hypersensitivity**	**Vasovagal Syndrome**
Yes	17	47	60	24	26
Perhaps	1	8	1	10	9
No	88	44	41	47	49
N/A	0	7	4	25	16
Total	106	106	106	106	106

Table 4.1: Falls Clinic patient epidemiology. N/A = Not applicable; i.e., either a test was not performed, or data did not exist for the test.

during HUT, and the clinical summary of the HUT written at a later date in the form of a letter to the patient's primary care physician. Positive tests for vasovagal syndrome were more reliable than negative tests, since in a number of cases the tilt test was halted prior to the recommended 40 minutes.

4.4 Preliminary Analysis

The database of signals demonstrates the different ways in which they vary in response to the cardiovascular challenge of HUT. The purpose of this section is to introduce as simply as possible the trends seen in the data streams.

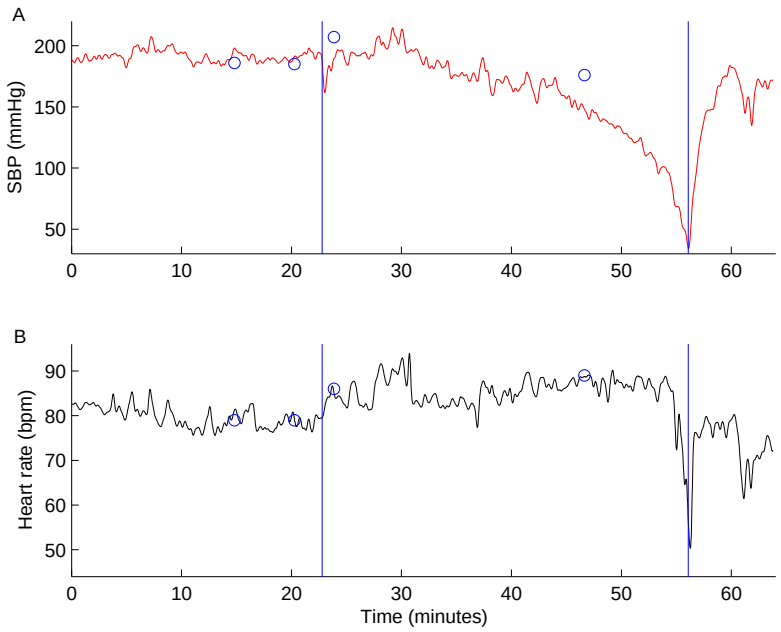

Figure 4.2: A plot of systolic blood pressure (**A**) and heart rate (**B**) for a patient suffering from both vasovagal syndrome and orthostatic hypotension, undergoing head-upright tilt table testing. The left vertical line indicates the time of tilt, while the right vertical line demarcates the return to the supine position. Blue circles represent BP and HR measurements from the oscillometric cuff.

4.4.1 Heart Rate and Blood Pressure

An example of HR and systolic BP for one patient is presented in Figure 4.2. After a baseline recording of approximately 22 minutes, the patient was tilted; immediately, a rise in HR was observed, but as described in Section 3.4, this is quite normal. However, the simultaneous decrease in systolic BP of more than 20 mmHg, accompanied by symptoms of light-headedness, demonstrated that the patient suffered from orthostatic hypotension. The BP recovered in less than two minutes to its baseline value, so the test continued, in an effort to diagnose comorbid syndromes. Less than ten minutes later, the BP began to decrease again, but this time more gradually. Eventually, approximately 55 minutes after the start of the recording, the unchecked descent in BP led to a form of cardiovascular collapse: HR plummeted and the patient reported feeling as though she would faint. Out of concern, the angle of the tilt table was returned to 0° — whereupon HR was immediately restored to a stable value near its baseline figure, and BP commenced a monoexponential recovery lasting several minutes. The physician in charge of the test diagnosed the patient not only with orthostatic hypotension but also with vasovagal syndrome.

For comparison, a second example is presented in Figure 4.3. As can be seen by the response of BP to

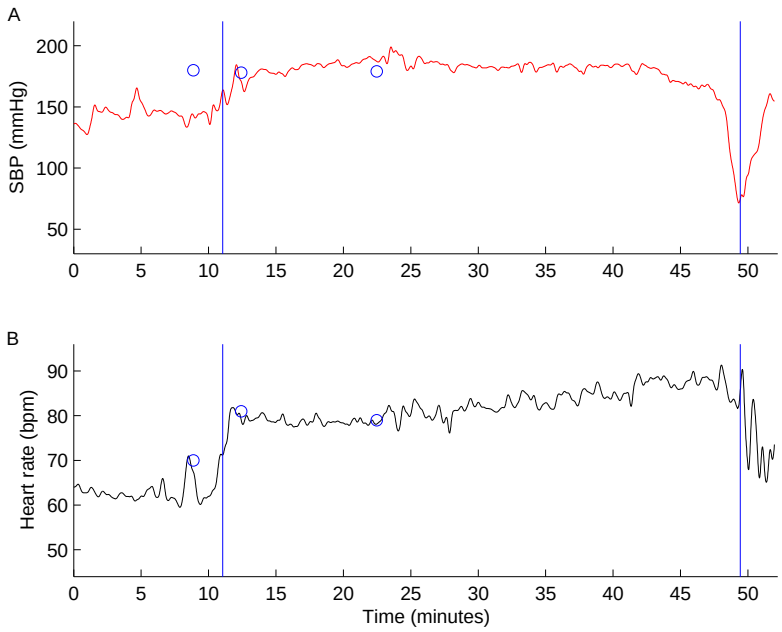

Figure 4.3: A plot of systolic blood pressure (**A**) and heart rate (**B**) for a patient with vasovagal syndrome undergoing head-upright tilt table testing. See the legend in Figure 4.2.

the first few minutes of tilt, this patient did not suffer from orthostatic hypotension. A second difference is that the BP remained steady for the first 30 minutes of tilt, before beginning its descent. A third difference is that HR did not decrease appreciably during syncope. Despite these differences, this patient was diagnosed with vasovagal syndrome as in the previous case.

Finally, asystoles of more than 3 seconds were rare in the data set, manifested in only three patients undergoing CSM, and in one patient as a result from prolonged HUT.

4.4.2 Arterial Oxygen Saturation

The supine values of arterial oxygen saturation (SaO_2) were similar for all patients, usually lying in the range of 90–100%. The effect of tilt on SaO_2 was imperceivable, and upon prolonged tilt SaO_2 did not change. However, as depicted in Figure 4.4A, some symptomatic patients experienced a sharp decrease in SaO_2 during syncope. Such sharp decreases were never preceded by a premonitory gradual fall.

The raw infrared attenuation signal from the pulse oximeter was expected to be of more interest, as it allows the calculation of pulse transit time (PTT). However, PTT in the supine position was similar for all patients (approximately 250–350 ms), regardless of diagnosis. Furthermore, although PTT sometimes

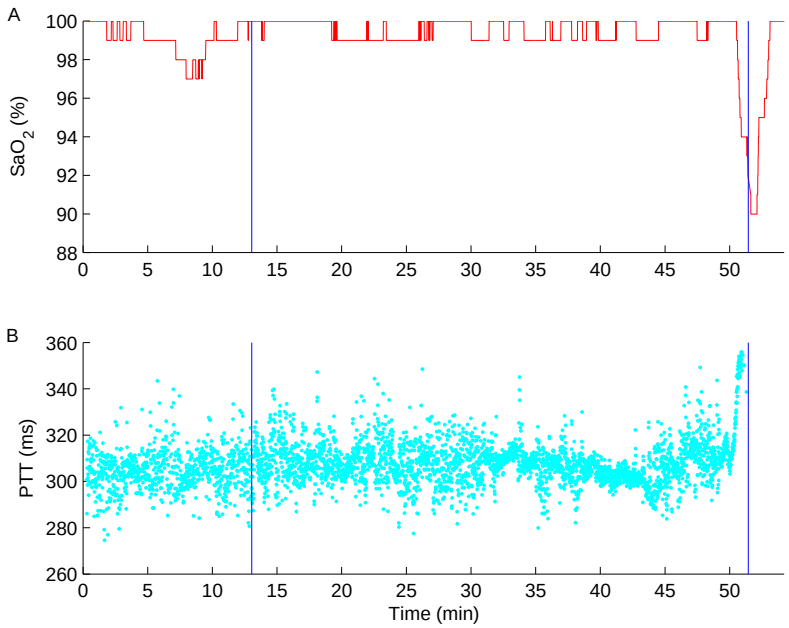

Figure 4.4: A plot of arterial oxygen saturation (SaO_2) (**A**) and pulse transit time (**B**), during head-up tilt testing of a patient with vasovagal syndrome. Vertical blue lines indicate the times of the tilt and the return to the supine position. Note the lack of change on tilt, followed by a precipitous change at the time of syncope (soon after 50 minutes).

changed on tilt (again regardless of diagnosis), the effect of tilt on PTT was often negligible. An example of this behaviour is seen in Figure 4.4B: the increase in PTT just prior to syncope mirrors the fall in BP which occurs at this time, but no earlier trends are discernible.

4.4.3 Near-Infrared Spectroscopy

An example of NIRS data for one patient is presented in Figure 4.5; the BP and HR of this patient were illustrated previously in Figure 4.3. The NIRS parameters remained relatively unchanged for most of HUT; yet, about 38 minutes into tilt, when the patient very suddenly lost postural tone and became unresponsive, the NIRO plots reflect this event (as postulated in Section 3.3.5). Figure 4.5 shows rapid decreases in TOI, THI, and O_2Hb concomitant with the BP collapse discernible in Figure 4.3. At this point the test was concluded, and the physician diagnosed the patient with vasovagal syndrome.

The autoregulatory curve for this patient is shown in Figure 4.6, with a cubic polynomial fit in black. During the course of HUT, this hypertensive patient's cerebral autoregulation changed from coping with high BP (upper right) to reach the flatter, more "normal" region of the curve (centre).

Chromophore	Vasovagal Patients	Non-vasovagal patients
O_2Hb	+0.42 ± 3.11	-0.19 ± 1.76
HHb	+0.67 ± 1.00	+0.48 ± 0.85
CtOx	-0.01 ± 0.27	+0.05 ± 0.18
TOI	-0.61 ± 1.44	-0.58 ± 1.26
THI	+0.41 ± 1.10	+0.30 ± 1.74

Table 4.2: The change in NIRO parameters immediately following tilt. Plus (minus) signs indicate an increase (decrease) relative to the supine recording. All values are expressed in μmol l^{-1}.

Shortly thereafter, BP and TOI both decreased sharply (lower left), as cerebral autoregulation failed to some extent. Haemodynamics were restored to baseline state once the test was terminated.

In Chapter 3, a possible link between tilt test positivity and steady decreases in O_2Hb was described. Analysis of the Falls Clinic data provided little evidence to support this claim: only two syncopal patients experienced a steady fall in O_2Hb during prolonged tilt, and several nonvasovagal patients demonstrated a similar trend. No obvious discriminatory patterns were perceived in the four other NIRO time series. For each, the mean value was measured during the final two minutes of supine data, and subtracted from the mean value measured in the first two minutes of data in the upright position. The results, given in Table 4.2, indicate no statistical significance via a Wilcoxon rank sum test. This was not unexpected, since the factors leading up to syncope can occur in the systemic cardiovasculature, as opposed to just the brain. O_2Hb and HHb were the parameters most sensitive to tilt, even though generalisations on their behaviour were difficult to formulate.

4.5 Variability of Vasovagal Syncope

The importance of recognising the heterogeneity of the population under study has already been underlined. As demonstrated by the contrast between Figures 4.2 and 4.3, the 26 Falls Clinic patients with vasovagal syndrome comprised a heterogeneous group: their responses to tilt involved BP increasing, decreasing, or staying the same, and HR evolved with similar variability. The only apparent common traits of these patients were the clinical diagnosis of vasovagal syncope and the fact that BP decreased substantially in the late stages of prolonged tilt. Syncope occurred in about half of the patients, because the test was often stopped seconds or perhaps minutes before syncope could occur.

Some of the VASIS criteria (see Section 2.3) can be applied only when the HR is known at the time of syncope. Since in the Oxford Falls Clinic the tests are often ended prior to syncope, less than half

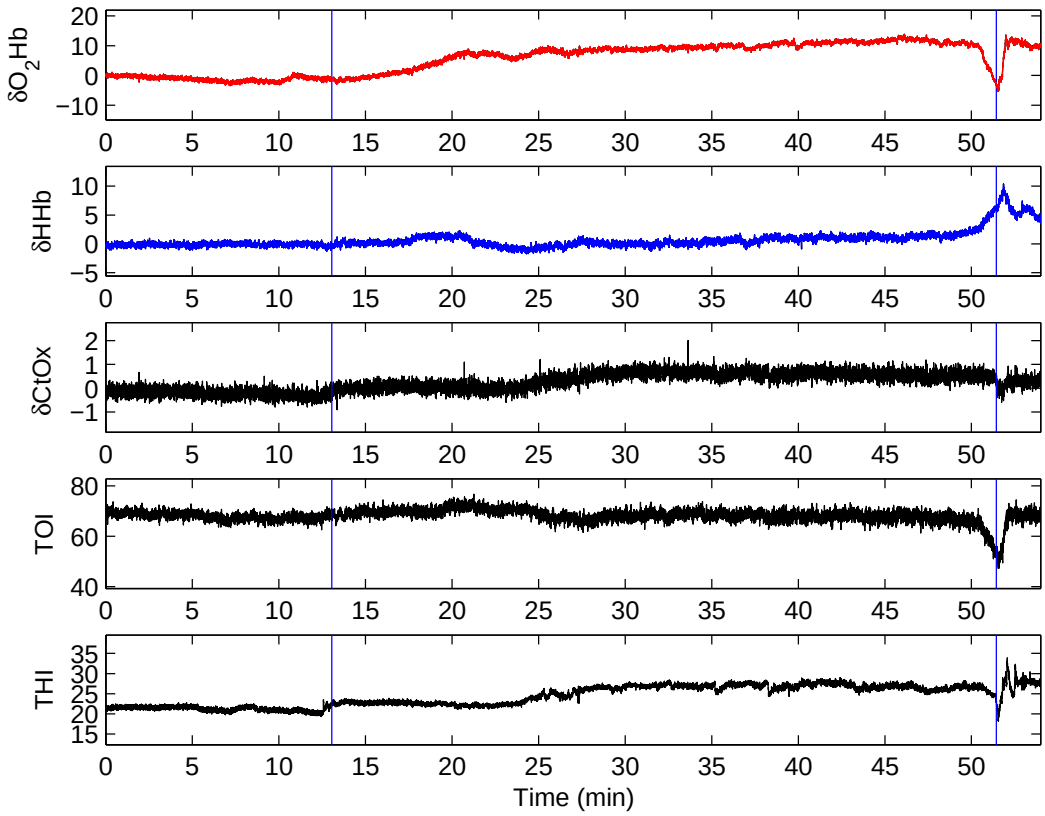

Figure 4.5: Evolution of NIRO parameters concurrent with the traces in Figure 4.3. The data were synchronised with that from the Software Monitor data acquisition system. O_2Hb = oxyhaemoglobin, HHb = deoxyhaemoglobin, CtOx = cytochrome oxidase (all in μmol L^{-1}). TOI = tissue oxygenation index, THI = total haemoglobin index (both are percentages). Blue vertical lines mark the beginning and end of the upright portion of the tilt test.

the vasovagal syndrome group could be classified according to VASIS criteria. Instead, an attempt was made to classify patients based on a count of the number of BP drops (each drop being regressed over minute intervals or other durations) in the initial stages of the upright portion of HUT (various limits were attempted, including the first 60% of the upright period, the first 15 minutes, etc.), but this test was too sensitive to artefact in the beat-by-beat determination of BP from the Finapres data.

Finally, the sub-division of patients based on a visual inspection of the general trends in BP following tilt was considered, by using Finapres data where they were deemed reliable, and oscillometric BP readings where these were available. This was motivated by the following: while vasovagal syncope as a result of HUT usually involves an apparently normal cardiovascular response to the early stages of standing or tilt, followed by haemodynamic collapse, it has been argued that this must be differentiated from the so-called

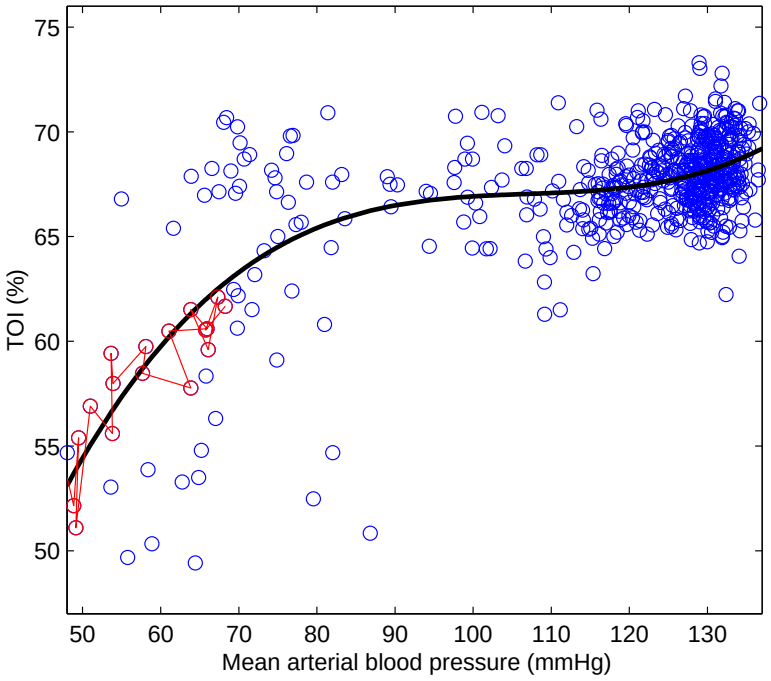

Figure 4.6: Autoregulatory curve for the patient in Figures 4.3 and 4.5, after downsampling the data to 0.5 Hz for clarity. TOI = tissue oxygenation index. The third-order line of best fit is indicated in black; data from the final 40 seconds prior to syncope are plotted in red.

"dysautonomic response" to orthostatism (see Section 2.3), as the treatment for the two problems may vary [26]. Most authors fail to make this distinction. In the current research as well, the distinction was ignored: too great a number of patients exhibited characteristics of both classes to be categorised either way. In other words, the clarity of the examples in Figures 4.2 and 4.3, demonstrating behaviour close to the two extremes, was uncommon.

Hence, the problem of heterogeneity amongst the vasovagal syncope population, while mitigated somewhat by the analysis of more than one data stream, hinders classification accuracy.

4.6 Automated Diagnosis of Syncope Using Heart Rate and Blood Pressure

Inspection of Figure 2.1 reveals that a rule-based analysis of HR and BP can be the foundation of an automated syncope classification algorithm, attempting to duplicate the diagnoses of the Falls Clinic physicians. The simple rules used are given in Table 4.3 and their application to the HUT data acquired from the patients listed in Table 4.1 is described in the sections that follow.

Syndrome	Criteria for Automated Diagnosis	Patients
OH	SBP decreased >20 mmHg within 3 min of tilt	104
VCSH	SBP decreased >50 mmHg during CSM, with lightheadedness	60
CCSH	Asystole of >3 s during CSM	71
VS	RPP < 7000 mmHg beats min^{-1} at end of HUT, or SBP decreased >50 mmHg below initial post-tilt value	63

Table 4.3: The rules of an automated diagnosis algorithm applied to the patients of the Falls Clinic. The number of patients analysed varied from test to test, since each test required different criteria for inclusion. CCSH = Cardioinhibitory Carotid Sinus Hypersensitivity, VCSH = Vasodepressor Carotid Sinus Hypersensitivity, OH = Orthostatic Hypotension, VS = Vasovagal Syndrome, CSM = Carotid Sinus Massage, HUT = Head-upright Tilt Test, SBP = Systolic Blood Pressure, RPP = Rate Pressure Product.

4.6.1 Orthostatic Hypotension

The results from the mercury sphygmomanometer used by the physician to diagnose orthostatic hypotension could not be saved directly to a hard disk, and hence the automated diagnosis of this disorder was approximated by other means. The Finapres systolic BP (SBP) data recorded immediately before and after tilt were used. To reduce the impact of sudden variations in the data owing to instrumentation error, a five-point median filter was applied to the time series.

An estimate of supine, pre-tilt SBP was calculated as the mean of the fifteen beats recorded just before the tilt. (The final three beats before tilt were discarded to prevent artefactual distortion.) The post-tilt minimum SBP was set as the lowest SBP datapoint recorded during the first three minutes following tilt. Subtracting this value from the pre-tilt SBP yielded the estimate of the maximum decrease for each patient.

One hundred and four patients had SBP data of sufficient quality to be analysed in this manner. Of these, only 63 (61%) were assigned the correct diagnosis. The low accuracy of the diagnoses can be explained by two factors. First, the tilt from which the mercury sphygmomanometer readings were attained was always different from the tilt during which the Finapres readings were recorded. It is therefore possible that, in some patients, BP decreased more in one tilt than in the other. The second reason is instrumentation error in the Finapres, a device which fails to meet all of the accuracy criteria defined by the American Association of Medical Instrumentation [85,147]. For example, Figure 4.7 shows the pre- and post-tilt values of Finapres SBP, versus those of the oscillometric brachial cuff SBP. The spread of values around the line of identity demonstrates that the continuous BP measurements made at the Falls Clinic are not well correlated with the oscillometric cuff BP values.

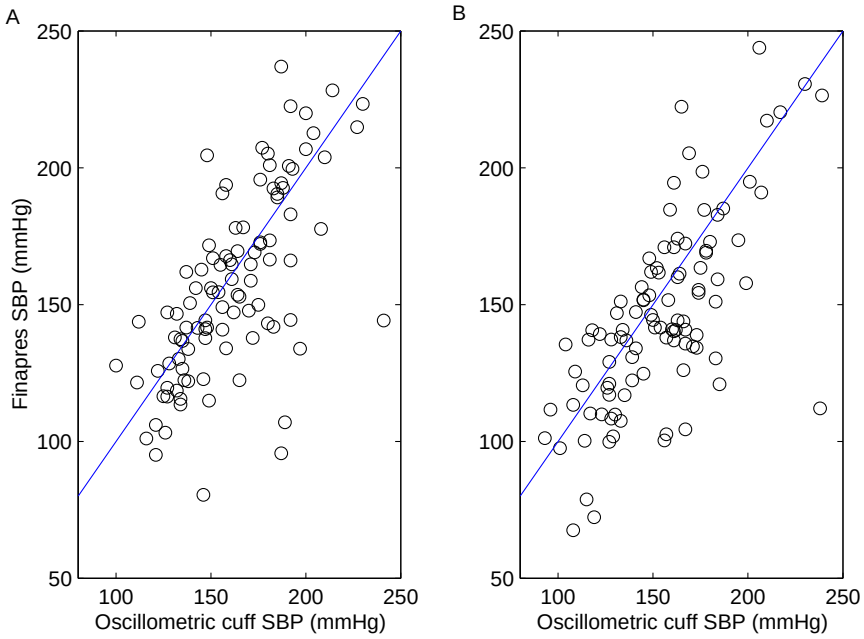

Figure 4.7: Plot of Finapres- versus oscillometric systolic blood pressure (SBP), during the supine baseline recording (**A**), and within several minutes of the tilt to the upright position (**B**). The Finapres SBP was calculated by averaging the data points within 10 seconds of the oscillometric cuff reading.

4.6.2 Vasodepressive Carotid Sinus Hypersensitivity

Symptoms of lightheadedness during CSM are one of the criteria in the diagnosis of VCSH. After these were noted by the physician, they were recorded in the database as a boolean value, since the automated diagnosis of VCSH required this information.

The second criterion for diagnosis is a decrease in SBP of more than 50 mmHg immediately following CSM. To evaluate this, a similar system to the automated diagnosis of orthostatic hypotension was used, with the exceptions that the start time of CSM was used rather than the time of tilt, and 50 mmHg was substituted for 20 mmHg.

Only 60 patients were analysed, since CSM was not performed in all patients. Of these, 54 (90%) were assigned the correct diagnosis. In five of the "incorrect" cases, the patient experienced a decrease in BP very close to 50 mmHg, so the physician's estimate based on visual inspection of the SBP graph disagreed with that of the algorithm. In the remaining incorrect case, the physician had used historical SBP data to estimate the pre-tilt value.

4.6.3 Cardioinhibitory Carotid Sinus Hypersensitivity

To diagnose CCSH automatically, only the RR tachogram was considered. A search was performed for RR intervals which exceeded 3 seconds and which occurred within 30 seconds of the start time of CSM. Uniquely among the four tests considered in this section, the automated CCSH diagnostic protocol matched closely the physician's own method of diagnosis.

Seventy-one patients were analysed, only three of whom were diagnosed with CCSH by the physician. In all cases, the algorithm matched the physician's diagnosis.

4.6.4 Vasovagal Syndrome

An automated diagnosis of vasovagal syndrome represents the most difficult challenge out of the four tests, since the symptoms are the least quantifiable.

One study found that neurally mediated syncope is often accompanied by a decrease in rate-pressure product (RPP) to a value below 7000 mmHg bpm [185]. Based on this finding, it was decided to implement an algorithm which calculated RPP during the last three minutes of the upright portion of HUT, excluding all data recorded following CSM. Vasovagal syndrome was diagnosed if the rate-pressure product fell below 7000 mmHg bpm.

However, since HUT was often terminated prior to syncope, the RPP of patients with vasovagal syndrome could not be expected to decrease below this threshold in all cases. Hence, a second test was used, based on the long-term trend in BP. A benchmark BP was established as the mean systolic BP during the last three minutes of the first five minutes of the upright portion of HUT. (The first two minutes of the upright portion of HUT were discarded, to ignore the BP transient upon tilt.) For the remainder of HUT, until the first CSM or the return to the supine position, a sliding thirty-beat window of averaged systolic BP was compared to this benchmark. Patients were diagnosed with vasovagal syndrome if at any time the window-averaged BP was more than 50 mmHg below the benchmark BP.

The second test, using BP instead of RPP, more closely matches the thought processes of the physician. However, it is still prone to error since physicians disregard some decreases in BP as artefactual, and such occurrences were too numerous to include as annotations in the database.

Sixty-three patients were analysed, all of whom experienced at least 30 minutes of HUT before CSM was initiated. Fifty-three patients (84%) were diagnosed accurately. The positive and negative predictive

values (PPV and NPV) were 0.71 and 0.94, respectively. Of the ten incorrect diagnoses, two were thought by the physician to have vasovagal syndrome, but their BP and RPP did not decrease to the extent required by the algorithm because the test was terminated early. The remaining eight incorrect diagnoses were "false positives", all caused by Finapres BP decreases which the physician deemed to be artefactual.

4.6.5 Conclusion — Automated Diagnosis of Syncope

The results of applying the rule-based algorithm to all patients are shown in Table 4.4. As can be seen, observing the decrease in Finapres SBP during HUT proved to be a poor method to diagnose patients with orthostatic hypotension. This inaccuracy was thought to be due primarily to the fact that the data known to the physician could not be made available to the algorithm, and secondarily to the limitations of the Finapres instrumentation. For example, 32 patients without orthostatic hypotension (31% of the total) were incorrectly diagnosed as positive for the disorder, since Finapres SBP fell by more than 20 mmHg. This implies that the Finapres device probably overestimated the transient decrease in SBP experienced after tilt. In addition, the false-negative rate (9 patients, or 9%) was the highest of all four syndromes under study, implying that Finapres data alone is insufficient to match the physician's diagnosis.

The algorithm was more accurate in the diagnosis of vasodepressive carotid sinus hypersensitivity. A modest number of false positives and false negatives (three patients in each category) was to be expected, since SBP during CSM sometimes fell by an amount close to the threshold of 50 mmHg. Understandably, such cases could be interpreted in one of two ways by the clinician. However, for the remaining 90% of patients the algorithm was accurate.

The algorithm was able to diagnose cardioinhibitory carotid sinus hypersensitivity perfectly. The false negative rate of 0% was due to the fact that all asystolic ECGs were examined very carefully by the physician in order to determine whether the threshold of 3.0 seconds had been crossed. The false positive rate of 0% was due in part to the accuracy of the QRS detection algorithm developed for the present purposes (see Appendix A).

Finally, the algorithm classified 53 patients (84% of the total of 64) correctly for having vasovagal syndrome or not. The false negative rate was very low (2 patients), since the thresholds for a positive diagnosis were set conservatively. For the same reason, the false-positive rate (8 patients) was high

Syndrome	TP	TN	FP	FN	No. of Patients
OH	50%	11%	31%	9%	104
VCSH	28%	62%	5%	5%	60
CCSH	3%	97%	0%	0%	71
VS	32%	52%	13%	3%	63

Table 4.4: The results from an automated diagnosis algorithm applied to the patients of the Falls Clinic. The diagnosis was deemed correct when it agreed with the decision of the physician. TP = True Positive, TN = True Negative, FP = False Positive, FN = False Negative. See Table 4.3 for other abbreviations.

compared to those for both types of CSH. However, it was still lower than the false-positive rate for orthostatic hypotension. The implications of these findings are that vasovagal syndrome can be diagnosed in an automated manner with a reasonable degree of accuracy; however, the fact that ten patients were still diagnosed incorrectly implies that either additional data may be required, or the method of diagnosis using the existing data should be improved.

Chapter 5

Signal Processing for Syncope Prediction: HRV

5.1 Introduction

Chapters 3 and 4 showed that HR, BP, and NIRO parameters may provide information to help to predict syncope. Chapter 3 (Section 3.4.4) showed that HRV may also be a useful predictive indicator. The reason it did not feature in the previous chapter is the lack of a clear clinical interpretation of HRV changes in the context of syncope diagnosis. The aim of this chapter is to lay the foundations for developing a useful HRV metric for syncope prediction.

5.2 The Need for Instantaneous Heart Rate Variability

One of the limitations from which most common HRV measurements suffer is the requirement of stationarity, i.e. the property that the dynamic characteristics of the analysed signal (standard deviation, spectral energy distribution, etc.) do not vary with time. However, stationarity in cardiovascular signals is often elusive, since even healthy cardiac dynamics exhibit transient changes [95]. As a result, "instantaneous HRV", which can track beat-to-beat changes in cardiac dynamics, began to be studied during the 1990s [125, 139]. (Of course, the concept of an instantaneous rate or instantaneous variability is not meaningful, but in the current work the term instantaneous will be used to refer to sample-by-sample estimates of a quantity.) Examples of instantaneous measures of HRV include LF energy, HF energy, and

LF/HF ratio, as described in Chapter 3 but computed on a sample-by-sample basis rather than being computed for a recording lasting several minutes.

Instantaneous changes in HRV are worth investigating in the context of vasovagal syndrome because of the instabilities of the autonomic nervous system implicated in the disorder. Since patients may faint because of over- or under-compensations of the different neural responses, a valid question to ask is whether patients with vasovagal syndrome exhibit an autonomic instability which might be identified by tracking the instantaneous changes in HRV in response to the HUT stimulus. For example, this instability could affect the variance of a measure of instantaneous HRV over a period of (perhaps) one minute.

To this end, the method of instantaneous centre frequency (ICF) was used. This relatively new approach was pioneered by Jasson *et al.* [88] and is gradually becoming better known [10, 95, 194]. The ICF can be defined as the first moment of area (similar to a centre of mass) in the frequency domain, and related calculations can be used to find the ICF_{LF} and ICF_{HF}. An important advantage of ICF over the other measures is the independence from arbitrary frequency bounds (for example, recall that in the calculation of LF/HF the LF- and HF regions are defined arbitrarily and do not take into account inter-individual variation).

5.3 The Calculation of Instantaneous Centre Frequency

5.3.1 Obtaining a Spectrum Using Time-Frequency Analysis

Signals which lack stationarity can be processed with one of several time-frequency transforms: Wavelet, Gabor, Choi-Williams, and others. Developed for quantum mechanics by Wigner [227] and introduced to signal processing fifteen years later by Ville [222], the Wigner-Ville distribution of a function $f(t)$ is:

$$W(t,\omega) = \int_{-\infty}^{\infty} f\left(t+\frac{\tau}{2}\right) f^*\left(t-\frac{\tau}{2}\right) e^{-i\omega\tau}\, d\tau \tag{5.1}$$

where * denotes complex conjugation. This equation provides a representation of $f(t)$ in the joint time-frequency domain, and is one of the most popular time-frequency analysis methods for biological signals [139]. After comparative evaluation with other time-frequency representations, it has been deemed to be superior for cardiovascular data [88, 95, 157], and was selected for the present work. Several particular reasons influenced the decision to use the Wigner-Ville distribution in the current work:

- Excellent time- and frequency-domain resolution
- The ability to optimize independently those two forms of resolution (explained below)
- Linear phase
- Efficacy in reducing artificial cross-terms

The Wigner-Ville distribution is a periodic function with period π. Hence, to avoid aliasing, sampling at *twice* the Nyquist rate is required [38]. Otherwise, the analytic signal should be used, i.e. an equivalent signal but with all negative frequencies suppressed. Hence, in Equation 5.1, $f(t)$ should not represent the original signal but rather a corresponding analytic signal. This analytic signal can be obtained easily using the Hilbert transform, $H[\cdot]$. For example, in the discrete case, where $f(n)$ is used instead of $f(t)$, this analytic signal is computed as:

$$f(n) = f_r(n) + i\,H[f_r(n)] \tag{5.2}$$

where $f_r(n)$ is the (real) original signal and $f(n)$ is the (complex) analytic signal.

The Wigner-Ville distribution of this finite discrete signal $f(n)$ is given as:

$$W(n,m) = \frac{N_h}{2} \sum_{k=-N_h+1}^{N_h-1} |h(k)|^2 f(n+k) f^*(n-k)\, e^{\frac{-2\pi i k m}{N_h}} \tag{5.3}$$

where $h(k)$ is a normalised symmetric windowing function, which acts as a form of frequency-smoothing. Equation 5.3 is seldom used in its pure form, and the Smoothed Pseudo Wigner-Ville Distribution (SPWVD) is employed instead:

$$W(n,m) = \frac{N_h}{2} \sum_{k=-N_h+1}^{N_h-1} |h(k)|^2 \sum_{p=-N_g+1}^{N_g-1} g(p)\, f(n+p+k) f^*(n+p-k)\, e^{\frac{-2\pi i k m}{N_h}} \tag{5.4}$$

Here, $g(p)$ and $h(k)$ represent independent time and frequency smoothing of order N_g and N_h, respectively. The advantage of smoothing is the removal of spurious cross-terms; in fact, spectral interference is so high in the pure Wigner-Ville distribution that it precludes implementation in most real applications [166]. However, the smoothed version, which trades off sufficient suppression of cross-terms on the one hand with adequate time-frequency resolution on the other, is used in many applications. A pictorial illustration of how the SPWVD is applied to the analytic signal is shown in Figure 5.1.

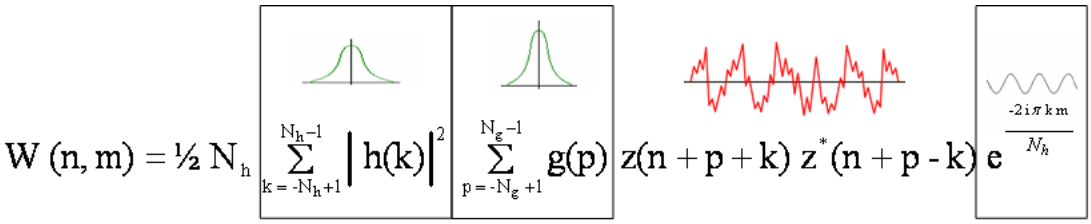

Figure 5.1: How the SPWVD operates. First, the analytic signal (red time series) is multiplied by a complex exponential (represented as a sinusoidal wave) of a given frequency (determined by *m*, the point in the time-frequency plane under consideration). The product is smoothed by an averaging window *g(p)* (narrow green distribution). Finally, the window *h(k)* (wide green distribution) is multiplied by the result to limit the contribution of the time series for a given point in the time-frequency plane, *W(n,m)*. Importantly, these two averaging operations can be adjusted (regarding the type or length of the window) independently of one other.

The Wigner spectrum of stationary signals is simply the classical spectrum [88]; clearly no advantage is to be gained in this case. Where the SPWVD is truly valuable is in the analysis of signals whose spectra vary rapidly with time. For example, a linear chirp signal reduces to a string of Kronecker delta functions in the time-frequency plane [166]. Short-time Fourier transforms (STFTs) cannot accurately track changes in a signal's spectrum that occur over the course of a few samples, which is a significant limitation for many biological signals. The human nervous and cardiovascular systems are known to modify blood pressure and cardiac contraction behaviour in just a few heart beats; hence the use of the SPWVD is much more appropriate than the STFT with a 60-second, or even 30-second, moving window.

5.3.2 Instantaneous LF/HF Ratio

A frequency band within a temporal slice of a time-frequency representation can be summed to provide the total spectral power in that band. For example, the LF[1] power at a given time can be computed as follows:

$$LF(t) = \int_{2\pi(0.04)}^{2\pi(0.15)} W(t,\omega)d\omega \tag{5.5}$$

In a similar manner, HF(t) can be calculated, and the ratio of the two time series is an instantaneous estimate of the LF/HF ratio:

$$LF/HF(t) = \frac{\int_{2\pi(0.04)}^{2\pi(0.15)} W(t,\omega)d\omega}{\int_{2\pi(0.15)}^{2\pi(0.40)} W(t,\omega)d\omega}. \tag{5.6}$$

[1] See note on p. 32.

This equation may be straightforwardly extended to express the LF/HF ratio of a discrete time series:

$$LF/HF(n) = \frac{\sum_{m=m_{L2}}^{m_{L2}} W(n,m)}{\sum_{m=m_{H1}}^{m_{H2}} W(n,m)}, \tag{5.7}$$

where the subscripted ms refer to the upper and lower boundary indices for the LF and HF spectral bands.

5.3.3 Instantaneous Centre Frequency

Recall from Section 5.2 that the ICF of a signal is a measure of the dominant frequency of a signal at any point in time; in the present work it is calculated as the time-dependent frequency average (i.e. first raw moment) of $W(n,m)$ from Equation 5.4. In continuous time, ICF is calculated from the SPWVD ($W(t,\omega)$ in Equation 5.3) as follows:

$$ICF(t) = \frac{\int_{-\infty}^{\infty} \omega W(t,\omega) d\omega}{\int_{-\infty}^{\infty} W(t,\omega) d\omega} \tag{5.8}$$

and in discrete time, ICF is:

$$ICF(n) = \frac{\sum_{m=0}^{m_{\max}} mW(n,m)}{\sum_{m=0}^{m_{\max}} W(n,m)}. \tag{5.9}$$

ICF can be calculated in other ways, without recourse to the computational complexity of the SPWVD [27]. For example, one method to estimate the ICF of a signal $x(t)$ [22] begins with the construction of an in-quadrature signal $y(t)$:

$$y(t) = \frac{1}{\pi t} * x(t). \tag{5.10}$$

where $*$ denotes convolution. The instantaneous frequency is then found as follows:

$$ICF(t) = \frac{d\left(\tan^{-1}\left(\frac{y}{x}\right)\right)}{dt}. \tag{5.11}$$

The equivalence of Equations 5.8 and 5.11 is proven in Appendix C. One limitation of the latter technique is its inability to generate other parameters resulting from the time-frequency representation; for example even related quantities such as ICF_{LF} (the ICF of the LF component of the tachogram) cannot be

determined. As a result, the SPWVD method was selected for the present research.

5.3.4 Summary

Before patient data can be analysed using the SPWVD method, validation using synthetic signals is required. To represent patient data as closely as possible, the problems of uneven sampling are incorporated into the artificial signals, and this is the subject of the next section.

5.4 Sampling Issues

Since the SPWVD works best on evenly sampled data, the (unevenly sampled) RR tachogram is resampled using interpolation. However, this approach introduces new problems: linear interpolation, and the alternative proposed by Berger *et al.* [18], each truncate higher frequencies and so cubic splines are preferred [39]. One problem with cubic splines is the generation of unacceptable oscillations when one RR interval is unusually longer than its predecessor; for example, as a result of asystole, as depicted in Figure 5.2. However, asystoles are sufficiently rare, and detectable, that this does not present an obstacle. In summary, the method of cubic splines outperforms the alternatives for the present purposes.

In the analysis of stationary signals, i.e. when the Fourier transform may be used instead of the SPWVD, a strategy to avoid the drawbacks of interpolation is to compute the spectrum directly from the unevenly sampled tachogram. The Lomb periodogram is an excellent candidate for this operation, since it weights the data on a point-by-point basis rather than on a per-interval basis. The Lomb periodogram of a time series x_j is:

$$P_N(\omega) \equiv \frac{1}{2\sigma^2}\left\{\frac{\left[\sum_j (x_j-\overline{x})\cos(\omega(t_j-\tau))\right]^2}{\sum_j \cos^2(\omega(t_j-\tau))} + \frac{\left[\sum_j (x_j-\overline{x})\sin(\omega(t_j-\tau))\right]^2}{\sum_j \sin^2(\omega(t_j-\tau))}\right\} \tag{5.12}$$

where $\tau \equiv \tan^{-1}(\frac{\sum_j \sin(2\omega t_j)}{2\omega \sum_j \cos(2\omega t_j)})$ [39]. It has been shown that the Lomb periodogram can provide a more accurate estimate of the power spectral density (PSD) of a tachogram than interpolation followed by a regular Fourier transform [39]. However, this method does not appear to have been combined with time-frequency analysis. Hence, the Lomb periodogram in its present form suffers from the problem of not being able to track the changes in the frequency content of a signal on a sample-by-sample basis.

Besides uneven sampling, a second problem in data processing is whether to use heart rate or heart

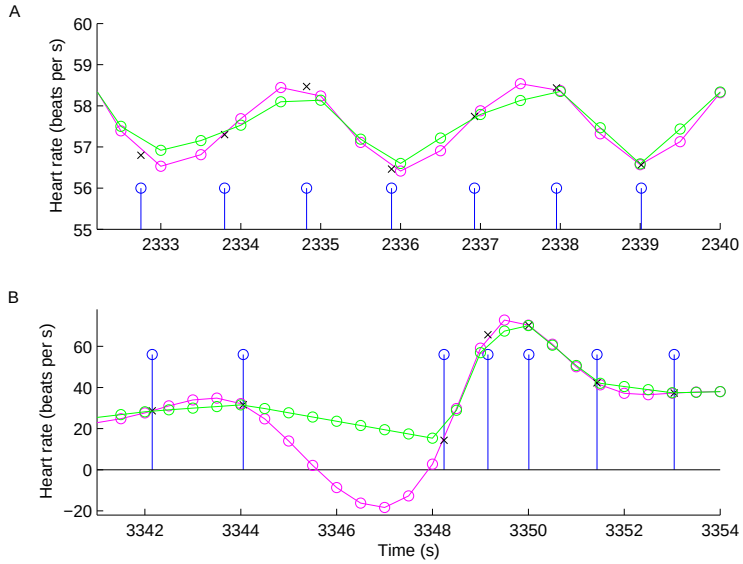

Figure 5.2: Interpolation of a heart rate event series (real data). Heart beats are indicated with vertical blue lines, and the corresponding sample-by-sample estimates of heart rate are plotted as black crosses. Linear and cubic-splines interpolations of the heart rate are shown in green and magenta, respectively. **A.** Cubic splines are better able to track sinusoidal rhythms; note the magenta line offers a closer approximation to the black crosses. **B.** However, during a four-second asystole triggered by carotid sinus massage, the linear interpolation is clearly superior; several data points interpolated using cubic splines are negative.

period. In the current research, heart period was preferred over heart rate, owing to the nonlinearity of the relationship between heart rate and efferent sympathetic and parasympathetic activities [159, 218].

5.5 Synthetic RR tachograms

This section will define the synthetic RR tachograms to be used in the validation of the instantaneous HRV computation.

5.5.1 Constant LF and HF Components

An artificial tachogram was generated with simple LF and HF components that remained constant throughout time. The properties of the time series were as follows:

- Length of 512 seconds, with a mean heart rate (HR) of 70 beats per minute
- No ectopic beats or artefacts
- LF and HF components, each modelled as a single sinusoid of 0.10 Hz or 0.25 Hz, respectively

The equation governing the tachogram generation was:

$$HR = 70 + A_L \sin(2\pi f_L t) + A_H \sin(2\pi f_H t) \tag{5.13}$$

$$f_L = 0.10\,\text{Hz},\ f_H = 0.25\,\text{Hz},\ A_L = 4,\ A_H = 3.2$$

where HR has units of beats per minute. The tachogram was constructed using the following algorithm:

- The heart rate was first generated at a sampling frequency of 1 kHz, using Equation 5.13
- Next, the RR interval time series was calculated (recall that heart rate is simply the inverse of RR interval length)
- The 1-kHz RR interval time series was downsampled unevenly, such that each RR value $y(\tau)$ was separated from the next by a time $\Delta\tau$ equal to the magnitude of its data point (i.e., $\Delta\tau = y(\tau)$)

The initial RR interval was set to occur at time $\tau = 1$ ms. The RR interval calculated at this time was added to a moving time index, to generate the next data point y. The value of the data point was also the next RR interval ($\Delta t = y$). This was repeated until the end of the time series.

5.5.2 Varying LF and HF Linearly

Next, an artificial tachogram was generated with characteristics more closely resembling patient data. The LF and HF components of the tachogram were each modelled by a single sinusoid which evolved over time as a result of frequency and amplitude variations. Over the 512 seconds, one frequency decreased linearly from 0.12 Hz to 0.08 Hz, while the other increased linearly from 0.21 Hz to 0.29 Hz. Over the same period, the amplitude of the LF (HF) component grew (receded) linearly by a factor of +67 (–40) per cent. Thus the equation was:

$$HR = 70 + A_L \sin(2\pi f_L t) + A_H \sin(2\pi f_H t) \tag{5.14}$$

$$f_L = 0.12 - \frac{0.04}{2}\frac{t}{512}\text{Hz},\quad f_H = 0.21 + \frac{0.08}{2}\frac{t}{512}\text{Hz},\quad A_L = 3 + 2\frac{t}{512},\quad A_H = 4.2 - 2\frac{t}{512}$$

5.5.3 Varying LF and HF Nonlinearly: Test tachogram

In real tachograms, LF and HF contributions wax and wane as a result of multiple factors, rather than changing monotonically and steadily as does the artificial tachogram generated from Equation 5.14.

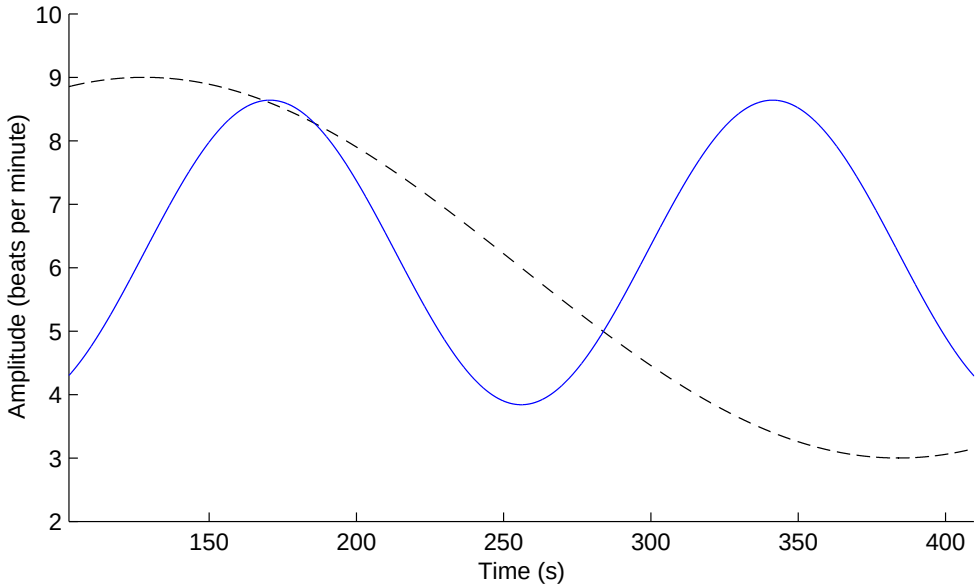

Figure 5.3: Amplitudes of the HF (solid blue line) and LF (dashed black line) components in the time series generated from Equation 5.15.

Hence, the LF and HF amplitudes were also varied nonlinearly and more rapidly. As illustrated in Figure 5.3, a sinusoidal modulation was chosen for both amplitudes, A_L and A_H. Frequency modulation (involving f_L and f_H) was kept the same as in Section 5.5.2. The equation governing this tachogram was:

$$HR = 70 + A_L \sin(2\pi f_L t) + A_H \sin(2\pi f_H t) \tag{5.15}$$

$$f_L = 0.12 - \frac{0.04}{2}\frac{t}{512}\text{Hz}, \quad f_H = 0.21 + \frac{0.08}{2}\frac{t}{512}\text{Hz},$$

$$A_L = 6\left[1 + 0.5\sin(2\pi\frac{t}{512})\right], \quad A_H = 4.8\left[1.3 + 0.5\cos(6\pi\frac{t}{512})\right]$$

5.5.4 Varying LF and HF Nonlinearly: Training tachogram

Finally, a more variable tachogram was used to set the two SPWVD smoothing parameters N_g and N_h, to ensure that the three less complex tachograms described above could be analysed. The overall time was reduced to 336 seconds to shorten the computations. The equation was:

$$HR = 70 + A_L \sin(2\pi f_L t) + A_H \sin(2\pi f_H t) \tag{5.16}$$

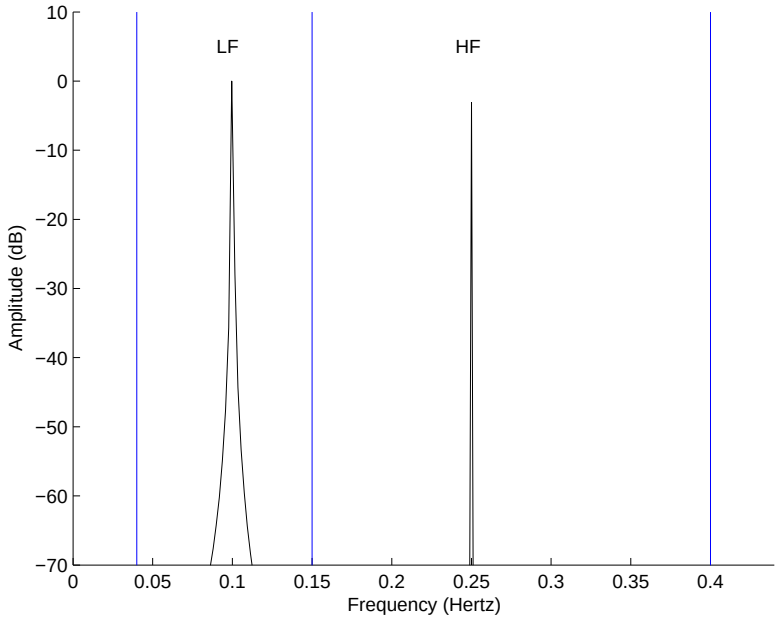

Figure 5.4: A 512-point Lomb periodogram of the simple signal generated from Equation 5.13. The two peaks correspond to the LF and HF components, and the vertical blue lines mark the ranges for calculating them (0.04–0.15 Hz and 0.15–0.4 Hz, respectively).

$$f_L = 0.12 - \frac{0.04}{2}\frac{t}{336}\text{Hz}, \quad f_H = 0.21 + \frac{0.08}{2}\frac{t}{336}\text{Hz},$$

$$A_L = \begin{cases} 2.4, & \text{if } t \leq 126 \\ 3\left[1 + 0.2\cos(\frac{40\pi t}{336})\right], & \text{if } t > 126 \end{cases} \qquad A_H = \begin{cases} 2.95, & \text{if } t \leq 126 \\ 2.8 + 0.4\frac{t}{336}, & \text{if } t > 126 \end{cases}$$

5.6 Results from the Lomb Periodogram

The Lomb periodogram of the simplest artificial tachogram (see Equation 5.13) is shown in Figure 5.4. HRV was calculated using the LF/HF ratio, employing bounds of 0.04–0.15 Hz for LF and 0.15–0.40 Hz for HF. The result was an LF/HF ratio of 1.55, nearly matching the expected value of $(\frac{4}{3.2})^2 = 1.56$.

Second, the Lomb periodogram of the artificial tachogram generated from Equation 5.14 is shown in Figure 5.5. The resulting LF/HF ratio is 1.54, in reasonable agreement with the expected mean value of 1.95 (obtained by averaging the changing LF/HF ratio over the duration of the time series). The discrepancy is likely to reflect the difficulty which the Lomb algorithm has in adapting to changes in LF/HF ratio.

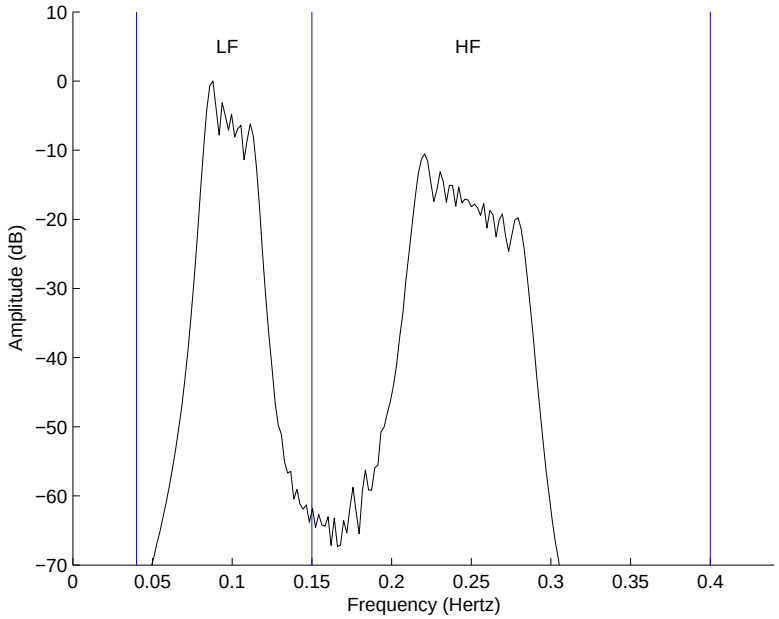

Figure 5.5: A 512-point Lomb periodogram of the signal generated from Equation 5.14. Each peak would be symmetrical were it not for amplitude modulation, i.e. a variation in A_L and A_H. For both the LF and HF components, spectral contributions were designed to be strongest at the lower frequencies (as is evident from the equation).

5.7 The Smoothed Pseudo Wigner-Ville Distribution

5.7.1 Choice of Smoothing Parameters N_g and N_h

The smoothing functions $g(p)$ and $h(k)$ for the SPWVD (see Section 5.3.1) can take a number of forms. The Hamming window function was selected:

$$w(n) = \begin{cases} 0.54 - 0.46\cos\left(\frac{2\pi n}{N}\right), & 0 \leq n \leq N, \\ 0, & \text{otherwise.} \end{cases} \tag{5.17}$$

where N is the order of the filter, in this case either N_g or N_h. Hamming windows provide a good trade-off between accuracy and versatility. In [139], it is recommended that the size N of these windows be chosen empirically, by visually comparing the results from various choices. This strategy was improved by calculating the RMS (root mean square) error for various window sizes. The RMS error E quantifies

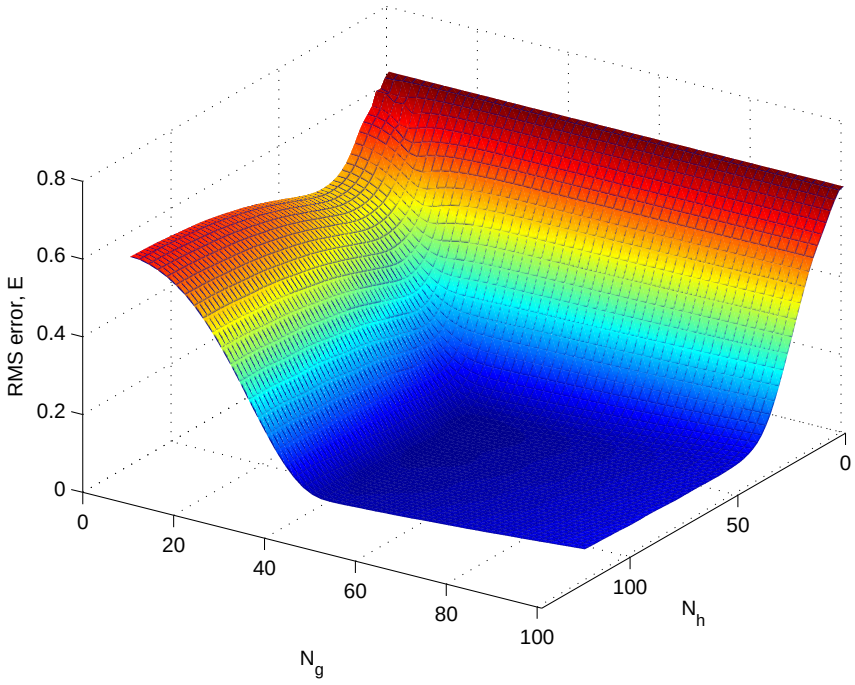

Figure 5.6: The effect of time and frequency smoothing filter orders (N_g and N_h respectively) on RMS error, E.

the degree of difference (error) between each of M data points, $x_o(t)$, and their expected values, $x_e(t)$:

$$E = \sqrt{\frac{1}{M}\sum_{t=1}^{M}\left[x_o(t) - x_e(t)\right]^2} \tag{5.18}$$

This formula was used as follows. First, $x_o(t)$ was calculated using the SPWVD for chosen values of N_g and N_h, applied to the tachogram generated from Equation 5.16. Second, the RMS error was calculated for the time series. These two steps were then repeated for new values of N_g and N_h, and the results plotted to compare the accuracy associated with various orders of filter (see Figure 5.6). As can be seen in the figure, at low values of N_g or N_h, insufficient smoothing occurred, so the RMS error was higher. This was due to oscillations from spurious spectral cross-terms. At very high values of N_g or N_h, too much smoothing occurred, and the RMS error rose again, due to insufficient time and frequency resolution. The minimum RMS error occurred with $N_g = 45$ and $N_h = 57$.

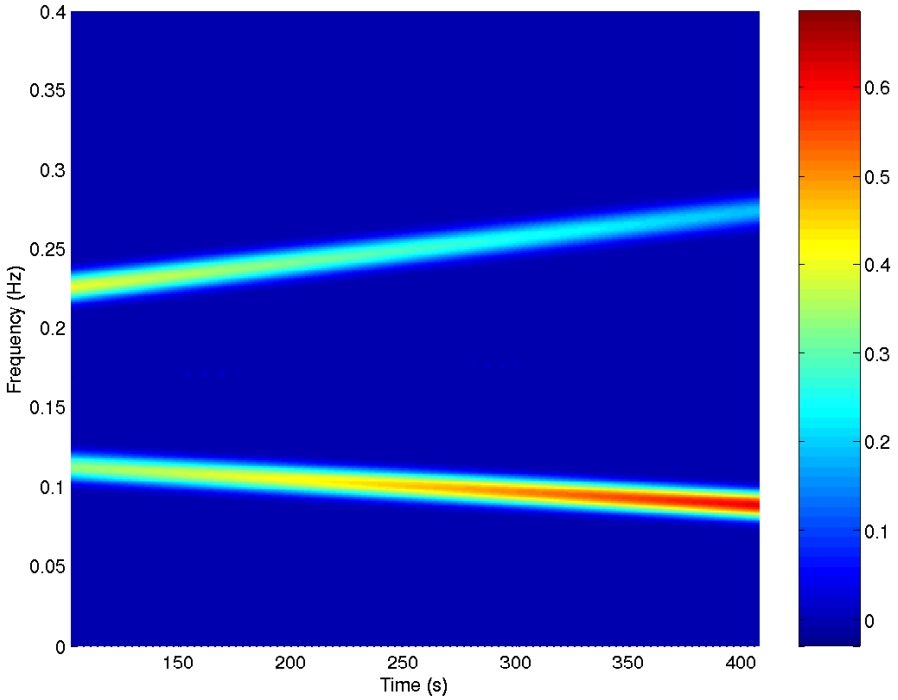

Figure 5.7: An SPWVD time-frequency representation of the artificially generated signal described in Equation 5.14. The first and last 20 per cent of the signal were ignored, since accurate results cannot be produced near the edges of time series. The colour bar at right indicates power, in units of s^2 Hz^{-1}.

5.7.2 Varying LF and HF Linearly

With the smoothing windows chosen as described in the previous section, the SPWVD of the tachogram generated from Equation 5.14 was calculated and compared with the Lomb periodogram. One step of pre-processing was necessary: resampling to ensure evenly-spaced data points. The uneven RR intervals were converted to evenly sampled values via cubic-splines interpolation. Since no artefacts or ectopic beats were present in the synthetic time series, this interpolation did not suffer from any of the artefactual effects described in Section 5.4. A sampling frequency of 3 Hz was selected as a trade-off between fast computation and a desire to avoid aliasing.

The time-frequency distribution and a plot of the LF/HF ratio versus time are shown in Figures 5.7 and 5.8, respectively. The effects of the variation in LF and HF amplitudes and frequencies are clearly detected by the SPWVD algorithm: i.e., changes in LF/HF ratio were tracked quite closely. Further, the mean LF/HF ratio of 1.68 is almost identical to the expected mean LF/HF ratio of 1.69 — no longer 1.95 as in Section 5.6; the value decreases because only the middle 60 per cent of the LF/HF plot was considered.

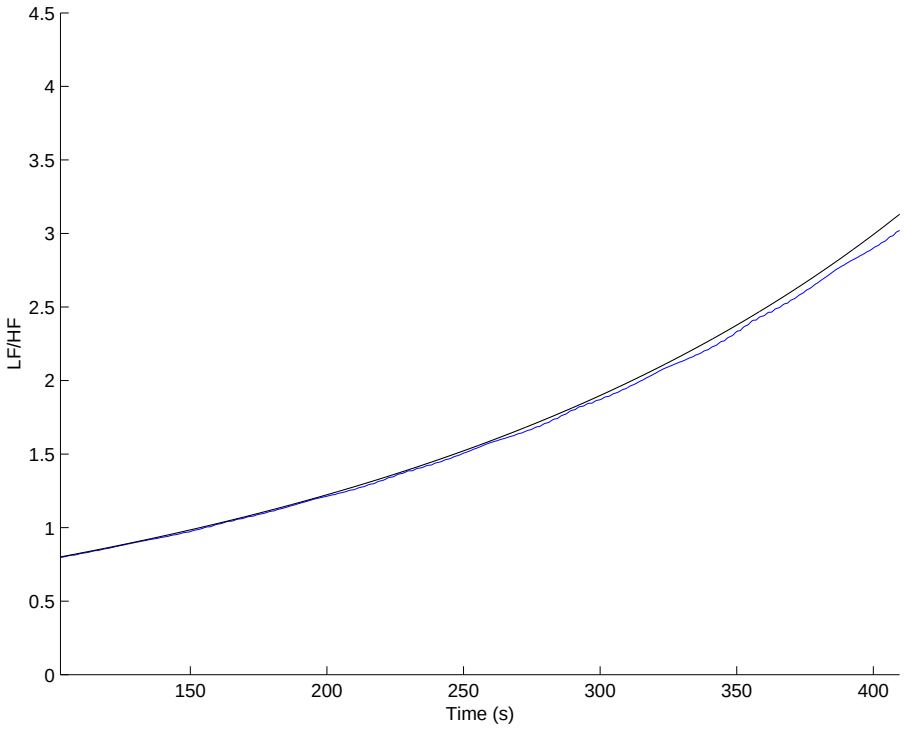

Figure 5.8: The expected (black line) and actual (blue line) LF/HF ratios for the RR tachogram resulting from Equation 5.14.

5.7.3 Varying LF and HF Nonlinearly

Finally, the test tachogram generated from Equation 5.15 was used. The graph of expected and actual LF/HF ratios is portrayed in Figure 5.9. There exists close agreement for most of the time series; however, when the LF/HF ratio changed abruptly near t = 250 s, the error rose to 3.6%. Note that the qualitative features of the graph remained well preserved. The ability of the SPWVD to track ICF accurately is demonstrated in Figure 5.10.

5.7.4 Conclusion

It has been shown that, on artificial data, the SPWVD performs better than the Lomb periodogram in tracking changes in the frequency components of a tachogram. The former method will be applied to real patient data in the next section; for comparison, the results of the latter method will also be presented.

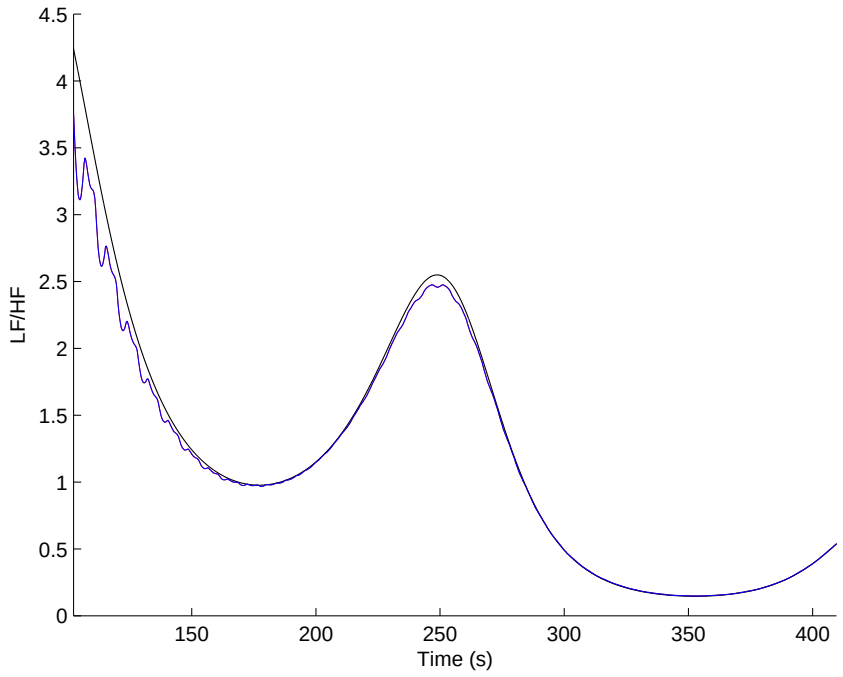

Figure 5.9: The expected (black line) and actual (blue line) LF/HF ratios for the time series generated from Equation 5.15.

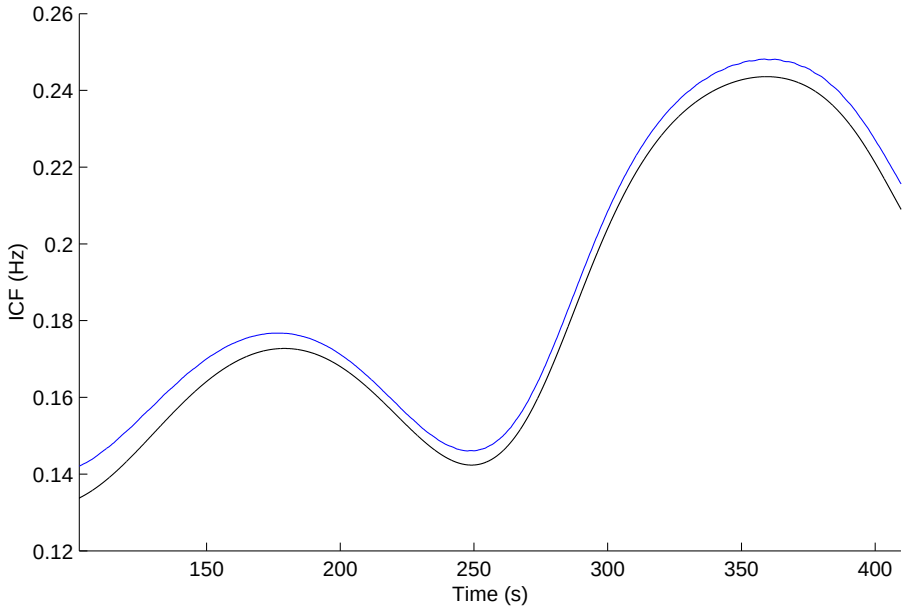

Figure 5.10: A comparison of the expected (black line) and actual (blue line) instantaneous frequency of the time series with nonlinearly time-varying LF and HF components.

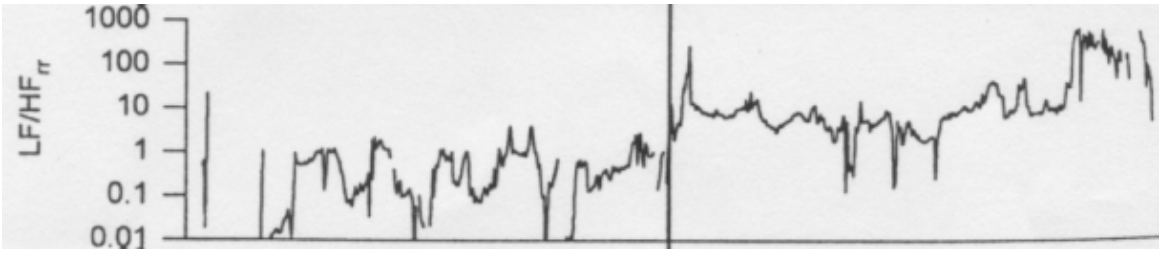

Figure 5.11: An example of how the instantaneous LF/HF ratio can vary with tilt [114]. The (linear) time axis spans 50 minutes. The vertical line in the centre represents a tilt to the upright position. Despite the logarithmic ordinate scale, burst-like activity is prominent.

5.8 Heart Rate Variability from Patient Data — Analysis of Normal Subjects

Data were analysed for two normal subjects aged 24 and 31, who had few artefacts and ectopic beats in their tachograms. Detrending using a 0.02-Hz high-pass Hamming-windowed filter was still required; the reason this was unnecessary for the artificial tachograms was that there was no change in mean heart rate in those time series. Data were divided into 50-per-cent-overlapping segments of 500 seconds, and only the middle 50% of each segment was used. Hence the first and last 25% of each segment were discarded — similar to the artificial tachograms, for which the first and last 20% of the signal were discarded, as is evident from the time axes in Figure 5.8.

The instantaneous LF/HF obtained by the SPWVD (see lower graphs in Figures 5.12, 5.13, and 5.14) resembled graphs in the literature (an example of which is depicted in Figure 5.11), in that the ratio tended to vary quickly and over a large range. Twofold and even fourfold variations over the course of a few seconds have been observed in previous research [88]. Further, other authors have reported that the majority of the burst activity in an LF/HF plot is due to sudden rises in LF power; examining LF and HF powers individually in the present subjects confirmed that finding.

One of the possible reasons for this burst-like activity is the lack of paced breathing in the studies. Paced breathing is respiration at prescribed intervals, and represents the only method which guarantees that the tachogram's HF peak falls within its "normal" range of 0.15–0.40 Hz. Without paced breathing, the strong respiratory peak may sometimes be found near 0.15 Hz, being classified alternately as LF or HF, which leads to an extremely variable LF/HF ratio.

The instantaneous LF/HF ratio was then averaged over five minute periods for comparison with the

ratio calculated using the Lomb periodogram [39]. As shown in Figures 5.12 and 5.13, close agreement in the overall trend existed. Some disagreement is to be expected: for example, the former method averaged a quotient (the mean LF/HF in a 5-minute period), whereas the latter calculated the quotient of two averages (the mean LF component divided by the mean HF component). Hence the nonlinearity of the operation of division played a small role.

5.9 Heart Rate Variability from Patient Data — Analysis of Falls Clinic Patients

5.9.1 Artefact and Ectopic Beat Removal

The young normal subjects analysed in Section 5.8 above produced smooth tachograms; usually, with patients undergoing HUT, more rigorous pre-processing is required to remove artefacts and ectopic beats. Despite the sensitivity of the SPWVD to artefact, the issue of artefact removal is rarely mentioned in the literature (although some guidelines are provided by Porges *et al.* [159]). A new method was developed, inspired in part by previous work in classical HRV analysis [21,37]. The first part of the procedure was the event series analysis described in Section A.5 of Appendix A. After obvious artefacts had been corrected in this manner, ectopic beats were identified to denote the period around them as dubious when later reporting results. This second-pass algorithm is summarised below:

1. The RR tachogram was first interpolated using the cubic-splines method (see Section 5.7.2).

2. A search began for values of HR which deviated by more than 20% from the average of the previous ten values (i.e., the previous $3\frac{1}{3}$ seconds, since the sampling frequency was 3 Hz).

3. These data points were labelled as aberrant, to reflect the fact that they were likely to be ectopic beats.

4. Further, where two aberrant data points flanked one or two non-aberrants, the non-aberrant data point(s) were relabelled as aberrant, since RR values are always dependent on neighbouring data points.

5. All aberrant data points were then recalculated. Each replacement heart rate was arbitrarily chosen to be the mean of the two nearest *previous* valid data points averaged with the mean of the two

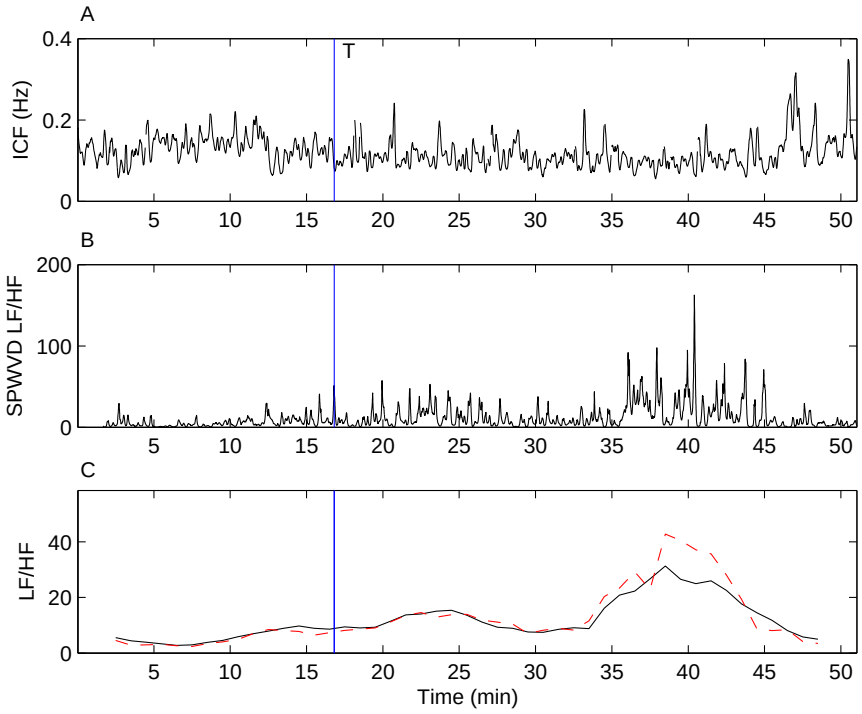

Figure 5.12: Instantaneous centre frequency (ICF) and LF/HF (Low- to high-frequency) ratio for the first normal subject, aged 31. **A**: ICF, calculated from the SPWVD. **B**: LF/HF, calculated from the SPWVD. **C**: LF/HF, calculated from the SPWVD and averaged over a five-minute sliding window (black line), and recalculated using the Lomb periodogram in [39] (dashed red line). A comparison of parts B and C suggests that information may be missed when time-frequency analysis is not used. T = tilt.

nearest *subsequent* valid data points.

6. Steps 2 through 5 were repeated until all aberrant beats were removed, or (rarely) until no further progress could be made. Typically, only a few passes were required.

The time series resulting from this procedure was an instantaneous heart rate signal (IHRS), ready for time-frequency analysis. The LF/HF ratio was calculated for all data points using the SPWVD; however, within the LF/HF time series, data points were discarded if their time index corresponded to, or was adjacent to, a time index earlier labelled as aberrant, thereby ensuring that no spurious data points remained in the final time series. This concluded the calculation of the instantaneous LF/HF ratio. Finally, the five-minute-averaged LF/HF ratio was calculated as before, but in five-minute segments where more than 20% of the LF/HF time series had been discarded, the calculation did not take place and the LF/HF was left undetermined.

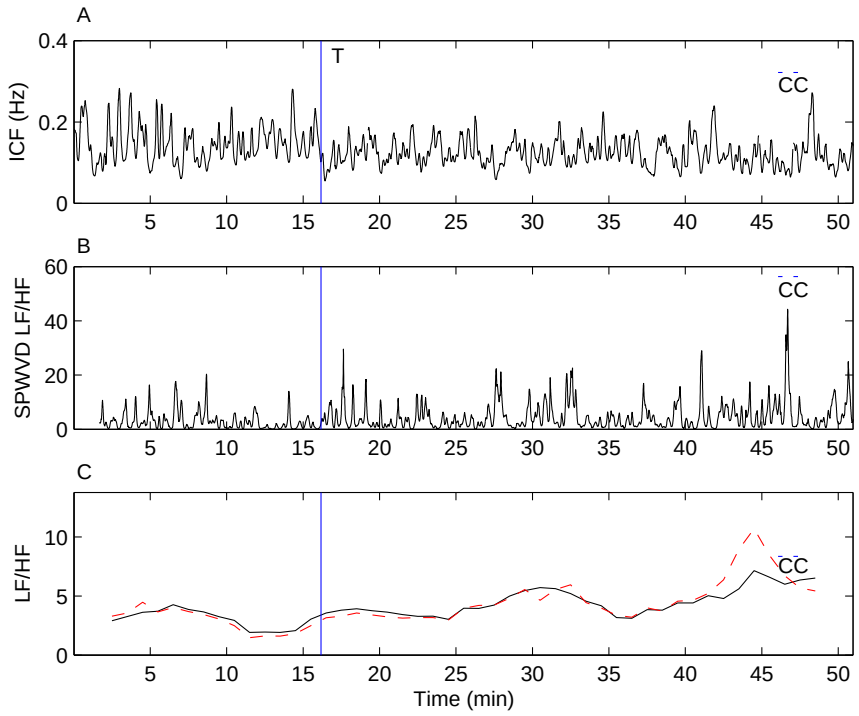

Figure 5.13: ICF and LF/HF ratio for the second normal subject, aged 24. For a description and legend, see Figure 5.12. The two small lines above the "C" each represent about 18 seconds of carotid sinus massage.

5.9.2 Typical Example of Falls Clinic Patients

Other patients previously analysed in [39] were examined, using the artefact and ectopic beat removal system described in Section 5.9.1 above.

A typical example of this analysis, for a 79-year-old Falls Clinic patient, can be found in Figure 5.14. This woman suffered from vasovagal syncope, and her symptoms were completely reproduced during the tilt test. Approximately 30 minutes after tilt, near $t \approx 3300s$, a marked bradycardia preceded an asystole lasting several seconds and subsequent loss of consciousness. The variations of the 5-minute average LF/HF ratio calculated using the SPWVD method and the Lomb periodogram method show reasonable agreement, but the data from the latter are consistently slightly lower. This is probably due to the inability of the Lomb periodogram algorithm to deal as effectively with artefacts and ectopic beats, which if not dealt with, can artificially increase the HF component and hence decrease LF/HF. Unrealistically, the LF/HF ratio even decreased to zero for a short time.

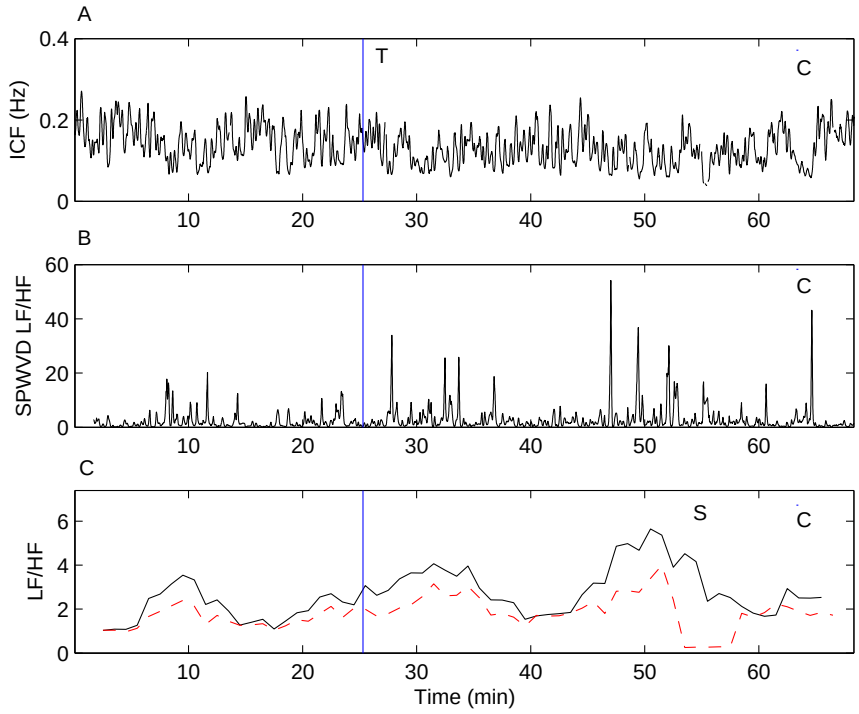

Figure 5.14: ICF and LF/HF ratio for a 79-year-old Falls Clinic patient with vasovagal syndrome. For a description and legend, see Figure 5.12. The "C" indicates 10 seconds of carotid sinus massage, and "S" indicates when syncope occurred.

5.10 Conclusion

This chapter has described the methods for computing an instantaneous HRV metric, based on the SPWVD. The analysis of well-defined artificial data demonstrated that the SPWVD is able to track rapid changes in simulated cardiac dynamics. Real patient data were used to show that the computation of 5-minute average LF/HF ratio using the SPWVD methods gave similar results to those produced using the Lomb periodogram. In addition, extra information was gleaned from the SPWVD analysis, for short-term changes in LF/HF were resolved over seconds rather than minutes. The next chapter describes how ICF was used as a parameter to predict syncope.

Chapter 6

Signal Processing for Syncope Prediction Early in HUT

6.1 Introduction

In this chapter, new signal analysis methods for the prediction of syncope are investigated and compared with existing methods, previously reviewed in Section 3.4. These methods were defined as tests T1–T29 in Tables 3.1 to 3.5. The methods were applied to data from 106 patients, previously described in Section 4.3. For reasons given below, it was necessary to exclude a number of patients from the data set (see Section 6.2).

6.2 Criteria for Inclusion for Analysis

6.2.1 First Inclusion Criterion: No Atrial Fibrillation

Patients with atrial fibrillation (AF) had to be excluded from HRV analysis. As explained in Section 3.4.3, the HRV models in the literature assume that HR is modulated by sympathetic and parasympathetic inputs to the heart. In contrast, the HR of an AF patient is known to be driven by chaotic impulses generated by the atria themselves [82]. As a result, the RR interval time series merely represents a (homoscedastic) stochastic process, and cannot reflect sympathovagal balance.

Various methods have been developed for the automatic detection of AF, including those using neural networks and Markov chains [211]. For the present purposes, the method described in Appendix E was

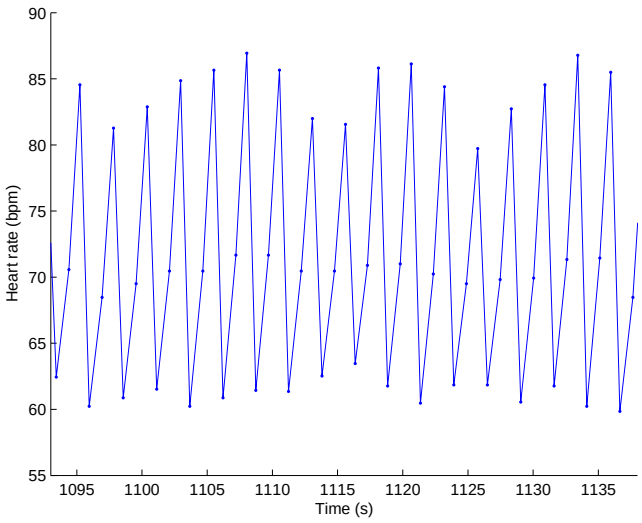

Figure 6.1: The RR tachogram recorded from a Falls Clinic patient experiencing cardio-respiratory synchronisation. The frequency of oscillation corresponds to the patient's respiration rate. Note that the RR interval decreased by approximately 22 bpm (approximately 30%) on every third beat. bpm = beats per minute.

used: RR interval histograms were computed for each patient, and compared with RR interval histograms computed from an online database [60] in which experts had annotated the presence or absence of atrial fibrillation.

Of the 106 patients, five had permanent AF, three had paroxysmal AF, and the remaining 98 (approximately 92%) were found to be entirely free of AF.

6.2.2 Second Inclusion Criterion: No Cardio-Respiratory Synchronisation

As interacting oscillatory systems, the cardiac and respiratory systems are subject to synchronisation [100,176,178,213,230]. For two self-sustained nonlinear systems, synchronisation occurs when their basic frequencies f_1 and f_2 evolve to satisfy the equation $nf_1 = mf_2 \mid n, m \in \mathcal{N}$. This phenomenon manifested itself as cardiorespiratory synchronisation (CRS) in some Falls Clinic patients; when it did so it tended to affect large sections of an RR tachogram but rarely the entire recording. One hundred patients out of 106 were entirely or mostly clear of CRS, based on visual inspection aided by simple detection software, which identified regions of the RR tachogram in which adjacent RR intervals consistently differed by 20% or more. This heuristically-derived figure resulted from the observation of known cases of CRS in Falls Clinic patient data (see Figure 6.1).

6.2.3 Third Inclusion Criterion: Age of 65 Years or More

The importance of age in the aetiology of vasovagal syncope was discussed in Section 3.4.3. An age of 65 was taken as the lower limit to define "elderly", on the advice of the collaborating physicians. Eighty-five patients out of 106 were 65 or older.

6.2.4 Fourth Inclusion Criterion: A Clear Diagnosis (Positive or Negative) of Vasovagal Syndrome

The most difficult criterion to assess was the diagnosis of vasovagal syndrome. Twenty-six patients were diagnosed with the disorder (eighteen by use of the first method described on page 45, i.e. losing consciousness or coming within seconds of doing so before the tilt test was terminated), and 49 patients did not show any evidence of the problem. Five patients were diagnosed with an unrelated type of orthostatic intolerance, such as POTS (postural orthostatic tachycardia syndrome). The remaining 26 patients either were not subjected to a long enough tilt test to be certain, or showed slight but not convincing vasovagal symptoms.

6.2.5 Fifth Inclusion Criterion: No Orthostatic Hypotension

In Section 2.4 it was mentioned that the nature of a doctor's investigation of syncope varies from clinic to clinic. In fact, HUT is often recommended only after orthostatic hypotension has been excluded from the diagnosis. For this reason, it was sometimes useful to examine the HUT response of Falls Clinic patients without orthostatic hypotension. As will become clear later in this chapter, it was hoped that this would clarify the prediction of vasovagal responses to tilt by excluding possible cardiovascular interference from orthostatic hypotension. Forty-three patients did not have orthostatic hypotension.

6.2.6 Sixth Inclusion Criterion: An Appropriate NIRO Recording

Forty-five patients had NIRO data acquired at 6 Hz during supine baseline recording and around the time of tilt. Sixty-one did not have this data.

6.3 Applying the Inclusion Criteria

6.3.1 Data Subset A: ECG Analysis

The first subset consisted of 46 patients (18 vasovagal and 28 non-vasovagal, 8 male and 38 female) who met the first four of the six inclusion criteria:

- No atrial fibrillation
- No cardio-respiratory synchronisation
- Age of 65 or more
- Clear diagnosis (positive or negative) of vasovagal syndrome

In addition, one patient was excluded because her ECG recording suffered from excessive amounts of artefact. Data Subset A was used for the syncope prediction algorithms which require only ECG data: T1–T23; and all but two of the new syncope predictors, described in Section 6.4 below.

6.3.2 Data Subset B: NIRS Analysis

The second subset consisted of 35 patients (13 vasovagal and 22 non-vasovagal, 9 male and 26 female) who met inclusion criteria 3, 4, and 6:

- An appropriate NIRO recording
- Age of 65 or more
- Clear diagnosis (positive or negative) of vasovagal syndrome

This subset was used for the two syncope prediction algorithms which rely on cerebral recordings from the NIRO apparatus. These tests are also described in Section 6.4 below.

6.3.3 Other Subsets

The syncope prediction tests of Tables 3.4 and 3.5, labelled T24–T29, require recordings from different instrumentation (e.g. Finapres or PPG) in addition to complying with inclusion criteria 3 and 4. The data subsets used for these six tests contained data from between 22 and 45 patients.

6.4 New Syncope Predictors

This section introduces three new methods to predict syncope. Each was designed while considering the first few minutes of data recorded after tilt.

6.4.1 Heart Rate Trend

Motivation

The Heart Rate Trend (HRT) is defined here as the result of a linear regression on the IHRS (see Section 5.9.1) during the first few seconds or minutes after tilt. The HRT is the slope of HR for a given duration.

The motivation for examining the HRT was to identify gradual changes in the IHRS, rather than test whether an arbitrarily chosen threshold was crossed (e.g. 18 beats per minute higher than the supine value, as described in Section 3.4.2) for an arbitrary duration (e.g. 10 or 30 seconds). The HR change following tilt in elderly vasovagal patients was found to be difficult to differentiate from that measured in elderly normal subjects, and hence a new predictor had to be investigated. The hypothesis was that patients prone to fainting are more likely to suffer from autonomic difficulties and hence may not be able to maintain their pulse rate (whether increased or not) when they assume the upright position. This would manifest itself as a greater decrease in pulse rate during the early phases of tilt than what would be expected in normal patients.

Methodology

Initially, two time periods of the IHRS were chosen for the purposes of syncope prediction: from 90 to 180 seconds after tilt (P1), and from 60 to 300 seconds after tilt (P2). These times were chosen as a compromise between accuracy and efficiency of calculation. (If the assessment period is too long, the utility of prediction is reduced; if too short, the data are more sensitive to artefacts.) Note that the first 60 (or 90) seconds after tilt were discarded in the P1 (or P2) calculation in order to allow the IHRS time to undergo its initial rise. During the first minute or so after tilt, it is typical for the IHRS to increase sharply as part of the natural autonomic response to standing.

Figures 6.2 and 6.3 illustrate the HRT for sample vasovagal and normal patients. As the red and black trend lines demonstrate in these typical examples, the average HRT seems to be more negative

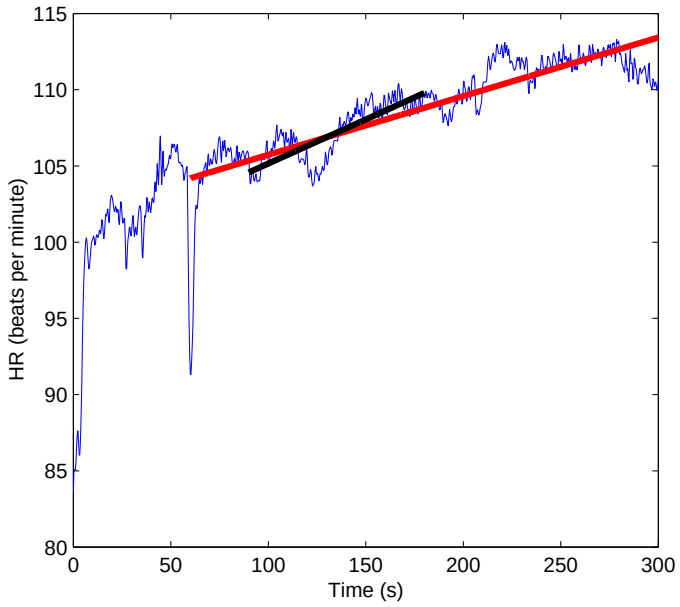

Figure 6.2: Graph of HRT for a Falls Clinic patient who had a negative diagnosis of vasovagal syndrome. The P1 and P2 trends are shown in black and red, respectively.

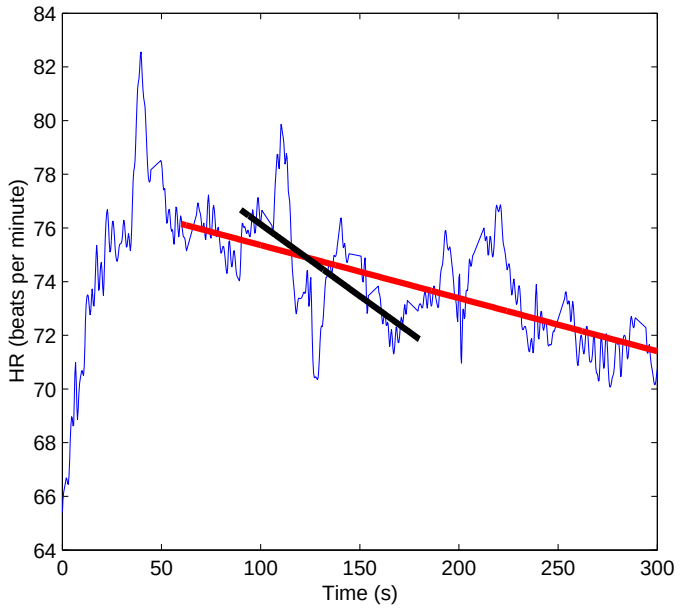

Figure 6.3: Graph of HRT for Falls Clinic patient diagnosed with vasovagal syndrome. The P1 and P2 trends are shown in black and red, respectively.

with vasovagal patients than with their tilt-negative counterparts.

The time taken for the IHRS to undergo its initial rise varies from person to person. Hence, a third time period (P3) was introduced for analysis, developed using the principle of "individually-determined time axes" [2]; i.e. the time axis of observation began at a point x seconds after tilt, as before, but rather

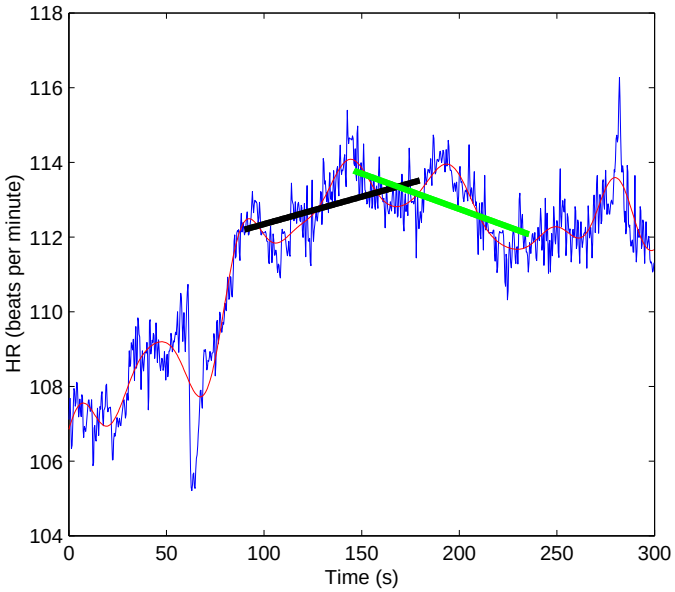

Figure 6.4: Comparison of HRT measurement techniques P1 (black line) and P3 (green line). Each is a linear regression recording a change in HR; however, the former begins 90 seconds after tilt for all patients, whereas the latter records the rate of fall in HR after the maximum has been achieved. The blue trace represents the raw RR tachogram, while the red line represents the low-pass filtered RR tachogram, using a cutoff frequency of 0.04 Hz.

than setting $x = 60$ or $x = 90$ seconds, x was determined on a per-patient basis. Specifically, P3 was defined to last for 90 seconds, with a start point x defined using the following algorithm:

1. Low-pass filter[1] the IHRS to exclude frequencies above 0.04 Hz.

2. For 180 seconds after the time of tilt, advance second by second a sliding 30-s window over the IHRS signal, computing the minimum IHRS value in each case. The 30-second window with the highest minimum IHRS is retained.

3. Define the start of P3, x, to be the midpoint of this 30-second period.

This procedure accounted for the varying rates at which pulses accelerated in response to tilt, so that in all cases, the initial IHRS rise upon tilt could be discarded, and the trend monitored thereafter.

The effect of this improvement on a particular patient is illustrated in Figure 6.4. While many patients have completed their initial HR rise by the time P1 begins, this is not true for all patients, as is the case in Figure 6.4. The rationale for P3 is that the start of the window, x, indicates the end of the early autonomic adjustment to tilt for each individual.

[1]This filtering is not applied to the IHRS used in the calculation of ICFV (see Section 6.4.2); it is used only for the determination of the time boundaries of P3.

6.4.2 Instantaneous Centre Frequency Variability

This section describes a novel HRV metric, known as "ICFV" (instantaneous centre frequency variability), to predict vasovagal syncope. ICFV is a measure of the instability of ICF over time. It is calculated as the standard deviation of ICF over a given interval, $[t_1, t_2]$:

$$\mathrm{ICFV}_{t_1 t_2} = \sqrt{\frac{\sum_{n=n_1}^{n_2} [\mathrm{ICF}(n) - \mu_{\mathrm{ICF}}]}{N}}, \tag{6.1}$$

where μ_{ICF} is the mean ICF in the interval and n_1 and n_2 are the discrete indices corresponding to t_1 and t_2, and $N = n_2 - n_1 + 1$.

Motivation

The variability of ICF was examined in an effort to identify autonomic instability, rather than assess the relative magnitude of various spectral bands. The hypothesis was that patients who experience difficulty in controlling their autonomic response to tilt (and hence are more prone to fainting) might have greater variability in their ICF (i.e. have higher ICFV). The avoidance of the use of spectral bandwidth power magnitudes was expected to provide a normalising effect to minimise the effects of ageing on HRV analysis. In addition, ICF variations are less susceptible to the problems of non-paced respiration than say LF/HF calculations (see Section 5.8).

Methodology

ICFV was calculated for the same three segments of the IHRS (P1, P2, and P3) as with HRT. The original motivation for introducing the new time period P3 was provided by the ICFV analysis rather than the HRT analysis. The intention was to identify the earliest reasonably stable period in the HR time series following tilt in which to measure ICFV; hence the need to begin measurement as soon as the initial HR rise had taken place.

6.4.3 Cerebral Indicators

Two NIRO-based methods were considered to derive new indicators of syncope prediction. The first considered the tilt-induced fall in $\mathrm{Hb}_{\mathrm{diff}}$. (Recall from Section 3.3.5 that $\mathrm{Hb}_{\mathrm{diff}}$ is the difference between oxy- and deoxyhaemoglobin concentration changes; hence a decrease in $\mathrm{Hb}_{\mathrm{diff}}$ is caused by oxygen de-

mand exceeding oxygen supply to the brain.) Mean values of Hb_{diff} were calculated for the final two minutes of baseline recording, and again for two minutes following the first three minutes of tilt. The difference between these two mean values was chosen as the metric to be investigated, referred to as HDD (haemoglobin difference drop).

The second method was based on the finding in a previous study [204] that the LF spectral energy of O_2Hb or TOI often increases in young normals on standing. For the current work, preliminary analysis first confirmed that the oscillations of O_2Hb were not correlated with those in diastolic BP. Next, O_2Hb LF was calculated for two minutes of baseline recording, as well as between minutes 3 and 5 in the upright position. The first three minutes after tilt were discarded because cerebral signals measured by NIRS require slightly longer than the IHRS to stabilise after tilt. The ratio of these two spectral energies was chosen as the metric to be investigated.

These two methods were chosen because it was thought that some vasovagal patients may suffer from poor cerebral reactivity. Hence, upon tilt, poor regulation of Hb_{diff} and blunted O_2Hb LF spectral energy increases were expected.

6.4.4 Summary

The new syncope prediction tests, described in the three previous sections, are summarised in tabular form in Table 6.1.

6.5 Results Obtained with Existing Predictors

6.5.1 Statistical Significance

The tests described in Tables 3.1 through 3.5 were applied to the Falls Clinic patients. Table 6.2 provides an overview of whether the statistics differed markedly between vasovagal and nonvasovagal patients. A nonparametric test known as the Wilcoxon rank sum evaluated this difference quantitatively. Parametric tests were avoided since not all data were normally distributed.

Out of 29 tests investigated at the 5% significance level, it is expected that approximately one to two of the tests through random chance should yield "statistically significant" results. The p values (0.046 and 0.019) of tests T11 and T23 were below 5%, but they were not high enough to withstand for example

Test	Parameter of Interest	Period(s) Measured	Positive Test Criterion	Patient Group
Heart rate:				
HRT P1	HR slope	90–180 s after tilt	Value is below some threshold	Subset A
HRT P2	HR slope	60–300 s after tilt	Value is below some threshold	Subset A
HRT P3	HR slope	An individually-calculated 90-s period soon after tilt	Value is below some threshold	Subset A
Heart rate variability:				
ICFV P1	ICFV	90–180 s after tilt	Value is above some threshold	Subset A
ICFV P2	ICFV	60–300 s after tilt	Value is above some threshold	Subset A
ICFV P3	ICFV	An individually-calculated 90-s period soon after tilt	Value is above some threshold	Subset A
Cerebral perfusion changes:				
HDD	Hb_{diff} (O_2Hb – HHb)	Final 2 min of baseline, Final 2 min of first 5 min after tilt	Difference is below some threshold	Subset B
LFO_2	LF (0.04–0.15 Hz)	Final 2 min of baseline, Final 2 min of first 5 min after tilt	Quotient is below some threshold	Subset B

Table 6.1: New syncope prediction tests, based on heart rate trend (HRT), instantaneous centre frequency variability (ICFV), haemoglobin difference drop (HDD), and low-frequency oxygen oscillations (LFO_2). min = minute.

a Bonferroni adjustment[2] to this confidence level.

Often, the lower the p value, the greater the chance that two patient groups may be classified successfully using some threshold which lies between the two distribution medians. However, this general rule does not always hold and it is necessary to test empirically the classification accuracy, regardless of the p value: discriminating between two distributions using a specific classifier is not the same activity as testing the similarity of their medians, as will be shown in the next section.

6.5.2 Classifier Design

The first of two issues to consider is the design of the classifier: given a data set acquired from vasovagal and nonvasovagal patients, it is desired to learn from the data how to classify future patients.

A simple approach is to identify the arithmetic mean of the medians of the two patient groups as a "threshold", and classify future patients according to whether their data points fall above or below the threshold. A shortcoming of this method is that, while the ideal threshold will usually lie between the two medians, it will in general be different from their mean.

[2] A Bonferroni adjustment is required when multiple statistical tests are evaluated simultaneously. For example, if the number of tests is 29, and a 95% confidence level is desired, the Bonferroni-adjusted significance level is $\alpha = 0.05/29 \approx 0.0017$. This is a form of what is known as "multiple-comparison correction".

Test	μ_v	σ_v	μ_n	σ_n	Units	TR	p value
Heart rate:							
T1	75.0	10.8	76.5	15.7	bpm	No	NS
T2	6.18	5.57	6.07	3.82	bpm	Yes	NS
T3	5.99	6.38	5.34	4.06	bpm	Yes	NS
T4	6.93	6.04	6.19	5.12	bpm	Yes	NS
T5	6.61	7.33	7.29	6.29	bpm	No	NS
T6	7.88	8.18	8.07	5.68	bpm	No	NS
T7	7.63	5.03	5.51	3.73	bpm	Yes	NS
T8	68.2	9.74	70.3	14.7	bpm	Yes	NS
T9	74.9	10.8	76.0	15.7	bpm	Yes	NS
T10	4.96	3.47	6.56	12.9	-	No	NS
T11	9.80	10.5	3.64	3.35	-	Yes	0.05
Heart rate variability:							
T12	0.936	1.14	0.636	1.56	s^2	Yes	NS
T13	1.47	1.33	1.05	1.20	s^2	Yes	NS
T14	13.2	17.1	24.8	23.2	%	Yes	NS
T15	1.98	2.65	1.70	2.31	s^2	No	NS
T16	63.8	21.2	50.9	21.8	%	Yes	NS
T17	81.6	91.3	80.6	133	%	No	NS
T18	2.95	2.42	1.57	1.47	-	Yes	NS
T19	3.54	0.383	3.47	0.400	-	No	NS
T20	1.74	0.969	1.28	0.961	-	No	NS
T21	115	207	86.5	153	%	No	NS
T22	3.98	5.84	6.03	9.60	%	No	NS
T23	-20.1	46.2	0.181	27.3	%	No	0.02
Blood pressure and baroreflex sensitivity:							
T24	712	337	690	392	-	Yes	NS
T25	7.00	5.06	4.12	2.26	ms	No	NS (0.06)
T26	3.28	1.15	4.35	4.59	ms	Yes	NS
Pulse transit time:							
T27	5.67	4.78	4.71	5.82	%	Yes	NS
T28	11.8	4.21	28.7	52.9	ms	No	NS
T29	12.7	4.47	26.6	47.3	ms	No	NS

Table 6.2: Wilcoxon rank sum results on 29 tests from the literature. μ and σ refer to the mean and standard deviation for vasovagal (v) and non-vasovagal (n) patients in Subset A, in units from the "Units" column (bpm = beats per minute). TR = Trend Reproduced, which is "Yes" if the relationship (> or <) between the two μs matches the published finding. p value = statistical p value returned by the Wilcoxon rank sum test (NS = not significant, using a significance threshold of 0.05).

A second method is to examine the receiver-operator characteristic (ROC), a plot of the true positive rate versus the false positive rate for all possible choices of threshold. This graph typically appears similar to that shown in Figure 6.5. The black dashed line represents the "line of no discrimination", corresponding to a truly random predictor. This predictor is correct 50% of the time, for, as the threshold (not shown) changes, the number of true positives rises no faster than the number of false positives. The ROC for an ideal classifier passes through the point (0,1); i.e. a threshold can be chosen such that the true-positive rate is 100% and the false-positive rate is 0%. Most classifiers lie between these two

Test	ROC Area	Sensitivity	Specificity	PPV	NPV	Accuracy
Heart rate:						
T1	0.63	0.67	0.58	0.62	0.64	0.62
T2	0.51	0.00	0.00	0.00	0.00	0.00
T3	0.60	0.25	0.58	0.38	0.44	0.42
T4	0.60	0.33	0.42	0.36	0.38	0.38
T5	0.61	0.50	0.55	0.55	0.50	0.52
T6	0.51	0.00	0.18	0.00	0.14	0.09
T7	0.64	0.58	0.67	0.64	0.62	0.62
T8	0.63	0.83	0.42	0.59	0.71	0.62
T9	0.64	0.67	0.50	0.57	0.60	0.58
T10	0.61	0.42	0.75	0.62	0.56	0.58
T11	0.73	0.75	0.67	0.69	0.73	0.71
Heart rate variability:						
T12	0.68	0.58	0.68	0.44	0.79	0.65
T13	0.66	0.67	0.50	0.36	0.78	0.55
T14	0.65	0.75	0.54	0.41	0.83	0.60
T15	0.54	0.58	0.46	0.32	0.72	0.50
T16	0.67	0.42	0.86	0.56	0.77	0.72
T17	0.54	0.75	0.43	0.36	0.80	0.53
T18	0.67	0.42	0.86	0.56	0.77	0.72
T19	0.54	0.17	0.32	0.10	0.47	0.28
T20	0.65	0.58	0.64	0.41	0.78	0.62
T21	0.53	0.33	0.57	0.25	0.67	0.50
T22	0.52	0.08	0.61	0.08	0.61	0.45
T23	0.74	0.58	0.71	0.47	0.80	0.68
Blood pressure and baroreflex sensitivity:						
T24	0.51	0.09	0.00	0.03	0.00	0.03
T25	0.68	0.64	0.60	0.41	0.79	0.61
T26	0.62	0.40	0.60	0.40	0.60	0.52
Pulse transit time:						
T27	0.59	0.43	0.00	0.18	0.00	0.14
T28	0.66	0.57	0.64	0.44	0.75	0.62
T29	0.65	0.43	0.50	0.30	0.64	0.48

Table 6.3: Leave-one-out cross-validation performance, on 29 tests from the literature. ROC Area = Area under the receiver-operator characteristic curve. Accuracy = Overall accuracy (fraction of patients who are diagnosed correctly). PPV = Positive Predictive Value, NPV = Negative Predictive Value.

extremes, as shown by the blue line in the figure. The area under this line, known as the ROC area, lies between 0 and 1 and gives a rough indication of the effectiveness of the classifier. The threshold which maximises overall accuracy for a given classifier is that which, when plotted on the ROC, lies at the minimum distance from the point (0,1), as shown by the red line in the figure.

6.5.3 Choice of Cross-Validation

The second issue to consider, once a classifier is chosen, is how to validate its accuracy. A common technique is the *hold-out* method, whereby the data is partitioned into a training set and a (usually

smaller) test set. The classifier is trained using data from the former, before the "new" data from the latter is tested as input to the classifier. The information contained in the test set data cannot be used to train the classifier.

A second technique is called "k-fold cross-validation", whereby the data is divided into k partitions. A single partition is then selected to form the test set, and the remaining $k-1$ partitions together form the training set. The classifier is trained and tested as with the hold-out method. Next, a new partition from the k possibilities is selected as the test set, and a new training set is formed from the remaining $k-1$ partitions. The process repeats a total of k times, and the average results of the k test sets are reported.

A shortcoming of k-fold cross-validation is that each of the *individual* classifiers considered is trained on a subset of the data, and hence some information is wasted. This is not a significant issue for large data sets, but in the case of a small data set such as the Falls Clinic data investigated in this thesis, it becomes more important. In the current work, k was set equal to n, the number of patients in the data set, in order to maximise the amount of training data available to each classifier. This method, n-fold cross-validation, is known more commonly as "leave-one-out cross-validation" (LOOCV).

To summarise, the technique used for cross-validation in this chapter is LOOCV, in which, repeatedly, a patient is removed from the data set (patient i), a classifier is designed using the data from the other $n-1$ patients (the training set), and finally patient i is classified using this classifier.

6.5.4 Results of Cross-Validating Classifiers

Single-parameter classifiers, cross-validated using LOOCV, were designed for tests T1–29, and the results are given in Table 6.3. These results show that one or two trends may be identifiable using traditional HRV analysis techniques, but classification was mostly inaccurate. To explain the poor performance of these tests, it should be noted that the promising results reported in the literature were attained by applying them to patients spanning a broad range of ages, rather than restricting their application to the elderly.

Several tests performed very poorly: for example, T2 and T24 had overall accuracies close to zero. This phenomenon is particular to tests which have ROC areas near 0.50, i.e. tests for which the ROC lies close to the line of no discrimination (for example, see Figure 6.6). In these cases, the appropriate threshold is very difficult to determine, since the line of no discrimination has zero convexity, unlike for

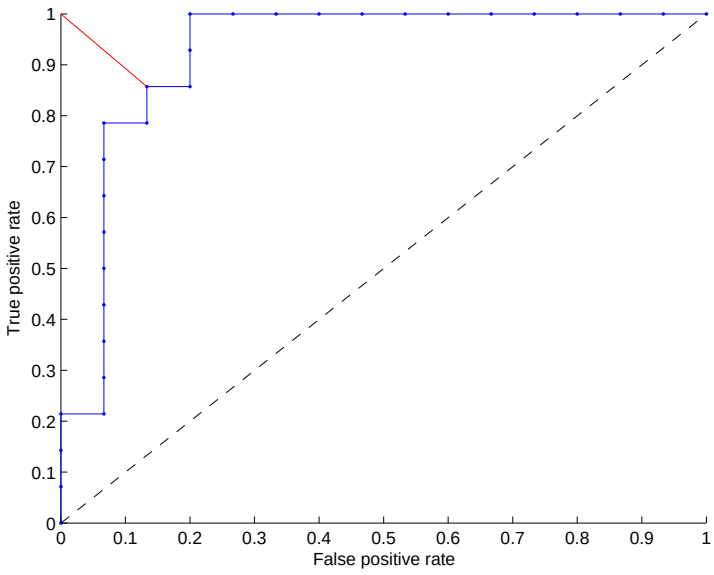

Figure 6.5: The receiver-operator characteristic (blue line) of an example data set. Each dot corresponds to a different choice of threshold to separate the two patient groups. The red line indicates the minimum distance between the curve and the point (0,1). The black dashed line is the line of no discrimination, corresponding to a classifier which makes random guesses.

example the blue line in Figure 6.5 which approaches (0,1) more clearly. When the ROC is perturbed during the removal of a single data point to form a test set for LOOCV, the selected threshold moves substantially, as demonstrated in the change from Figure 6.6 to 6.7.

6.6 Results Obtained with the New Predictors

Sample traces of the ICF for vasovagal and normal patients are shown in Figures 6.8 and 6.9. Note that the vasovagal patient experiences a greater variability in ICF after tilt. Examples of $\mathrm{Hb}_{\mathrm{diff}}$ during HUT are plotted in Figures 6.10 and 6.11. The normal subject was better able to maintain the value of $\mathrm{Hb}_{\mathrm{diff}}$ during HUT.

The tests described in Table 6.1 were applied to the Falls Clinic data, and the data are summarised in Table 6.4. All of the ICFV tests, and one of the HRT tests, yielded statistically significant results between the two patient groups. The results of LOOCV, as applied in Section 6.5 above, are given in Table 6.5.

An optimal threshold to differentiate vasovagal syndrome patients from normal subjects can be determined for most of the tests. This is represented simply by the median of the n thresholds calculated

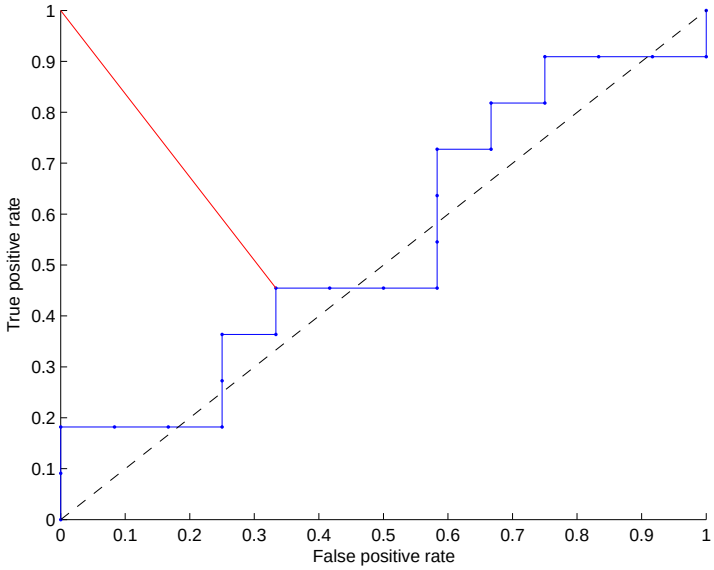

Figure 6.6: The receiver-operator characteristic (blue line) for T2, with data from the first of the thirty patients missing. The bottom-right end of the red line indicates the threshold point: in this case it was calculated that patients with values of T2 above 8.2 will be classified as having vasovagal syndrome. However, not much confidence can be placed in this finding, since the area under the curve is approximately 0.50; i.e. the blue line is in all cases close to the black line.

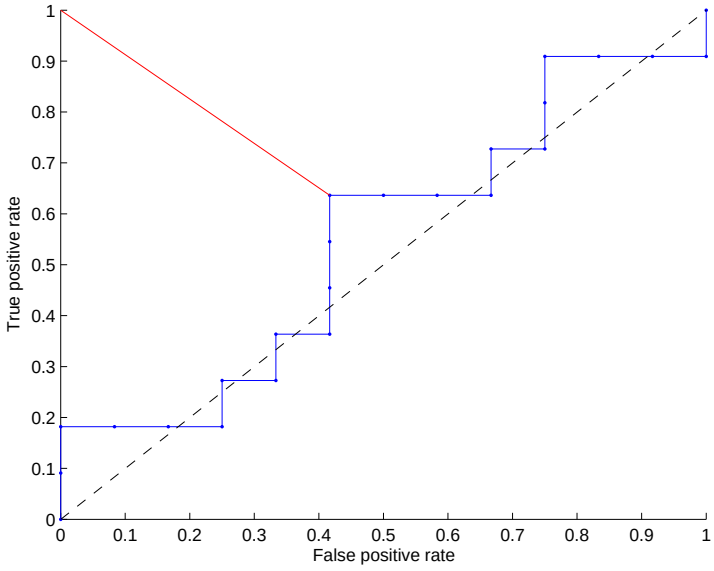

Figure 6.7: The receiver-operator characteristic for T2, with data from the second of the thirty patients missing. The perturbation in the line, as compared with Figure 6.6, has caused the threshold to change substantially: now patients with values of T2 *below* 6.5 will be classified as having vasovagal syndrome.

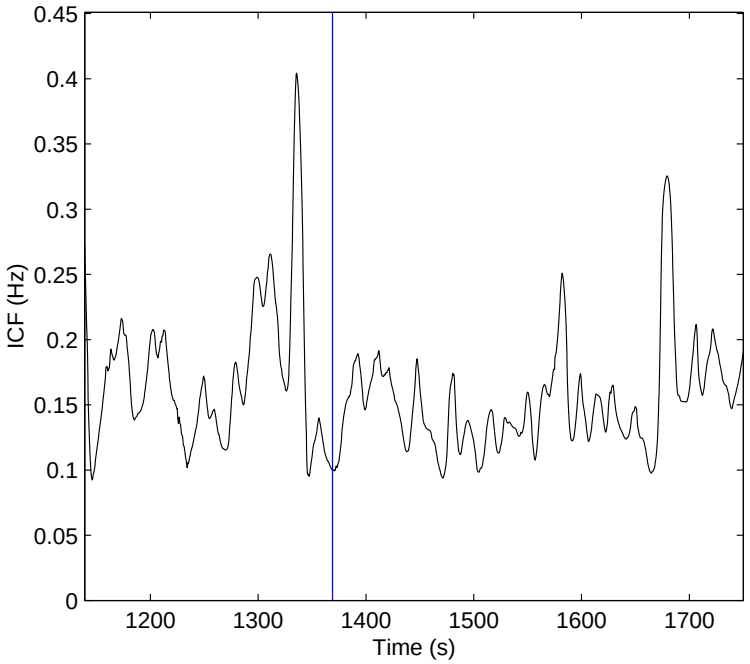

Figure 6.8: Graph of ICF for a Falls Clinic patient with a negative diagnosis of vasovagal syndrome. The blue line indicates the time of tilt.

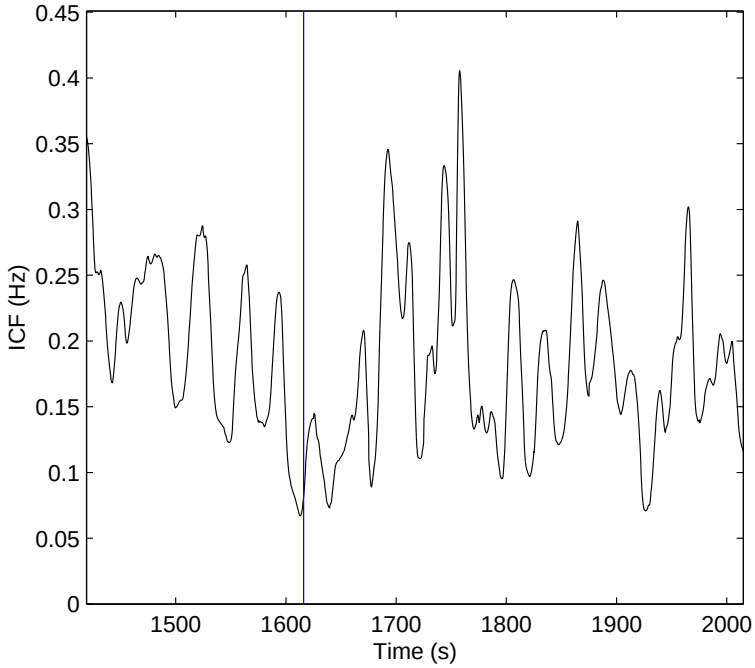

Figure 6.9: Graph of ICF for a Falls Clinic patient diagnosed with vasovagal syndrome. The blue line indicates the time of tilt.

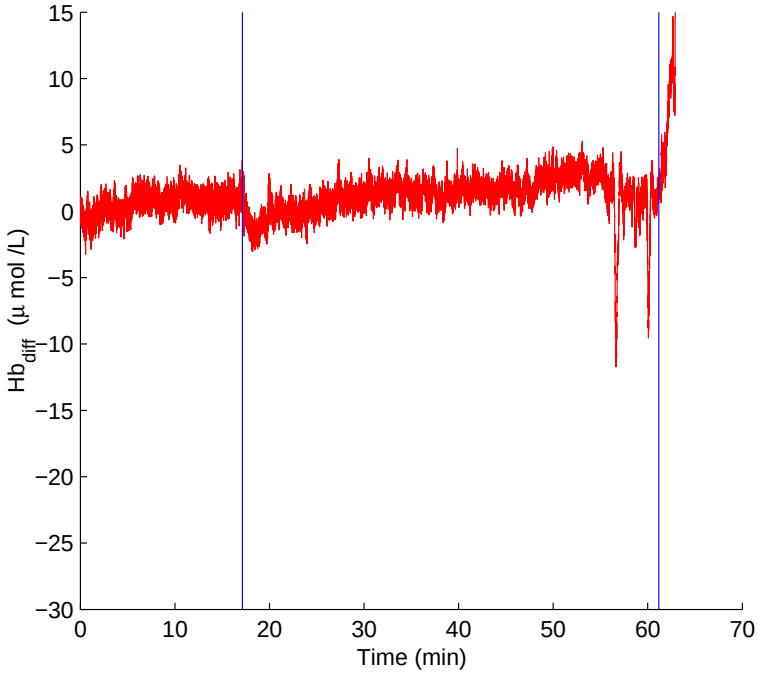

Figure 6.10: Plot of Hb_{diff} versus time for a Falls Clinic patient with a negative diagnosis of vasovagal syncope. Hb_{diff} estimates the imbalance between cerebral oxygen demand and supply; since for this patient it remains close to zero, oxygen levels in the brain remain adequate during the tilt test. The first blue line represents a tilt to the upright position, and the second blue line represents a return to the supine position.

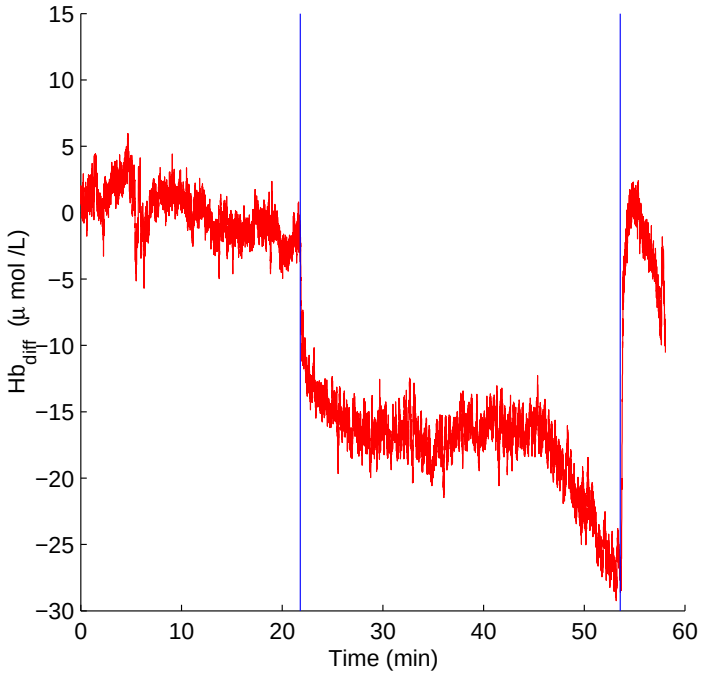

Figure 6.11: Plot of Hb_{diff} versus time for a Falls Clinic patient with vasovagal syncope. Note the decrease at the time of tilt (left blue line), followed by the precipitous drop from minutes 46 through 53, prior to syncope. Oxygen demand exceeds oxygen supply during the tilt test.

Test	μ_v	σ_v	μ_n	σ_n	Units	p value
Heart rate:						
HRT P1	-0.77	3.25	0.06	1.61	$\frac{\text{bpm}}{\text{min}}$	NS
HRT P2	-0.25	0.77	-0.10	0.61	$\frac{\text{bpm}}{\text{min}}$	NS
HRT P3	-2.76	2.37	-0.95	2.12	$\frac{\text{bpm}}{\text{min}}$	0.01
Heart rate variability:						
ICFV P1	0.064	0.020	0.048	0.026	Hz	0.02
ICFV P2	0.060	0.014	0.053	0.022	Hz	0.04
ICFV P3	0.062	0.023	0.046	0.023	Hz	0.01
Cerebral behaviour:						
HDD	-1.52	3.69	-0.997	2.20	$\frac{\mu\text{mol}}{\text{L}}$	NS
LFO_2	4.06	6.99	3.38	4.21	–	NS

Table 6.4: Wilcoxon rank sum results for eight tests developed for the current research. See Table 6.2 for a description of the symbols, and Section 6.4 for a description of the tests.

by LOOCV. In each case, this data set is the same as that used to generate the corresponding values in Table 6.5.

For HRT, the optimal threshold was found to be -1.94 beats/min^2 during P3. The classifier tested whether the heart rate changed at a rate faster or slower than approximately -2 beats/min^2 over the course of the time period P3. Similarly, for ICFV, the optimal threshold to differentiate vasovagal syncope patients from normal subjects was 0.056 Hz during P3. A threshold for the NIRS parameters was impossible to obtain owing to the lack of discrimination in these parameters.

For each of the tests, the number of patients is not large enough to consider splitting the data set into a training and test set, to confirm the accuracy of the optimal threshold. Instead, the overall accuracy (percentage correctly classified) and other metrics can be plotted to evaluate the behaviour of classification as the choice of threshold varies. The plots for the best classifier, ICFV P3, are given in Figure 6.12.

6.6.1 Discussion

From the table, it is clear that the HRT and NIRS signals are not good predictors of syncope among the Falls Clinic patients. The new ICFV technique performed generally better than the HRT and NIRS tests and better than the existing predictors found in the literature. The ICFV results may imply that some elderly vasovagal patients experience a greater degree of haemodynamic instability immediately after the

Test	ROC Area	Sensitivity	Specificity	PPV	NPV	Accuracy
Heart rate:						
HRT P1	0.61	0.50	0.50	0.39	0.61	0.50
HRT P2	0.52	0.39	0.43	0.30	0.52	0.41
HRT P3	0.73	0.72	0.68	0.59	0.79	0.70
Heart rate variability:						
ICFV P1	0.88	0.67	0.71	0.60	0.77	0.69
ICFV P2	0.92	0.78	0.71	0.64	0.83	0.74
ICFV P3	0.94	0.78	0.86	0.78	0.86	0.83
Cerebral perfusion changes:						
HDD	0.52	0.20	0.00	0.11	0.00	0.08
LFO_2	0.53	0.30	0.53	0.27	0.56	0.45

Table 6.5: Leave-one-out cross-validation performance of eight tests developed for the current research. PPV = Positive Predictive Value, NPV = Negative Predictive Value. See Section 6.4 for a description of the tests.

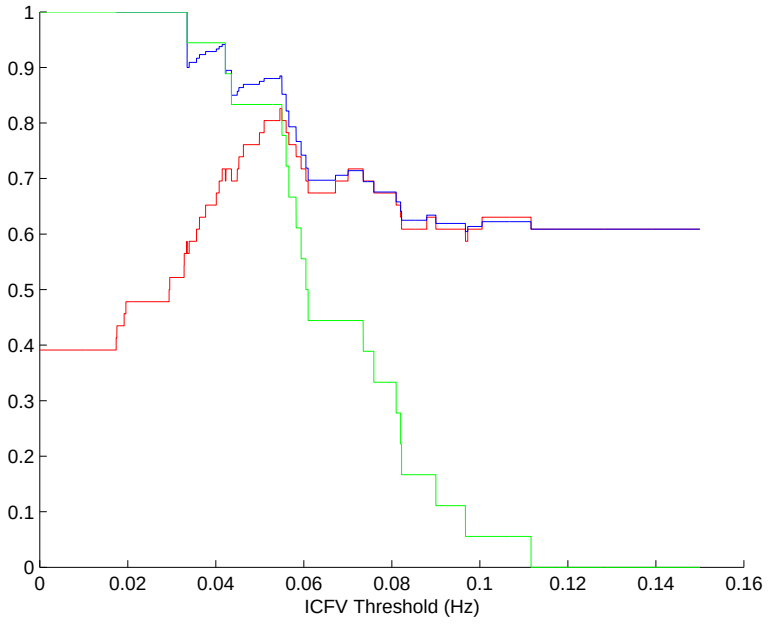

Figure 6.12: Classification accuracy (red line), negative predictive value (blue line), and specificity (green line) versus ICFV P3 threshold. As expected, the accuracy peaks at the optimal threshold of 0.056 Hz, calculated as the median of the thresholds used in the leave-one-out cross-validation.

early response to tilt is complete.

The inability to classify patients using HRT represents a partial negative result. Contrary to the hypothesis presented in Section 6.4.1, elderly patients appear to be able to maintain approximately adequate HR in the early response to upright tilt, regardless of their propensity to faint.

The classification inaccuracies involving the NIRS data may have been due in part to instrumentation error. For example, the change in Hb_{diff} on standing was not negative for all subjects, which represents an

unexpected finding. In addition, it may be that cerebral perfusion changes during the early response to tilt are broadly similar for vasovagal patients and nonvasovagal subjects, despite differences seen among other orthostatic conditions in the literature such as pure autonomic failure or multiple system atrophy [40].

Since 18 patients were analysed using ICFV P3, the number of false negatives can be calculated from Table 6.5 to be two, or less than 9%. This led to a NPV of 0.86. In contrast, the highest NPV observed among the tests taken from the literature was 0.83 (see T14 in Table 6.3). Hence ICFV P3 outperforms the best test previously proposed, in this data set. However, the number of false negatives is still too high by clinical standards: recall that if HUT is aborted based on the (negative) results of the prediction, the diagnosis of vasovagal syndrome will never be made. The patient may then be erroneously assigned an alternate diagnosis, perhaps resulting in improper medication. The number of false negatives is reduced to zero if the choice of threshold is lowered from 0.056 Hz to 0.033 Hz, as can be seen in Figure 6.12; however, this occurs at the expense of overall accuracy, which is reduced to an unacceptable 0.59. At a threshold of 0.056 Hz, the accuracy, NPV, and PPV are 0.80, 0.86, and 0.78 respectively.

6.6.2 Multi-parameter Classifier

The combination of several discriminatory parameters can in some cases yield results better than classification based on a single parameter. Here two of the most accurate published predictors (T23 and T25 — see Table 6.3) are combined with the two most accurate new predictors (HRT P3 and ICFV P3), in a four-parameter classifier. The number of patients for whom all four parameters may be calculated is 40 (15 vasovagal and 25 nonvasovagal), which is reduced to 30 patients (15 patients of each type) in the balanced data set in the analysis that follows.

A linear classifier was constructed to combine the four parameters:

$$y = a_0 + \sum_{i=1}^{4} a_i x_i \tag{6.2}$$

where the classifier output y is intended to be positive for vasovagal syndrome patients and negative for nonvasovagal patients, a_i are the linear coefficients (weights), and x_i are the four parameters. These parameters were adjusted to have zero mean and unit variance, so that later, the relative effect of each of the four on y could be compared by simply examining the magnitudes of a_i.

To maximise the discriminatory capability of y, the weights a_i were set as follows. Let V and N

represent the set of vasovagal and nonvasovagal patients, respectively, with mean feature vectors μ_V and μ_N. The covariance matrices of the two classes are

$$\Sigma_V = \frac{1}{M_V} \sum_{n \in V} (\mathbf{x}^n - \mu_V)(\mathbf{x}^n - \mu_V)^T \tag{6.3}$$

$$\Sigma_N = \frac{1}{M_N} \sum_{n \in N} (\mathbf{x}^n - \mu_N)(\mathbf{x}^n - \mu_N)^T \tag{6.4}$$

where M_V and M_N represent the number of points $\mathbf{x}$ in the vasovagal and nonvasovagal classes, respectively. From these, the within-class scatter matrix [135] can be computed as a weighted sum of the class covariance matrices:

$$\mathbf{S}_W = \frac{M_V}{M}\Sigma_V + \frac{M_N}{M}\Sigma_N \tag{6.5}$$

where $M = M_V + M_N$. The between-class scatter matrix $\mathbf{S}_B$ is the weighted covariance of the class means:

$$\mathbf{S}_B = \frac{M_V}{M}(\mu_V - \mu)(\mu_V - \mu)^T + \frac{M_N}{M}(\mu_N - \mu)(\mu_N - \mu)^T \tag{6.6}$$

where μ is the mean of all feature vectors. A method known as canonical variates analysis (CVA) can maximise the ratio of these two scatters, by optimising the choice of projection vectors $\mathbf{u}_i$ in the expression

$$\frac{\mathbf{u}^T \mathbf{S}_B \mathbf{u}}{\mathbf{u}^T \mathbf{S}_W \mathbf{u}}. \tag{6.7}$$

It can be shown [135] that the vectors which maximise Equation 6.7 are generalised eigenvectors of $\mathbf{S}_W$ and $\mathbf{S}_B$, i.e. solutions of the equation

$$\mathbf{S}_B \mathbf{u} = \lambda \mathbf{S}_W \mathbf{u}. \tag{6.8}$$

In a problem with p classes, CVA produces $p - 1$ eigenvectors; here, $p = 2$ (vasovagal vs. nonvasovagal) so the one eigenvector produced corresponds to the single optimal projection vector for the data.

Using this technique, the five weights a_i were determined 30 times, using a division into training and test data sets that mirrored the leave-one-out methodology described earlier in this section. The plot of

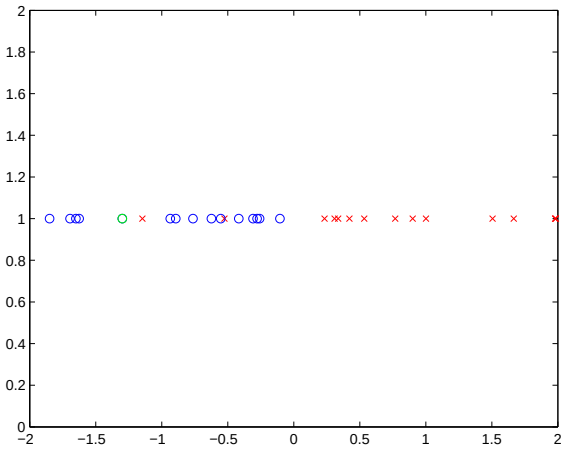

Figure 6.13: The results of a linear classifier using four input parameters: T23, T25, HRT P3, and ICFV P3. Red crosses represent vasovagal syndrome patients and blue circles represent patients without the syndrome. The green circle represents the test patient in a given run, who is classified correctly as not having vasovagal syndrome.

y for an example run is given in Figure 6.13; note that 29 patients are depicted in red and blue in the diagram, as this is the size of every training data set. (The 30th patient is green.)

In this manner the optimal weights for the linear classifier were calculated as the mean of the 30 runs, viz. $\{a_1, a_2, a_3, a_4\} = \{0.186, -0.000217, -0.251, 0.821\}$. The average PPV, NPV, and overall accuracy for the linear classifier were found to be 0.93, 0.88, and 0.90 respectively. These values are higher than those achieved with the best-performing single-parameter classifiers (0.78, 0.86, and 0.83 respectively; see Table 6.5).

6.7 Conclusion

This chapter reported on new syncope predictors, investigated in an attempt to differentiate positive from negative tilt test results from the first few minutes of data recorded after tilting. The significance of finding a predictor of vasovagal syncope positivity during the early stage of HUT cannot be over-emphasised. If the test could be terminated early for some patients, the time saved would enable a greater number of patients to undergo the procedure. At present, many patients who would benefit from HUT are not offered the test, due to healthcare resource limitations. Thresholds for ICFV and HRT were found to be 0.056 Hz and -1.94 beats/min^2, respectively. Although not all of the algorithms, tested using LOOCV, performed as accurately as expected, the ICFV techniques performed well. The accuracy was still less

than 100%, but this may have been due to factors beyond the control of any algorithm, such as the expert labels concerning which patients had vasovagal syndrome and which did not; the inherent reproducibility problems related to HUT; instrumentation limitations, etc. Importantly, ICFV also performed better than the methods published previously.

Four of the most predictive parameters were input to a linear classifier, in an effort to combine their capabilities. The overall accuracy and the negative predictive value were 0.90 and 0.88 respectively. These figures are slightly better than those of the best individual classifiers (0.83 and 0.86, respectively).

An important question to consider is whether data-driven syncope prediction of any higher accuracy (slightly closer to 100%) is possible in such a heterogeneous population. The next two chapters will investigate whether physiological modelling can enhance the ability of a signal analysis system to predict syncope.

Chapter 7

The Cause of Vasovagal Syncope

7.1 Introduction

Vasovagal syncope involves a reversal of cardiovascular tone which has puzzled researchers for decades. Suddenly, blood pressure transitions from a stable pattern to one of dramatic collapse; an elevated heart rate may give way to a bradycardia; plasma catecholamine levels alter markedly; systemic vasoconstriction is replaced by abrupt vasodilation. As mentioned in Chapter 2, the trigger of this rapid withdrawal of the sympathetic nervous system is poorly understood and hotly debated.

Prior to the development of any informed model to predict the occurrence of vasovagal syncope, the most important physiological factors must be identified. The next section outlines the physiology required to underpin the modelling; this is complemented by a description of the nervous system in Appendix B. Following the physiological background is an identification of three possible syncopal mechanisms, and the details of the pathways in each case. The purpose of this chapter is to describe these pathways in preparation for the model development which will occur in Chapter 8.

7.2 Physiological Background

7.2.1 Genesis of Vasovagal Syncope

Many stimuli are known to evoke vasovagal syncope and other forms of neurocardiogenic syncope; the primary causes were listed in the left column of Figure 2.4. Elements such as hypovolaemia, the sight of blood, boredom, stuffy rooms, and prior consumption of alcohol can also act to antagonise the car-

diovascular system to increase the likelihood of syncope [201]. The stimuli most relevant to the present research are prolonged standing or HUT, and emotion (e.g. fear, stress, anxiety).

It is fortunate that, from a haemodynamic point of view, the effects of vasovagal syncope appear not to depend on the type of external stimulus, whether it is emotion, pain, prolonged standing, lower body negative pressure, or head-up tilt [90, 167]. The existence of this common final pathway simplifies the approach to modelling. Carotid sinus syndrome will be excluded for the present time as it is a form of neurocardiogenic but not vasovagal syncope, and is believed to differ slightly in its outcome (most notably, bradycardia is more often implicated).

7.2.2 Afferent Pathways: The "Inputs" for Vasovagal Syncope

As can be seen from Figure 2.4, the afferent (incoming) signal triggering vasovagal syncope often originates from the central nervous system (shown specifically as the cerebral cortex) or from the peripheral nervous system (shown as various receptors). Appendix B offers a brief outline of these two nervous systems. A third source (not shown) is the humoral system, and these three sources comprise the three paradigms to be considered in Section 7.3.

7.2.3 The Integration of the Vasovagal Response

It is not known precisely what role the brain plays in the vasovagal response. Several of the proposed triggers for vasovagal syncope discussed in this chapter rely on the existence of a "Vasovagal Syncope Centre" (VSC) in the brain, responsible for integrating inputs and initiating a vasovagal response when necessary. Reasonable candidates for the VSC are:

- The hypothalamus
- The medulla
- The cerebrum: insular cortex, temporal lobe, anterior cingulate gyrus
- An interaction among the above

The most likely locations of a VSC are within the hypothalamus or the medulla (in particular, the NTS) [162]. Mohrman *et al.* [130] state that depressor centres in the anterior hypothalamus, which can receive signals from the cortex, activate a region within the medullar cardiovascular centres to initiate

the vasovagal response. This is in agreement with Hainsworth *et al.* [90], who explain that the electrical stimulation of a localised region of the hypothalamus elicits the characteristic pattern of bradycardia and peripheral vasodilation. It is interesting that this stimulated region is just lateral to the "defence area" (see Appendix B) — based on that connection, Hainsworth *et al.* hypothesise that the VSC is either triggered by the defence area, or that the VSC is activated by similar emotional inputs to the defence area but at a higher threshold [90]. These hypotheses have not been tested clinically.

Some cases of vasovagal syncope may be caused by localised seizure activity resulting from a vascular anomaly, tumour, or other cause, within the cerebral cortex. Direct electrical stimulation of the anterior cingulate gyrus, i.e. the cortical section of the limbic system, has been shown to produce a vasovagal response in cats [64]. Two other particular areas of interest are the insular cortex, located between the frontal and temporal lobes [13], and the temporal lobe itself [64].

Finally, Aaronson *et al.* [1] believe that a single vasomotor centre in the brainstem does not exist; rather, control may lie in the interaction amongst the brainstem, hypothalamus, cerebral cortex, and cerebellum. This is likely to be the case in at least some episodes of neurocardiogenic syncope.

7.2.4 Efferent Pathways: The Symptoms of Vasovagal Syncope

More is known about the efferent pathways of vasovagal syncope than its initiation and integration. Recall from Chapter 1 that the compound term "vasovagal" refers firstly to vasodilation and secondly to bradycardia. The vasodilation is believed to be caused by a sympathetic withdrawal, often [14] but not necessarily [131,172] following intense sympathetic activity. Although this withdrawal causes vasodilation, the symptoms may be confined to the muscle vasculature as opposed to that of the skin and bone, which may even vasoconstrict [169].

On the other hand, the bradycardia is not a result of sympathetic withdrawal, being vagally mediated. It is also known that the bradycardia presents in patients less often than the vasodilation, and it is for this reason that vasovagal syncope is often referred to as "vasodepressor" syncope instead [167]. Since the sympathetic and parasympathetic nervous systems have a push-pull effect on one another, the sequence of their activities throughout the environmental stimulus is probably very important in determining the precise nature of the symptoms [13]. Large increases in circulating catecholamines (adrenaline and noradrenaline) have often been seen prior to syncope, and these may play several roles as well.

The symptoms associated with vasovagal syncope are extreme, and it is possible that peripheral mech-

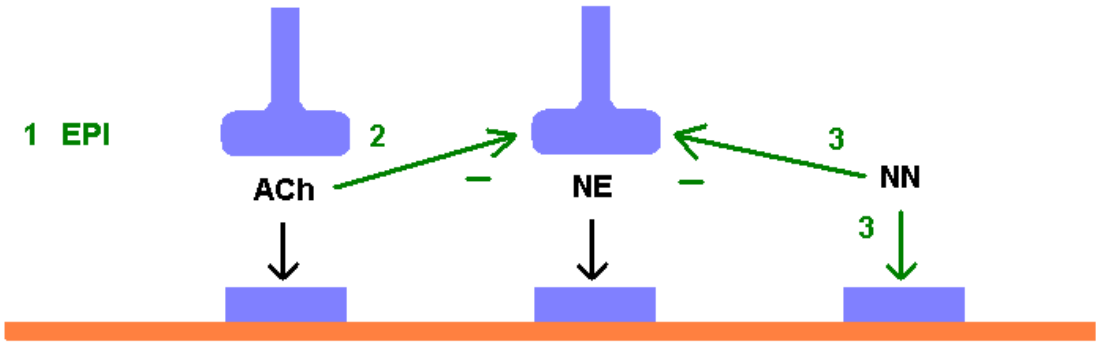

Figure 7.1: Three potential peripheral contributors to vasovagal syncope. The rectangles represent, from left to right, receptors for parasympathetic, sympathetic, and neurohumoral inputs in a blood vessel. The numbers correspond to the enumerated pathways in the text. ACh = acetylcholine, EPI = epinephrine, NE = norepinephrine, NN = noncatecholamine neurohumours, minus signs (–) = presynaptic inhibition.

anisms, not just a VSC, assist in their production. In other words, perhaps the dramatic vasodilation and bradycardia are a result not just of a centrally-mediated phenomenon, but also of end-organ hypersensitivity. Benditt [13] lists three possible peripheral enhancements which may accompany the vasovagal response (see Figure 7.1):

1. **Accentuated receptor antagonism:** The sympathetic mediator epinephrine acts somehow at the heart to accentuate the parasympathetic drive towards bradycardia, as well as at peripheral blood vessels to accentuate parasympathetically-mediated vasodilation.

2. **Presynaptic feedback inhibition:** Acetylcholine is known to inhibit noradrenaline release, and could hence accentuate a vasodilation driven by sympathetic withdrawal.

3. **Circulating hormones other than adrenaline and noradrenaline:** These include vasoactive peptides (e.g. vasoactive intestinal peptide, calcitonin gene-related peptide) and purinergic agonists (e.g. adenosine) which have been found in increased concentrations near the time of syncope. Once released from perivascular nerves, these hormones elicit a direct vasodilatory effect through specialised receptors, and may decrease norepinephrine release from the sympathetic nervous system.

7.3 Physiology of the Three Vasovagal Syncope Paradigms

7.3.1 The Bezold-Jarisch Reflex

The Bezold-Jarisch reflex is a concept which originated in 1867 from the Austrian dermatologist Albert von Bezold and was revisited extensively in 1937 by Adolf Jarisch, Jr. In 1956, Sharpey-Schafer first proposed that it could be responsible for vasovagal syncope [172]. Following the now famous experiments of Öberg *et al.* published in 1972 [141], linking the reflex to vasovagal syncope in cats, it has been considered the most likely cause for fainting in humans, albeit with reservations. The Bezold-Jarisch reflex is occasionally described as the definitive component of vasovagal syncope [24, 25], although most researchers are more circumspect.

Important to the reflex are anti-hypertensive chemoreceptors [1, 169] or more likely mechanoreceptors [13, 66, 96] in the left ventricle of the heart, providing feedback via unmyelinated C fibres to the medulla. These receptors are ordinarily responsible for signalling increases in blood pressure; hence, as expected, their activation can lead to drastic medullar measures to lower the blood pressure — notably sinus bradycardia and/or peripheral vasodilation. (It is quite possible that the aforementioned Vasovagal Syncope Centre plays a role here.) A summary of the reflex is illustrated in Figure 7.2.

The hypothesis proposed by Sharpey-Schafer is that prior to syncope, the cardiac left ventricle contracts forcefully around a relatively small stroke volume; hence the aforementioned ventricular receptors become activated accidentally, and the Bezold-Jarisch reflex is initiated. When this incorrect signal is presented to the medulla, blind sympathoinhibition and parasympathetic activation ensues. Following the resulting dramatic fall in blood pressure and/or heart rate, syncope becomes unavoidable.

The question of whether this cardiac underfilling coupled with excessive force of contraction is sufficient to cause vasovagal syncope has been a matter of debate. Several problems exist with the hypothesis:

1. Vasovagal syncope, or at least its vasodilatory component, can occur in heart transplant patients [49]. As the afferent pathway of the Bezold-Jarisch reflex has obviously been severed in such cases, this is the most prevalent obstacle to accepting the reflex as the only cause of vasovagal syncope.

2. Not all episodes of vasovagal syncope are preceded by a nearly empty left ventricle, nor a high cardiac contractility [73]. Moreover, several studies have refuted the common claim that sympathetic activity is always heightened in the minutes prior to its eventual syncopal withdrawal [131, 172].

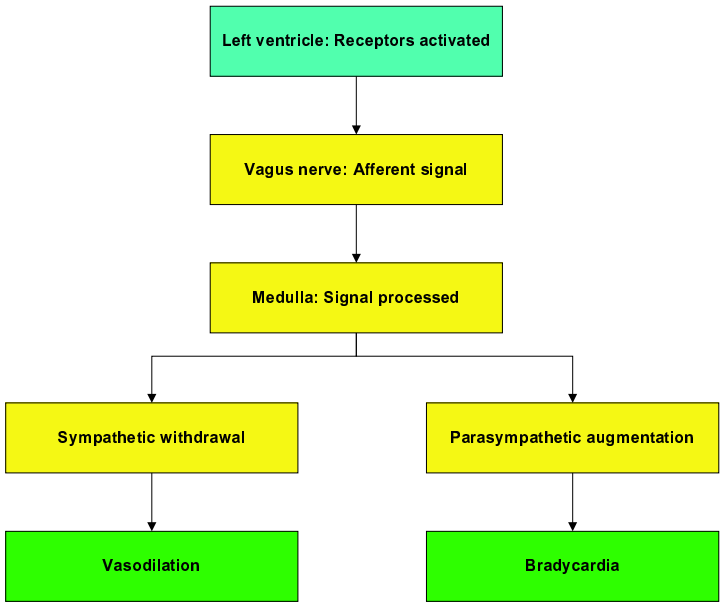

Figure 7.2: The Bezold-Jarisch reflex.

3. Recent experiments involving the sympathetic activation of near-empty dog hearts were unable to initiate the Bezold-Jarisch reflex [228]. Further, owing to ethical approval limitations the reflex has not once been demonstrated in humans as a cause for vasovagal syncope [86].

A fourth contention perhaps of less importance is the possibility of the transience of the reflex. Hainsworth [73] states that upon initiation of the reflex, the baroreceptors would become unloaded very quickly — the implication being that there should exist an immediate compensatory mechanism. However, baroreceptors should not be expected to perform in such extreme hypotension: Berne *et al.* [20] indicate that baroreceptors are ineffective below a certain threshold, usually a mean arterial pressure of about 60 mmHg (although this varies from subject to subject). Benditt [66] suggests that an interaction of central and peripheral elements may disable the baroreceptors during vasovagal syncope. Hence the transience of the effects of a Bezold-Jarisch reflex is a possible but unlikely concern.

In short, several serious issues cast doubt on the plausibility of the connection between syncope and the Bezold-Jarisch reflex. However, the lack of a convincing alternative — coupled perhaps with the momentum acquired during several decades — has sustained the Bezold-Jarisch reflex's position in the literature as the primary suspect for vasovagal syncope.

7.3.2 Central Nervous Processing

The fact that the brain is involved in the vasovagal response is not disputed. Many healthy people experience their only fainting episodes in life as a result of emotional or painful stimuli, such as fear or venipuncture. The more interesting question is whether the role of the brain in syncope ends there. In other words, must a vasovagal syncope stimulus, such as prolonged standing, extreme emotion, etc., affect the heart excessively and thereby initiate a Bezold-Jarisch reflex? Or can the loss of consciousness originate from a more direct mechanism?

While the pathways of the PNS were illustrated clearly in Figure 2.4, triggers within the CNS are more difficult to map. However, it can be expected that errors in central processing would leave a biochemical mark in the brain. Indeed, a few centrally-released neurotransmitters, many of which have been found in elevated concentrations prior to syncope, have been implicated in triggering or integrating the vasovagal response in the brain:

- Serotonin
- Nitric oxide
- Opioids (especially endorphins)
- Pancreatic polypeptide
- Vasopressin[1]

More generally, it has been suggested that the response of the brain to a signal generated elsewhere in the body, or the alteration of processing by central pathways, or both, may cause vasovagal syncope [73, 90, 172]. Details of most of these claims are sparse, but opioids [74] and serotonin [67] seem to be under particular scrutiny. For example, serotonin levels increase substantially prior to vasodilation, and serotonin blockade may curb vasodilation [67]. In addition, a decrease in cerebral perfusion, such as occurs during prolonged tilt in some patients, may lead to a small cerebral ischaemia. This ischaemia in turn may initiate a vasospasm [65] beginning a chain of events leading to syncope.

In either the case of neurotransmitter problems or ischaemia, a Vasovagal Syncope Centre (see Section 7.2.3) in the brain might be triggered by cerebral neural activity, rather than by the Bezold-Jarisch reflex. Figure 7.3 summarises the three most likely pathways.

[1] Although vasopressin acts as a neurotransmitter in the brain, its hormonal aspects will also be addressed in Section 7.3.3.

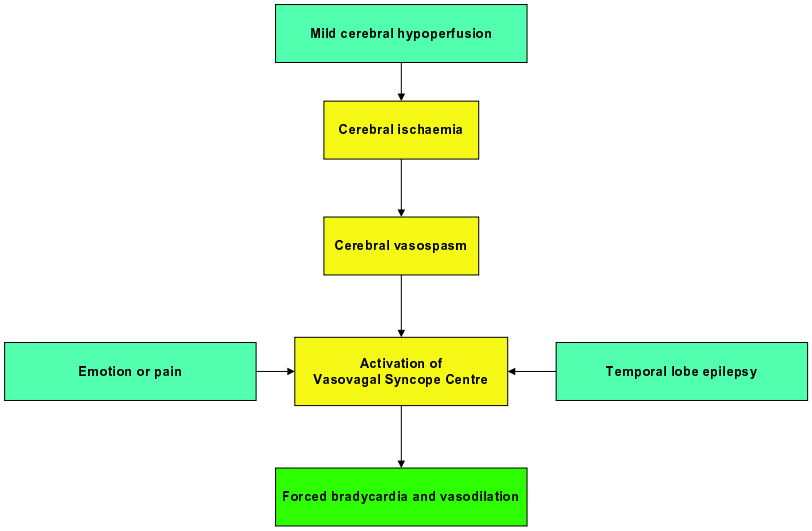

Figure 7.3: The role of the putative cerebral Vasovagal Syncope Centre, examining three possible CNS input paths. Note that only one of the three inputs (blue) would ordinarily be activated for a given syncopal episode.

7.3.3 The Endocrine System

Arterial baroreceptors act as dampeners of sudden fluctuations in blood pressure; however, they are only able to mitigate short-term disturbances owing to a resetting mechanism, to be described later in this section. In this sense, they act merely as band-pass filters. For the long-term control of blood pressure and blood volume the body relies on the endocrine system (hormones), notably vasopressin and the outputs of the RAA (renin-angiotensin-aldosterone) system [226]. For example, plasma vasopresssin has been found in elevated concentrations prior to vasovagal syncope [74, 171]. The RAA system, used for medium- and long-term control of arterial blood pressure [167], has recently been described as "crucial" for preventing syncope in healthy people [3].

Vasopressin

Vasopressin, also known as ADH (antidiuretic hormone), is a peptide whose normal function is to suppress renal water excretion. It is produced in the hypothalamus when a rise in osmolality[2] is detected by specialised receptors. However, vasopressin is also produced when pressure receptor traffic decreases, i.e. when blood pressure decreases.

In raised concentrations, usually resulting from a decrease in blood pressure, vasopressin adopts a

[2]Osmolality is defined as the concentration of osmotically active particles per kg of water. In the blood, 95% of these particles are the ions Na^+, Cl^-, and HCO_3^-.

more cardiovascular role. The hormone acts as a vasoconstrictor in most tissues, except in the brain and heart — where it functions as a vasodilator. As a result of this inconsistency, vasopressin redistributes blood to the two most important organs during episodes of hypovolaemia (low blood volume).

A third role of vasopressin which may be important in the context of vasovagal syncope is the resetting of baroreceptors. The reason that baroreceptors are only useful for short-term regulation is that in the face of long-term challenges, they are adjusted to new operating points. It is thought that in some patients, such resetting may be responsible for initiating the vasovagal attack [86]. Indeed this process has been shown to launch a positive feedback loop leading to rapid hypotension, during experimentation with haemorrhage [221]. (As explained in Chapter 8, haemorrhage and prolonged standing share several similarities.)

The resetting might be accomplished by a sudden release of endogenous opioids in the brain (see Section 7.3.2), which has been observed during haemorrhage [133]. It may also be accomplished by circulating vasopressin, since this hormone enhances baroreflex inhibition of the sympathetic nervous system [52]. Indeed, high vasopressin concentrations have been observed prior to syncope [171], and the carotid sinus baroreceptors have long been considered a possible site of the vasovagal syncope trigger [108, 223].

In summary, while vasopressin mainly serves the purpose of fluid retention in the kidneys, in higher concentrations triggered by hypovolaemia its blood redistributive effects become evident. In addition, it greatly enhances reflexes and in particular baroreflexes.

The Renin-Angiotensin-Aldosterone System

The kidneys play the dominant role in controlling blood volume, through the RAA system as summarised in Figure 7.4.

Renin: Renin is an enzyme released by the kidneys under any of four conditions: low renal arterial perfusion pressure, low delivery of sodium chloride to the kidneys, an increase in renal sympathetic nerve activity, or an increase in circulating catecholamines. Hence, there are several ways in which low blood volume or pressure can be sensed by the organ.

Angiotensin: Renin cleaves the plasma alpha-2-globulin "angiotensinogen", to liberate a decapeptide called angiotensin I. Angiotensin I is then cleaved further by an enzyme found on the the surface of

endothelial cells: ACE (angiotensin converting enzyme). The result of this activity, which occurs mostly in the lung blood, is an octapeptide called angiotensin II.

Aldosterone: Angiotensin II drives the release of the steroidal hormone aldosterone from the adrenal cortex.

The two hormones angiotensin II and aldosterone represent the primary functional products of the RAA system. The effects of angiotensin II are to increase blood pressure through:

(a) Direct vasoconstrictor action on the vascular smooth muscle

(b) Neuromodulation to increase the impact of sympathetic nerve activity, locally at various places in the body

(c) Stimulation of sympathetic vasoconstrictor outflow from the brainstem

(d) Suppression of any reflex bradycardia initiated from the brainstem

(e) Enhancement of Ca^{2+} current in the heart, to increase cardiac contractility

It also increases blood volume through:

(f) Promotion of vasopressin release

(g) Inhibition of natriuresis (excreting Na^+ in the urine)

(h) Development of thirst

The effects of aldosterone are to bolster blood volume by retention of Na^+ in the kidneys, and reabsorption of Na^+ from several glands (e.g. salivary, sweat).

It has been proposed [220] that some patients with cardioinhibitory vasovagal syncope suffer from a blunted activation of the RAA system upon standing. As a result, the sympathetic nervous system must work harder to address the orthostatic challenge, and syncope results when that system eventually fails to compensate completely.

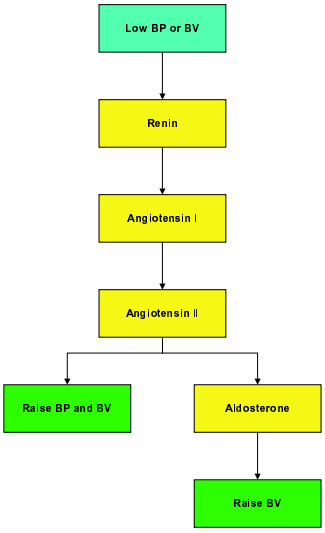

Figure 7.4: A summary of the RAA system. See text for the specific effects of angiotensin II and aldosterone. BP = blood pressure, BV = blood volume.

7.4 Conclusion

This chapter has described three possible causes of vasovagal syncope: the Bezold-Jarisch reflex, central nervous processing, and the endocrine system. Each of these causes is a contender worthy of modelling; unfortunately, given that the Falls Clinic patients are non-invasively monitored, there is a limit on which pathways could be modelled with confidence. The next chapter describes the construction of a model which can incorporate as many of the relevant parameters as possible.

Chapter 8

Physiological Modelling

8.1 Introduction

As was discussed in Chapter 1, investigation with multiple parameters can be supported by physiological modelling to progress beyond mere "black box" analysis. Hence, in this chapter, candidate models from the literature are reviewed for their relevance to the prediction of orthostatic vasovagal syncope. This is followed by a description of the model created for the current work (referred to as the Orthostasis Model). Finally, the method used to estimate the key parameters in the model is explained and applied to the problem of syncope prediction.

8.2 Foundations of the Physiological Model

Since the late 1960s, several groups have attempted to model the response of the human cardiovasculature to short-term orthostasis [29,41,48,80,104,154,193] and/or lower-body negative pressure [41,77,80,128, 129,154,197]. This activity is summarised in Table 8.1. None of the models contains all of the elements needed for the present work; during the early stages of model development it was decided to choose the most relevant model and extend it as appropriate.

A deterministic, lumped-parameter model was chosen for the task of representing the human cardiovasculature. Since the aim of the latter is to monitor and control blood flow through various compartments with different properties, a system of ordinary differential equations (ODEs) such as those provided by most of the models in Table 8.1 is appropriate; introducing PDEs or stochastic processes would have added an unnecessary layer of complexity. Most of the models are nonlinear, since they make use of ex-

Principal author	Year	Purpose	Pulsatile	Reference
Orthostasis Models:				
Snyder	1969	Tilt	Yes	[193]
Boyers	1972	Tilt	No	[29]
Croston	1974	Tilt, LBNP	Yes	[41]
Leonard	1979	Tilt	No	[104]
Melchior	1992	LBNP	No	[128]
Sud	1993	LBNP	Yes	[197]
Melchior	1994	LBNP	Yes	[129]
Heldt	2002	Tilt, LBNP	Yes	[80]
Peterson	2002	Tilt, LBNP	Yes	[154]
Hao	2003	LBNP	Yes	[77]
Fink	2004	Tilt	No	[48]
Related Models:				
Beneken	1967	Blood loss	Yes	[16]
Guyton	1967	Long-term circulation regulation	No	[69]
Guyton	1972	Long-term circulation regulation	No	[70]
Srinivasan	1972	Various	No	[195]
deBoer	1987	Baroreflex	Yes	[42]
Ursino	1994	Baroreflex	No	[215]
Ursino	2000	Hypoxia, haemorrhage	Yes	[217]
Ursino	2000	Cerebrovasculature	N/A	[219]

Table 8.1: Cardiovascular models from the literature. The "Purpose" of some of the Related Models has been simplified to relate them to the current work. N/A = Not applicable (the cerebrovascular model [219] was validated for non-pulsatile flow but can nonetheless be connected to some pulsatile models of the systemic vasculature).

ponential, logarithmic and sigmoidal relationships, as well as multiplying or dividing the state variables by one other. Although nonlinearity increases complexity, it does not pose too great a computational challenge in the present work.

The clearly defined and carefully validated Ursino models [215,217,219] were chosen to set the foundations for the current work. Once these three models were combined to form a single system of equations, the resulting model was then modified to accommodate orthostasis by adding and subtracting several mechanisms. While doing so, the aim was to create an assembly with the following subsystems, collectively referred to as the "Orthostasis Model":

Haemodynamics:	• Lumped parameter compartments (volumes, resistances, and compliances)
Cerebrovasculature:	• Primarily cerebral autoregulation
Feedback regulation:	• Sympathetic and parasympathetic, afferent and efferent pathways • Effectors
Posture:	• Viscoelastic properties of smooth muscle • Hydrostatic pressure changes • Venous collapse • Blood pooling in dependent areas • Decreased compliance at high pressure

The Orthostasis Model is capable of simulating most of the cascade of the physiological response to standing, illustrated in Figure 8.1. The diagram was created based on a literature review of the main activities which occur as a subject stands [13, 57, 72, 74, 89, 138, 158, 167, 174, 183, 226]. The three green boxes depict the main challenge which must be overcome: less blood is available for the heart to pump. The central vertical column depicts what activities occur immediately upon standing, leading finally to the box labelled "arterial blood pressure decreases". The pathways in the lower left and lower right of the diagram illustrate the response of stretch receptors. The pathways in the upper left and upper right of the diagram represent, respectively, very fast and very slow mechanisms which provide extra compensation to the orthostatic challenge.

While this flowchart does not encapsulate all equations in the model, it does summarise the salient activities of interest as a subject stands up. The angiotensin II response in the upper right of the figure (discussed in Chapter 7), and the muscular response in the upper left (not applicable in the case of passive standing) were excluded from the Orthostasis Model for the purposes of syncope prediction.

Haemodynamics lies at the heart of the model, and an overview is presented in Figure 8.2.

8.3 The Ordinary- and Delay Differential Equations

The state space, intermediate variables, and constants of the DDE system are identified in Appendix D; what follows is a description of how these entities are related. The present section provides the differential equations, and the next section completes the model with expressions for the intermediate variables. The nature of the 26 differential equations divides as follows: 2 cardiac, 10 vascular, 10 feedback, and 4 cerebral equations.

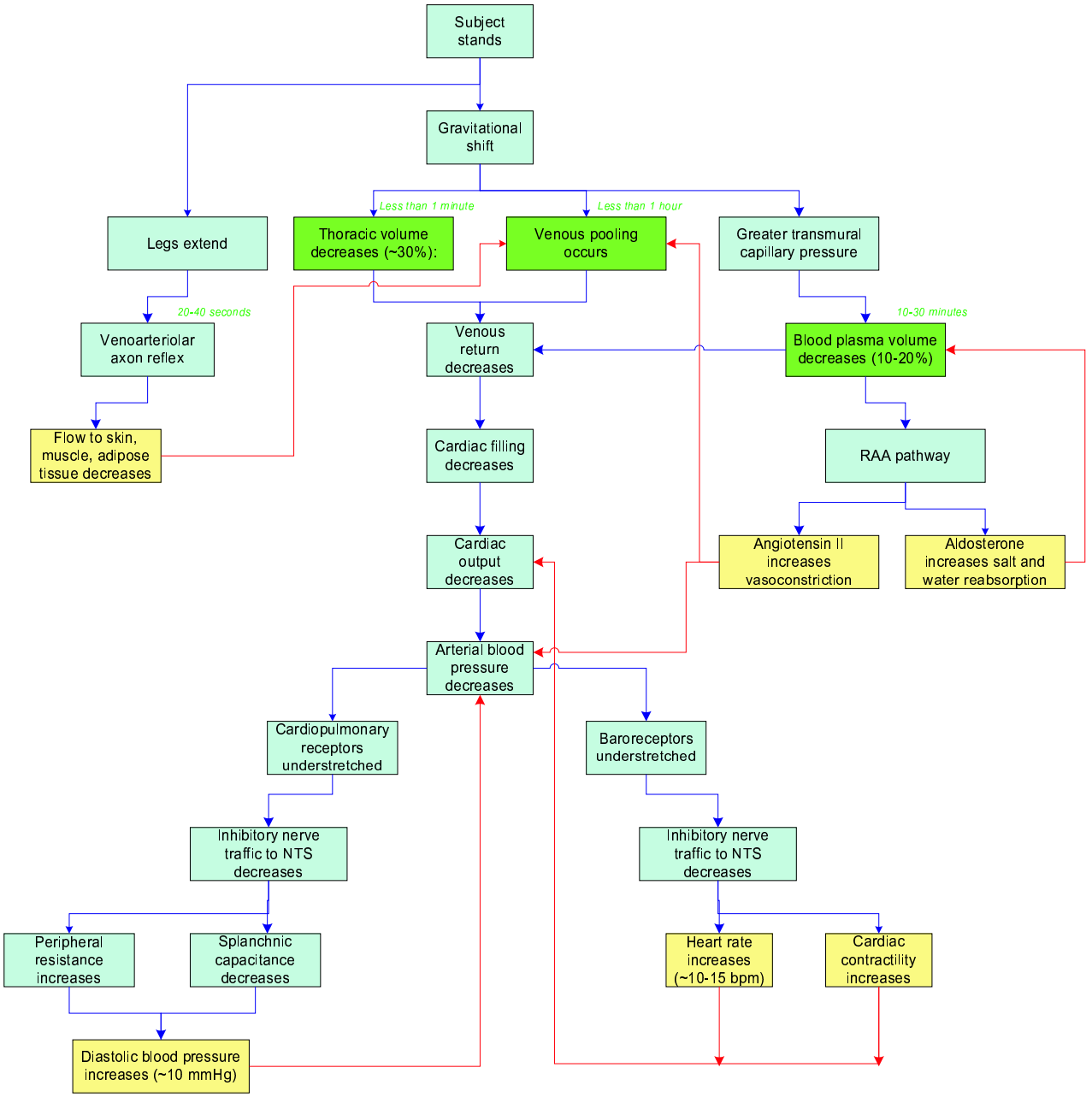

Figure 8.1: The normal response to standing. Green boxes represent the three key challenges associated with orthostasis; blue boxes and arrows represent causal relationships; yellow boxes and red arrows represent the primary pathways of negative feedback; BPM = beats per minute; RAA = renin angiotensin aldosterone; NTS = nucleus tractus solitari.

8.3.1 Cardiac and Pulmonary Pressures and Flows

The equations for cardiac and pulmonary haemodynamics were mostly based on simple relationships found in fluid dynamics, for instance Darcy's Law. They are easily derived by examining Figure 8.2.

$$\frac{dP_{la}}{dt} = \frac{1}{C_{la}} \left[\frac{P_{pv} - P_{la}}{R_{pv}} - F_{ol} \right] \tag{8.1}$$

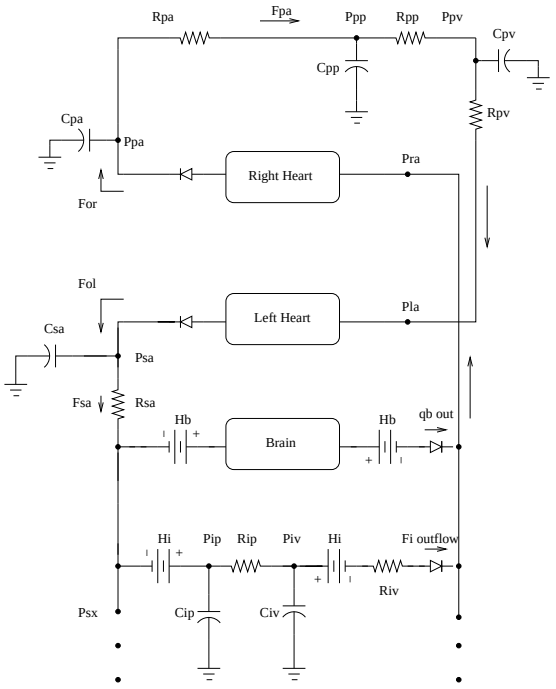

Figure 8.2: Haemodynamics of the Orthostasis Model. i = {s,h,le,ue,lm,um}, representing the splanchnic, cardiac, lower/upper extrasplanchnic, and lower/upper muscular compartments. Note the cerebral circulation (not shown) is similar to the cerebrovascular model of Ursino.

$$\frac{dP_{ra}}{dt} = \frac{1}{C_{ra}}\left[\frac{P_{sv}-H_s-P_{ra}}{R_{sv}} + \frac{P_{uev}-H_u-P_{ra}}{R_{uev}} + \frac{P_{lev}-H_l-P_{ra}}{R_{lev}} + \ldots \right.$$
$$\left. \frac{P_{umv}-H_u-P_{ra}}{R_{umv}} + \frac{P_{lmv}-H_l-P_{ra}}{R_{lmv}} + \frac{P_{hv}-H_h-P_{ra}}{R_{hv}} + q_{b\text{out}} - F_{or}\right] \tag{8.2}$$

In Equation 8.2, the H terms represent additional hydrostatic pressures which required careful estimation before they were introduced, for they underpin the short-term response to passive tilt. When the pressures were modified from zero, to simulate a tilt, they acted to decrease the blood pressure in the brain, carotid sinus, upper body, and coronary arteries, and increase the blood pressure in the splanchnic and lower-body circulations. These pressures were computed according to the Hydrostatic Equation: $\Delta P = \rho g d$, where ΔP is the pressure caused by a fluid column of length d and density ρ, and g is the acceleration due to gravity. Hence the pressure alteration occurred at the rate of 82 mmHg per metre of vertical displacement, where a displacement of 0 m corresponds to the HIP (hydrostatic indifference point, located near the base of the heart). For example, this led to the adjustments listed in Table 8.2 for the 75° tilt of a 173-cm person. Each of these values can be derived by multiplying sin(75°) by the corresponding entry

Compartment	Hydrostatic change (mmHg)
Cerebral circulation	-32
Carotid sinus	-23
Upper body (skeletal muscle and extrasplanchnic circulation)	-14
Coronary circulation	-6
Splanchnic circulation	13
Lower body (skeletal muscle and extrasplanchnic circulation)	55

Table 8.2: Hydrostatic adjustments of a 173-cm patient upon 75° tilt.

in Table D.8.

8.3.2 Pressures of the Systemic Vascular System

As in the previous subsection, the equations for the pressures and flows of the systemic vasculature can be derived by examination of Figure 8.2:

$$\frac{dP_{sx}}{dt} = \frac{F_{sa} - \mathrm{PR}_{\mathrm{sum}}}{C_{sp} + C_{uep} + C_{lep} + C_{ump} + C_{lmp} + C_{hp} + C_{bp}} \tag{8.3}$$

where for clarity, "$\mathrm{PR}_{\mathrm{sum}}$" is defined as:

$$\mathrm{PR}_{\mathrm{sum}} = \frac{P_{sp} - P_{sv}}{R_{sp}} + \frac{P_{up} - P_{uev}}{R_{uep}} + \frac{P_{lp} - P_{lev}}{R_{lep}} + \frac{P_{up} - P_{umv}}{R_{ump}} + \frac{P_{lp} - P_{lmv}}{R_{lmp}} + \frac{P_{hp} - P_{hv}}{R_{hp}} + q_b \tag{8.4}$$

$$\frac{dP_{pp}}{dt} = \frac{1}{C_{pp}}\left[F_{pa} - \frac{P_{pp} - P_{pv}}{R_{pp}}\right] \tag{8.5}$$

$$\frac{dP_{pv}}{dt} = \frac{1}{C_{pv}}\left[\frac{P_{pp} - P_{pv}}{R_{pp}} - \frac{P_{pv} - P_{la}}{R_{pv}}\right] \tag{8.6}$$

$$\frac{dP_{sa}}{dt} = \frac{F_{ol} - F_{sa}}{C_{sa}} \tag{8.7}$$

$$\frac{dP_{pa}}{dt} = \frac{F_{or} - F_{pa}}{C_{pa}} \tag{8.8}$$

Before Equations 8.12-8.16 are given, it should be noted that venous valves act as a diode, and hence some temporary variables require definition:

$$F_{hv_{\mathrm{out}}} = \max\left(0, \frac{P_{hv} - H_h - P_{ra}}{R_{hv}}\right) \qquad F_{lmv_{\mathrm{out}}} = \max\left(0, \frac{P_{lmv} - H_l - P_{ra}}{R_{lmv}}\right) \tag{8.9}$$

$$F_{lev_{\mathrm{out}}} = \max\left(0, \frac{P_{lev} - H_l - P_{ra}}{R_{lev}}\right) \qquad F_{umv_{\mathrm{out}}} = \max\left(0, \frac{P_{umv} - H_u - P_{ra}}{R_{umv}}\right) \tag{8.10}$$

$$F_{sv_{\mathrm{out}}} = \max\left(0, \frac{P_{sv} - H_s - P_{ra}}{R_{sv}}\right) \tag{8.11}$$

These temporary expressions, necessary to prevent the backwards flow of blood in the veins of the lower body and thereby combat gravitational pooling, are incorporated into the next five differential equations:

$$\frac{dP_{sv}}{dt} = \frac{1}{C_{sv}}\left[\frac{P_{sp} - P_{sv}}{R_{sp}} - F_{sv_{\text{out}}} - \frac{d\Delta V_{usv}}{dt}\right] \tag{8.12}$$

$$\frac{dP_{umv}}{dt} = \frac{1}{C_{umv}}\left[\frac{P_{up} - P_{umv}}{R_{ump}} - F_{umv_{\text{out}}} - C_u\frac{d\Delta V_{umv}}{dt}\right] \tag{8.13}$$

$$\frac{dP_{lmv}}{dt} = \frac{1}{C_{lmv}}\left[\frac{P_{lp} - P_{lmv}}{R_{lmp}} - F_{lmv_{\text{out}}} - C_l\frac{d\Delta V_{umv}}{dt}\right] \tag{8.14}$$

$$\frac{dP_{lev}}{dt} = \frac{1}{C_{lev}}\left[\frac{P_{lp} - P_{lev}}{R_{lep}} - F_{lev_{\text{out}}} - C_l\frac{d\Delta V_{uev}}{dt}\right] \tag{8.15}$$

$$\frac{dP_{uev}}{dt} = \frac{1}{C_{uev}}\left[\frac{P_{lp} - P_{uev}}{R_{uep}} - F_{uev_{\text{out}}} - C_u\frac{d\Delta V_{uev}}{dt}\right] \tag{8.16}$$

8.3.3 Feedback Regulatory Actions

Acting upon the vasculature described in Figure 8.2 was a simple network of neural feedback. This feedback regulation is illustrated in Figure 8.3. Most of the equations are provided in the next section; however, the state variables will be described here. For $j = \{s, e, m\}$:

$$\frac{d\Delta R_{jp}}{dt} = \frac{-\Delta R_{jp} + \sigma_{Rjp}}{\tau_{Rjp}} \qquad \frac{d\Delta V_{usv}}{dt} = \frac{-\Delta V_{usv} + \sigma_{Vusv}}{\tau_{Vusv}} \tag{8.17}$$

and for the cardiac feedback,

$$\frac{d\Delta T_s}{dt} = \frac{-\Delta T_s + \sigma_{Ts}}{\tau_{Ts}} \qquad \frac{d\Delta T_v}{dt} = \frac{-\Delta T_v + \sigma_{Tv}}{\tau_{Tv}} \tag{8.18}$$

8.3.4 Cerebral Equations

The brain model (see Figure 8.4) is based largely on a model developed by Ursino *et al.* to observe the effect that changes in systemic arterial pressure (SAP) and arterial carbon dioxide pressure ($PaCO_2$) induce on cerebral blood flow (CBF) and intracranial pressure (ICP) [219]. The model was simplified for

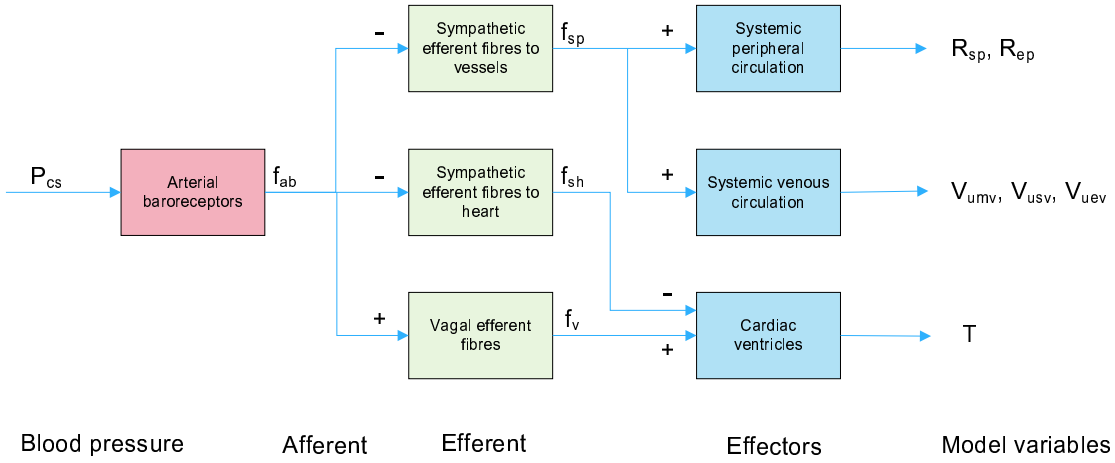

Figure 8.3: Feedback regulation in the Orthostasis Model. P_{cs} = carotid sinus pressure, $f_{ab}, f_{sp}, f_{sh}, f_v$ = firing frequency of arterial baroreceptors, and peripheral (sympathetic) and cardiac (sympathetic and vagal) efferent nerves.

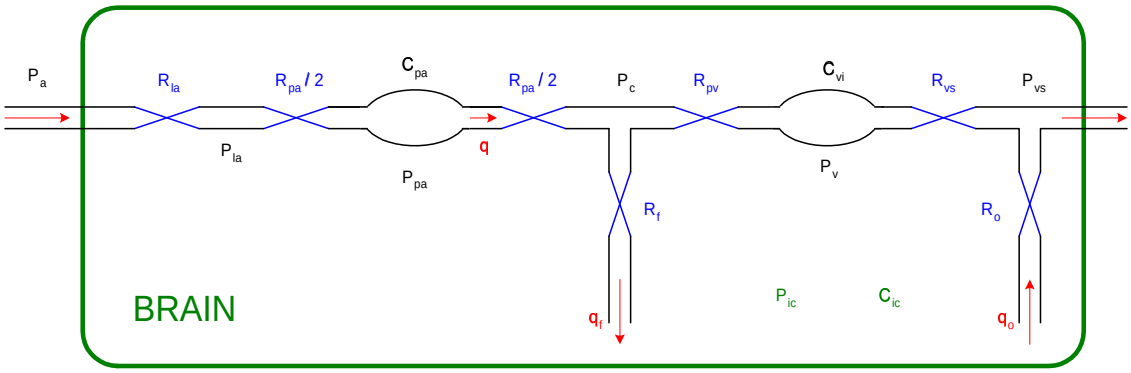

Figure 8.4: Biomechanical schematic of the cerebrovascular system constructed by Ursino. P_a = systemic arterial pressure; q = tissue cerebral blood flow; la = large intracranial arteries; pa = pial arteries; c = capillaries; pv = proximal cerebral veins; vi = v = intracranial veins; vs = terminal intracranial veins; R_f and R_o refer to the resistances to CSF formation and outflow, respectively; P_{ic} and C_{ic} refer to intracranial pressure and compliance, respectively. [219]

the present purposes, to focus on the following structures:

- Large intracranial arteries (resistance)
- Pial arterial system (resistance and compliance)
- Venous intracranial circulation (resistance and compliance)

The equations for the brain model are as follows:

$$\frac{dV_{pa}}{dt} = \frac{P_a - P_{pa_b}}{R_{la_b} + R_{pa}/2} - \frac{P_{pa_b} - P_c}{R_{pa}/2} \tag{8.19}$$

$$\frac{dP_v}{dt} = \frac{1}{C_{vi}} \frac{dV_{vi}}{dt} \tag{8.20}$$

$$\frac{dx_{\text{aut}}}{dt} = \frac{-x_{\text{aut}} + G_{\text{aut}}(q_b - q_n)/q_n}{\tau_{\text{aut}}} \tag{8.21}$$

Calculating $\frac{dP_{pa_b}}{dt}$ requires an intermediate differential equation that does reflect directly one of the state variables:

$$\frac{dC_{pa}}{dt} = \frac{\Delta C_{pa}}{k_{C_{pa}}} \frac{e^{\frac{x_{CO_2} - x_{\text{aut}}}{k_{C_{pa}}}}}{\left[1 + e^{\frac{x_{CO_2} - x_{\text{aut}}}{k_{C_{pa}}}}\right]^2} \frac{d(x_{CO_2} - x_{\text{aut}})}{dt} \tag{8.22}$$

This differential is then incorporated as follows:

$$\frac{dP_{pa_b}}{dt} = \frac{1}{C_{pa_b}} \left[\frac{dV_{pa}}{dt} + \frac{dC_{pa}}{dt}(P_{ic} - P_{pa_b})\right] \tag{8.23}$$

8.3.5 Humoral and Viscoelastic Effects

Finally, for long-term orthostasis, it is necessary to consider the effects of angiotensin-II and viscoelastic creep:

$$\frac{dA2}{dt} = \frac{-A2 + G_{A2}/pv}{\tau_{A2}} \tag{8.24}$$

$$\frac{dV_{vc}}{dt} = \frac{-V_{vc} + V_{vcf}}{\tau_{vc}} \tag{8.25}$$

8.4 Intermediate Variables

To determine the state-space derivatives, the calculation of a number of intermediate variables is required.

8.4.1 Cardiac Variables

Stroke volume increases with atrial pressure, according to the Frank-Starling mechanism. Here this relationship is modelled using a constant of proportionality known as cardiac effectiveness, which is measured in ml mmHg^{-1}. (See k_r and k_l below.) In addition, cardiac performance is also affected by the load against which the heart is working. A corrective factor L is therefore needed for each half of the heart (left and right), which is assumed to increase with the square root of arterial pressure [215]. Multiplying stroke volume by this corrective factor L and dividing it by the heart period T yields the cardiac output (flow), F_o.

$$L_r = \begin{cases} \sqrt{\frac{Ppan}{Ppa}}, & \text{if } P_{pa} > P_{pan}, \\ 1, & \text{otherwise} \end{cases} \quad (8.26)$$

$$F_{or} = k_r(P_{ra} - P_{ra,0})\frac{L_r}{T} \quad (8.27)$$

$$L_l = \begin{cases} \sqrt{\frac{Psan}{Psa}}, & \text{if } P_{sa} > P_{san}, \\ 1, & \text{otherwise} \end{cases} \quad (8.28)$$

$$F_{ol} = k_l(P_{la} - P_{la,0})\frac{L_l}{T} \quad (8.29)$$

8.4.2 Miscellaneous Cardiovascular Variables

$$F_{pa} = \frac{P_{pa} - P_{pp}}{R_{pa}} \quad (8.30)$$

$$F_{sa} = \frac{P_{sa} - P_{sx}}{R_{sa}} \quad (8.31)$$

$$V_u = V_{ustatic} + V_{usv} + V_{uev} + V_{umv} \quad (8.32)$$

$$\begin{aligned} PC_{\text{subtotal}} =& C_{sa}P_{sa} + C_{sp}P_{sp} + (C_{uep} + C_{ump})P_{up} + (C_{lep} + C_{lmp})P_{lp} + C_{hp}P_{hp} + C_{umv}P_{umv} \ldots \\ &+ V_{lev} + V_{lmv} + V_{sv} + C_{hv}P_{hv} + C_{ra}P_{ra} + C_{la}P_{la} + C_{pa}P_{pa} + C_{pp}P_{pp} + C_{pv}P_{pv} \end{aligned} \quad (8.33)$$

$$V_{\text{brain}} = C_{pa_b}(P_pa_b - P_{ic}) + C_{vi}(P_v - P_{ic}) \quad (8.34)$$

$$P_{uev} = \frac{V_t + V_i - PC_{\text{subtotal}} - V_{\text{brain}} - V_{rv} - V_{lv} - V_u - V_{vc} - V_{vco}}{C_{uev}} \quad (8.35)$$

8.4.3 Afferent and Efferent Neural Pathways

The afferent pathway is comprised of a signal transmitted from the arterial baroreceptors to the vasomotor centre. The frequency of this signal is given by

$$f_{ab} = \frac{f_{abmin} + f_{abmax}e^{\frac{P_{cs}-P_n}{k_{ab}}}}{1 + e^{\frac{P_{cs}-P_n}{k_{ab}}}} \quad (8.36)$$

The effects of respiration have been incorporated in the model, by considering the frequency of the output of the chemoreceptors and pulmonary stretch receptors (f_{ac} and f_{ap}, respectively). However, since a suitable respiration signal was not recorded in most patients, these frequencies have been set to constant values (f_{acn} and f_{apn}), and the pathways have not been included in Figure 8.3.

For the sympathetic activity to the heart, peripheral resistances, and veins ($j = \{h, p, v\}$ respectively), the efferent signals are as follows:

$$f_{sj} = \min\left(f_{esmax}, f_{es\infty} + f_{es_0} - f_{es\infty} e^{k_{es}(W_{bsj} f_{ab} + W_{csj} f_{ac} + W_{psj} f_{aj} - \theta_{sj})}\right) \tag{8.37}$$

$$f_v = \frac{f_{ev\,0} + f_{ev\,\infty} e^{\frac{f_{ab} - f_{ab\,0}}{k_{ev}}}}{1 + e^{\frac{f_{ab} - f_{ab\,0}}{k_{ev}}}} + W_{cv} f_{ac} - W_{pv} f_{ap} - \theta_v \tag{8.38}$$

8.4.4 Effectors for Reflex Regulation

The differential equations for the feedback variables in Section 8.3.3 required the following intermediate parameters, for $j = \{s, e, m\}$:

$$\sigma_{R_{jp}} = \begin{cases} G_{R_{jp}} \log[f_{sp}(t - D_{R_{jp}}) - f_{esmin} + 1], & \text{if } f_{sp} \geq f_{esmin}, \\ 0, & \text{otherwise} \end{cases} \tag{8.39}$$

$$\sigma_{Vujv} = \begin{cases} G_{V_{ujv}} \log[f_{sp}(t - D_{Vujv}) - f_{esmin} + 1], & \text{if } f_{sv} \geq f_{esmin}, \\ 0, & \text{otherwise} \end{cases} \tag{8.40}$$

and for T_s:

$$\sigma_{T_s} = \begin{cases} G_{T_s} \log[f_{sh}(t - D_{T_s}) - f_{esmin} + 1], & \text{if } f_{sh} \geq f_{esmin}, \\ 0, & \text{otherwise} \end{cases} \tag{8.41}$$

$$\sigma_{Tv} = G_{T_v} f_v(t - D_{Tv}) \tag{8.42}$$

Finally, for $\pi = \{R_{sp}, R_{ep}, R_{sm}, V_{usv}, V_{uev}, V_{umv}, \}$:

$$\pi = \Delta\pi + \pi_0 \tag{8.43}$$

and for heart period,

$$T = \Delta T_s + \Delta T_v + T_0 \tag{8.44}$$

8.4.5 Upper- and Lower-Body Division

Recall that u and l refer to the upper- and lower-body divisions, respectively. For $i = \{u, l\}$ and $j = \{e, m\}$:

$$R_{ijp} = R_{ijp0} R_{jp} \frac{R_{ujp0} + R_{ljp0}}{R_{uep0} R_{lep0}} \tag{8.45}$$

8.4.6 Cerebrovascular Variables

The following intermediate parameters were required in the computation of cerebral variables:

$$R_{pa_b} = k_R \left(\frac{C_{pan}}{V_{pa}} \right)^2 \tag{8.46}$$

$$C_{vi} = \frac{1}{k_{ven}(P_v - P_{ic} - P_v 1)} \tag{8.47}$$

$$k_{Cpa} = \frac{\Delta C_{pa}}{4} \tag{8.48}$$

$$q_b = \frac{P_{pa_b} - P_c}{R_{pa}/2} \tag{8.49}$$

$$q_{b\text{out}} = \frac{P_v - P_{vs}}{R_{vs}} + q_o \tag{8.50}$$

$$A_{CO_2} = \frac{1}{1 + e^{-k_{CO_2} \frac{q_b - q_n}{q_n - b_{CO_2}}}} \tag{8.51}$$

$$R_{vs} = \begin{cases} R'_{vs}, & \text{if } P_v > 2 \text{ (patient supine)}, \\ \frac{2R'_{vs}}{P_v}, & \text{otherwise (patient upright)} \end{cases} \tag{8.52}$$

$$\frac{dV_{vi}}{dt} = \frac{P_{pa_b} - P_v}{R_{pv_b} + R_{pa}/2} - \frac{P_v - H_b - P_{ra}}{R_{vs}} \tag{8.53}$$

$$\Delta C_{pa} = \begin{cases} \Delta C_{pa_1}, & \text{if } x_{CO_2} > x_{\text{aut}}, \\ \Delta C_{pa_2}, & \text{otherwise} \end{cases} \tag{8.54}$$

$$C_{pa_b} = \frac{(C_{pan} - \frac{\Delta C_{pa}}{2}) + (C_{pan} + \frac{\Delta C_{pa}}{2}) e^{\frac{x_{CO_2} - x_{\text{aut}}}{k_{Cpa}}}}{1 + e^{\frac{x_{CO_2} - x_{\text{aut}}}{k_{Cpa}}}} \tag{8.55}$$

8.4.7 Additional Postural Effects

The progression of the tilt to the upright position, $c_T \in [0,1]$, is calculated as

$$c_T = \begin{cases} 0, & \text{if } t < t_{\text{start}} \text{ (patient supine)}, \\ \frac{t - t_{\text{start}}}{t_{\text{end}} - t_{\text{start}}}, & \text{if } t_{\text{start}} < t < t_{\text{end}} \text{ (moving patient upright)}, \\ 1, & \text{if } t > t_{\text{end}} \text{ (patient in upright position)} \end{cases} \tag{8.56}$$

From this, the hydrostatic pressures H_i can be calculated for $i = \{s, u, l, b, h, c\}$ — i.e. splanchnic, upper body, lower body, brain, heart, and carotid sinus, respectively — as simply $H_i = (c_T)(H_{iT})$.

As the simulated patient is tilted, it is necessary to compute the time derivative of the hydrostatic equation for blood flow to the brain:

$$\frac{dH_b}{dt} = \begin{cases} 0, & \text{if } t < t_{\text{start}} \text{ (patient supine)}, \\ \frac{Hb_{\text{final}}}{t_{\text{end}} - t_{\text{start}}}, & \text{if } t_{start} < t < t_{\text{end}} \text{ (moving patient upright)}, \\ 0, & \text{if } t > t_{end} \text{ (patient in upright position)} \end{cases} \tag{8.57}$$

Blood pooling in the lower extremities is calculated as

$$V_i = \begin{cases} 0, & \text{if } t < t_{\text{end}} \text{ (patient supine or moving upright)} \\ V_i = V_{i\text{final}} \left(1 - e^{\frac{t_{\text{end}} - t}{\tau_{V_i}}}\right), & \text{if } t > t_{\text{end}} \text{ (patient in upright position)} \end{cases} \tag{8.58}$$

Venous collapse (applicable only in the upright posture [154]) is modelled as

$$R_{uev} = \begin{cases} R_{uev0}, & \text{if } P_{uev} > 2 \text{ (patient supine)}, \\ \frac{2R_{uev}}{P_{uev}}, & \text{otherwise (patient upright)} \end{cases} \tag{8.59}$$

$$R_{umv} = \begin{cases} R_{umv0}, & \text{if } P_{umv} > 2 \text{ (patient supine)}, \\ \frac{2R_{umv}}{P_{umv}}, & \text{otherwise (patient upright)} \end{cases} \tag{8.60}$$

$$R_{hv} = \begin{cases} R_{hv0}, & \text{if } P_{hv} > 2 \text{ (patient supine)}, \\ \frac{2R_{hv}}{P_{hv}}, & \text{otherwise (patient upright)} \end{cases} \tag{8.61}$$

Certain compliances change from a "HI" value to a "LOW" value when the pressure of the corresponding compartment exceeds PNC (see Table D.8). This affects the calculation of the compartment's

stressed volume; for $j = \{s, le, lm\}$ (splanchnic, lower extrasplanchnic, and lower muscular circulations):

$$V_{jv} = \begin{cases} C_{jv} P_{jv}, & \text{if } P_{jv} < \text{PNC} \\ (\text{PNC}) C_{jv\text{LOW}} + (P_{jv} - \text{PNC}) C_{jv\text{HI}}, & \text{otherwise} \end{cases} \tag{8.62}$$

$$C_{bp} = \frac{C_{pa_b} C_{ic}}{C_{pa_b} + C_{ic}} \tag{8.63}$$

This nonlinearity in the dependent venous compliances was one of two important considerations in designing the model, to accommodate the hydrostatic pressures discussed on page 116. (The second was the behaviour of venous valves.) This characterisation of compliances is necessary to prevent orthostatic hypotension in a normal subject: if veins were too compliant at high pressure, the entire blood volume of the circulation would simply accumulate in the lower body.

Overall viscoelastic effects are modelled as

$$V_{vco} = \begin{cases} 0, & \text{if } t < t_{\text{end}} \text{ (patient supine or moving upright)} \\ V_{vco} = \Delta V_{vco} \left(1 - e^{\frac{t_{\text{end}} - t}{\tau_{vco}}}\right), & \text{if } t > t_{\text{end}} \text{ (patient in upright position)} \end{cases} \tag{8.64}$$

Additionally, viscoelastic creep in the lower muscular and lower extrasplanchnic circulations is represented as:

$$V_{vcf} = k_{VC}(P_{lmv} - \text{PNC}) \tag{8.65}$$

This allowed for a more realistic adaptation to pressure increases — by allowing the overall circulation to compensate partially for the loss of blood volume during standing.

The peripheral pressures are calculated using P_{sx} as follows. For $j = \{s, u, l, b, h\}$ (splanchnic, upper-body, lower-body, cerebral, and coronary circulations):

$$P_{jp} = P_{sx} + H_j. \tag{8.66}$$

Finally, normalised plasma volume is calculated as:

$$p_v = \frac{V_t + V_i}{V_t} \tag{8.67}$$

8.4.8 The Long-term Response to Tilt

It is known that in the normal response to standing, blood volume decreases over the course of 15-40 minutes. This is due to the increased transmural pressure in the lower capillaries, driving blood out of the vessels and into interstitial space. Negative feedback mechanisms in the body usually act to curb the blood loss so that it does not exceed approximately 10% of the total. The physiological effects of prolonged standing share many similarities with those of haemorrhage simply because of this decrease in circulating blood volume [20,90]. The time-dependent blood loss $V_i(t)$ is modelled as a monoexponential function:

$$V_{\text{final}} = c_{\text{loss}} V_{\text{total}} \tag{8.68}$$

$$V_i(t) = V_{\text{final}} \left(1 - e^{\frac{-t}{\tau_{V_i}}}\right) \tag{8.69}$$

where V_{total} represents the total blood volume (5 litres), V_{final} represents the blood lost upon long-term standing (500 ml if $c_{\text{loss}} = 0.10$), $V_i(t)$ represents the blood loss at time t, and τ_{V_i} represents the time constant associated with the decrease (10 minutes). Although the degree of blood loss is small, it is enough to cause syncope in the tilted patient (arterial blood pressure collapses as per Type 3 syncope in Figure 2.1). The fact that a redistribution in blood can cause syncope is in agreement with expectations, as even healthy subjects can lose consciousness 10 to 20 minutes after tilt [130] if no compensatory mechanisms occur — in particular, slight muscular contractions in the legs to prevent blood pooling.

8.5 Model Validation

Of the 26 differential equations, eight contain a delay, reflecting the fact that the information generated in one part of the body cannot arrive instantaneously at another part. Hence, strictly speaking the model is not an ODE system but a DDE (delay differential equation) system, of the following form:

$$\mathbf{y}'(t) = f\Big(t, \mathbf{y}(t), \mathbf{y}(t-\tau_1), \mathbf{y}(t-\tau_2), \ldots, \mathbf{y}(t-\tau_7)\Big) \tag{8.70}$$

The numerical solving of DDEs is not yet as efficient as the state-of-the-art ODE software, but accurate programs exist. For the current work, the *dde23* function in Matlab is used. The algorithm is based on the explicit Runge-Kutta method.

Using this solution procedure, validation of the Orthostasis Model occurred in two phases. The first phase focused on the simulation of a normal 173-cm patient lying quietly, in order to compare the model parameters to published values [106,107]. All constants were set to their default values. The state space

was initialised by assuming that the heart was initially at rest (for example, V_{lv} was set initially to the constant V_{ulv}, and so on) and by assuming that pressures could be approximated within an order of magnitude using the equation

$$\text{Unstressed vessel volume} = \text{Pressure} \times \text{Vessel compliance}.$$

The model was run for five minutes, during which time the state space adapted to its supine equilibrium. This equilibrium was found to be independent of the initial state space, provided the latter was within range of physiological plausibility (for example, initialisations which led to a negative heart rate caused problems). A selection of the equilibrium values appears in Table 8.3; a longer list is given in Appendix D. For comparison in the table, typical values are also given, measured in healthy subjects of usually unspecified ages from the literature [105–107]. The boundaries of the ranges do not necessarily reflect definitions of pathology; hence it is acceptable for the model baseline values to lie outside the range as long as they are similar.

Second, the response to a simulated tilt was observed. This response was gauged as follows:

1. The model was run for a 173-cm simulated patient as before. Baseline "pre-tilt" values were calculated as the final data points in this period, as before.

2. A tilt from 0° to 75° in 10 seconds was imposed, incurring hydrostatic effects in the blood pressure. The state variables changed to adapt the cardiovasculature to the upright position.

3. The simulated patient was observed for 2 minutes after tilt, to ensure new equilibrium values were reached. "Post-tilt" values were calculated as the final data points in this 2-minute period.

The differences between the pre- and post-tilt values were calculated for four key parameters encompassing different aspects of the cardiovasculature: upper-body blood volume, stroke volume, cardiac output, and splanchnic resistance. These changes were compared to the expected values reported by Rowell [174] (see Table 8.4). As can be seen, the differences between the model's results and Rowell's figures were small in all cases.

Also, the time courses of several model parameters were plotted and compared to those collected by Wieling *et al.* [75] from a healthy subject (see Figure 8.5). Although the published results from this single subject cannot necessarily be expected to represent average behaviour, they provide an interesting mode

Quantity	Units	Normal value	Model baseline
Systolic BP	mmHg	122 ± 30 [107]	115
Diastolic BP	mmHg	75 ± 20 [107]	80
Heart rate	bpm	65–75 [106]	67
Cardiac output	ml s^{-1}	76–100 [106]	91
Stroke volume	ml	70–80 [106]	83
Total peripheral resistance	mmHg s ml^{-1}	0.58–1.1 [105]	1.32

Table 8.3: Selected baseline outputs of the Orthostasis Model. The values of "normal" haemodynamics were taken from single sources in the literature [105–107]. bpm = beats per minute.

Quantity	Pre-tilt	Post-tilt	Change	Expected Change
Upper-body blood volume (ml)	2487	2054	–433 ml	–600 ml
Stroke volume (ml)	80	55	–31%	–40%
Cardiac output (ml s^{-1})	91	75	–18%	–22%
Splanchnic resistance (mmHg s ml^{-1})	3.4	4.9	+44%	+45%

Table 8.4: Sample baseline and post-tilt outputs of the Orthostasis Model, compared with normal values ("expected change") from [174]. bpm = beats per minute.

of comparison. For example, the model's response to tilt seems slightly underdamped, which is perhaps due to the fact that not all feedback paths can be included in the model.

In summary, the model behaved reasonably well during supine rest and upright tilt. A third validation of the model might involve setting the model constants (defined for healthy young subjects in Appendix D) to values appropriate for elderly patients. The model could then in theory be run as above and the results compared to published parameter time courses, as was done in Figure 8.5. However, neither such constants nor such parameter time courses could be found in the literature, so the existing constants were maintained.

8.6 Parameter Estimation

In the previous section, all constants were set to default values, and running the model yielded a certain reproducible state-space behaviour. However, actual clinical data varies from patient to patient: no single set of constants can duplicate each patient's vital signs. Hence, to fit the model to a given patient, the constants must be adjusted. This is achieved by iteratively comparing the model's behaviour to that observed in the patient's data and adjusting the constants accordingly, until a stopping criterion is satisfied. This is a form of what is known as parameter estimation.

The "Identifiability Problem" classifies a model into one of the following three categories:

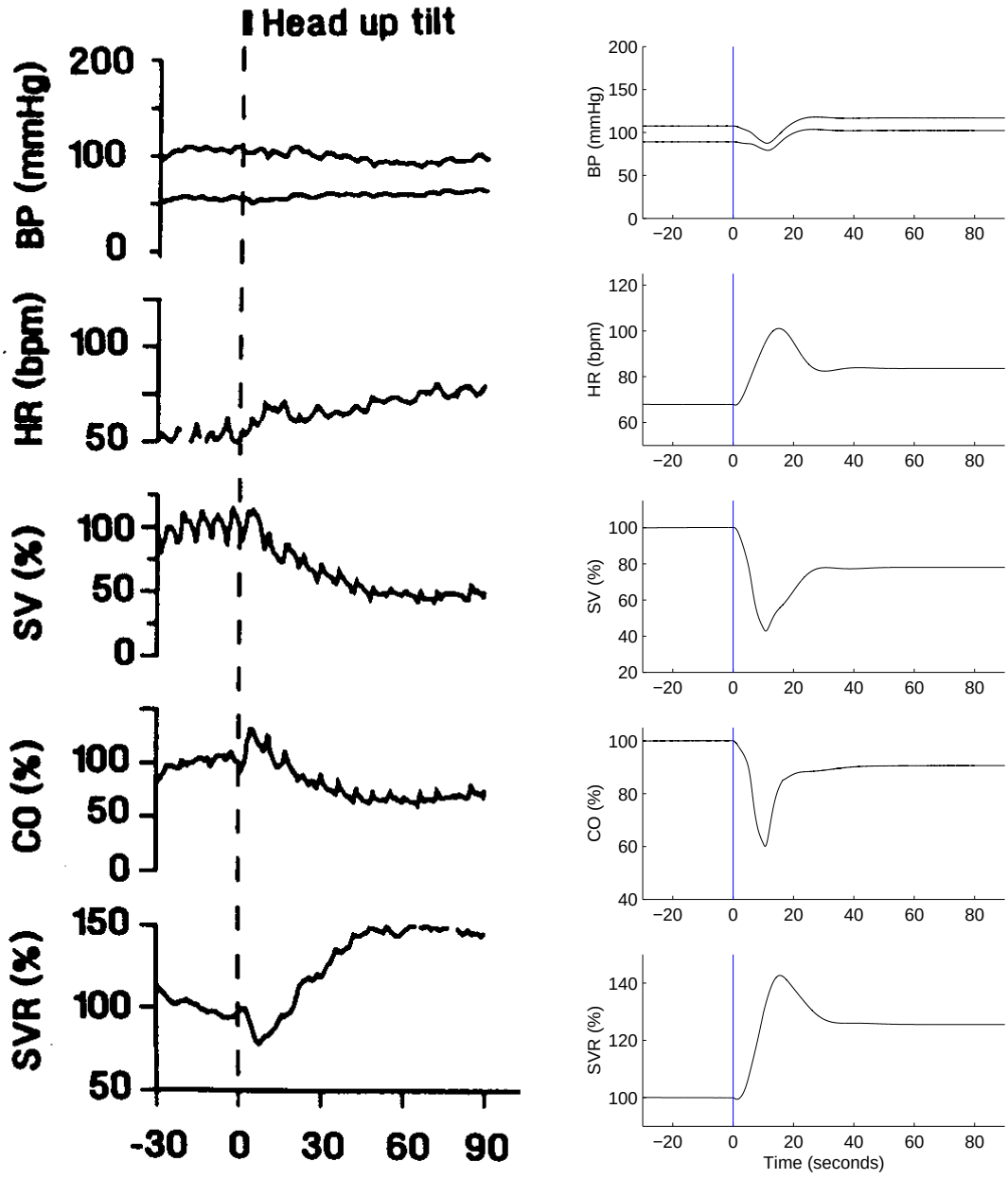

(a) Wieling *et al.*

(b) Model predictions

Figure 8.5: Blood pressure (BP), heart rate (HR), stroke volume (SV), cardiac output (CO), and systemic vascular resistance (SVR) responses to a 75° head-up tilt. Data collected from a healthy subject by Wieling *et al.* [75] are compared with the results from the current model. Some differences exist, due to natural inter-patient variations.

Uniquely identifiable: Sufficiently accurate parameter estimation always results in the same outcome; each model parameter can assume only one possible value in this single "correct answer".

Nonuniquely identifiable: At least one parameter can assume more than one (but a finite number of) possible values. Note that in each of these answers, an equally good fit to the data still occurs.

Nonidentifiable: At least one parameter can assume any of an infinite number of values.

With the number of model constants (~150) greatly exceeding the number of independent parameters calculated from the four available datastreams (see Section 1.4.2) for use in parameter estimation, the Orthostasis Model is classified as "nonidentifiable". Several methods to deal with nonidentifiability exist [33]:

- Model reparameterisation
- Incorporation of additional knowledge
- Design of a more informative experiment
- Setting elusive parameters as constants

The final technique was employed for the current work: most of the values available from the literature were kept constant during parameter estimation.

Identifying which parameters to estimate and which to keep constant is an important task. Not all the findings from the previous chapter can be used fully, since certain parameters of interest within syncopal patients (such as those characterising the activation of endocrine pathways) are impossible to estimate using the noninvasive monitoring of the Falls Clinic. The list of key parameters to estimate thus represents the intersection of parameters of clinical interest with parameters that can be extracted reliably from the available data set.

This intersection is important to consider: simply choosing the most clinically important parameters, rather than clinically important parameters which can be estimated reliably, may be responsible for misleading results. In a cerebrovascular model, Ursino *et al.* [219] selected six parameters to estimate in patients, keeping the remaining parameters constant. These six were chosen based solely on their clinical relevance. Recently, Payne [151] performed a sensitivity analysis on three of these six parameters, and found that two of them (cerebrospinal fluid outflow resistance and the intracranial elastance coefficient) had virtually no effect on the model outputs, whilst the third parameter (cerebral autoregulation gain, G_{aut}) had very little effect compared to several other parameters. In particular, G_{aut} had less than half of the effect of each of five other parameters which were not considered for estimation by Ursino *et al.* This implies that at least three of the six constants selected for parameter estimation are not able

to be calculated sufficiently accurately from the Ursino cerebrovascular model: either the model requires adjustment or the constants are not as clinically relevant as is supposed by the authors.

For the present work, of the ~150 parameters, the subset to be estimated was designated as:

P_n: baroreceptor operating point, mmHg

k_{lr}: cardiac effectiveness multiplier, dimensionless

k_{ab}: a parameter inversely related to baroreflex gain, mmHg

G_{T_s}: gain of sympathetic activity on sino-atrial node, s

G_{T_v}: gain of parasympathetic activity on sino-atrial node, s

W_{bsp}: parameter relating baroreflex activity to peripheral vasoconstriction, dimensionless

V_t: total blood volume, ml

Here, k_{lr} is a constant which is multiplied by the cardiac effectivenesses of the left and right ventricles (k_l and k_r respectively; each is measured in ml mmHg^{-1}). The Bezold-Jarisch reflex can be linked to hypovolemia (low V_t) or venous pooling. The latter can be caused by, among other things, a poor baroreflex arc (high k_{ab} or low absolute values of G_{T_s} or G_{T_v}) or a lack of sufficient vasoconstriction (low W_{bsp}). Problems in the endocrine system or central nervous processing can be manifested in the resetting of baroreceptors (affecting k_{ab}, G_{T_s}, and/or G_{T_v}), or blood volume control (affecting V_T). The parameters P_n and k_{lr} are not expected to be linked to any particular vasovagal syncope mechanism, but estimates are still required prior to determining the other parameters.

The sequential parameter estimation scheme to estimate these parameters will be described in the next section.

8.6.1 Supine Parameters

It was assumed that the mean supine BP was itself the best estimate of the baroreceptor operating point P_n. Hence, P_n was the easiest of the seven parameters to estimate.

To calculate the cardiac effectiveness multiplier k_{lr}, the model was analysed under steady state conditions; this reduced the model to a system of eight linear equations with eight unknowns:

$$F = \frac{P_{pa} - P_{pp}}{R_{pa}} \quad (8.71)$$

$$F = \frac{P_{sx} - P_{ra}}{R_{eq}} \quad (8.72)$$

$$F = \frac{P_{pp} - P_{pv}}{R_{pp}} \quad (8.73)$$

$$F = \frac{P_{pv} - P_{la}}{R_{pv}} \quad (8.74)$$

$$F = \frac{P_{sa} - P_{sx}}{R_{sa}} \quad (8.75)$$

$$F = a_r(P_{ra} - P_{ra,0}) \quad (8.76)$$

$$F = a_l(P_{la} - P_{la,0}) \quad (8.77)$$

$$V_T = \sum_i P_i C_i + V_u \quad (8.78)$$

where $F = F_{ol} = F_{or}$, $\sum_i P_i C_i$ refers to the sum of volumes contained in the compliant vessels, $a_r = \frac{k_r L_r}{T}$, and $a_l = \frac{k_l L_l}{T}$. Since steady state conditions are being analysed, $L_l = L_r = 1$, and T is set to the resting heart period measured in the patient.

The eight unknowns were solved using Gaussian elimination, and the computed systemic arterial pressure (P_{sa}) was compared with the actual mean supine BP. The difference was used to adjust k_{lr} and the system of equations was re-solved iteratively in this manner until a solution was found. (A solution was deemed acceptable when k_{lr} and P_{sa} required updating by less than 10^{-4} units, where one unit was defined as the initial guess for k_{lr} in the former case, and 1 mmHg in the latter case.) The style of iteration was a variant of the Powell dogleg method [160, 161] provided by The MathWorks Inc. This optimization algorithm is very similar to the Levenberg-Marquardt method (a "model trust region" approach) but the Jacobian matrix is approximated rather than calculated explicitly.

The final supine parameter to estimate was k_{ab}. Equation 8.44 was differentiated with respect to the carotid sinus afferent firing frequency f_{cs}, and the resulting derivative $\frac{\partial T}{\partial f_{cs}}$ was used as follows. Baroreflex sensitivity was calculated using the spectral technique described in Section 3.4.5, and it was assumed that

$$\text{BRS} = \frac{\partial \text{RR}}{\partial \text{BP}} = \frac{\partial T}{\partial f_{cs}} \frac{\partial f_{cs}}{\partial P_{cs}}. \quad (8.79)$$

Since BRS and $\frac{\partial T}{\partial f_{cs}}$ were known quantities, $\frac{\partial f_{cs}}{\partial P_{cs}}$ could be determined easily by rearranging Equation 8.79. Finally, differentiating Equation 8.36 with respect to P_{cs} and setting $P_{cs} = P_n$ yields the estimate for k_{ab} as required:

$$k_{ab} = \frac{f_{\max} - f_{\min}}{4 \frac{\partial f_{cs}}{\partial P_{cs}}}. \quad (8.80)$$

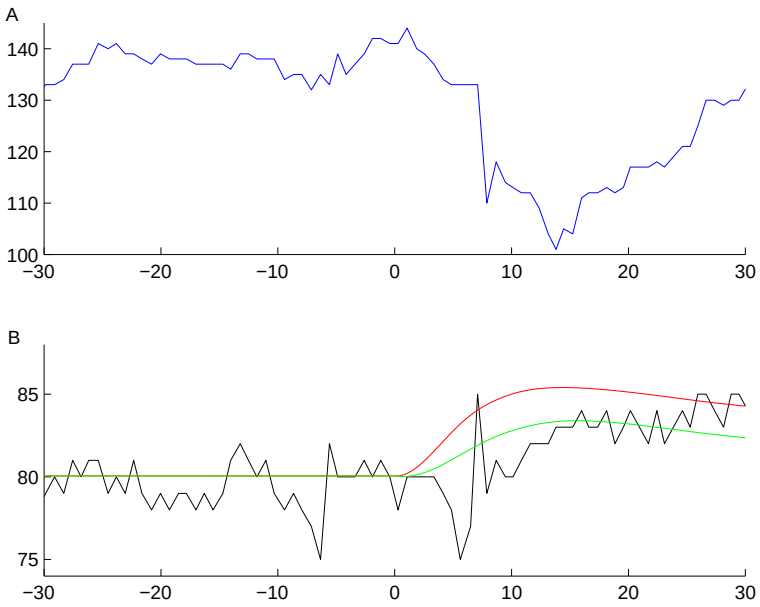

Figure 8.6: Demonstration of the optimisation of ANS gains. **A.** The decrease of mean blood pressure observed in a patient following tilt. **B.** The patient's simultaneous heart rate response (black line), and the heart rate response expected by the model (red line), using the default values of the gains G_{T_s} and G_{T_v}. The green line indicates the model's response after the optimal values for the gains were determined.

8.6.2 Parameters from the Initial Response to Tilt

The two branches of the ANS — sympathetic and parasympathetic — operate with different reaction times. The latter acts rapidly, within the course of a single heartbeat, while the former is more sluggish, requiring several heart beats to attain full effect. Wieling [225] found that qualitative examination of post-tilt HR could be used to estimate their relative strengths. For the current work, the first 45 seconds of the mean BP (MBP) time series following tilt were input to the Orthostasis Model, and the resulting HR response examined. To match this expected HR response to the actual HR response from the ECG, two parameters were adjusted: G_{T_s} and G_{T_v}, reflecting the gain of the sympathetic and parasympathetic nervous systems acting on the sino-atrial node. Each parameter was constrained ($G_{T_s} < 0, G_{T_v} > 0$), so that the sympathetic (parasympathetic) effect never increased (decreased) heart period. The two-dimensional optimisation was achieved using a nonlinear minimisation routine: the Nelder-Mead simplex (direct search) method. Figure 8.6 illustrates typical results.

8.6.3 Parameters from the Early Adjustment to Tilt

For the final stage of parameter estimation, the first two minutes of MBP after tilt were examined. (Such a long period was not necessary for the estimation of G_{T_s} and G_{T_v}, since most or sometimes all of the increase in HR occurs within the first 45 seconds.) The parameters adjusted to match the expected and actual MBP time series were W_{bsp} and V_t, reflecting peripheral vasoconstriction and total blood volume respectively. The Nelder-Mead simplex method was again used to achieve the optimal parameter fit.

8.6.4 Selection of the Data Set

Using the sequence of parameter estimation described above, seven model parameters of interest could be determined for each patient, for the purpose of syncope prediction. The patients selected for this analysis were those for whom the seven parameters could be estimated, and who were assigned a clear diagnosis with respect to vasovagal syndrome. This excluded patients with excessive artefacts in their RR tachograms or BP time series, patients who did not undergo prolonged HUT, and patients with uncertain diagnoses. The size of this data set, labelled Subset C, was 40 patients (15 vasovagal and 25 nonvasovagal). When setting the parameters of a classifier, a balanced data set consisting of 15 patients of each type was used, as before.

8.7 Predictions from Parameter Estimation

8.7.1 Comparison of Parameter Sets

Out of the many characteristics which can be evaluated in the Falls Clinic patients, it was hypothesised that these could be divided into two nearly distinct groups: those related to age, weight, height, etc., and those related to the presence of vasovagal syndrome. The problem was then to estimate the parameters in the former group from the supine data in order to adjust ("normalise") the model for a particular patient, before estimating the parameters in the latter group to form the diagnosis.

Hence, for the patients in Subset C, the first three of seven parameters were estimated using the supine data, following the parameter estimation sequence of Section 8.6, and the remaining four were first assigned their default values (G_{T_s} = -0.13 s, G_{T_v} = 0.09 s, W_{bsp} = -1 s, V_t = 5.0 L, as per Appendix D). These seven-dimensional vectors were then compressed to two-dimensional vectors, using a technique called Neuroscale. The technique will be discussed more thoroughly and with more applications in

Section 9.3, but in the present section it is only necessary to appreciate that a seven-dimensional vector can be approximated as a two-dimensional vector, for the purposes of *visualising* differences between patient groups. Such a visualisation is given in Figure 8.7A. Recall that all differences among data points are due to the variance in only the first three of seven parameters: P_n (61–174 mmHg), k_{lr} (0.33–4.98), and k_{ab} (8.1–67 mmHg).

Next, the four upright parameters were estimated rather than set to their default values, using the procedure of Sections 8.6.2 and 8.6.3. The resulting new seven-dimensional vectors were input as test vectors to the same Neuroscale network. The visualisation of the new data points is given in Figure 8.7B. The ranges for the four final parameters were also observed individually: G_{T_s} (-0.24–0 s), G_{T_v} (0–0.11 s), W_{bsp} (0.04 – 1.41 s), and V_t (4.5-5.7 L).

The data points are more spread out than those of Figure 8.7A, since in the first graph four of the seven parameters are fixed for all patients, whereas in the second graph all seven parameters are permitted to vary. Hence no information is gleaned from the observation that the data points have become more diffuse. The information of interest is whether the data points have moved in characteristic patterns for vasovagal syncope patients as compared to nonvasovagal subjects. This is difficult to determine precisely from the two figures, so the vectors which connect the new two-dimensional points to the old ones are plotted in Figure 8.8. These vectors show no characteristic movement in the 2D space for either patient group. Hence, the present method is unable to discriminate syncopal from nonsyncopal patients, and the four estimated parameters do not appear to be predictive of syncope.

8.7.2 Combination of the Four Parameters

The distributions of the four parameters are given in Figure 8.9. As can be seen, no parameter on its own is capable of differentiating vasovagal patients from nonvasovagal patients. Next the parameters are plotted one against each other in turn, to see if any combination of two parameters can differentiate between the two patient classes (see Figure 8.10). It is interesting to note that the ANS gains — G_{T_s} and G_{T_v} — separate patients into two distinct groups, representing high or low levels of ANS activity. However, no pair of the four signal processing parameters can separate the patients into vasovagal and nonvasovagal groups.

In Chapter 6, a linear classifier was used to combine four parameters, each offering some discriminatory information between the two patient groups. The four upright parameters estimated from the

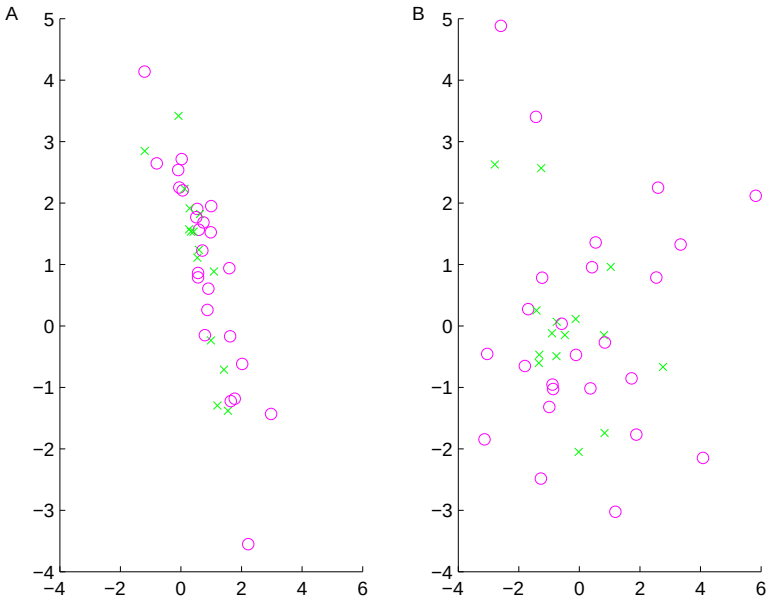

Figure 8.7: Dimensionality reduction of seven model parameters. In **A**, the three supine parameters have been estimated for each patient, but the four upright parameters have been left as their default values. **B:** The projections onto 2-D space after the four upright parameters have been estimated. Crosses and circles represent patients with and without vasovagal syndrome, respectively.

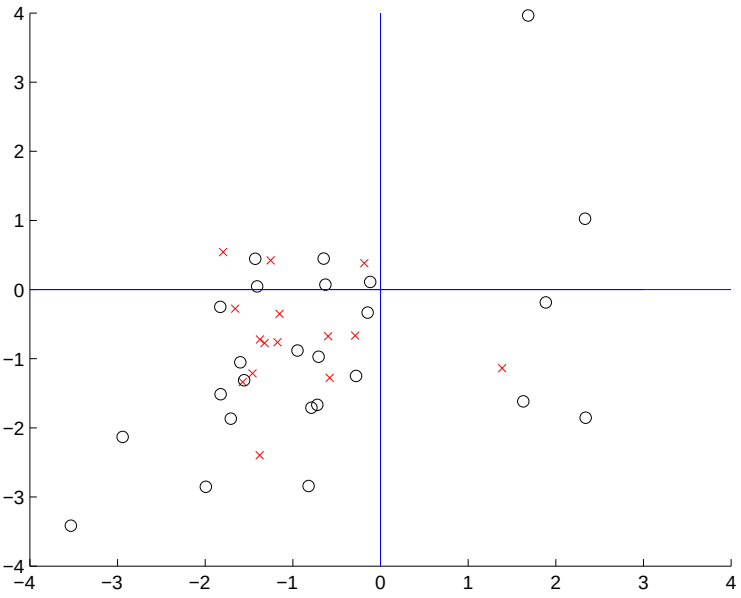

Figure 8.8: The vectors connecting the 2D points in Figure 8.7A to the corresponding points in B. Significant overlap exists between the two patient groups, confounding classification.

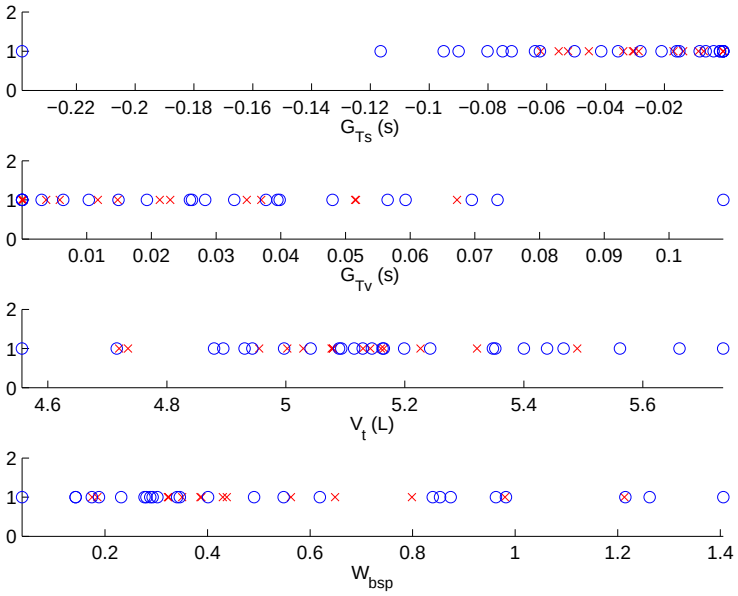

Figure 8.9: The distribution of the four post-tilt feature vectors in vasovagal (red crosses) and nonvasovagal (blue circles) patients. See page 131 for an explanation of the four parameters.

Orthostasis Model can be analysed in a similar way. Applying canonical variates analysis (CVA) to these four parameters yielded the four-dimensional projection vector which best differentiates between the two patient classes: $\mathbf{u}_i = \{0.73, -0.46, -0.48, 0.12\}$ (see Section 6.6.2 for a detailed explanation of $\mathbf{u}_i$). Multiplying this vector by the 4D feature vector of each patient ($\{G_{T_s}, G_{T_v}, V_t, W_{bsp}\}$) yielded 30 scalars, representing the 30 patients. Finally, an attempt was made to classify the patients using LOOCV on these scalars, in a manner similar to that performed in Section 6.5.4. The positive predictive value (PPV), NPV, and overall accuracy following LOOCV were 0.65, 0.69, and 0.67 respectively.

8.7.3 Long-term HUT

As described in the previous chapter, the endocrine system assists with the maintenance of BP during prolonged HUT. A natural extension of the parameter estimation scheme would be to estimate G_{A2} (angiotensin-II gain, see Equation 8.24) from the post-tilt data, considering the hypothesis that patients with low G_{A2} should be more prone to fainting. This parameter is difficult to estimate reliably, owing to the many factors controlling BP during HUT. However, an attempt was made, using the Nelder-Mead simplex method on systolic BP data to achieve the optimal parameter fit for G_{A2}. All post-tilt BP data were used, with the exception of the final three minutes before syncope, which in many syncopal patients

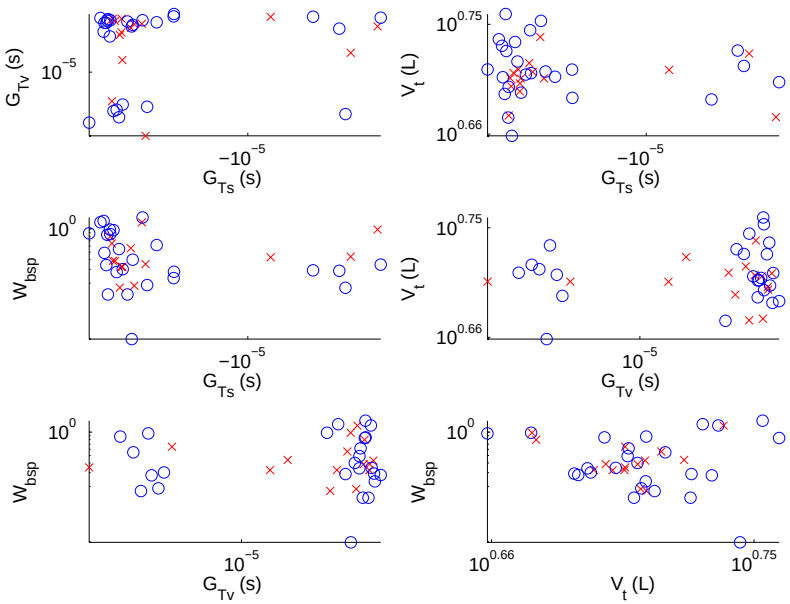

Figure 8.10: An alternate representation of the data contained in Figure 8.9. Here, each parameter is plotted against the other in turn, to examine the joint discriminatory capability of each pair. Logarithmic axes are used for clarity; see page 131 for an explanation of the four parameters.

are influenced by factors other than the RAA system. While the mean G_{A2} in syncopal patients was found to be lower than that of nonsyncopal patients ($p < 0.05$ using the Wilcoxon signed rank test), the parameter was a poor classifier (NPV = 0.63). This was arguably due to the strong overlap between the two patient groups' G_{A2} values. The implication of this finding is that either G_{A2} is too difficult to measure accurately, or that it plays a role in some patients' propensity to faint but not others.

8.8 Conclusion

With the aid of a model, it was hoped that a more informed syncope prediction could be achieved. However, the results demonstrate that this approach does not offer an advantage over the signal processing work of Chapter 6: the accuracy of a linear classifier using the four model parameters as inputs is low. Table 8.5 compares the accuracies of the best results from Chapters 4, 6, and 8.

There are several problems which proved too difficult to overcome in the physiological modelling: firstly, there were many parameters which could not be measured directly. Most of the parameters in the Orthostasis Model were not estimated from the Falls Clinic population but were set as constants, often taken from the models of Ursino *et al.*

Section	Variables	Time period	PPV	NPV	Accuracy
4.6.4	BP, RPP	All available data	0.71	0.94	0.84
6.5	LF (T14)	Early response to HUT	0.41	0.83	0.60
6.6	ICFV P3	Early response to HUT	0.78	0.86	0.83
6.6.2	LC: Signal Processing	Early response to HUT	0.93	0.88	0.90
8.7.2	LC: Ortho. Model	Early response to HUT	0.65	0.69	0.67

Table 8.5: A comparison of the classification performance for various methods to predict or diagnose automatically the presence of vasovagal syndrome. LC = Linear Combination.

Secondly, these constants have been calculated largely from healthy young volunteers, as opposed to the elderly. This is due to the relatively poor characterisation of elderly people in the physiological literature; healthy young volunteers are usually recruited in most studies.

A third factor is the reliance of the parameter estimation upon accurate Finapres data, in particular the decrease in BP after tilt. As noted previously, although the Finapres is a very popular instrument for the measurement of beat-to-beat changes in BP, it does not meet the standards of accuracy established by the American Association of Medical Instrumentation.

A fourth factor may be the most important: it is possible that not all of the parameters necessary for syncope prediction in the elderly can be derived from the first few minutes of BP, HR, or NIRS data following tilt. The thoroughness of the investigation into these data streams in the present work makes this a definite possibility: the information which they provide has not been able to predict vasovagal syncope in the elderly based on the early response to tilt.

A question which arises is whether the approaches in Chapters 6 and 8 can be combined to improve accuracy. It could be argued that signal processing has already played an important role in the determination of some of the model parameters; for example, the calculation of k_{ab} requires BRS, the result of processing an RR tachogram and a BP time series. Hence the question is whether the signal processing methods of Chapter 6 could be used to enhance the model-fitting process. There are two problems, however, with this approach. The first is related to the characteristics of the Falls Clinic data set: the new patient subset would have to be formed from the intersection of Subsets A, B, and C, which would significantly reduce the amount of data available for analysis. The second problem is more general: the new signal processing metrics developed in Chapter 6 have not yet been studied by others, and hence have not been linked quantitatively to parameters in the Orthostasis Model, for example via animal or human studies. For these two reasons, the modelling approach of the current chapter was developed separately from the techniques of Chapter 6.

Chapter 9

Signal Processing for Syncope Prediction During Prolonged HUT

9.1 Introduction

It is clear from the analysis in Chapters 6 and 8 that vasovagal syncope cannot be predicted sufficiently accurately based on the first few minutes after tilt. The next step is to expand the analysis by exploring the evolution of signal processing parameters during the course of HUT. It is possible that parameters might evolve according to characteristic patterns which could differentiate fainters from normals before the end of the test.

9.2 Selection of Parameters for Prolonged Monitoring

One of the best early predictors in Chapter 6 was BRS; monitoring the changes in HR and ICF were also very effective. For these reasons, these three parameters are also considered in the current chapter, but adapted to deal with prolonged monitoring. In addition, PP (pulse pressure) is included because it might be inversely related to vasoconstriction [146], which is implicated in the minutes preceding vasovagal syncope as discussed in Chapter 7. A fifth potentially useful parameter is RPP, which is supposed to decrease prior to syncope, as discussed in Chapter 3. In summary, the following parameters were selected as indicators of cardiac, vascular, and neural activity:

1. **BRS -** Baroreflex sensitivity: via spectral technique

2. ICFV - Instantaneous centre frequency variability

3. ΔRPP - Rate-pressure product difference: current RPP minus baseline average RPP[1]

4. PP - Pulse pressure: PP = SBP - DBP

5. ΔHR - Heart rate difference: current HR minus baseline average HR

Secondly, the analysis of HRV (see tests T12–T21 in Table 3.2) was extended to represent a measure of a patient's evolving cardiovascular dynamics during HUT. The RR tachogram during the entire course of HUT, from supine to upright and back to supine, was computed and ectopic beats were removed using the procedure described in Section 5.9.1. In a sliding window of 90 seconds, the Fourier spectrum of the RR tachogram was computed and divided into eight equal-width frequency bands from 0 to 0.5 Hz, encompassing all oscillations of interest. The energies in these bands became the eight time-varying parameters of interest.

Finally, HRV was analysed in a more generic manner. In a sliding window, the reflection coefficients of a 10th-order autoregressive (AR) model of the RR tachogram were computed, in order to attempt to track the dominant frequencies in the HRV spectrum. The mth reflection coefficient ($0 < m \leq 10$) of the data $x(t)$ in each window represents the partial correlation between $x(t)$ and $x(t+m)$, holding $x(t+1), x(t+2), \ldots, x(t+m-1)$ constant [149]. Reflection coefficients were computed rather than the actual AR coefficients since they are constrained to the interval $[-1, 1]$, and hence do not require any form of normalisation to cope with different amplitude ranges.

In summary, three different multi-dimensional representations were investigated in the search for trends in the plots of cardiovascular state:

- Eight equal-width frequency bands of the Fourier spectrum of the RR tachogram
- Ten reflection coefficients of an AR model characterising the RR tachogram
- An ensemble of five averaged secondary parameters from the ECG and BP data streams, as discussed above.

Each was computed for the duration of HUT, where possible. Eighteen vasovagal syndrome patients and 28 nonvasovagal patients were selected, who had an age of 65 of more and were free of AF and CRS.

[1] Recall that RPP = SBP $\times$ HR.

These numbers are slightly larger than those associated with Subset A: six patients have been added. The recordings of these patients were affected by artefacts in the first few minutes after tilt, but higher quality data were recorded during the rest of HUT.

9.2.1 Choice of Baroreflex Sensitivity Calculation

Of the five BRS methods reviewed in Section 3.4.5, the spectral technique was selected for the current work. The justifications for this choice are as follows:

- The spectral technique provides a continuous-time trace, tracking changes in BRS during the course of a tilt test
- It allows the separate evaluation of sympathetic and parasympathetic components (depending on whether α_{LF} or α_{HF} is chosen)
- It does not suffer unduly from only having short sequences of reliable data, as is the case for some patients for whom there is a large amount of artefact around the time of tilt

9.3 Dimensionality Reduction

The trajectories over time of the three representations cannot be visualised easily in their original form, since they are high dimensional. However, they can be visualised approximately in two dimensions via dimensionality-reduction techniques, mapping each feature vector $\mathbf{x}_i$ to a 2D data point $\mathbf{y}_i$. Sammon mapping [177] is one such method, aiming to make the Euclidean distances d_{ij} in 2D between pairs of image patterns as close as possible to the Euclidean distances d^*_{ij} between the corresponding pairs of patterns in the original high-dimensional space. This is done by minimising the "Sammon stress"[2],

$$E_{\text{sam}} = \sum_{i=1}^{N} \sum_{j>i}^{N} (d_{ij} - d^*_{ij})^2. \tag{9.1}$$

In such a manner, 2D trajectories for each patient could be constructed.

Following the preliminary investigation with Sammon mapping, the second objective was to search for typical deviations from normality (as assessed by visual inspection of the entire data set) that might predict a positive test. However, a problem of Sammon mapping is that creating the map requires $\mathcal{O}(N^2)$

[2]This version of the Sammon stress is a simplified form [135] of the original metric [177].

calculations, since E_{sam} sums $\frac{1}{2}N(N-1)$ distance pairs. A second problem is that Sammon mapping acts as a look-up table, so that previously unseen data cannot be located in the projection map without rerunning the optimisation procedure. Hence, to visualise all patient data simultaneously would require one optimisation of all $\frac{1}{2}N(N-1)$ distance pairs, which is too large a computational challenge.

This problem is solved by Neuroscale [135], an extension of Sammon mapping which parameterises the 2D mapping so that $\mathbf{y}_i = G(\mathbf{x}_i; \mathbf{w})$ for arbitrary $\mathbf{x}_i$, where $\mathbf{w}$ represents the Neuroscale model parameters. To fit the model, the patient data were first subsampled every two minutes, generating a training set of approximately 1000 data points (an average of approximately 22 data points per patient). Hence the number of distance pairs involved was approximately 5×10^5, representing a manageable computational load. The data points were constructed as the feature vectors described above, after normalisation using a zero-mean, unit-variance transform. This transform ensured that each element in a feature vector offered a comparable contribution to the vector's magnitude. In this manner the Euclidean distance between points was not dominated by large-magnitude features, and small-magnitude features were not ignored.

Second, the model parameters were determined by nonlinear optimisation after setting the partial derivatives of E_{sam} to zero:

$$\frac{\partial E_{\text{sam}}}{\partial w_{kr}} = \sum_{i=1}^{N} \frac{\partial E_{\text{sam}}}{\partial \mathbf{y}_i} \frac{\partial \mathbf{y}_i}{\partial w_{kr}} = 0 \tag{9.2}$$

where k refers to the index of an RBF (radial basis function), and $r \in \{1, 2\}$ for a 2D map. $\frac{\partial E_{\text{sam}}}{\partial \mathbf{y}_i}$ is the derivative of Equation 9.1:

$$\frac{\partial E_{\text{sam}}}{\partial \mathbf{y}_i} = -2 \sum_{j \neq i} \left(\frac{d_{ij}^* - d_{ij}}{d_{ij}} \right) (\mathbf{y}_i - \mathbf{y}_j) \tag{9.3}$$

and, if the output of the kth RBF is represented by z_k,

$$\frac{\partial \mathbf{y}_i}{\partial w_{kr}} = \delta_{ir} z_k \tag{9.4}$$

where δ_{ir} is the Kronecker delta function.

Following Neuroscale training, "test data" (patient-specific, high time-resolution data) could be input to the RBF network for each patient. A high time resolution was permissible since the computation of network outputs of a trained RBF is very fast compared to the training itself. Trajectories were calculated

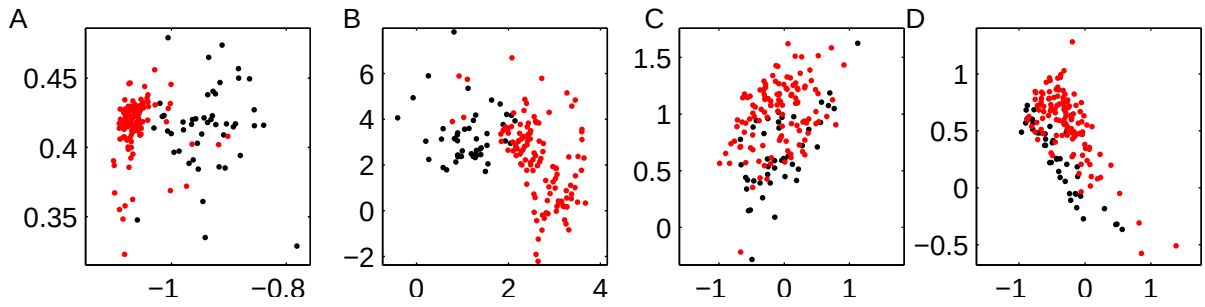

Figure 9.1: Changes in patient state throughout an experiment, as measured using (**A**) Fourier transform spectral band amplitudes, (**B**) AR reflection coefficients, (**C**) an ensemble of five parameters explained in the text, or (**D**) a pair of parameters described in Section 9.4.4. Sammon mapping was used to visualise the high-dimensional data. Black and red dots indicate pre- and post-tilt data, respectively, in a single patient without vasovagal syndrome. In each of the four representations, pre- and post-tilt data are distinguishable, as was the case for most patients. The time separation between each data point is 20 seconds.

for all 46 patients using a resolution of 20 seconds.

9.4 Results

Results are given in Figures 9.1 through 9.4, considering different segments of prolonged HUT. Figure 9.1 provides example trajectories of the feature vectors for a single patient for the entire duration of HUT. Figure 9.2 compares the mean baseline feature vector to that recorded immediately after tilt, for all available patients. Figure 9.3 compares the same pre-tilt feature vector to that averaged over the last five minutes in the upright portion of HUT. Finally, Figure 9.4 compares the pre-tilt feature vector to the final data point recorded in the upright segment of HUT.

9.4.1 Fourier Transform

Although some patient trajectories showed no obvious trend, the majority tended to shift permanently from one region of the Sammon map to another following tilt, as shown in Figure 9.1A. This finding was in line with published findings (see Section 3.4.3) that spectral power tends to change upon tilt.

When Neuroscale was used to visualise the entire patient data set, no generalisations could be made regarding the distribution of the normal versus vasovagal data in the 2D space: the direction of the shift from pre-tilt to immediate post-tilt did not seem to be affected by the diagnosis assigned to the patient (see Figure 9.2A/E). For this reason, it is concluded that the Neuroscale visualisation of spectral band amplitudes in the RR tachogram offers no benefit for syncope prediction.

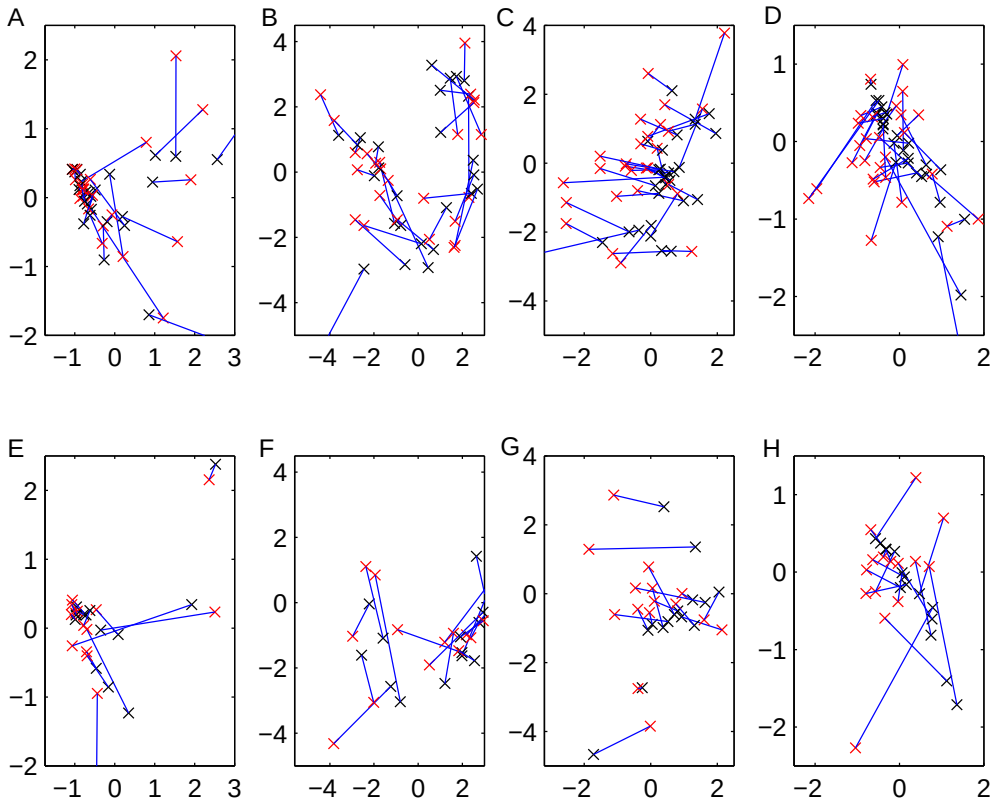

Figure 9.2: Comparison of nonvasovagal (top row) and vasovagal (bottom row) patients in a 2D visualisation, using the following input vectors: (**A**/**E**) Fourier transform spectral band amplitudes, (**B**/**F**) AR reflection coefficients, (**C**/**G**) an ensemble of five parameters, (**D**/**H**) a pair of parameters described in Section 9.4.4. Letters A-D are as in Figure 9.1 for nonvasovagal patients, and E-H represent the corresponding data for patients with vasovagal syndrome. The black crosses represent the mean pre-tilt vector (the last five minutes of data taken during the quiet baseline recording), and the red crosses represent the mean post-tilt vector (from 2 to 5 minutes after tilt). The lines connecting each pair of points indicate the direction of shift as a result of the initial response to tilt. In each of the four cases, the two patient groups could not be distinguished.

To confirm that the method does not differentiate between the two patient groups during prolonged HUT, the last few minutes (Figure 9.3A/E) and seconds (Figure 9.4A) of tilt were examined, when differences in the Fourier transform should be greatest. These differences were found to be negligible as is evident from the figures.

9.4.2 AR Reflection Coefficients

As with the Fourier transform trajectories, two phases (pre- and post-tilt) were observable in the AR reflection coefficient trajectories (see Figure 9.1B).

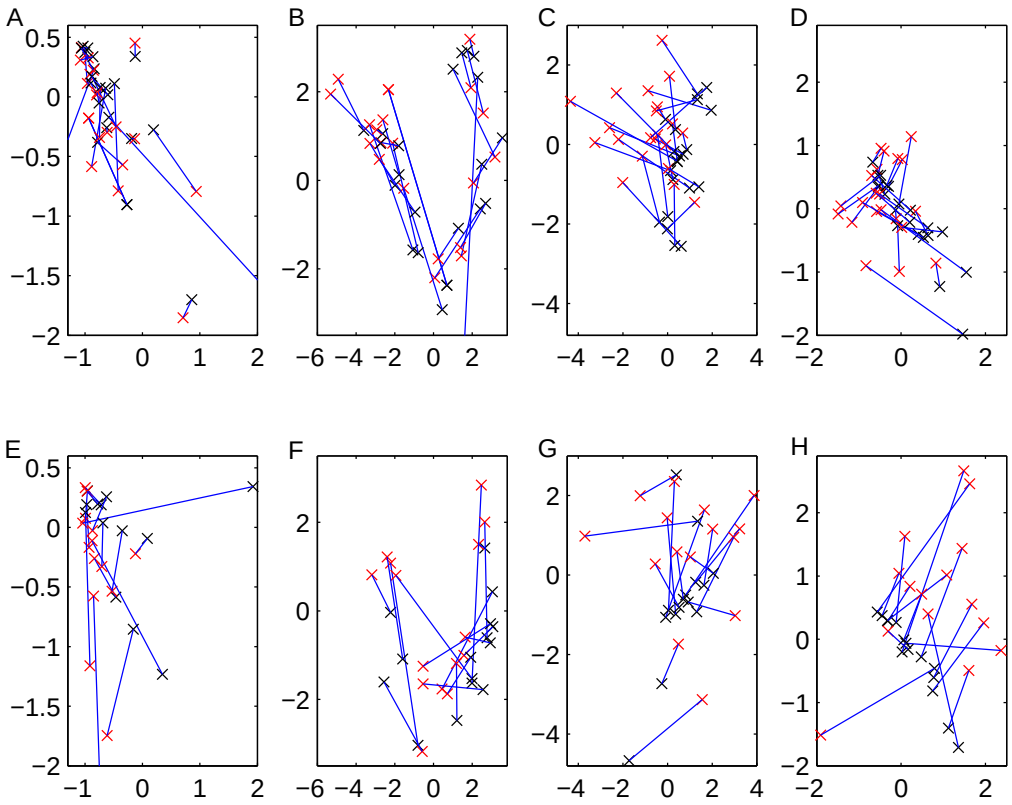

Figure 9.3: Comparison of nonvasovagal (top row) and vasovagal (bottom row) patients in a 2D visualisation, using the following input vectors: (**A/E**) Fourier transform spectral band amplitudes, (**B/F**) AR reflection coefficients, (**C/G**) an ensemble of five parameters, (**D/H**) a pair of parameters described in the text. Letters A-H are as in Figure 9.2. The black crosses represent the mean pre-tilt vector (the last five minutes of data taken during the quiet baseline recording), and the red crosses represent the *late* post-tilt vector (the last 5 minutes in the upright position). The lines connecting each pair of points indicate the direction of shift as a result of the late response to tilt. In cases A/E and B/F, the two patient groups could not be distinguished. In contrast, the direction of the blue lines differed between C and G, as well as between D and H, indicating that vasovagal syndrome could be identified using either of these two input representations.

Figure 9.2B/F plots the averaged pre- and post-tilt results for each patient. These plots demonstrate that no differences could be discerned between the post-tilt reactions of vasovagal and nonvasovagal patients. As with the Fourier transform input representations, Figures 9.3B/F and 9.4B show that AR reflection coefficients also cannot differentiate, on their own, between the two patient groups toward the end of HUT, when maximal differences would have been expected. The similarity of these results with those obtained with the Fourier transform coefficients is probably due to the fact that AR reflection coefficients and spectral energy bands encode similar information.

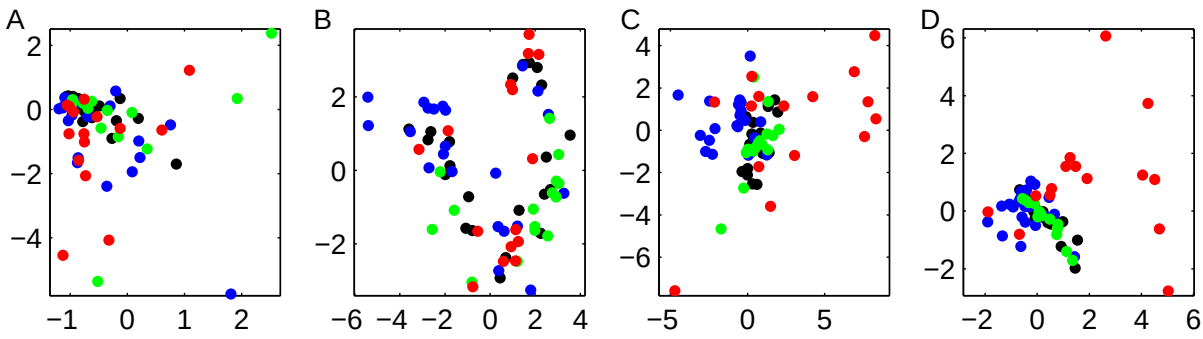

Figure 9.4: Comparison of nonvasovagal patients with vasovagal patients in a 2D visualisation using Neuroscale, with letters A-D as in Figure 9.1. The black and green dots represent the mean baseline data of nonvasovagal and vasovagal patients, respectively. The blue and red dots represent, for the same two groups respectively, the data recorded at the end of HUT, immediately before the return to the supine position. In D, and to some extent in C, the red dots only are in a separate region of the graph, indicating that the two patient groups behave differently at the end of HUT.

9.4.3 Ensemble of Physiological Parameters

As previously mentioned, the parameters were transformed to each have zero mean and unit variance, to cope with their differences in dynamic range. As with the Fourier transform bands and AR reflection coefficients, the five-dimensional feature vectors were visualised in 2D for individual patients (see Figure 9.1C) and general pre-/post-tilt behaviour were compared across patients (see Figure 9.2C/G). This grouping of five parameters was not found to behave consistently within either patient group to be useful to predict syncope. During late HUT, some differences begin to appear between the two patient groups. The blue lines in Figure 9.3C have a greater tendency to point leftwards than those in Figure 9.3G. Figure 9.4C also shows that the late-HUT points for the two patient groups occupy slightly different regions of the Neuroscale visualisation.

9.4.4 Projection of Physiological Parameters

Of the five physiological parameters, it is possible that the predictive capability of those carrying useful information was reduced by those not carrying such information. Hence reductions of the ensemble to fewer than five parameters were investigated.

In Section 6.6.2 it was noted that the relative utility of each parameter in a linear classifier can be determined by examining the magnitude of its corresponding weight a_i. In this manner, less useful parameters can be identified and, if desired, discarded. Therefore, by performing CVA on the five physiological parameters, a ranking of effectiveness can be achieved.

A "final feature vector" was considered; this refers to the five aforementioned physiological parameters, for the final data point recorded in the upright segment of HUT. Following CVA, the elements of the eigenvector were 0.16 (BRS), 0.06 (ICFV), -0.98 (ΔRPP), 0.09 (PP), and 0.06 (ΔHR). Hence, at the end of HUT, it is shown that ΔRPP and BRS contribute most of the classification information in the feature vector: they differ to a greater extent than PP, ICFV, or ΔHR, when vasovagal and nonvasovagal patients are compared. (This is despite the good performance of ICFV during early syncope prediction — see Section 6.6.) When the ensemble is reduced from five to just these two parameters, the elements are recomputed as 0.11 (BRS) and -0.99 (ΔRPP). The result of reducing the ensemble for one patient is plotted in Figure 9.2D/H, where pre- and post-tilt behaviour are different as expected. In addition, Figures 9.3D/H and 9.4D imply that the combination of ΔRPP and BRS (after zero-mean, unit-variance transformation) is able to differentiate between patients toward the end of HUT.

9.5 Evolution of Parameters during Prolonged HUT

The capacity of the four methods to differentiate between patients can be tracked from the start to the end of HUT. For each of the methods, the mean data point μ at time t of each of the two patient groups was calculated. The Euclidean distance between the two means was determined as:

$$\delta(t) = \|\mu_{\mathbf{V}}(t) - \mu_{\mathbf{N}}(t)\| = \sqrt{\left[\mu_{\mathbf{V}}(t) - \mu_{\mathbf{N}}(t)\right]^T \left[\mu_{\mathbf{V}}(t) - \mu_{\mathbf{N}}(t)\right]} = \sqrt{\sum_{i=1}^{D} \left[\mu_{\mathbf{V}\,i}(t) - \mu_{\mathbf{N}\,i}(t)\right]^2} \qquad (9.5)$$

where V indicates vasovagal patients and N nonvasovagal patients, and T represents transposition of the D-dimensional vectors. The hypothesis motivating this investigation was that a clear increase in $\delta(t)$ many minutes prior to syncope might be used as a predictor.

For comparison, the distance between a point and its group's centre, averaged over all points ($\eta(t)$) was also considered. Hence $\delta(t)$ is compared with an intra-group variability, $\eta(t)$:

$$\eta(t) = \frac{1}{M} \sum_{j=1}^{M} ||\mathbf{x}_j(t) - \mu_{C_j}(t)|| \qquad (9.6)$$

where the M vectors (data points) $\mathbf{x}_j$ are each associated with a class C_j of either V or N as in Equation 9.5.

The results are plotted in Figure 9.5. As shown on the righthand side of the plots, an increase in

$\delta(t)$ was found to occur in three of the four cases, starting several minutes before syncope. In A and B, $\delta(t)$ does not exceed $\eta(t)$, indicating that classification performance would be expected to be poor. However, in C and D the significant rise in $\delta(t)$ toward the end of HUT signifies the differing responses of the two patient groups to prolonged orthostasis. Since the mean inter-cluster distance exceeds the mean point-to-centre distance, some degree of classification is possible.

In summary, as the intra-group variability $\eta(t)$ is not significantly smaller than the the inter-group distance $\delta(t)$ in Figure 9.5A-B, accurate discrimination between the two groups in these high-dimensional spaces is not possible. However, discrimination is possible with the combination of ΔRPP and BRS, as shown in part D of the figure. Based on these results, a linear classifier was constructed as

$$y = a_1 x_1 + a_2 x_2 \tag{9.7}$$

where x_i are the parameters ΔRPP and BRS after zero mean and unit variance normalisation, a_i are the weights (-0.99 and 0.11), and the result y should be high for vasovagal syndrome patients and low for nonvasovagal patients. The method of classification is similar to that used in Section 6.6.2.

The final data point (that closest to the return to supine) yielded the highest accuracy: the area under the receiver-operator characteristic curve was 1.00, as determined by the leave-one-out method. Hence the two patient groups were separated perfectly. The area was lower for the preceding data points, but exceeded 0.80 for the final 150 seconds of HUT. This implies that there exists some degree of predictive information in the 2.5 minutes preceding syncope. The overall accuracy of the classifier remained above 0.80 for more than a minute before syncope, as can be seen in Figure 9.6. This could be exploited by an algorithm offering early warning of syncope. For example, in cases where patient comfort is particularly important, a tilt test may be halted one minute early with a success rate of approximately 80%.

9.6 Conclusion

The investigations of this chapter used data from the entire course of HUT. Visualisation of the evolution of these parameters in 2D space did not reveal typical patterns in the data which could differentiate between the two patient groups in the early stages of HUT. However, the rate-pressure product and baroreflex sensitivity were able to discriminate between the two patient groups shortly before syncope. One conclusion from this is that different parameters are appropriate for syncope prediction during

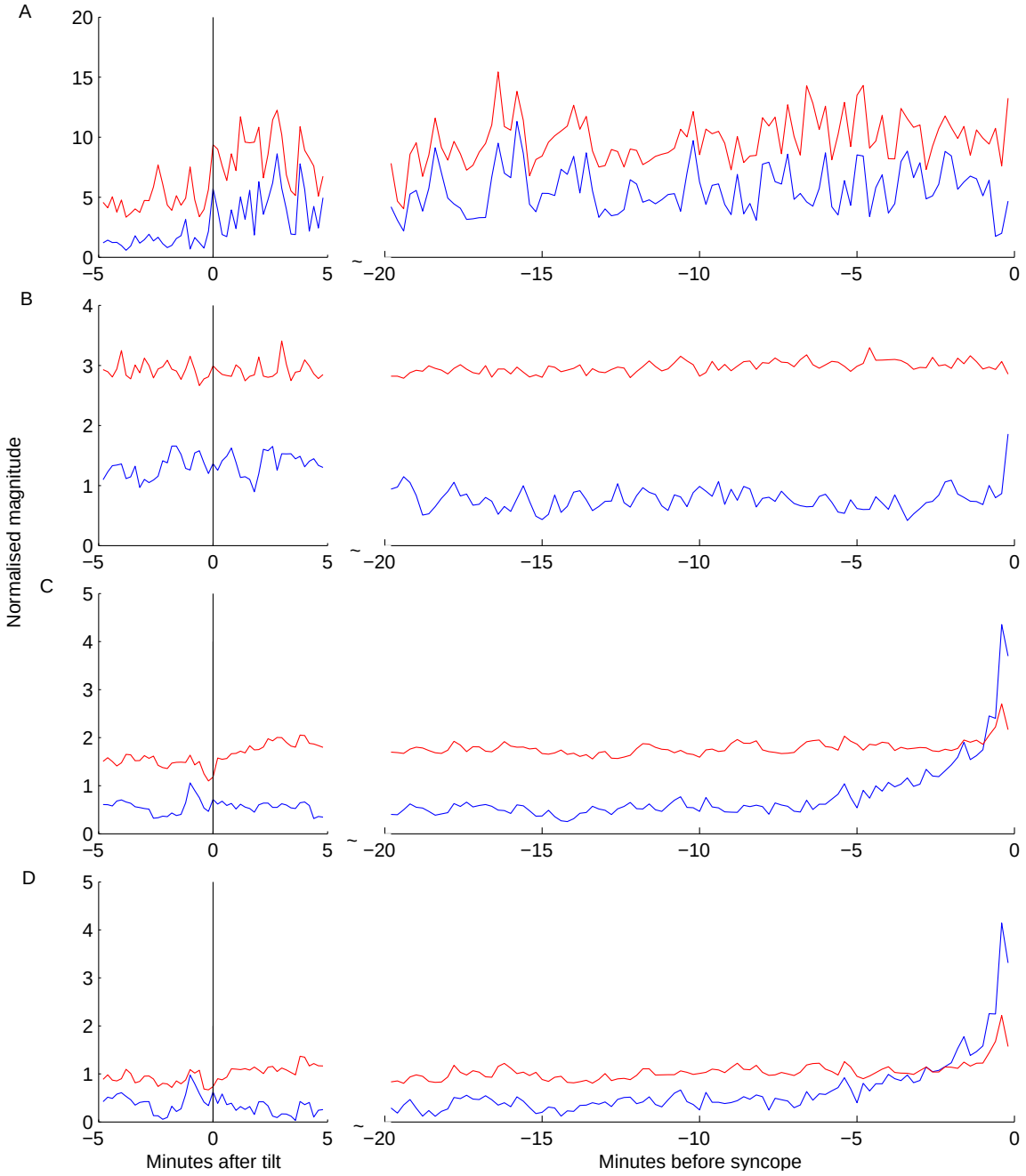

Figure 9.5: Using high-dimensional space to compare patients' cardiovascular dynamics, as calculated with (**A**) Fourier transform, (**B**) AR reflection coefficients, (**C**) an ensemble of five parameters explained in the text, or (**D**) a pair of parameters as explained in the text. On the left are shown the five minutes before and after the patient was tilted to the upright position (the time of tilt is indicated by a vertical black line), and on the right are shown the 20 minutes preceding either syncope (for vasovagal syndrome patients) or the return to the supine position (for nonsyncopal patients). The blue line represents Euclidean distance $\delta(t)$, and the red line represents the average intracluster distance, $\eta(t)$.

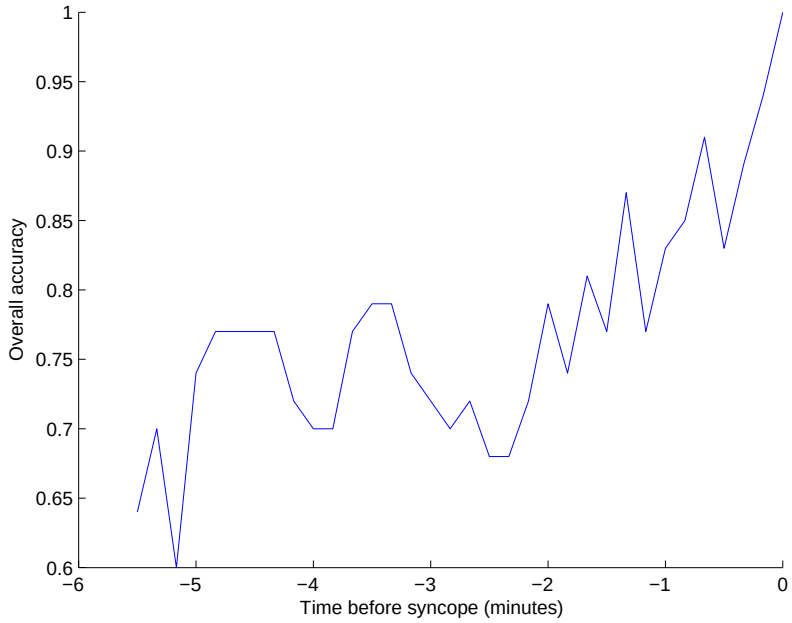

Figure 9.6: Overall accuracy as a function of time, for a classifier based on the optimal combination of ΔRPP and BRS (compare Figure 9.5D).

different periods of HUT.

An expanded version of Table 8.5 is given as Table 9.1. The combination of RPP and BP has an accuracy of 100% at the end of the HUT test but does not offer significant predictive benefit. However, HUT may be terminated early with 80% accuracy, preventing the patient from experiencing the discomfort associated with syncope. A clinician could combine an indicator from such an algorithm together with his own observation of patient symptoms, while making a diagnosis.

Section	Variables	Time period	PPV	NPV	Accuracy
4.6.4	BP, RPP	All available data	0.71	0.94	0.84
6.5	LF (T14)	Early response to HUT	0.41	0.83	0.60
6.6	ICFV P3	Early response to HUT	0.78	0.86	0.83
6.6.2	LC: Signal Processing	Early response to HUT	0.93	0.88	0.90
8.7.2	LC: Ortho. Model	Early response to HUT	0.65	0.69	0.67
9.5	BP, RPP	Data point at end of HUT	1.00	1.00	1.00
9.5	BP, RPP	1 min before end of HUT	0.76	0.87	0.83
9.5	BP, RPP	2 min before end of HUT	0.68	0.86	0.79

Table 9.1: A comparison of the classification performance for various methods to predict or diagnose automatically the presence of vasovagal syndrome. LC = Linear Classifier.

Chapter 10

Conclusions

10.1 Summary of the Thesis

The first two chapters stressed the importance of syncope prediction, and provided the clinical background necessary to understand the problem. The diagnosis of syncope, including a description of the various pathologies responsible for fainting, was reviewed and vasovagal syncope was identified as being poorly understood.

Chapter 3 described previous work on the quantitative analyses of BP, HR, SaO_2, and NIRS time series, and presented the relevant concepts underlying time-frequency analysis. Since even healthy patients experience persistent nonstationarity in their haemodynamics, the Smoothed Pseudo-Wigner Ville Distribution was characterised as being well suited to their analysis.

Chapter 4 explained how the data set used in the thesis was acquired. The data set was then investigated with the aim of generating automatic diagnoses. It was shown that orthostatic hypotension was difficult to assess, whereas it was easier to diagnose carotid sinus hypersensitivity and vasovagal syndrome more accurately. In particular, the use of the rate-pressure product (blood pressure multiplied by heart rate) during the time of syncope combined with monitoring the decrease of systolic blood pressure during prolonged HUT, yielded an 84% accuracy rate for the diagnosis of vasovagal syndrome.

Chapter 5 explored the use of time-frequency analysis in RR tachograms. After the smoothing parameters of the SPWVD were chosen based on artificial data, the optimised transform was validated on artificial data. The computed LF/HF ratio followed the expected value with a maximum tracking error of just 3.6%. Finally, the application of the SPWVD transform to the clinical data showed it to be superior

to the Lomb periodogram.

Chapter 6 investigated whether it was possible to predict vasovagal syncope well in advance of its occurrence. Classical techniques from the literature gave poor results on the Falls Clinic data set: out of 29 tests, only four achieved an overall accuracy greater than 0.70, and none more than 0.75. The largest negative predictive value (NPV) was 0.83. The most significant contribution of this chapter was the development of a new form of time-frequency analysis of RR tachograms. As a classifier, the ICFV during time period P3 performed well (NPV: 0.86). A linear classifier using a total of four input parameters increased the NPV marginally to 0.88. Several factors which may have reduced the maximum possible accuracy attainable in the data set were listed.

Chapter 7 identified and analysed the three most probable mechanisms of vasovagal syncope. Chapter 8 considered these pathways during the development of the Orthostasis Model. Once the model was validated by comparison with physiological findings in the literature, it was used to underpin parameter estimation from the clinical data introduced in Chapter 4. Three parameters (baroreceptor operating point, cardiac effectiveness, and baroreflex gain) were extracted from each patient's supine baseline recording in order to normalise the model for that patient, after which four new parameters (sympathetic and parasympathetic gains at the sino-atrial node, peripheral vasoconstriction gain, and total blood volume) were estimated from the data collected in the upright position. The modelling approach, however, was found to offer no improvement upon the signal processing results: a linear classifier using the four parameters estimated in the upright position yielded an NPV of just 0.69, as compared to 0.86 for the best signal processing technique. This finding may have been due to the amount of inference in the model, increased vulnerability to Finapres artefact, or other reasons discussed in Chapter 8.

Finally, Chapter 9 returned to the problem of predicting syncope based on signal processing parameters, but this time using data from mid- and late HUT. Two-dimensional data visualisation of signal processing parameters did not reveal patterns characteristic to patients with vasovagal syndrome, during prolonged HUT. However, it was shown that information derived from the rate-pressure product and baroreflex sensitivity, could be used to terminate the test approximately 2 minutes before syncope was expected to occur. A weighted combination of the two parameters gave a prediction accuracy of 80%. This achieves the secondary aim of increasing patient comfort, by halting a test early.

The first key conclusion from the thesis is that it is very difficult to predict vasovagal syncope early in HUT (within the first few minutes after tilt) with great accuracy. A second conclusion is that the use

of physiological modelling does not help, because it requires the values of too many unknown variables to be extracted. Finally, the third key conclusion is that the test can be terminated early to increase patient comfort by avoiding syncope.

10.2 Future Work

Signal Processing

Prospective testing of the predictive value of ICFV during time period P3 (see Section 6.4.2) requires more data to be collected. Appendix F shows that a minimum of 68 patients would be needed in a randomised controlled trial.

The instrumentation described in the thesis produced a number of noninvasive data streams. An alternative to using the Finapres for beat-by-beat BP is to develop a BP estimation algorithm based on PTT (see Section 3.4.7). This was attempted for the current research but thus far without success. The search for a reliable BP estimator from PTT has been on-going since the early 1920s [30], motivated by the knowledge that changes in blood pressure are often associated with changes in vasoconstrictive tone, which in turn affect the speed of transmission of pulse waves in blood vessels.

The methods used to classify the data could also be extended. For example, an alternative to producing parameters for canonical variates analysis would be to use phase space dissimilarity measures [81]. Statistical distribution functions would be derived from the original time series, and these functions could be compared for patients with different diagnoses. A second alternative would be to compute a large number of metrics from the time series, and apply the relatively new technique of false discovery rate (FDR) to identify significant patterns [17].

Physiological Modelling

The following improvements should be considered:

Hydrostatic changes of the cardiac pump: Although hydrostatic changes upon tilt are imposed on the coronary blood flow, the cardiac pump itself (described in Equations 8.30 through 8.1, and 8.26 through 8.29) is not affected. In fact, the atria lie approximately 4 cm above the hydrostatic indifference point in the upright position.

Spatial limitations of the pericardium: The left and right ventricles compete for space within a

limited pericardium; this is one of the causes of lowered left ventricular stroke volume on standing. The model currently overlooks this effect which may be why stroke volume did not decrease as much as reported in the literature.

Increasing the effects of atherosclerosis: As the arteries harden, their compliance and resistance change. The change in compliance is currently estimated using a simple formula but the (smaller) change in resistance is more difficult to estimate. If a characterisation of this change, or even an empirical relationship between arterial resistance and compliance, could be determined from the literature, then the arterial resistance of a given patient could be estimated more accurately.

Angiotensin II: Given the multiplicity of generation mechanisms for renin, and hence angiotensin II (see Section 7.3.3), accurate modelling is difficult. However, the model would be improved if it could be expanded to reflect the differences between antagonising the actions of angiotensin II versus blocking it altogether, the results could be combined with an upcoming clinical trial.

The most significant extension of the model regards the representation of breathing. An extended version of the Orthostasis Model has been developed to accommodate respiration rate and tidal volume, but the instrumentation used at the Falls Clinic is unable to provide these time series reliably. Should the instrumentation be improved, this is an area for further study which will assist with the parameter estimation.

Incorporating NIRS data into the model should also be considered more carefully in future. For the present work, it was not included since some patients experienced a rise in O_2Hb upon tilt concurrent with a fall in arterial BP, and it was not clear how best to reflect this behaviour in the model. Payne showed recently that TOI may be represented in a simple extension of the Ursino cerebrovascular model [153]. An expression relating TOI to cerebral blood flow and volume was derived:

$$TOI = 1 - \frac{V_v\, k_q}{(V_a + V_v) q_b} \tag{10.1}$$

where k_q is a constant, q_b represents blood flow rate, and V_a and V_v represent the volume of blood per unit volume of tissue, in the arterial and venous systems respectively. However, in Falls Clinic patients, TOI usually did not change noticeably upon tilt. Moreover, the supine baseline value of TOI is dependent on optode positioning: in some cases this affects the reading by up to 10 percentage points. One way of

mitigating this second problem might be to assume that all patients had the same supine level of TOI, and scale their entire traces accordingly.

Data Acquisition

In future HUT studies, a Valsalva manoeuvre (attempting to expire air while keeping the throat closed) could be introduced. The observation of the impact which the manoeuvre has on BP and HR may assist with the model parameter estimation, and in some cases identify patients with sympathetic neurocirculatory failure.

The most significant improvement which could be made would be the acquisition of further patient data. If the height and weight of every patient were recorded, this additional data could be used to normalise some of the constants in the Orthostasis Model on a per-subject basis. The availability of more training data would also make it possible to investigate nonlinear classifiers, such as the multi-layer perceptron, which could be trained without the risk of over-fitting. A larger data set could also be subdivided to take into account the inter-patient heterogeneity of vasovagal syncope.

Appendix A

Peak Detection Algorithms

A.1 Introduction

This appendix describes the algorithms developed for the current research to overcome the problems associated with peak detection in the ECG and PPG traces. Owing to the similarity between these two tasks, the discussion will be limited to the ECG algorithms, with comparison to the PPG made at the end.

The QRS complex was introduced in Figure 1.2 in Chapter 1. Various methods of detecting the QRS complexes in an ECG have been proposed [54,76,83,84,145,209]. Two major problems in QRS detection are:

Noise: e.g. muscle noise, electrode pop, electrical mains interference, baseline wander, and high T waves

Morphological variability in the R waves: e.g. a wide, high-amplitude beat will have a lower R-wave slope, confounding some derivative-based approaches

For these reasons, even the best automated QRS complex detectors cannot match the level of human analysis. In the present work, an algorithm whose fundamentals are based loosely on those of the algorithm of Pan and Tompkins [145] was employed (see Figure A.1). The procedure was chosen for its simplicity and accuracy, and tailored with the following assumptions in mind:

- A rest period occurs at some point within the first five minutes of the recording
- The ECG is acquired using three leads

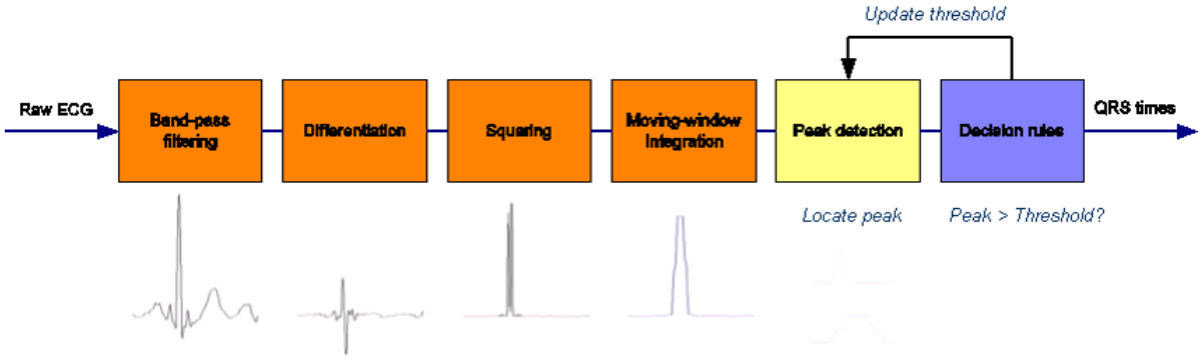

Figure A.1: An overview of the QRS detection algorithm.

- The subjects were elderly, and hence ectopic beats should be expected

In addition to this algorithm, pre- and post-processing was needed to improve the accuracy the resulting event series. The QRS detection algorithm was based on four signal processing sections: ECG time-stamping, QRS localisation, multi-lead integration, and event series analysis. In the following sections, each of these blocks is discussed in turn, and the algorithm is validated quantitatively using well-known annotated ECGs available publically from the MIT-BIH database [60].

A.2 ECG Time-Stamping

The time stamps associated with the ECG data points were uneven and inaccurate. They were therefore replaced by an evenly-sampled time vector, calculated as part of the post-processing of the original data.

A summary of the algorithm used to post-process each ECG is illustrated in Figure A.2. It consisted of the following steps:

1. The raw ECG was represented as a two-column matrix, containing the data points in mV and their respective time stamps in seconds.

2. Towards the end of a clinical experiment, as the patient was being disconnected from the ECG monitor, the device sometimes recorded time stamps at a slower rate than normal. To prevent these times from affecting the accurate calculation of F_s in step 4, the ECG was truncated. Although a rule-based algorithm detecting patient disconnection was written for the PPG recordings, the termination points of ECG recordings were also confirmed visually.

3. If any gaps greater than 3 seconds existed in the recording, steps 4 through 7 were applied to each

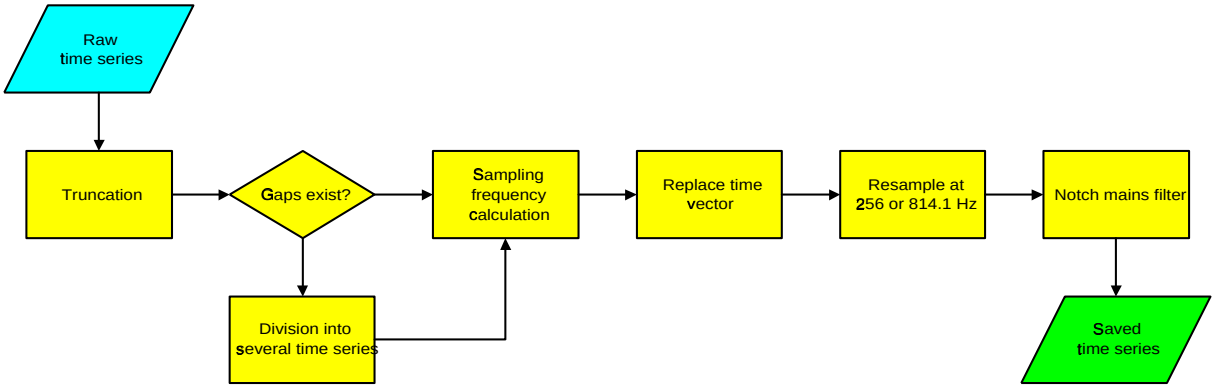

Figure A.2: Assigning time stamps to the ECG or PPG. The electrical mains notch filter (50 Hz) is not applied in the case of the PPG signal, as the time series reflects IR attenuation rather than electric potential.

block of continuous data in turn. If the time series were instead treated as a whole, the calculations in step 4 would have been inaccurate.

4. The "mean sampling frequency" of an ECG record consisting of N data points, ranging from a start time of t_{start} to an end time of t_{final}, was estimated using the following formula:

$$F_s = \frac{N-1}{t_{\text{final}} - t_{\text{start}}} \tag{A.1}$$

5. The new time vector started with the first time stamp of the ECG, and ended with a value very close to the final time stamp of the ECG. In between, the points were sampled evenly at a rate of F_s.

6. The new two-column matrix, consisting of the original data points assigned to the new time stamps, was linearly interpolated at 256 Hz. This standardisation simplified all subsequent software.

7. The matrix was filtered using a 100-point FIR notch filter, removing electrical mains interference near 50 Hz.

8. Finally, the result of steps 4 through 7 for each continuous block of the ECG was combined into an $m \times 2$ matrix, with $m/256$ representing the length of the ECG recording in seconds.

A.3 QRS Localisation

The identification of QRS complexes within the refined ECG time series followed the Pan and Tompkins algorithm, divided into three sections: preprocessing, peak detection, and decision making (recall Figure A.1).

Preprocessing

Preprocessing consisted of four stages:

Band-pass filter: To reduce noise and focus on the frequencies of interest. The desirable passband to maximise QRS energy is 5-15 Hz. (Pan and Tompkins used 5-12.)

Differentiation: To find the slope of the signal (QRS complexes are spikes). A nearly linear frequency response between 0 and 30 Hz was obtained using:

$$y(n) = \frac{1}{8T}[-a(n-2) - 2a(n-1) + 2a(n+1) + a(n+2)]. \tag{A.2}$$

Squaring: To intensify the slope, in order to restrict T-waves from being taken as QRS complexes. Not only were all data points made positive, but the higher frequencies (i.e. the QRS frequencies) were emphasised:

$$y(n) = [x(n)]^2. \tag{A.3}$$

Moving window integration: To consider slope and width together, for an approximation of morphology. In the equation

$$y(n) = \frac{1}{N}[x(n-N+1) + x(n-N+2) + ... + x(n)], \tag{A.4}$$

N was chosen as the width of the widest QRS complex. With a greater value of N, the QRS complexes and T-waves could have merged together; with a smaller value, a single QRS complex could have produced several peaks in the integration waveform.

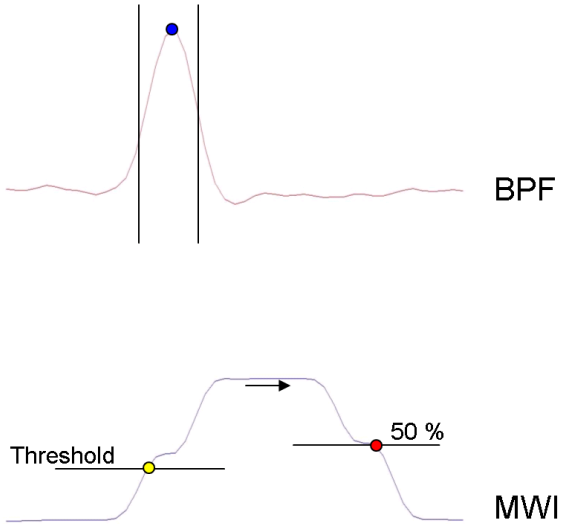

Figure A.3: Detection of peaks using fiducial marks. The MWI trace was analysed from left to right. After it exceeded the threshold (yellow circle) from Equation A.5, a search for the fiducial point (red circle) began. This point occurred when the MWI descended below 50% of the maximum obtained after the yellow circle was assigned. Next, a range of times (denoted by the two vertical lines) was defined usually as from 125 to 225 ms before the fiducial point. The maximal BPF point (blue circle) within this range was easily determined. Finally, the QRS complex time was calculated as the first moment of the BPF trace within 80 ms of this point (i.e. the "centre of mass" of the QRS complex). BPF = Band-pass filtered; MWI = Moving Window Integration.

Fiducial Point Determination (Peak Detection)

The objective of fiducial point determination was to identify a consistent point of interest in the ECG which could be used to determine the time of the R peak. A fiducial mark could have been set at various points in the MWI trace, each of which mapped uniquely onto a feature of the QRS complex. For the current algorithm, the method described in Figure A.3 was developed.

Decision Making

Once a peak was identified, it had to be tested for validity, based on its amplitude. To this end, running estimates of peak height and noise levels were maintained, calculated as the median of the previous eight values. A threshold was maintained, to compare the expected with the actual peak heights:

$$\text{Threshold} = \text{Noise} + 0.189\,(\text{Peak} - \text{Noise}) \tag{A.5}$$

Two thresholds were used: the first applied to the output of the BPF, and the second to the output of the MWI. If the current MWI peak exceeded the MWI threshold, and the corresponding BPF peak

exceeded the BPF threshold, the peak was labelled as a QRS complex.

When both peaks were exceeded, a morphology test was performed. An interval of ten typical QRS complex widths, centred on the putative QRS complex, was compared with a similar interval for an "archetypal" (see below) case. The comparison was achieved using Pearson's correlation coefficient R between the two intervals. If Pearson's R was above 0.5, the beat was accepted; furthermore, if it was above 0.75 the current beat was recorded as the new archetype. If Pearson's R was below 0.5 but above a certain threshold (usually 0.43), a second assessment was performed: if the current morphology interval correlated closely (Pearson's $R > 0.80$) with any interval in the subsequent 1.2 seconds, the beat was not rejected. This exception was necessary since some patients do not exhibit a consistent archetypal QRS complex for more than several minutes at a time.

In summary, the decision-making algorithm accepted peaks which exceeded the MWI and BPF thresholds, and passed the morphology test. Special cases arose from time to time, and these were dealt with systematically:

- If 1.66 average beat-to-beat intervals passed with no new peak detection, the algorithm returned to the last detected beat, and continued with a 50-70% lower threshold. (Average beat-to-beat interval was determined using the mean of the eight most recent RR intervals.)
- Irregular heart rates were special cases
- A refractory period of 200 ms was imposed after a QRS complex: no detections were allowed during this time
- A probationary period of 160 ms followed the refractory period: the detection was rejected if its maximal slope was less than 50% of the maximal slope of the preceding QRS complex

Initialisation

A number of parameters had to be initialised whenever the algorithm was used to analyse a new ECG signal. This occurred in two learning phases:

Learning phase 1: Initialised detection thresholds using 2 s of signal

Learning phase 2: Initialised RR-interval average and RR-interval limit values, using two beats

A.4 Interpreting the Multi-Lead ECG

Three-lead ECGs were monitored in the Falls Clinic (see Section 3.3). Reasonable results (not shown) could be obtained by examining only the ECG lead with the highest signal-to-noise ratio (SNR); however, in most cases the accuracy of QRS detection increased by including the two other ECG leads. This is due to the fact that artefacts could affect one or two ECG leads at a time whilst leaving the third relatively unaffected.

Hence, the three ECG leads were each processed individually using the aforementioned QRS detection algorithm, and the resulting three event series were summed on the basis of their respective SNRs. All QRS points were accepted when the SNR in the associated region of the time series (calculated using an autocorrelation function) exceeded a certain threshold. Of course, a number of these QRS points were removed later as a result of post-processing (discussed in Section A.5). So in combining the three ECG leads, it was preferable to err on the side of inclusion rather than exclusion.

A.5 Event Series Analysis

The final step in processing the ECG involved the removal from the event series of simple false positives and false negatives, based on timing information alone. The amplitude of the ECG signal played no role in this step.

- If the beat-to-beat variation in RR interval did not vary by more than 20%, the beat was accepted as correct.
- If the current RR interval was less than 80% of the previous one, the neighbouring QRS times were examined with a rule-based system to determine the most suitable action in line with the previous behaviour of the event series. Usually this involved deleting or repositioning a heartbeat.
- If the current RR interval was more than 120% of the previous one, another rule-based system was employed. This usually resulted in the insertion or repositioning of a heartbeat.

Generally, the approximate heart rate determined using the results of the peak detection algorithm was assumed to be accurate — that is to say, if the event series analysis was found to remove every other heartbeat, or insert an extra heartbeat after every beat, or reposition every other heartbeat, appropriate action was taken. This involved, firstly, confirming that the original time series fell within an acceptable

heart rate range; secondly, disregarding the last 4 decisions; thirdly, re-initialising a few key parameters; and fourthly, re-initialising the algorithm from the point where the problem occurred.

Beats that resulted from repositioning or insertion were labelled as specious, since in these cases their timing represented merely an approximation: the arithmetic average of the two neighbouring heartbeat times. This labelling aided later analysis of instantaneous parameters such as HR or HRV: regions with low confidence were omitted.

A.6 Validation of the Algorithm

The algorithm was applied to the MIT-BIH Normal Sinus Rhythm Database, to prove its efficacy. Eighteen ECGs, each of varying duration, were selected, for a total of over 11.4 million normal heartbeats. The sensitivity and positive predictive value were each 99.96%. (Note that specificity has no meaning in a beat-detection algorithm, since an infinite number of true negatives exist.)

A.7 PPG Peak Detection

The peak detection algorithm written for the PPG was similar to the algorithm designed for the ECG. However, since the signal was in general noisier, with less synchronisation amongst the different leads[1], and showed more variability in its morphology, several key differences exist. For example, event series analysis and morphology checks were not used, and the special cases listed in Section A.3 were not applied.

The algorithm was based on the procedure of Germuska [58], with the following enhancements:

- The threshold applied to the cubed waveform was calculated as the mean of the ranked middle 50% of the previous eight peaks. This change was thought to reflect "normality" better than a simple mean of the previous two beats.
- A 450-ms probationary period was enforced after each peak detection. This was inspired by the similar condition used in the ECG analysis.
- All fiducial points of possible interest were calculated: 0, 25, 50, 75, and 100% of the rise of each peak, in addition to each peak's point of maximal slope.

[1] Recall that the three ECG leads should be expected to produce QRS complexes simultaneously; however, the features of the four PPG optodes were expected to occur at different times, owing to the time required to conduct a pulse wave from one point to another, as described in Section 3.4.7.

- The differentiation equation of choice was the same as for the ECG (see Equation A.2), since it was not necessary to restrict the analysis to causal techniques.
- The signal was upsampled by a factor of approximately 10 (to 814.1 Hz) using cubic splines interpolation, so that fiducial points could be indexed more accurately.

Appendix B

The Human Nervous System

The human nervous system is traditionally divided into the central and peripheral nervous systems (CNS and PNS, respectively). Both of these systems play an essential role in vasovagal syncope.

B.1 Central Nervous System

The CNS can be divided into four parts:

1. Forebrain
    - Cerebral hemispheres (for high-level processing such as "thinking") *
    - Thalamus (relays sensory inputs to cerebral hemispheres)
    - Hypothalamus (for homeostasis and basic behavioural regulation) *
2. Cerebellum (for balance and motor control)
3. Brainstem
    - Midbrain (for many basic unconscious activities)
    - Pons (literally, "bridge" - bundles of nerves)
    - Medulla (for cardiac and respiratory regulation) *
4. Spinal cord (for transmission and simple processing of nerve activity) *

Asterisked areas are especially important in the genesis of vasovagal syncope. For example, the cerebral hemispheres can provide emotional responses such as fear or anxiety. The spinal cord is important for

relaying afferent (incoming) and efferent (outgoing) nerve traffic. The hypothalamus releases hormones as well as hosting the "defence area", a behavioural nucleus responsible for integrating the fight-or-flight regime known as the defence reaction.

Finally, the medulla is responsible for the control of breathing, heart rate, peripheral resistance, and other autonomic functions. An area of particular interest for many of these tasks is the nucleus tractus solitarius (NTS), which processes input from the following sources:

- The vagus, glossopharyngeal, and other cranial nerves
- The hypothalamus
- The spinal cord
- The brainstem
- Plasma hormones (as the medulla lies near a weakness in the blood-brain barrier)

Besides having a large number of inputs, the NTS also has numerous outputs [13]:

- Sympathetic nuclei in the spinal cord
- Parasympathetic nuclei in the medulla
- Other brain stem nuclei
- The forebrain

B.2 Peripheral Nervous System

The PNS, responsible for connecting the CNS to muscles and glands, comprises two elements:

Sensory neurons: Convey input from sensory receptors to the CNS

Motor neurons: Convey output from the CNS to muscles and glands

Somatic division: Innervates skeletal muscle

Autonomic division: Innervates smooth muscle, the heart, and glands

The autonomic division, also known as the autonomic nervous system (ANS), is governed by three forces:

Sympathetic: Prepares the organism for exertion (in the extreme, the defence reaction)

Parasympathetic: Regulates visceral function in a state of relaxation

Enteric: Controls digestion

The enteric system is ignored in the current research as it is a largely independent unit. The sympathetic and parasympathetic[1] systems act in a push-pull manner, and are thought to influence the content of different frequency bands in the heart rate variability (HRV) spectrum.

[1]For the purposes of this thesis, parasympathetic is synonymous with "vagal", as the parasympathetic avenues of interest involve the vagus nerve.

Appendix C

Instantaneous Frequency Equality

In Section 5.3.3, it was claimed that two particular methods of calculating ICF were equivalent; the object of this appendix is to prove their equality. The equality is stated in Ville's seminal paper introducing the SPWVD (Smoothed Pseudo-Wigner Ville Distribution) [222] but here a rigorous path is pursued.

C.1 Delineation of the Proof

For a complex signal $x(t) = a(t)e^{i\phi(t)}$, the instantaneous frequency (ICF or $\phi'(t)$) of $x(t)$ can be expressed as $\phi'(t) = \frac{d\phi(t)}{dt}$. Consider a simple way of deriving this quantity: $\phi'(t) = \frac{d\left(\tan^{-1}(\frac{y}{x})\right)}{dt}$, where $y(t)$ is an in-quadrature signal, $y(t) = \frac{1}{\pi t} * x(t)$. (To assist an intuitive understanding, the two functions $x(t)$ and $y(t)$ are separated by $\pi/2$ radians on a circle in the complex plane; the rate at which their tangent varies will reflect directly the rate at which the pair of functions moves around this circle.)

Next consider the following quantity:

$$\alpha(t) = \frac{\int_{-\infty}^{\infty} \omega W(t,\omega) d\omega}{\int_{-\infty}^{\infty} W(t,\omega) d\omega} \tag{C.1}$$

where $W(t,\omega)$ is the Wigner transform of $x(t)$. The object of the proof is to show that $\alpha(t) = \phi'(t)$.

C.2 Basic Properties

The starting point of the proof is one of the definitions of the Dirac function:

$$\delta(\tau) = \frac{1}{2\pi}\int_{-\infty}^{\infty} e^{i\omega\tau} d\omega. \tag{C.2}$$

Differentiating the left and right sides with respect to τ, we obtain:

$$\delta'(\tau) = \frac{1}{2\pi}\int_{-\infty}^{\infty} i\omega e^{i\omega\tau} d\omega \tag{C.3}$$

which can be rewritten as:

$$\int_{-\infty}^{\infty} \omega e^{-i\omega\tau} d\omega = -i2\pi\delta'(\tau) \tag{C.4}$$

A property of the derivative of the Dirac function is that for any $h(\tau)$,

$$\int_{-\infty}^{\infty} \delta'(\tau)h(\tau)d\tau = -h'(0). \tag{C.5}$$

C.3 The Proof

Multiplying C.4 by an arbitrary function $h(\tau)$ and integrating over all time,

$$\int_{-\infty}^{\infty}\int_{-\infty}^{\infty} \omega h(\tau)e^{-i\tau\omega} d\omega d\tau = -i2\pi\int_{-\infty}^{\infty} \delta'(\tau)h(\tau)d\tau. \tag{C.6}$$

The right-hand side of C.6 can be simplified with the aid of C.5:

$$\int_{-\infty}^{\infty}\int_{-\infty}^{\infty} \omega h(\tau)e^{-i\tau\omega} d\omega d\tau = i2\pi h'(0) \tag{C.7}$$

Then, inserting $h(\tau) = g(t+\tau/2)g^*(t-\tau/2)$, for arbitrary $g(t)$, into the simplified C.6 we reach the following general identity:

$$\int_{-\infty}^{\infty}\int_{-\infty}^{\infty} \omega g\left(t+\frac{\tau}{2}\right) g^*\left(t-\frac{\tau}{2}\right) e^{-i\omega\tau} d\omega d\tau = -\pi i\left[g'(t)g^*(t) - g(t)g^{*\prime}(t)\right]. \tag{C.8}$$

Turning to the specific case where $g(t) = x(t)$, C.8 becomes:

$$\int_{-\infty}^{\infty} \omega W(t,\omega) d\omega = 2\pi a^2(t)\phi'(t). \tag{C.9}$$

Since $W(t,\omega)$ satisfies the marginals,

$$\frac{1}{2\pi}\int_{-\infty}^{\infty} W(t,\omega) d\omega = |x(t)|^2 \tag{C.10}$$

and since $|x(t)|^2 = a^2(t)$, the left-hand side of C.10 can be substituted easily into C.9, to yield:

$$\phi'(t) = \frac{\int_{-\infty}^{\infty} \omega W(t,\omega) d\omega}{\int_{-\infty}^{\infty} W(t,\omega) d\omega} = \alpha(t). \tag{C.11}$$

Appendix D

The Orthostasis Model

This appendix describes the constants, state space, and intermediate variables of the Orthostasis Model developed in Chapter 8.

Descriptions of the constants are provided in Tables D.1 through D.8. These values were almost always taken from the literature [16, 113, 152, 154, 174, 215–217, 219]. Although the Falls Clinic patients were of advanced age, it is not possible to obtain invasive cardiovascular parameters from the elderly. Instead, such parameters are obtained from young healthy subjects or via animal experimentation.

Table D.9 lists the 26 state variables comprising the DDE system. Recall that the model does not require any input for it forms a closed loop. Hence, for each of the state variables, it is possible to give a "Typical value". This is the value which is observed when the default constants are used and the model is run until all state variables settle to a homeostatic equilibrium.

Tables D.10 and D.11 describe the intermediate variables which can be derived from the state variables and are often used in the calculation of the latter. For example, the heart period, T, is the sum of the two state variables ΔT_s and ΔT_v, plus the model constant T_0. This intermediate variable is then used in the calculation of the state variable P_{pa} (see Equations 8.8 and 8.27).

Constant	Value	Description
Systemic volumes:		
V_{usa}	0	Unstressed systemic arterial volume
V_{usp}	274.4	Unstressed splanchnic peripheral volume
V_{uep}	134.64	Unstressed extrasplanchnic peripheral volume
V_{ump}	105.8	Unstressed muscular peripheral volume
V_{ubp}	72.13	Unstressed brain peripheral volume
V_{uhp}	24	Unstressed heart peripheral volume
V_{ubv}	294.64	Unstressed brain venous volume
V_{uhv}	98.21	Unstressed heart venous volume
Pulmonary volumes:		
V_{upa}	0	Unstressed pulmonary arterial volume
V_{upp}	123	Unstressed pulmonary peripheral volume
V_{upv}	120	Unstressed pulmonary venous volume
Cardiac volumes:		
V_{ula}	25	Unstressed left atrial volume
V_{ura}	25	Unstressed right atrial volume
V_{ulv}	16.77	Unstressed left ventricular volume
V_{urv}	40.8	Unstressed right ventricular volume
Overall volumes:		
V_t	5.0×10^3	Total blood volume in supine position
$V_{u_{static}}$	1297	Total immutable component of unstressed volumes

Table D.1: Volume constants in the Orthostasis Model, expressed in ml of blood. The variation in the number of significant figures results from the fact that they were not reported to a consistent number of figures in the literature.

Constant	Value	Description
Systemic resistances:		
R_{hpn}	19.71	Coronary peripheral resistance set-point
R_{hv0}	0.224	Coronary venous resistance
R_{sa}	0.06	Systemic arterial resistance
R_{sv}	0.038	Splanchnic venous resistance
R_{uev0}	0.039	Upper extrasplanchnic venous resistance
R_{lev}	0.036	Lower extrasplanchnic venous resistance
R_{umv0}	0.048	Upper muscular venous resistance
R_{lmv}	0.045	Lower muscular venous resistance
Extrasplanchnic Peripheral Basal Resistances:		
R_{uep0}	3.40	Upper extrasplanchnic peripheral basal resistance
R_{lep0}	3.17	Lower extrasplanchnic peripheral basal resistance
R_{ump0}	4.32	Upper muscular peripheral basal resistance
R_{lmp0}	4.03	Lower muscular peripheral basal resistance
Pulmonary resistances:		
R_{pa}	0.023	Pulmonary arterial resistance
R_{pp}	0.0894	Pulmonary peripheral resistance
R_{pv}	5.6×10^{-3}	Pulmonary venous resistance
Cardiac resistances:		
R_{la}	2.5×10^{-3}	Left atrial resistance
R_{ra}	2.5×10^{-3}	Right atrial resistance

Table D.2: Resistance constants in the Orthostasis Model, expressed in mmHg s ml^{-1} of blood. Resistance names ending in "0" are basal values, and the actual value is calculated after taking into account effector mechanisms.

Constant	Value	Description
Systemic compliances:		
C_{sa}	0.28	Systemic arterial compliance
C_{sp}	2.05	Splanchnic peripheral compliance
C_{uep}	0.301	Upper extrasplanchnic peripheral compliance
C_{lep}	0.367	Lower extrasplanchnic peripheral compliance
C_{ump}	0.236	Upper muscular peripheral compliance
C_{lmp}	0.289	Lower muscular peripheral compliance
C_{hp}	0.119	Coronary peripheral compliance
$C_{sv\mathrm{LOW}}$	61.11	Splanchnic venous compliance, LPC
C_{uev}	9	Upper extrasplanchnic venous compliance
$C_{lev\mathrm{LOW}}$	11	Lower extrasplanchnic venous compliance, LPC
C_{umv}	7.07	Upper muscular venous compliance
$C_{lmv\mathrm{LOW}}$	8.64	Lower muscular venous compliance, LPC
C_{hv}	3.57	Coronary venous compliance
$C_{sv\mathrm{HI}}$	4.7	Splanchnic venous compliance, HPC
$C_{lev\mathrm{HI}}$	0.846	Lower extrasplanchnic venous compliance, HPC
$C_{lmv\mathrm{HI}}$	0.665	Lower muscular venous compliance, HPC
Pulmonary compliances:		
C_{pa}	0.76	Pulmonary arterial compliance
C_{pp}	5.8	Pulmonary peripheral compliance
C_{pv}	25.37	Pulmonary vernous compliance
Cardiac compliances:		
C_{la}	19.23	Left atrial compliance
C_{ra}	31.25	Right atrial compliance

Table D.3: Compliance constants in the Orthostasis Model, expressed in ml mmHg^{-1} of blood. "HI" parameters were calculated as $\frac{\text{LOW parameter}}{\text{NCF}}$, where NCF is listed in Table D.8. HPC = high-pressure conditions, LPC = low-pressure conditions.

Constant	Value	Units	Description
Resistances:			
R_{pv_b}	0.88	mmHg s ml^{-1}	Proximal cerebral veins' resistance
R'_{vs}	0.366	mmHg s ml^{-1}	Terminal vein resistance
R_{la_b}	0.6	mmHg s ml^{-1}	Large intracranial resistance
Compliances:			
C_{pan}	0.205	ml mmHg^{-1}	Basal pial arteriolar capacitance
ΔC_{pa_1}	2.87	ml mmHg^{-1}	Amplitude of sigmoidal curve to calculate C_{pa}
ΔC_{pa_2}	0.164	ml mmHg^{-1}	Amplitude of sigmoidal curve to calculate C_{pa}
Other cerebral haemodynamic parameters:			
P_c	0	mmHg	Cerebral capillary pressure
k_R	13.1×10^3	mmHg^3 s ml^{-1}	Factor in hyperbolic constant relating R_{pa} and V_{pa}
τ_{aut}	20	s	Autoregulation time constant (for x_{aut})
k_{CO_2}	15	–	Factor in power used to calculated A_{CO_2}
b_{CO_2}	0.5	–	Term in power used to calculated A_{CO_2}
q_n	12.5	ml s^{-1}	CBF autoregulatory set point
G_{aut}	3	s mmHg^{-1}	Autoregulation gain
$\tau_{CO_{2b}}$	40	s	CO_2 reactivity time constant
G_{CO_2}	8	s mmHg^{-1}	CO_2 reactivity gain
x_{CO_2}	0	–	Degree of CO_2 reactivity effect

Table D.4: Cerebral constants in the Orthostasis Model.

Constant	Value	Units	Description
Carotid sinus (baroreflex) afferent pathway:			
P_n	92	mmHg	Pressure at which no baroreflex occurs
k_{ab}	11.758	mmHg	Related to slope of a static function for baroreflex
f_{abmin}	2.52	Hz	Lower saturation of baroreflex frequency discharge
f_{abmax}	47.78	Hz	Upper saturation of baroreflex frequency discharge
Afferent chemoreflex pathway:			
τ_{ac}	2	s	Time constant for chemoreceptor dynamics
f_{acmin}	0.835	Hz	Lower saturation of frequency discharge
f_{acmax}	12.3	Hz	Upper saturation of frequency discharge
$\tilde{P}_{O_2ac}$	45	mmHg	Pa_{O_2} at the central point of a sigmoid function
k_{ac}	29.27	mmHg	Parameter for sigmoid
K_H	3	–	Dimensionless constant used in CO_2's effect
f	1.4	–	Dimensionless constant used in CO_2's effect
Afferent pulmonary stretch receptors pathway:			
τ_p	2	s	Time constant for f_{ap}
G_{ap}	2.329×10^{-4}	Hz ml^{-1}	Stretch receptor gain
Sympathetic efferent pathway:			
f_{es8}	2.1	Hz	Minimum frequency for f_{es}
f_{es0}	16.11	Hz	Maximum frequency for f_{es}
f_{esmin}	2.66	Hz	Minimum frequency for the effectors to take effect
f_{esmax}	60	Hz	Maximum possible frequency for f_{sp} and f_{sh}
k_{es}	0.0675	s	Exponential power used in f_{es} calculation
W_{bsp}	-1	s	Peripheral sympathetic baroreceptor weight
W_{bsv}	-1	s	Unstressed volume baroreceptor sympathetic weight
W_{bsh}	-1	s	Coronary sympathetic baroreceptor weight
W_{csp}	5	s	Peripheral sympathetic chemoreceptor weight
W_{csv}	5	s	Unstressed volume sympathetic chemoreceptor weight
W_{csh}	1	s	Coronary sympathetic chemoreceptor weight
W_{psp}	-0.34	s	Peripheral sympathetic pulmonary weight
W_{psv}	-0.34	s	Unstressed volume sympathetic pulmonary weight
W_{psh}	0	s	Coronary sympathetic pulmonary weight
Vagal efferent pathway:			
f_{ev0}	3.2	Hz	Maximum frequency for f_{ev}
f_{ev8}	6.3	Hz	Minimum frequency for f_{ev}
f_{ab0}	25	Hz	Central value on f_{cs} axis for determining f_{ev}
k_{ev}	7.06	Hz	Exponential power constant used in f_{ev} calculation
W_{cv}	0.2	s	Unstressed volume chemoreceptor weight
W_{pv}	0.103	s	Unstressed volume pulmonary weight
θ_v	-0.68	Hz	Offset term

Table D.5: Feedback regulation constants in the Orthostasis Model. Hz represents neural firing in spikes s^{-1}.

Constant	Value	Units	Description
Cardiac constants:			
$P_{la,0}$	2.8	mmHg	Minimum left-atrial pressure
$P_{ra,0}$	1.82	mmHg	Minimum right-atrial pressure
k_l	20.02	ml mmHg^{-1}	Left-ventricular cardiac effectiveness
k_r	34.02	ml mmHg^{-1}	Right-ventricular cardiac effectiveness
P_{san}	100	mmHg	Basal value of systemic arterial pressure
P_{pan}	17	mmHg	Basal value of pulmonary arterial pressure
CNS hypoxic response:			
P_{aCO_2n}	40	mmHg	Normal CO_2 arterial pressure
θ_{spn}	13.32	Hz	Basal value of peripheral sympathetic offset term
θ_{svn}	13.32	Hz	Basal value of unstressed volume sympathetic offset term
θ_{shn}	3.6	Hz	Basal value of coronary sympathetic offset term

Table D.6: Miscellaneous constants in the Orthostasis Model. CNS = Central Nervous System. Hz represents neural firing in spikes s^{-1}. Basal values of the CNS hypoxic response represent normoxia and normocapnia.

Gain	Value (υ/Hz)	Time constant	Value (s)	Delay	Value (s)	Basal constant	Value (υ)	υ
G_{Rsp}	0.695 *	τ_{Rsp}	6	D_{Rsp}	2	R_{sp0}	2.49	mmHg s ml^{-1}
G_{Rep}	1.94	τ_{Rep}	6	D_{Rep}	2	R_{ep0}	1.655	mmHg s ml^{-1}
G_{Rmp}	2.47	τ_{Rmp}	6	D_{Rmp}	2	R_{mp0}	2.106	mmHg s ml^{-1}
G_{Vusv}	-265.4	τ_{Vusv}	20	D_{Vusv}	5	V_{usv0}	1435.4	ml
G_{Vuev}	-74.21	τ_{Vuev}	20	D_{Vuev}	5	V_{uev0}	640.73	ml
G_{Vumv}	-58.29	τ_{Vumv}	20	D_{Vumv}	5	V_{umv0}	503.26	ml
G_{Ts}	-0.13	τ_{Ts}	2	D_{Ts}	2	T_0	0.58	s
G_{Tv}	0.09	τ_{Tv}	1.5	D_{Tv}	0.2			s

Table D.7: Effector parameters (gains, time constants, delays, and basal constants) in the Orthostasis Model. All gains and basal constants make use of the unit "υ" reported in the right-most column. For an example of how these four types of parameters are used, see Equations 8.40 and 8.17. * G_{Rsp} increases to 1.22 upon tilt to reflect abdominal contraction.

Constant	Value	Units	Description
Hydrostatic effects:			
CSF_B	0.8	–	Extent to which CSF experiences hydrostatic changes
H_s	13	mmHg	Splanchnic circulation pressure gradient
H_u	-14	mmHg	Upper-body circulation pressure gradient
H_l	57	mmHg	Lower-body circulation pressure gradient
H_b	-29	mmHg	Cerebral circulation pressure gradient
H_h	-6	mmHg	Coronary circulation pressure gradient
H_c	-24	mmHg	Carotid sinus pressure gradient
Viscoelastic creep:			
k_{VC}	6.5	ml mmHg^{-1}	Viscoelastic creep gain in individual compartments
τ_{vc}	600	s	Time constant for viscoelastic creep
ΔV_{vco}	-200	ml	Overall viscoelastic creep, compensating for blood plasma loss
τ_{vco}	600	s	Time constant for overall viscoelastic creep
Other constants:			
NCF	13	–	Nonlinear compliance factor, to decrease C's under HPC
PNC	6.5	mmHg	Threshold pressure between LPC and HPC

Table D.8: Postural constants in the Orthostasis Model. H_b was estimated based on CSF_B [174, 216], and ΔV_{vco} from [16].

Variable	Typical value	Units	Description
Cardiac state:			
P_{la}	6	mmHg	Left atrial pressure
P_{ra}	4	mmHg	Right atrial pressure
Vascular state:			
P_{pa}	16	mmHg	Pulmonary arterial pressure
P_{pp}	14	mmHg	Pulmonary peripheral pressure
P_{pv}	7	mmHg	Pulmonary venous pressure
P_{sa}	95	mmHg	Systemic arterial pressure
P_{sx}	90	mmHg	Systemic arteriolar pressure
P_{sv}	5	mmHg	Splanchnic venous pressure
P_{umv}	4	mmHg	Upper muscular venous pressure
P_{lmv}	4	mmHg	Lower muscular venous pressure
P_{uev}	4	mmHg	Upper extrasplanchnic venous pressure
P_{lev}	4	mmHg	Lower extrasplanchnic venous pressure
Feedback state:			
ΔR_{sp}	0.7	mmHg s ml^{-1}	Splanchnic peripheral resistance adjustment
ΔR_{ep}	1.9	mmHg s ml^{-1}	Extrasplanchnic peripheral resistance adjustment
ΔR_{mp}	2.4	mmHg s ml^{-1}	Muscular peripheral resistance adjustment
ΔV_{usv}	-260	ml	Splanchnic venous unstressed volume adjustment
ΔV_{uev}	-73	ml	Extrasplanchnic venous unstressed volume adjustment
ΔV_{umv}	-57	ml	Muscular venous unstressed volume adjustment
ΔT_s	-0.14	s	Sympathetically-mediated adjustment to heart period
ΔT_v	0.44	s	Vagally-mediated adjustment to heart period
Cerebral state:			
V_{pa}	10	ml	Pial arteriolar volume
P_{pa_b}	38	mmHg	Pial arteriolar pressure
P_v	7	mmHg	Cerebral venous pressure
x_{aut}	-0.18	–	Degree of autoregulatory effect
Miscellaneous:			
$A2$	1	–	Normalised concentration of angiotensin II
V_{vc}	0	ml	Volume change due to viscoelastic creep

Table D.9: Cardiac, vascular, and feedback state variables in the Orthostasis Model. "Typical values" are observed under equilibrium conditions, when all model constants are set to their default values.

Variable	Typical value	Units	Description
Cardiac:			
T	0.88	s	Heartbeat period
F_{ol}	83	ml s^{-1}	Blood flow exiting the left ventricle
F_{or}	83	ml s^{-1}	Blood flow exiting the right ventricle
F_{sa}	83	ml s^{-1}	Systemic arterial flow
F_{pa}	83	ml s^{-1}	Pulmonary arterial flow
L_l	1	–	Left cardiac output afterload effect
L_r	1	–	Right cardiac output afterload effect
Vascular:			
V_u	3540	ml	Total unstressed volume
P_{hv}	5	mmHg	Coronary venous pressure
P_{cs}	95	mmHg	Carotid sinus pressure
Feedback:			
f_{ab}	26	Hz	Afferent baroreflex firing rate
f_{sp}	4	Hz	Firing rate of the efferent sympathetic fibres to arteries
f_{sh}	5	Hz	Firing rate of the efferent sympathetic fibres to the heart
f_{sv}	4	Hz	Firing rate of the efferent vagal fibres to veins
f_v	5	Hz	Firing rate of the efferent vagal fibres to the heart
R_{uep}	7	mmHg s ml^{-1}	Upper extrasplanchnic peripheral resistance
R_{lep}	7	mmHg s ml^{-1}	Lower extrasplanchnic peripheral resistance
R_{ump}	9	mmHg s ml^{-1}	Upper muscular peripheral resistance
R_{lmp}	9	mmHg s ml^{-1}	Lower muscular peripheral resistance
R_{sp}	3	mmHg s ml^{-1}	Splanchnic peripheral resistance
R_{hp}	20	mmHg s ml^{-1}	Coronary peripheral resistance
V_{usv}	1170	ml	Splanchnic venous unstressed volume
V_{uev}	570	ml	Extrasplanchnic venous unstressed volume
V_{umv}	450	ml	Muscular venous unstressed volume

Table D.10: Cardiac, vascular, and feedback variables in the Orthostasis Model. "Typical values" are observed under equilibrium conditions, when all model constants are set to their default values.

Variable	Typical value	Units	Description
Cerebral:			
R_{vs}	0.37	mmHg s ml^{-1}	Resistance of the terminal intracranial veins
R_{pa_b}	6	mmHg s ml^{-1}	Resistance of pial arterioles
C_{vi}	11	ml mmHg^{-1}	Intracranial venous compliance
C_{pa_b}	0.56	ml mmHg^{-1}	Pial arteriolar pressure
ΔC_{pa}	3	ml mmHg^{-1}	Pial arteriolar compliance adjustment
$\frac{dV_{vi}}{dt}$	0	ml s^{-1}	Rate of change of intracranial venous volume
q_b	11.7	ml s^{-1}	Blood flow from pial arterioles to capillaries
A_{CO_2}	0	–	Corrective factor to depress CO_2 reactivity at low CBF levels
Postural:			
pv	1	–	Normalised total blood volume ($pv \lesssim 1$)
V_i	0	ml	Haemorrhage volume
C_{sv}	61	ml mmHg^{-1}	Splanchnic venous compliance
V_{sv}	305	ml	Splanchnic venous volume
C_{lmv}	9	ml mmHg^{-1}	Lower muscular venous compliance
V_{lmv}	38	ml	Lower muscular venous volume
C_{lev}	11	ml mmHg^{-1}	Lower extrasplanchnice venous compliance
V_{lev}	49	ml	Lower extrasplanchnice venous volume
V_{vc}	0	ml	Volume change due to muscular/extrasplanchnic visco. creep
V_{vco}	0	ml	Overall volume change due to viscoelastic creep
R_{uev}	0.05	mmHg s ml^{-1}	Upper extrasplanchnic venous resistance
R_{umv}	0.04	mmHg s ml^{-1}	Upper muscular venous resistance
R_{hv}	0.22	mmHg s ml^{-1}	Coronary venous resistance
α	70	$^\circ$	Final tilt angle
c_T	0	–	Tilt progression extent ($0 \leq c_T \leq 1$; 0 is incomplete, 1 complete)

Table D.11: Cerebral, respiratory, and postural variables in the Orthostasis Model. CBF = Cerebral blood flow.

Appendix E

Atrial Fibrillation Detection

To detect atrial fibrillation (AF) in Chapter 6, an algorithm described by Tateno and Glass [211] was modified and executed. In brief, RR-interval histograms were computed and compared with those from an online database, according to the following steps.

A. Training

Data from the online MIT (Massachusetts Institute of Technology) Atrial Fibrillation Database (AFDB) were downloaded [60]. This data set contained 300 AF episodes within the 10-hour recordings of 25 patients. During each AF episode, blocks of 100 consecutive beats were considered at a time. The median RR interval value was calculated and used to bin the 100-beat set into one of 9 different classes, corresponding to median values between 300-399 ms, 400-499 ms, ... , 1100-1199 ms. For each class, a density histogram of ΔRR[1] was calculated after accumulating that class's data from all patients. The result was a set of nine standard density histograms for AF, sorted by median RR interval.

In their original paper, Tateno and Glass used the mean, rather than median, but this was problematic for two reasons. First, it was susceptible to skew by the long RR intervals that result from gaps in the recording. These gaps may have been due to technical failure or, more commonly, to regions of artefact in which no beats were detected. Second, their binning system, which only covered RR intervals of less than 1200 ms, was insufficient for evaluating their data set. Spanning several patients, a total of about 6 minutes of data needed to be discarded for RR intervals in excess of 1200 ms.

[1]The differenced RR time series.

B. Testing

For a test data set, density histograms of 100-beat segments were compared with the standard histograms developed previously. The best-suited instrument for this comparison was the Kolmogorov-Smirnov test, as it provided a measure of the dissimilarity between two distributions, by returning a familiar statistical p value. For p larger than some critical threshold, it could be said that the distributions were not significantly different from one another. For the present work, $p < 0.01$ was associated with a positive identification of AF.

Before the AF test was applied to Falls Clinic data, its performance on the training set was assessed. As indicated in the final row of Table E.1, classification performance was quite good. Part of the reason the results were imperfect was that errors existed in the MIT-BIH annotations. As in the case of QRS detection described in Appendix A, the present work led to the discovery and reporting of these errors.

C. Excluding Falls Clinic patients with AF

The final step was to identify Falls Clinic patients with AF. The test was used in conjunction with visual inspection; the latter was used since regions of artefact or CRS can masquerade as AF. A rule-based system could easily have substituted for this visual inspection. An example of a patient experiencing paroxysmal (intermittent) AF is shown in Figure E.1.

There were two main limitations of the AF test. The first was that localisation of the onset or end of AF episodes were difficult to detect, as each analysed sequence comprised of 100 beats. This was not a major issue for the current work, as the aim of applying the algorithm was simply identification of occasional or constant AF, as opposed to measuring the timing of its beginning and end. Secondly, in some patients, the median RR interval could rise in excess of 1200 ms. For these few 100-beat sequences, the presence of AF had to be evaluated by eye.

Subject	TP	TN	FP	FN	Sensitivity	Specificity	PPV	NPV
00735	303	39288	29	0	100	99.93	91.27	100
03665	10889	40934	168	673	94.18	99.59	98.48	98.38
04015	494	41257	31	2122	18.88	99.92	94.1	95.11
04043	9179	47087	5455	93	99	89.62	62.72	99.8
04048	511	39011	302	9	98.27	99.23	62.85	99.98
04126	3023	37943	270	1523	66.5	99.29	91.8	96.14
04746	30175	16880	698	19	99.94	96.03	97.74	99.89
04908	5180	54760	630	1089	82.63	98.86	89.16	98.05
04936	31449	13597	8232	267	99.16	62.29	79.25	98.07
05091	60	36441	78	82	42.25	99.79	43.48	99.78
05121	31634	15273	2125	748	97.69	87.79	93.71	95.33
05261	582	44118	352	381	60.44	99.21	62.31	99.14
06426	52347	1397	688	622	98.83	67	98.7	69.19
06453	237	34274	208	17	93.31	99.4	53.26	99.95
06995	26649	24604	776	3059	89.7	96.94	97.17	88.94
07162	36119	0	3078	0	100	0	92.15	–
07859	40262	0	19922	0	100	0	66.9	–
07879	37110	16451	2925	7	99.98	84.9	92.69	99.96
07910	6615	29697	104	74	98.89	99.65	98.45	99.75
08215	33000	10176	79	0	100	99.23	99.76	100
08219	13585	40653	609	4345	75.77	98.52	95.71	90.34
08378	1764	35683	191	7776	18.49	99.47	90.23	82.11
08405	43390	13677	1654	34	99.92	89.21	96.33	99.75
08434	2284	37319	26	120	95.01	99.93	98.87	99.68
08455	43654	15238	559	0	100	96.46	98.74	100
Total	460495	685758	49189	23060	95.23	93.31	90.35	96.75

Table E.1: Beat-by-beat assessment of AF based on ΔRR using data in the MIT AFDB (atrial fibrillation database). Each heart beat was accompanied by an expert label indicating whether it occurred as a result of AF or not; these expert labels were compared with the results of the automated algorithm, for 25 patients. The final row indicates that the classification accuracy was good. TP = True Positive, TN = True Negative, FP = False Positive, FN = False Negative. PPV = Positive Predictive Value, NPV = Negative Predictive Value.

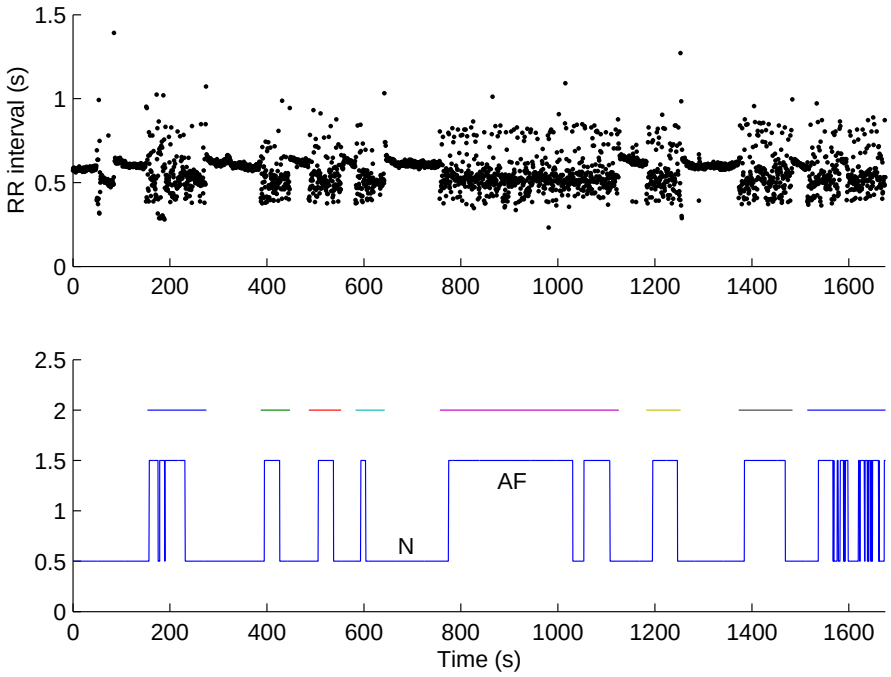

Figure E.1: Evaluating MIT AFDB patient 04043 with the AF algorithm. The upper plot depicts the RR intervals. In the lower plot, the outcome of the algorithm (blue line) of either atrial fibrillation (AF) or normal (N) is compared with the expert labels (coloured horizontal lines).

Appendix F

Power Calculation for Prospective Testing

The results obtained in Section 6.5 suggest that ICFV may be a metric worthy of further study. The number of patients recommended for a prospective clinical trial can be determined using a statistical power calculation. Such calculations on non-parametric data are difficult; however, since the data are close to being normally distributed, a reasonable approximation can be obtained by assuming they are Gaussian.

The following methodology is employed. Let x and y correspond to the ICFV values associated with normal and vasovagal patients, respectively, and n_x and n_y correspond to the number of samples in either case. The null hypothesis is that the mean post-tilt values of ICFV for the two groups are identical. The prospective trial will be designed to have an 80% chance of rejecting the null hypothesis at the 5% significance level, based on the test statistic [170]

$$z = \frac{\overline{y} - \overline{x}}{\sqrt{s^2 \left(\frac{1}{n_x} + \frac{1}{n_y}\right)}} \tag{F.1}$$

where s is calculated using the retrospective data, as

$$s^2 = \frac{\sum (x - \overline{x})^2 + \sum (y - \overline{y})^2}{n_x + n_y - 2} = 5.25 \times 10^{-4}. \tag{F.2}$$

Letting X represent a random variable with a standard normal probability distribution, the value of x

such that $Pr(X \leq x) = p$ can be found in a distribution table [43] for a given p. To obtain results for which $p < 0.05$ in the prospective study with an 80% chance of success, the sum of the two tabled values of x corresponding to $p = 0.80$ and $p = 0.975$ would represent z in Equation F.1; i.e.,

$$z_{p<0.05} = x_{p=0.80} + x_{p=0.975} = 0.842 + 1.960 = 2.802. \tag{F.3}$$

Assuming that $n_x = 1.6n_y$, $\overline{y} = 0.0624$ and $\overline{x} = 0.0461$, as was approximately the case for the retrospective data, Equation F.1 has one remaining unknown: n_x. This can be isolated:

$$n_x = \frac{2.6z^2s^2}{(\overline{y} - \overline{x})^2} = 26. \tag{F.4}$$

Finally, the estimate of the total number of patients required in a prospective study would be $n = n_x + n_y = 2.6n_y = 68$.

Bibliography

[1] P.I. Aaronson and J.P.T. Ward. *The Cardiovascular System at a Glance.* Blackwell Publishing, 2003.

[2] S. Akselrod, Y. Barak, Y. Ben-Dov, L. Keselbrener, and A. Baharav. Estimation of autonomic response based on individually determined time axis. *Auton Neurosci Basic Clin*, 90:13–23, 2001.

[3] P. Alboni, D. Benditt, L. Bergfeldt, J.J. Blanc, P.E. Bloch Thomsen, et al. Task force report: Guidelines on management (diagnosis and treatment) of syncope. *Eur Heart J*, 22:1256–1306, 2001.

[4] M.L. Appel, R.D. Berger, J.P. Saul, J.M. Smith, and R.J. Cohen. Beat to beat variability in cardiovascular variables: Noise or music? *J Am Coll Cardiol*, 14:1139–48, 1989.

[5] E. Asensio, J. Oseguera, A. Loria, M. Gomez, and J. Dorantes R. Narvaez, et al. Clinical findings as predictors of positivity of head-up tilt table test in neurocardiogenic syncope. *Arch Med Res*, 34(4):287–91, 2003.

[6] M. Bacon and J.A.H. Grunstein. A diagnostic service for eliciting carotid sinus hypersensitivity and vasovagal symptoms in a district general hospital. *Age Ageing*, 29:501–4, 2000.

[7] F. Badilini, P. Maison-Blanche, and P. Coumel. Heart rate variability in passive tilt test: comparative evaluation of AR and FFT spectral analyses. *Pacing Clin Electrophysiol*, 21(5):1122–32, 1998.

[8] A. Baharav, L. Kesselbrenner, O. Oz, T. Lehrman-Sagie, and S. Akselrod. The autonomic control in vasovagal syncope investigated by spectral and time-dependent analysis of heart rate fluctuations. In *Proceedings*, volume 28, pages 269–72. Comput Cardiol, 1993.

[9] M. Bahjaoui-Bouhaddi, S. Cappelle, M.T. Henriet, G. Dumoulin, J.P. Wolf, and J. Regnard. Graded vascular autonomic control versus discontinuous cardiac control during gradual upright tilt. *J Auton Nerv Syst*, 79:149–55, 2000.

[10] C. Baillard, P. Gonçalves, L. Mangin, B. Swynghedauw, and P. Mansier. Use of time frequency analysis to follow transitory modulation of the cardiac autonomic system in clinical studies. *Autonom Neurosci*, 90:24–8, 2001.

[11] M. Béchir, C. Binggeli, R. Corti, R. Chenevard, L. Spieker, F. Ruschitzka, et al. Dysfunctional baroreflex regulation of sympathetic nerve activity in patients with vasovagal syncope. *Circulation*, 107(12):1620–5, 2003.

[12] E. Bellard, J.O. Fortrat, D. Schang, J.M. Dupuis, J. Victor, and G. Lefthériotis. Changes in the transthoracic impedance signal predict the outcome of a 70-degree head-up tilt test. *Clin Sci*, 104(2):119–126, 2003.

[13] D.G. Benditt. Neurally mediated syncopal syndromes: pathophysiological concepts and clinical evaluation. *Pacing Clin Electrophysiol*, 20(2):572–584, 1997.

[14] D.G. Benditt, C. Ermis, B. Padanilam, N. Samniah, and S. Sakaguchi. Catecholamine response during haemodynamically stable upright posture in individuals with and without tilt-table induced vasovagal syncope. *Europace*, 5(1):65–70, 2003.

[15] D.G. Benditt, D.W. Ferguson, B.P. Grubb, W.N. Kapoor, J. Kugler, B.B. Lerman, et al. Tilt table testing for assessing syncope. *JACC*, 28(1):263–75, 1996.

[16] J.E.W. Beneken and B. De Wit. *Physical bases of circulatory transport: Regulation and exchange*, chapter 1 ("A physical approach to hemodynamic aspects of the human cardiovascular system"), pages 1–45. W.B. Saunders, 1967.

[17] Y. Benjamini and Y Hochberg. Controlling the false discovery rate: A practical and powerful approach to multiple testing. *J Roy Stat Soc, Ser B*, 57:289–300, 1995.

[18] R. Berger, S. Akselrod, D. Gordon, and R. Cohen. An efficient algorithm for spectral analysis of heart rate variability. *IEEE Trans Biomed Eng*, 33(9):900–904, 1986.

[19] R.D. Berger, J.P. Saul, and R.J. Cohen. Transfer function analysis of autonomic regulation: I. The canine atrial rate response. *Am J Physiol*, 25:H142–152, 1989.

[20] R.M Berne and M.N. Levy. *Cardiovascular Physiology*. Mosby Inc., eighth edition, 2001.

[21] G.G. Berntson, K.S. Quigley, J.F. Jang, and S.T. Boysen. An approach to artifact identification: Application to heart period data. *Psychophysiology*, 27(5):586–598, 1990.

[22] C. Berthomier. Instantaneous frequency and energy distribution of a signal. *Signal Proc*, 5:31–45, 1983.

[23] B. Bertin, P. Mansier, I. Makeh, P. Briand, W. Rostene, B. Swynghedauw, et al. Specific atrial overexpression of G protein coupled human beta-1-adrenoceptors in transgenic mice. *Cariovasc Res*, 27:1606–12, 1993.

[24] D.M. Bloomfield. Introduction. *Am J Cardiol*, 84:1Q–2Q, 1999.

[25] D.M. Bloomfield. Strategy for the management of vasovagal syncope. *Drugs Aging*, 19(3):179–202, 2002.

[26] D.M. Bloomfield, R. Sheldon, B.P. Grubb, H. Calkins, and R. Sutton. Panel Consensus — Putting it together: A new treatment algorithm for vasovagal syncope and related disorders. *Am J Cardiol*, 84(33):33Q–39Q, 1999.

[27] B. Boashash. Estimating and interpreting the instantaneous frequency of a signal, Part 1: Fundamentals. *Proc IEEE*, 80:520–538, 1992.

[28] M. Boulos, S. Barron, E. Nikolski, and W. Markiewicz. Power spectral analysis of heart rate variability during upright tilt test: A comparison of patients with syncope and normal patients. *Cardiol*, 87:28–32, 1996.

[29] D.G. Boyers, J.G. Cuthbertson, and J.A. Luetscher. Simulation of the human cardiovascular system: a model with normal response to change in posture, blood loss, transfusion, and autonomic blockade. *Simulation*, 18:197–205, 1972.

[30] J.C. Bramwell and A.V. Hill. Velocity of transmission of the pulse wave and elasticity of the arteries. *Lancet*, 1:891–2, 1922.

[31] M. Brignole, C. Menozzi, A. Del Rosso, S. Costa, G. Gaggioli, N. Bottoni, et al. New classification of haemodynamics of vasovagal syncope: Beyond the VASIS classification. *Europace*, 2:66–76, 2000.

[32] M. Brignole, B. Sartore, and R. Prato. Role of body position during carotid sinus stimulation test in the diagnosis of cardioinhibitory carotid sinus syndrome. *G Ital Cardiol*, 14:69–72, 1983.

[33] J.D. Bronzino, editor. *The Biomedical Engineering Handbook*. IEEE Press, 2000.

[34] B.J. Carey, P.J. Eames, R.B. Panerai, and J.F. Potter. Carbon dioxide, critical closing pressure and cerebral haemodynamics prior to vasovagal syncope in humans. *Clin Sci*, 101:351–8, 2001.

[35] F. Carré, P. Maison-Blanche, L. Ollivier [*sic*], P. Mansier, B. Chevalier, R. Vicuna, et al. Heart rate variability in two models of cardiac hypertrophy in rats in relation to the new molecular phenotype. *Am J Physiol*, 266:H1872–8, 1994.

[36] S. Cencetti, A. Lagi, M. Cipriani, L. Fattorini, G. Bandinelli, and L. Bernardi. Autonomic control of the cerebral circulation during normal and impaired peripheral circulatory control. *Heart*, 82(3):365–72, 1999.

[37] M.N. Cheung. Detection of and recovery from errors in cardiac interbeat intervals. *Psychophysiology*, 18(3):341–6, 1981.

[38] T.A.C.M. Claasen and W.F.G. Mecklenbräuker. The aliasing problem in discrete-time Wigner distributions. *IEEE Trans Acoust, Speech, Signal Processing*, 31:1067–1072, 1983.

[39] G. Clifford. *Mathematical methods for heart rate variability.* PhD thesis, University of Oxford, December 2002.

[40] W.N.J.M. Colier, R.A. Binkhorst, M.T.E. Hopman, and B. Oeseburg. Cerebral and circulatory haemodynamics before vasovagal syncope induced by orthostatic stress. *Clin Physiol*, 17:83–94, 1997.

[41] R.C. Croston and D.G. Fitzjerrell. Cardiovascular model for the simulation of exercise, lower body negative pressure, and tilt experiments. In *Proc 5th Ann Pittsburgh Conf Modeling Simulation*, pages 471–6, 1974.

[42] R.W. deBoer, J.M. Karemaker, and J. Strackee. Hemodynamic fluctuations and baroreflex sensitivity in humans: a beat-to-beat model. *Am J Physiol*, 253(22):H680–H689, 1987.

[43] M.H. DeGroot and M.J. Schervish. *Probability and Statistics.* Addison Wesley, third edition, 2002.

[44] M. Ebden and N. Townsend. *Operating Manual for the Software Monitor Project*, 2.2 edition, November 2002.

[45] D.L. Eckberg. Sympathovagal balance: A critical appraisal. *Circulation*, 96:3224–3232, 1997.

[46] C.E. Elwell. *A Practical Users Guide to Near Infrared Spectroscopy.* UCL Reprographics, 1995.

[47] C.E. Elwell, R. Springett, E. Hillman, and D.T. Delpy. *Oxygen Transport to Tissue XXI*, chapter 8 ("Oscillations in cerebral haemodynamics"). Plenum Publishers, 1999.

[48] M. Fink, J.J. Batzel, and F. Kappel. An optimal control approach to modeling the cardiovascular-respiratory system: An application to orthostatic stress. *Cardiovascular Engineering: An International Journal*, 4(1):27–38, 2004.

[49] A.P. Fitzpatrick, N. Banner, A. Cheng, M. Yacoub, and R. Sutton. Vasovagal reactions may occur after orthotopic heart transplantation. *J Am Coll Cardiol*, 21:1132–7, 1993.

[50] A.P. Fitzpatrick and R. Sutton. Blood pressure and heart rate during positive and negative 60^o head-up tilt-testing. *Eur J C P E*, 1:42–7, 1991.

[51] A.P. Fitzpatrick, G. Theodorakis, P. Vardas, and R. Sutton. Methodology of head-up tilt testing in patients with unexplained syncope. *J Am Coll Cardiol*, 17(1):125–30, 1991.

[52] J.S. Floras, P.E. Aylward, F.M. Abboud, and A.L. Mark. Inhibition of muscle sympathetic nerve activity in humans by arginine vasopressin. *Hypertension*, 10:409–16, 1987.

[53] J. Freitas, S. Pereira, P. Lago, O. Costa, M.J. Carvalho, and A. Falcão de Freitas. Impaired arterial baroreceptor sensitivity before tilt-induced syncope. *Europace*, 1(4):258–65, 1999.

[54] G.M. Friessen, T.C. Jannett, M.A. Jadallah, S.L. Yates, S.R. Quint, and H.T. Nagle. A comparison of the noise sensitivity of nine QRS detection algorithms. *IEEE Trans Biomed Eng*, 37(1):85–98, 1990.

[55] P. Fung, G. Dumont, C. Ries, C. Mott, and M. Ansermino. Continuous noninvasive blood pressure measurement by pulse transit time. In *Proceedings of the 26th IEEE EMBC*, pages 738–41, 1–5 September 2004.

[56] R. Furlan, S. Piazza, S. Dell'Orto, F. Barbic, A. Bianchi, L. Mainardi, et al. Cardiac autonomic patterns preceding occasional vasovagal reactions in healthy humans. *Circulation*, 98:1756–1761, 1998.

[57] W.F. Ganong. *Review of Medical Physiology.* McGraw Hill, 2003.

[58] R. Germuska. The use of pulse transit time (Technical Report), 2002.

[59] G. Gielerak, K. Makowski, E. Kramarz, M. Cholewa, E. Dluzniewska, A. Roszczyk, et al. Heart rate variability during head-up tilt test in patients with syncope of unknown origin. *Kardiol Pol*, 57(11):399–406, 2002.

[60] A.L. Goldberger, L.A.N. Amaral, L. Glass, J.M. Hausdorff, P.Ch. Ivanov, R.G. Mark, et al. PhysioBank, PhysioToolkit, and PhysioNet: Components of a new research resource for complex physiologic signals. *Circulation*, 101(23):e215–e220, 2000 (June 13). Circulation Electronic Pages: http://circ.ahajournals.org/cgi/content/full/101/23/e215.

[61] W. Grimm, M. Degenhardt, J. Hoffman, V. Menz, A. Wirths, and B. Maisch. Syncope recurrence can better be predicted by history than by head-up tilt testing in untreated patients with suspected neurally mediated syncope. *Eur Heart J*, 18(9):1465–9, 1997.

[62] W. Grimm, A. Wirths, J. Hoffmann, V. Menz, and B. Maisch. Heart rate variability during head-up tilt testing in patients with suspected neurally mediated syncope. *Pacing Clin Electrophysiol*, 21(11):2411–15, 1998.

[63] B. Grubb and B. Olshansky. *Syncope: Mechanisms and Management.* Futura Publishing Co., Inc., Armonk, New York, 1998.

[64] B.P. Grubb. Pathophysiology and differential diagnosis of neurocardiogenic syncope. *Am J Cardiol*, 84:3Q–9Q, 1999.

[65] B.P. Grubb, G. Gerard, K. Roush, P. Temesy-Armos, P. Montford, L. Elliot, et al. Cerebral vasoconstriction during head-upright tilt-induced vasovagal syncope: A paradoxic response. *Circulation*, 84:1157–1164, 1991.

[66] B.P. Grubb and B. Karas. Review: Clinical disorders of the autonomic nervous system associated with orthostatic intolerance — an overview of classification, clinical evaluation, and management. *Pacing Clin Electrophysiol*, 22(5):798–810, 1999.

[67] B.P. Grubb and D. Kosinski. Serotonin and syncope: an emerging connection? *Eur J C P E*, 5:306–14, 1996.

[68] B.P. Grubb, D. Samoil, D. Kosinkski, D. Wolfe, P. Brewster, L. Elliott, et al. Cerebral syncope: Loss of consciousness associated with cerebral vasoconstriction in the absence of systemic hypotension. *Pacing Clin Electrophysiol*, 21:652–658, 1998.

[69] A.C. Guyton and T.G. Coleman. *Physical bases of circulatory transport: Regulation and exchange*, chapter 11 ("Long-term regulation of the circulation: Interrelationships with body fluid volumes"), pages 179–202. W.B. Saunders, 1967.

[70] A.C. Guyton, T.G. Coleman, and H.J. Granger. Circulation: overall regulation. *Annu Rev Physiol*, 34:13–46, 1972.

[71] C.E. Guzmán, G.M. Sánchez, M.F. Márquez, A.G. Hermosillo, and M. Cárdenas. Differences in heart rate variability between cardioinhibitory and vasodepressor responses to head-up tilt table testing. *Arch Med Res*, 30(3):203–11, 1999.

[72] R. Hainsworth. *Autonomic failure: a textbook of clinical disorders of the autonomic nervous system*, chapter 39 ("Syncope and fainting"). Oxford University Press, third edition, 1992.

[73] R. Hainsworth. Syncope: What is the trigger? *Heart*, 89(2):123–4, 2003.

[74] R. Hainsworth and A.L. Mark, editors. *Cardiovascular reflex control in health and disease*, chapter 18 ("Haemorrhage and shock"), pages 463–90. Saunders, 1993.

[75] R. Hainsworth and A.L. Mark, editors. *Cardiovascular reflex control in health and disease*, chapter 2 ("Importance of reflexes in the circulatory adjustments to postural changes"), pages 35–63. Saunders, 1993.

[76] P.S. Hamilton and W.J. Tompkins. Quantitative investigation of QRS detection rules using the MIT/BIH arrhythmia database. *IEEE Trans Biomed Eng*, BME-33(12):1157–1165, 1986.

[77] W.Y. Hao, J.Y. Bai, X. Wu, and L.F. Zhang. Simulation study of the effects of hypovolaemia on cardiovascular response to orthostatic stress. *Med Biol Eng Comput*, 41(1):44–51, 2003.

[78] M.P.M. Harms, W.N.J.M. Colier, W. Wieling, J.W.M. Lenders, N.H. Secher, and J.J. van Lieshout. Orthostatic tolerance, cerebral oxygenation, and blood velocity in humans with sympathetic failure. *Stroke*, 31:1608–1614, 2000.

[79] K.E. Hauer. Discovering the cause of syncope: A guide to the focused evaluation. *Postgrad Med*, 113(1):31–8, 2003.

[80] T. Heldt, E.B. Shim, R.D. Kamm, and R.G. Mark. Computational modeling of cardiovascular response to orthostatic stress. *J Appl Physiol*, 92:1239–1254, 2002.

[81] L.M. Hively and V.A. Protopopescu. Advanced physiological monitoring of FCS soldiers. In *24th Army Science Conference Proceedings*, pages 1–8, 2004.

[82] A.R. Houghton and D. Gray. *Making sense of the ECG*. Arnold, 1997.

[83] Y.H. Hu, S. Palreddy, and W.J. Tompkins. A patient-adaptable ECG beat classifier using a mixture of experts approach. *IEEE Trans Biomed Eng*, 44(9):891–900, 1997.

[84] Y.H. Hu, W.J. Tompkins, J.L. Urrusti, and V.X. Afonso. Applications of artificial neural networks for ECG signal detection and classification. *J Electrocardiol*, 26 Supplement:66–73, 1993.

[85] B.P.M. Imholz, W. Wieling, G.J. Langewouters, and G.A. van Montfrans. Continuous finger arterial pressure: Utility in the cardiovascular laboratory. *Clin Auton Res*, 1:45–53, 1991.

[86] M.C. Jacobs, D.S. Goldstein, J.J. Willemsen, P. Smits, T. Thien, R.A. Dionne, et al. Neurohumoral antecedents of vasodepressor reactions. *Eur J Clin Invest*, 25:754–61, 1995.

[87] M.A. James and J.F. Potter. Orthostatic blood pressure changes and arterial baroreflex sensitivity in elderly subjects. *Age Ageing*, 28:522–530, 1999.

[88] S. Jasson, C. Médigue, P. Maison-Blanche, N. Montano, L. Meyer, C. Vermeiren, et al. Instant power spectrum analysis of heart rate variability during orthostatic tilt using a time-/frequency-domain method. *Circulation*, 96(10):3521–6, 1997.

[89] P.C. Johnson. *Handbook of Physiology. The Cardiovascular System: Vascular Smooth Muscle, sect. 2*, volume II, chapter 15 ("The myogenic response"), pages 409–? American Physiological Society, Bethesda, MD, 1980.

[90] D. Jordan and J. Marshall, editors. *Cardiovascular Regulation*. Portland Press, 1995.

[91] W.N. Kapoor, M. Karpf, Y. Maher, R.A. Miller, and G.S. Levey. Syncope of unknown origin: the need for a more cost-effective approach to its diagnostic evaluation. *JAMA*, 247:2687–91, 1982.

[92] M. Kempa, D. Kozlowski, S. Sielski, R. Galaska, I. Romanowska, J. Staniewicz, et al. The usefulness of the "VASIS" classification in the evaluation of vasovagal syncope types. *HeartWeb*, 2(1):Article No. 96110005, 1996.

[93] R.A. Kenny, D. O'Shea, and S.W. Parry. The Newcastle protocols for head-up tilt table testing in the diagnosis of vasovagal syncope, carotid sinus hypersensitivity, and related disorders. *Heart*, 83:564–569, 2000.

[94] L. Keselbrener, A. Baharav, Y. Ben-Dov, S. Diamant, A. Berger, Y. Sivan, et al. Time-frequency decomposition of heart rate and blood pressure variability in reflex syncope. *Comput Cardiol*, xxiv:219–22, 1997.

[95] J. Kettunen and L. Keltikangas-Järvinen. Intraindividual analysis of instantaneous heart rate variability. *Psychophysiology*, 38(4):659–68, 2001.

[96] P.N. Kizakevich, E. Kaufman, N. Cragg, W.J. Jochem, S.M.Teague, and J.R. Hordinsky. Beat-by-beat monitoring of systemic vascular resistance during head-up tilt for assessment of orthostatic stress response. In *Proceedings of the Seventh Symposium on Computer-Based Medical Systems*, volume xi, pages 82–7. IEEE, 1994.

[97] G.E. Kochiadakis, P.J. Lees, E.M. Kanoupakis, N.E. Igoumenidis, G.I. Chlouverakis GI, and P.E. Vardas. Reproducibility of time domain indexes of heart rate variability in normal subjects and patients with vasovagal syncope. *Comput Cardiol*, 24:41–3, 1997.

[98] G.E. Kochiadakis, P.J. Lees, E.M. Kanoupakis, N.E. Igoumenidis, E.G. Manios, and P.E. Vardas. Spectral analysis of heart rate variability in the analysis of autonomic nervous system activity during tilt-table testing in patients with unexplained syncope. *Comput Cardiol*, 24:367–9, 1997.

[99] G.E. Kochiadakis, A.T. Rombola, E.M. Kanoupakis, E.N. Simantirakis, G.I. Chlouverakis, and P.E. Vardas. Assessment of autonomic function at rest and during tilt testing in patients with vasovagal syncope. *Am Heart J*, 134(3):459–66, 1997.

[100] K. Kotani, K. Takamasu, Y. Ashkenazy, H.E. Stanley, and Y. Yamamoto. Model for cardiorespiratory synchronization in humans. *Phys Rev E*, 65:051923–1–9, 2002.

[101] C. Kouakam, D. Lacroix, N. Zghal, R. Logier, D. Klug, P. Le Franc, et al. Inadequate sympathovagal balance in response to orthostatism in patients with unexplained syncope and a positive head up tilt test. *Heart*, 82(3):312–8, 1999.

[102] A. Lagi, S. Cencetti, V. Corsoni, D. Georgiadis, and S. Bacalli. Cerebral vasoconstriction in vasovagal syncope: Any link with symptoms? *Circulation*, 104:2694–2698, 2001.

[103] Jr. L.C. McHenry, J.F. Fazekas, and J.F. Sullivan. Cerebral hemodynamics of syncope. *Am J Med Sci*, 241:173–8, 1961.

[104] J.I. Leonard, C.S. Leach, and J.A. Rummel. Computer simulations of postural change, water immersion and bedrest: an integrative approach for understanding the spaceflight response. *Physiologist*, 22:S31–2, 1979.

[105] A.S. Levey. Special report from the NKF Task Force on Cardiovascular Disease. *Am J Kidney Diseases*, 32(5):Suppl 3, 1999.

[106] J. Levick. *An Introduction to Cardiovascular Physiology.* Arnold Publishers, 2000.

[107] M.G. Levitzky. *Pulmonary Physiology.* McGraw-Hill, sixth edition, 2003.

[108] T. Lewis. A lecture on vasovagal syncope and the carotid sinus mechanism. *BMJ*, 14:873–6, 1932.

[109] M. Linzer, M. Pontinen, D.T. Gold, G.W. Divine, A. Felder, and W.B. Brooks. Impairment of physical and psychosocial function in recurrent syncope. *J Clin Epidemiol*, 44:1037–43, 1991.

[110] N. Lippman, K.M. Stein, and B.B. Lerman. Failure to decrease parasympathetic tone during upright tilt predicts a positive tilt-table test. *Am J Cardiol*, 75:591–5, 1995.

[111] L.A. Lipsitz, J. Mietus, G.B. Moody, and A.L. Goldberger. Spectral characteristics of heart rate variability before and during postural tilt — Relation to aging and risk of syncope. *Circulation*, 81:1803–1810, 1990.

[112] C.C. Lu, A. Diedrich, C.S. Tung, S.Y. Paranjape, P.A. Harris, D.W. Byrne, et al. Water ingestion as prophylaxis against syncope. *Circulation*, 108:2660–2665, 2003.

[113] E. Magosso and M. Ursino. A mathematical model of CO_2 effect on cardiovascular regulation. *Am J Physiol Heart Circ Physiol*, 281:H2052–H2052, 2001.

[114] L.T. Mainardi, A.M. Bianchi, R. Furlan, S. Piazza, R. Barbieri, V. di Virgilio, et al. Multivariate time-variant indentification of cardiovascular variability signals: A beat-to-beat spectral parameter estimation in vasovagal syncope. *IEEE Trans Biomed Eng*, 44(10):978–989, 1997.

[115] M. Malik, A.J. Camm, J.T. Bigger, G. Breithardt, S. Cerutti, R.J. Cohen, et al. Heart rate variability: Standards of measurement, physiological interpretation, and clinical use. *Circulation*, 93(5):1043–1065, 1996.

[116] Z. Mallat, E. Vicaut, A. Sangaré, J. Verschueren, G. Fontaine, and R. Frank. Prediction of head-up tilt test result by analysis of early heart rate variations. *Circulation*, 96:581–4, 1997.

[117] L. Mangin, A. Kobeissi, D. Lelouche, Y. D'Hérouville, P. Mansier, B. Swynghedauw, et al. Simultaneous analysis of heart rate variability and myocardial contractility during head-up tilt in patients with vasovagal syncope. *J Cardiovasc Electrophysiol*, 12(6):639–44, 2001.

[118] P. Mansier, C. Médigue, N. Charlotte, C. Vermeiren, E. Coraboeuf, E. Deroubai, et al. Decreased heart rate variability in transgenic mice overexpressing atrial beta-1-adrenoceptors. *Am J Physiol*, 271:H1465–72, 1996.

[119] E. Marangoni, A. Zucchi, P. Ferraris, F. Lissoni, S. Belletti, and C. Panciroli. A study on blood pressure and heart rate variations during head-up tilt testing supporting evidence for the two-phase model of postural syncope. *New Trends Arrhythmias*, 9(2):207–210, 1993.

[120] A. Marrone, A.D. Polosa, and G. Scioscia. Multiscale analysis of blood pressure signals. *Phys Rev E*, 60(1):1088–91, 1999.

[121] A. Marrone, A.D. Polosa, G. Scioscia, S. Stramaglia, and A. Zenzola. Wavelet analysis of blood pressure waves in vasovagal syncope. *Physica A*, 271(3):458–69, 1999.

[122] A. Martinez-Coll, M.K. Morgan, P.G. Cooper, H.T Nguyen, and S.N. Hunyor. *Oxygen Transport to Tissue XXI*, chapter 15 ("Cerebral tissue oxygen saturation (SrO_2 from near infrared spectroscopy (NIRS) measurements following 90^o-head-up tilt"). Plenum Publishers, 1999.

[123] W. Mayhew, S. Askew, Y. Zheng, J. Porrill, G.W.M. Westby, P. Redgrave, et al. Cerebral vasomotion: A 0.1-hz oscillation in reflected light imaging of neural activity. *Neuroimage*, 4:183–93, 1996.

[124] A.D. McGavigan and S. Hood. The influence of sex and age on response to head-up tilt-table testing in patients with recurrent syncope. *Age Ageing*, 30:295–8, 2001.

[125] C. Médigue, C. Vermeiren, P. Bourgin, C. Debouzy, and P. Escourrou. Cardiovascular perturbations involved in periodic leg movements during sleep. *Comput Cardiol*, pages 477–480, 1995.

[126] D.J. Mehagnoul-Schipper, W.N.J.M. Colier, and R.W.M.M. Jansen. Reproducibility of orthostatic changes in cerebral oxygenation in healthy subjects aged 70 years or older. *Clin Physiol*, 21(1):77–84, 2001.

[127] D.J. Mehagnoul-Schipper, L.C.M. Vloet, W.N.J.M. Colier, W.H.L. Hoefnagels, and R.W.M.M. Jansen. Cerebral oxygenation declines in healthy elderly subjects in response to assuming the upright position. *Stroke*, 31:1615–1620, 2000.

[128] F.M. Melchior, R.S. Srinivasan, and J.M. Clère. Mathematical modeling of human cardiovascular response to LBNP. *Physiologist*, 35(Suppl 1):S204–5, 1992.

[129] F.M. Melchior, R.S. Srinivasan, P.H. Thullier, and J.M. Clère. Simulation of cardiovascular response to lower body negative pressure from 0 to -40 mmHg. *J Appl Physiol*, 77(2):630–40, 1994.

[130] D.E. Mohrmann and L.J. Heller, editors. *Cardiovascular Physiology.* McGraw-Hill, 2003.

[131] C.A. Morillo, D.L. Eckberg, K.A. Ellenbogen, L.A. Beightol, J.B. Hoag, K.U. Tahvanainen, et al. Vagal and sympathetic mechanisms in patients with orthostatic vasovagal syncope. *Circulation*, 96:2509–13, 1997.

[132] C.A. Morillo, G.J. Klein, D.L. Jones, and R. Yee. Time and frequency domain analyses of heart rate variability during orthostatic stress in patients with neurally mediated syncope. *Am J Cardiol*, 74:1258–1262, 1994.

[133] H. Morita, Y. Nishida, H. Motochigawa, N. Uemura, H. Hosomi, and S.F. Vatner. Opiate receptor-mediated decrease in renal nerve activity during hypotensive hemorrhage in conscious rabbits. *Circ Res*, 63:165–72, 1988.

[134] R. Mosqueda-Garcia, R. Furlan, R. Fernandez-Violante, T. Desai, M. Snell, Z. Jarai, et al. Sympathetic and baroreceptor reflex function in neurally mediated syncope evoked by tilt. *J Clin Invest*, 99(11):2736–44, 1997.

[135] I.T. Nabney. *Netlab: Algorithms for Pattern Recognition.* Springer, 2002.

[136] M. Nakagawa, N. Takahashi, T. Iwao, H. Yonemochi, T. Ooie, M. Hara, et al. Evaluation of autonomic influences on QT dispersion using the head-up tilt test in healthy subjects. *Pacing Clin Electrophysiol*, 22(8):1158–63, 1999.

[137] J.E. Naschitz, I. Rosner, M. Rozenbaum, M. Fields, H. Isseroff, J.P. Babich, et al. Patterns of cardiovascular reactivity in disease diagnosis. *Q J Med*, 97:141–51, 2004.

[138] N. Nijhawan and D.C. Warltier. *Cardiovascular Physiology*, chapter 6 ("Regulation of the cardiovascular system"). BMJ, second edition, 2000.

[139] P. Novak and V. Novak. Time/frequency mapping of the heart rate, blood pressure, and respiratory signals. *Med Biol Eng Comput*, 31:103–110, 1993.

[140] V. Novak, P. Novak, T. Kus, and R. Nadeau. Slow cardiovascular rhythms in tilt and syncope. *J Clin Neurophysiol*, 12:64–71, 1995.

[141] B. Öberg and P. Thorén. Increased activity in left ventricular receptors during hemorrhage or occlusion of caval veins in the cat. — A possible cause of the vaso-vagal reaction. *Acta Physiol Scanda*, 85:164–173, 1972.

[142] J.H. Oh, J.S. Kim, H.C. Kwon, K.P. Hong, J.E. Park, J.D. Seo, et al. Predictors of positive head-up tilt test in patients with suspected neurocardiogenic syncope or presyncope. *Pacing Clin Electrophysiol*, 26(2 pt 1):593–8, 2003.

[143] B. Olshansky. Syncope evaluation at a crossroad: For which patients? *Circulation*, 104:7–8, 2001.

[144] M. Pagani, F. Lombardi, S. Guzzetti, O. Rimoldi, R. Furlan, et al. Power spectral analysis of heart rate and arterial pressure variabilities as a marker of sympathovagal interaction in man and conscious dog. *Circ Res*, 59:178–193, 1986.

[145] J. Pan and W. Tompkins. A real-time QRS detection algorithm. *IEEE Trans Biomed Eng*, BME-32(3):230–6, 1985.

[146] T.G. Papaioannou, A. Protogerou, C. Papamichael, D. Mathioulakis, S. Tsangaris, E. Karatzis, et al. Experimental and clinical study of the combined effect of arterial stiffness and heart rate on pulse pressure: differences between central and peripheral arteries. *Clin Exper Pharm Physiol*, 32:210–17, 2005.

[147] G. Parati, R. Casadei, A. Gropelli, M. Di Rienzo, and G. Mancia. Comparison of finger and intra-arterial blood pressure monitoring in rest and during laboratory tests. *Hypertension*, 13:647–655, 1989.

[148] G. Parati, M. Di Rienzo, and G. Mancia. How to measure baroreflex sensitivity: from the cardiovascular laboratory to daily life. *J Hypertension*, 18:7–19, 2000.

[149] J. Pardey, S. Roberts, and L. Tarassenko. A review of parametric modelling techniques for EEG analysis. *Med Eng Phys*, 18(1):2–11, 1996.

[150] S.W. Parry, D. Richardson, D. O'Shea, B. Sen, and R.A. Kenny. Diagnosis of carotid sinus hypersensitivity in older adults: Carotid sinus massage in the upright position is essential. *Heart*, 83:22–3, 2000.

[151] S. Payne. Analysis of the Ursino/Lodi model of cerebral autoregulation. unpublished, 16 August 2002.

[152] S. Payne. Interaction between the cardiovascular and respiratory control systems: A mathematical model. Internal SPANN Report, 17 October 2003.

[153] S.J. Payne and L. Tarassenko. Tissue oxygenation index as a measure of cerebral autoregulation. In *Proceedings of the 2nd conference, Feb 16–18, Innsbruck, Austria*, pages 546–550. BioMED, 2004.

[154] K. Peterson, E.T. Ozawa, G.M. Pantalos, and M.K. Sharp. Numerical simulation of the influence of gravity and posture on cardiac performance. *Ann Biomed Eng*, 30:247–59, 2002.

[155] G. Piccirillo, C. Naso, A. Moisè, M. Lionetti, M. Nocco, S. Di Carlo, et al. Heart rate and blood pressure variability in subjects with vasovagal syncope. *Clin Sci*, 107(1):55–67, 2004.

[156] M. Pitzalis, G. Parati, F. Massari, P. Guida, M. Di-Rienzo, B. Rizzon, et al. Enhanced reflex response to baroreceptor deactivation in subjects with tilt-induced syncope. *J-Am-Coll-Cardiol*, 41(7):1167–73, 2003.

[157] S. Pola, A. Macerata, M. Emdin, and C. Marchesi. Estimation of the power spectral density in nonstationary cardiovascular time series: Assessing the role of the time-frequency representations (TFR). *IEEE Trans Biomed Eng*, 43(1):46–59, 1996.

[158] S.W. Porges. Orienting in a defensive world: Mammalian modifications of our evolutionary heritage. A polyvagal theory. *Psychophysiology*, 32:301–318, 1995.

[159] S.W. Porges and E.A. Byrne. Research methods for measurement of heart rate and respiration. *Biol Psychol*, 34:93–130, 1992.

[160] M.J.D. Powell. *Numerical Methods for Nonlinear Algebraic Equations*, chapter 6 ("A hybrid method for nonlinear equations"). Gordon and Breach, London, 1970.

[161] M.J.D. Powell. *Numerical Methods for Nonlinear Algebraic Equations*, chapter 7 ("A Fortran Subroutine for Solving Systems of Nonlinear Algebraic Equations"). Gordon and Breach, London, 1970.

[162] E.S. Prakash and Madanmohan. When the heart is stopped for good: hypotension-bradycardia paradox revisited. *Adv Physiol Educ*, 29:15–20, 2005.

[163] M. Prinz-Zaiss, A.N. Yeap, V. Moguilevski, L. Trigg, and B.P. McGrath. Power spectral analysis of heart rate variability during graded head-up tilting in patients with vasodepressor syncope. *Clin Exp Pharm Physiol*, 22:472–474, 1995.

[164] E. Pruvot, J.M. Vesin, J. Schlaepfer, and M. Fromer. Autonomic imbalance assessed by heart rate variability analysis in vasovagal syncope. *Pacing Clin Electrophysiol*, 17:2201–6, 1994.

[165] M. Ptizalis, F. Massari, P. Guida, M. Iacoviello, F. Mastropasqua, B. Rizzon, et al. Shortened head-up tilt test guided by systolic pressure reductions in neurocardiogenic syncope. *Circulation*, 105:146–8, 2002.

[166] S. Qian and D. Chen. Joint time-frequency analysis. *IEEE Sig Proc Mag*, 3:52–67, 1999.

[167] K.J. Quan, M.D. Carlson, and M.D. Thames. Mechanisms of heart rate and arterial blood pressure control: Implications for the pathophysiology of neurocardiogenic syncope. *Pacing Clin Electrophysiol*, 20(3):764–74, 1997.

[168] A. Radaelli, S. Perlangeli, M.C. Cerutti, L. Mircoli, I. Mori, L. Boselli, et al. Altered blood pressure variability in patients with congestive heart failure. *J Hypertens*, 17(12):1905–10, 1999.

[169] R.F. Rea and M.D. Thames. Neural control mechanisms and vasovagal syncope. *J Cardiovasc Electrophysiol*, 4(5):587–95, 1993.

[170] J.A. Rice. *Mathematical Statistics and Data Analysis*. Duxbury Press, second edition, 1994.

[171] G.A. Riegger and A. Wagner. Excessive secretion of vasopressin during vasovagal reaction. *Am Heart J*, 121:602–3, 1991.

[172] R.M. Robertson, E. Medina, N.Shah, R. Furlan, and R. Mosqueda-Garcia. Neurally mediated syncope: Pathophysiology and implications for treatment. *Am J Med Sci*, 317(2):102–109, 1999.

[173] R. Rossen, H. Kabat, and J.P. Anderson. Acute arrest of cerebral circulation in man. *Arch Neurol Psychiatr*, 50:510–28, 1943.

[174] L.B. Rowell. *Human cardiovascular control*. Oxford University Press, 1993.

[175] G.A. Ruiz, C. Madoery, F. Arnaldo, C. Menéndez, and M.C. Tentori. Frequency-domain analysis of heart rate variability during positive and negative head-up tilt table testing: Importance of age. *Pacing Clin Electrophysiol*, 23(3):325–32, 2000.

[176] S. Rzeczinski, N.B. Janson, A.G. Balanov, and P.V.E. McClintock. Regions of cardiorespiratory synchronization in humans under paced respiration. *Phys Rev E*, 66:051909–1–9, 2002.

[177] J.W. Sammon. A nonlinear mapping for data structure analysis. *IEEE Trans Comput*, 18(5):401–9, 1969.

[178] C. Schäfer, M.G. Rosenblum, H. Abel, and J. Kurths. Synchronization in the human cardiorespiratory system. *Phys Rev E*, 60(1):857–70, 1999.

[179] R. Schondorf, J. Benoit, and T. Wein. Cerebrovascular and cardiovascular measurements during neurally mediated syncope induced by head-up tilt. *Stroke*, 28:1564–8, 1997.

[180] R. Schondorf, R. Stein, R. Roberts, J. Benoit, and W. Cupples. Dynamic cerebral autoregulation is preserved in neurally mediated syncope. *J Appl Physiol*, 91:2493–2502, 2001.

[181] R. Schondorf and W. Wieling. Vasoconstrictor reserve in neurally mediated syncope. *Clin Autonom Res*, 10:53–55, 2000.

[182] M.L. Schroeter, O. Schmiedel, and D.Y. von Cramon. Spontaneous low-frequency oscillations decline in the ageing brain. *J Cereb Blood Flow Metab*, 24:1183–91, 2004.

[183] R. Schubert and M.J. Mulvany. The myogenic response: established facts and attractive hypotheses. *Clin Sci*, 96:313–26, 1999.

[184] E.P. Sharpey-Schafer. Emergencies in general practice: syncope. *Br Med J*, 1:506–9, 1956.

[185] R. Sheldon and S. Killam. Methodology of isoproterenol-tilt table testing in patients with syncope. *J Am Coll Cardiol*, 19:773–9, 1992.

[186] R. Sheldon and M.L. Koshman. A randomized study of tilt test angle in patients with undiagnosed syncope. *Can J Cardiol*, 17(10):1051–7, 2001.

[187] R. Sheldon, S. Rose, and M.L. Koshman. Comparison of patients with syncope of unknown cause having negative or positive tilt-table tests. *Am J Cardiol*, 80(5):581–5, 1997.

[188] R. Sheldon, E. Sexton, and M.L. Koshman. Usefulness of clinical factors in predicting outcomes of passive tilt tests in patients with syncope. *Am J Cardiol*, 85(3):360–4, 2000.

[189] R.S. Sheldon, M.L. Koshman, and W.F. Murphy. Electroencephalographic findings during presyncope and syncope induced by tilt table testing. *Can J Cardiol*, 14(6):811–6, 1998.

[190] W.K. Shen, P.A. Low, R.F. Rea, C.M. Lohse, D.O. Hodge, and S.C. Hammill. Distinct hemodynamic profiles in patients with vasovagal syncope: A heterogeneous population. *J Am Coll Cardiol*, 35(6):1470–1477, 2000.

[191] S. Silvani, G. Ciucci, E. Verità, G.G. Rebucci, and A. Maresta. Correlazione tra tipo di postivà del tilt test ed elettroencefalogramma simultaneo: risultati preliminari [The correlation between the type of positivity of the tilt test and a simultaneous electroencephalogram: the preliminary results]. *Ital Heart J Suppl*, 1(1):103–9, 2000.

[192] P. Sleight, M.T. La Rovere, A. Mortara, G. Pinna, R. Maestri, and S. Leuzzi. Physiology and pathophysiology of heart rate and blood pressure variability in humans: Is power spectral analysis largely an index of baroreceptor gain? *Clin Sci*, 88:103–9, 1995.

[193] M.F. Snyder and V.C. Rideout. Computer simulation studies of the venous circulation. *IEEE Trans Biomed Eng*, BME-16:325–34, 1969.

[194] H. Sorsa and V. Turjanmaa. Time-frequency analysis of cardiovascular signals. In *Proceedings of the XVI IMEKO World Congress, Vienna, September 25-28*, volume TC 13, pages 113–8. IMEKO 2000 International Measurement Confederation, 2000.

[195] R. Srinivasan and H.B. Nudelman. Modeling the carotid sinus baroreceptor. *Biophys J*, 12:1171–82, 1972.

[196] S.A. Strickberger, D.W. Benson, I. Bioaggioni, D.J. Callans, M.I. Cohen, K.A. Ellenbogen, et al. AHA/ACCF scientific statement on the evaluation of syncope. *Circ*, 113(2):316–27, 2006.

[197] V.K. Sud, R. Srinivasan, J.B. Charles, and M.W. Bungo. Effects of lower-body negative pressure on blood flow with applications to the human cardiovascular system. *Med Biol Eng Comput*, 31:569–75, 1993.

[198] M. Sumiyoshi, Y. Nakata, Y. Mineda, T. Tokano, M. Yasuda, and Y. Nakazato. Does an early increase in heart rate during tilting predict the results of passive tilt testing? *Pacing Clin Electrophysiol*, 23(12):2046–51, 2000.

[199] R. Sutton. Indications, methodology, and classification of results of tilt table testing. *Am J Cardiol*, 84:10Q–19Q, 1999.

[200] R. Sutton, M. Petersen, M. Brignole, A. Raviele, C. Menozzi, and P. Giani. Proposed classification for tilt induced vasovagal syncope. *Eur J C P E*, 3:180–3, 1992.

[201] R. Sutton and M.E.V. Petersen. The clinical spectrum of neurocardiogenic syncope. *J Cardiovasc Electrophysiol*, 6(7):569–76, 1995.

[202] S. Suzuki, S. Takasaki, T. Ozaki, and Y. Kobayashi. A tissue oxygenation monitor using NIR spatially resolved spectroscopy. *Proc SPIE*, 3597:582–592, 1999.

[203] E. Szufladowicz, R. Maniewski, E. Kozluk, A. Zbiec, A. Nosek, and F. Walczak. Near-infrared spectroscopy in evaluation of cerebral oxygenation during vasovagal syncope. *Physiol Meas*, 25:823–6, 2004.

[204] I. Tachtsidis, C.E. Elwell, C.W. Lee, T.S. Leung, M. Smith, and D.T. Delpy. Spectral characteristics of spontaneous oscillations in cerebral haemodynamics are posture dependent. *Adv Exp Med Biol*, 540:31–6, 2003.

[205] I. Tachtsidis, C.E. Elwell, T.S. Leung, K. Bleasdale-Barr, K. Hunt, N. Toms, et al. Rate of change in cerebral oxygenation and blood pressure in response to passive changes in posture: a comparison between pure autonomic failure patients and controls. *Adv Exp Med Biol*, 566:187–93, 2005.

[206] I. Tachtsidis, C.E. Elwell, T.S. Leung, C.W. Lee, M. Smith, and D.T. Delpy. Investigation of cerebral haemodynamics by near infrared spectroscopy in young healthy volunteers reveals posture dependent spontaneous oscillations. *Physiol Meas*, 25(2):437–45, 2004.

[207] K. Takayasu, U. Osamu, K. Miwako, N. Tadahiro, and T. Iida. Orthostatic hypotension in elderly persons during passive standing: A comparison with young persons. *J Gerontol*, 56(5):M273–80, 2001.

[208] A. Takei, Y. Ohnishi, and M. Yokoyama. Elevated parasympathetic nerve tone in isoproterenol-induced neurally mediated syncope during head-up tilt testing. *Jpn Circ J*, 65(4):320–4, 2001.

[209] L. Tarassenko, G. Clifford, and N. Townsend. Detection of ectopic beats in the electrocardiogram using an auto-associative neural network. *Neural Proc Letters*, 14:15–25, 2001.

[210] L. Tarassenko, N. Townsend, G. Clifford, L. Mason, J. Burton, and J. Price. Medical signal processing using the software monitor. Technical report, IEE, 2001.

[211] K. Tateno and L. Glass. A method for detection of atrial fibrillation using RR intervals. *Comput Cardiol*, 27:391–4, 2000.

[212] H.L. Thomson, K. Wright, and M. Frenneaux. Baroreflex sensitivity in patients with vasovagal syncope. *Circulation*, 95(2):395–400, 1997.

[213] E. Toledo, M.G. Rosenblum, J. Kurths, and S. Akselrod. Cardiorespiratory synchronization: Is it a real phenomenon? *Comput Cardiol*, 26:237–40, 1999.

[214] N.W. Townsend and R. Germuska. Pulse transit time and blood pressure: nomenclature and physiology. Pending publication, 2003.

[215] M. Ursino, M. Antonucci, and E. Belardinelli. Role of active changes in venous capacity by the carotid baroreflex: Analysis with a mathematical model. *Am J Physiol Heart Circ Physiol*, 267:H2531–H2546, 1994.

[216] M. Ursino and C.A. Lodi. A simple mathematical model of the interaction between intracranial pressure and cerebral hemodynamics. *J Appl Physiol*, 82(4):1256–1269, 1997.

[217] M. Ursino and E. Magosso. Acute cardiovascular response to isocapnic hypoxia. I. A mathematical model. *Am J Physiol Heart Circ Physiol*, 279:H149–H165, 2000.

[218] M. Ursino and E. Magosso. Role of short-term cardiovascular regulation in heart period variability: A modeling study. *Am J Physiol Heart Circ Physiol*, 284:H1479–H1493, 2003.

[219] M. Ursino, A. Ter Minassian, C. Lodi, and L. Beydon. Cerebral hemodynamics during arterial and CO_2 pressure changes: in vivo prediction by a mathematical model. *Am J Physiol Heart Circ Physiol*, 279:2439–2455, 2000.

[220] M. Vanderheyden, M. Goethals, P. Nellens, E. Andries, and P. Brugada. Different humoral responses during head-up tilt testing among patients with neurocardiogenic syncope. *Am Heart J*, 135:67–73, 1998.

[221] R.G. Victor, P. Thoren, D.A. Morgan, and A.L. Mark. Differential control of adrenal and renal sympathetic nerve activity during hemorrhagic hypotension in rats. *Circ Res*, 64:686–94, 1989.

[222] J. Ville. Théorie et applications de la notion de signal analytique. *Cables et Transm*, 1:61–74, 1948.

[223] M.B. Waxman, D.A. Cameron, and R.W. Wald. Editorial: Role of ventricular vagal afferents in the vasovagal reaction. *J Am Coll Cardiol*, 21:1138–41, 1993.

[224] K.H. Wesseling, B. De Wit, G.M.A. van der Hoeven, J. van Goudoever, and J.J. Settels. Physiocal, calibrating finger vascular physiology for finapres. *Homeostasis*, 36(2):67–82, 1995.

[225] W. Wieling. *Autonomic failure: a textbook of clinical disorders of the autonomic nervous system*, chapter 15 ("Non-invasive continuous recording of heart rate and blood pressure in the evaluation of neurocardiovascular control"). Oxford University Press, third edition, 1992.

[226] W. Wieling and J.J. van Lieshout. *Clinical Autonomic Disorders*, chapter Maintenance of postural normotension in humans. Lippincott-Raven Publishers, 1997.

[227] E.P. Wigner. On the quantum correction for thermodynamic equilibrium. *Phys Rev*, 40:749–759, 1932.

[228] C. Wright, M.J. Drinkhill, and R. Hainsworth. Reflex effects of independent stimulation of coronary and left ventricular mechanoreceptors in anaesthetized dogs. *J Physiol*, 528:349–58, 2000.

[229] Y. Yokoi and K. Aoki. Relationship between blood pressure and heart rate variability during graded head-up tilt. *Acta Physiol Scand*, 165(2):155–61, 1999.

[230] J. Zariffa, M. Ebden, and B. Bardakjian. A synaptic input portal for a mapped clock oscillator model of neuronal electrical rhythmic activity. *J Neural Eng*, 1(3):158–64, 2004.